University of Augsburg

Cumulative Doctoral Thesis

Imprints of the upper troposphere and the stratosphere on column-averaged methane

Author:
M.Sc. Andreas Ostler

Supervisor:
PD Dr. Ralf Sussmann

A thesis submitted in fulfillment of the requirements for the degree of

Dr. rer. nat.

in the

Faculty of Applied Computer Science
University of Augsburg

January 2017

Erstgutachter:	PD Dr. Ralf Sussmann, KIT, Garmisch-Partenkirchen
Zweitgutachter:	Prof. Dr. Jucundus Jacobeit, University of Augsburg

Tag der mündlichen Prüfung: 19.12.2016

Für Verena

Declaration of authorship

I, M.Sc. Andreas Ostler, declare that this thesis titled, "Imprints of the upper troposphere and the stratosphere on column-averaged methane" and the work presented in it are my own. I confirm that:

- This work was done wholly or mainly while in candidature for a research degree at this University.
- Where any part of this thesis has previously been submitted for a degree or any other qualification at this University or any other institution, this has been clearly stated.
- Where I have consulted the published work of others, this is always clearly attributed.
- Where I have quoted from the work of others, the source is always given. With the exception of such quotations, this thesis is entirely my own work.
- I have acknowledged all main sources of help.
- Where the thesis is based on work done by myself jointly with others, I have made clear exactly what was done by others and what I have contributed myself.

Signed: _____

Date: _____

Summary

Methane is the second most important anthropogenic greenhouse gas and there is renewed strong increase of atmospheric methane since 2007. Although the overall global budget of methane emissions is well constrained, the quantitative attribution to the underlying sources remains an up-to-date open scientific question. The column-averaged dry-air mixing ratio of methane, denoted as XCH_4, is a special atmospheric measure attainable only via ground-based and satellite-derived observations. The resulting data enable a global spatiotemporal overview of the atmospheric methane concentrations and, thus, are very suitable for the quantification of methane emission sources by means of inverse modeling. However, even the strongest surface emission fluxes only produce a slight change in the XCH_4 signal in relation to the co-resident background level in XCH_4. For this reason, an accurate quantification of methane emissions from XCH_4 data only is possible, if observations and simulations of XCH_4 achieve high accuracy (<0.3 %). Meeting this standard requires that XCH_4 as a vertically integrating measure correctly accounts for the existing methane concentrations of various height layers. Therefore, this work examines the effects of atmosphere dynamical processes in the upper troposphere and the stratosphere on the accuracy of XCH_4 observations, and simulations, respectively. At the same time, this dissertation shall contribute to an improved understanding of the factors controlling the atmospheric quantity XCH_4.

This dissertation was conducted at the Karlsruhe Institute of Technology, Institute of Meteorology and Climate Research – Atmospheric Environmental Research (KIT IMK–IFU). It comprises three independent scientific studies (Sussmann et al., 2013; Ostler et al., 2014, 2016), which all are linked to each other. Each individual study is supported by ground-based Fourier Transform Infrared (FTIR) observations of XCH_4 as well as simulations from the Atmospheric Chemistry Transport Model (ACTM). The FTIR measurements originate from several measurement sites and were performed in the framework of the Total Carbon Column Observing Network (TCCON), and the Network for the Detection of Atmospheric Composition Change (NDACC), respectively.

The first article (Sussmann et al., 2013) compares quasi-coincident XCH_4 data sets, that were derived according to NDACC- and TCCON-type retrieval methods from the respective solar absorption spectra. This NDACC−TCCON comparison was realized with

XCH_4 data sets from the sites Garmisch (Germany) and Wollongong (Australia). For both sites, a nearly perfect overall agreement in XCH_4 observations from NDACC and TCCON was detected. By contrast, the seasonal comparison of NDACC and TCCON retrievals shows quasi-periodic XCH_4 differences which can be reduced, but not entirely be eliminated by the use of improved, ACTM-modeled a priori knowledge of the vertical concentration distributions.

The reasons for these seasonal XCH_4 differences are examined in the second article (Ostler et al., 2014) using additional XCH_4 data of the sites Karlsruhe (Germany), Izaña (the Canaries, Spain) and Ny-Ålesund (Spitsbergen, Norway). Two representing case studies illustrate that polar vortex-induced stratospheric subsidence or stratosphere-troposphere exchange processes are an activator for significant XCH_4 variations of up to 1.7 % ($\sim$30 ppb). This dynamically induced variability is connected with variability in the vertical distribution of methane concentrations, which only can be reproduced to some extent by FTIR observations with limited vertical sensitivity and unrealistic a priori information. Therefore, the differing vertical sensitivity of NDACC and TCCON observations produces seasonal varying XCH_4 disagreements in the presence of quasi-periodic events with high atmosphere dynamical variability. The accuracy of TCCON XCH_4 data is only affected by stratospheric subsidence within the polar vortex region. In contrast, NDACC XCH_4 data primarily loose accuracy by means of stratosphere-troposphere exchange processes. Both problems could be circumvented by improved a priori information.

The third study (Ostler et al., 2016) analyzes the dependence of the model−TCCON XCH_4 agreement on the model representation of stratospheric CH_4 based on the 2010 measurement time series from 11 selected TCCON sites. To do this, a triplet of model stratospheric CH_4 fields – model simulations and two satellite-based data sets – was converted into model XCH_4 data. The XCH_4 model−TCCON comparison was conducted with three well-established chemical transport models: ACTM, TM5 (Tracer Model, version 5) and LMDz (Laboratoire de Météorologie Dynamique model with Zooming capability). It becomes evident, that the range of stratospheric CH_4 concentrations, derived from different models and satellites, is large and translates into a significant range of XCH_4 values. Most striking is a large model XCH_4 bias of 2.1 % ($\sim$38 ppb) for ACTM, which is likely to originate from model errors in the simulation of stratospheric transport causing a high bias in stratospheric CH_4 compared to satellite data. The application of the two satellite CH_4 data sets significantly reduces the ACTM XCH_4 bias to 0.2 % (3.3 ppb), whereas their effect on the model XCH_4 bias is ambiguous for TM5 and LMDz, i.e. respective model XCH_4 biases (0.5 % and 0.4 %) can both be increased (to 0.6 % and 1.1 %) and reduced (to 0.2 %). This implies that the satellite data uncertainty is hindering a more accurate evaluation of model stratospheric CH_4

and, hence, its contribution to XCH_4. At the same time, the origin of model-to-model differences in stratospheric CH_4 needs a better assessment in order to take full benefit of XCH_4 data for the inverse modeling of regional CH_4 emissions.

Zusammenfassung

Methan ist das zweitwichtigste anthropogene Treibhausgas. Seit 2007 gibt es erneut einen starken Zuwachs an atmosphärischen Methan. Obwohl das globale Budget an Methanemissionen sich gut abgrenzen lässt, bleibt die quantitative Zuteilung zu den unterliegenden Quellen eine offene wissenschaftliche Fragestellung. Das säulen-gemittelte Mischungsverhältnis von Methan, bekannt als XCH_4, ist ein besonderes atmosphärisches Maß, welches nur durch bodengebundene und satellitenbasierte Messungen ermittelt werden kann. Daraus resultierende Daten ermöglichen einen globalen räumlichen und zeitlichen Überblick über den Methangehalt der Atmosphäre und sind somit sehr gut für die Quantifizierung von Methanquellen über inverse Modellierung geeignet. Allerdings erzeugen selbst die stärksten bodennahen Emissionsflüsse nur eine geringfügige Änderung im XCH_4-Signal bezogen auf das stets vorhandene XCH_4-Hintergrundniveau. Deswegen ist eine akkurate Quantifizierung von Methanemissionen aus XCH_4-Daten auch nur möglich, wenn bei der Messung und Simulation von XCH_4 eine hohe Genauigkeit ($<$0.3 %) erzielt wird. Die Erfüllung dieser Anforderung verlangt, dass XCH_4 als vertikal intergrierendes Maß die vorhandenen Methankonzentrationen aus verschiedenen Höhenbereichen korrekt berücksichtigt. Diese Arbeit untersucht daher die Auswirkungen von atmosphärendynamischen Prozessen in der oberen Troposphäre und der Stratosphäre auf die Genauigkeit von XCH_4-Messungen bzw. XCH_4-Simulationen. Gleichzeitig soll diese Dissertation dazu beitragen, das Verständnis, durch welche Faktoren die atmospherische Größe XCH_4 kontrolliert wird, zu verbessern.

Diese Dissertation wurde am Karlsruhe Institut für Technologie, Institut für Meteorologie und Klimaforschung – Atmosphärische Umweltforschung (KIT IMK–IFU) durchgeführt und besteht im wesentlichen aus drei eigenständigen wissenschaftlichen Arbeiten (Sussmann et al., 2013; Ostler et al., 2014, 2016), die in einem logischen Zusammenhang zueinander stehen. Jede einzelne der drei Studien basiert auf bodengebundenen Fourier-Tranformations-Infrarot (FTIR) XCH_4-Messungen, sowie Simulationen des Chemie-Transport-Modells ACTM (Atmospheric Chemistry Transport Model). Die verwendeten FTIR-Messungen stammen von verschiedenen Messstandorten und wurden im Rahmen des Total Carbon Column Observing Network (TCCON) oder des Network for the Detection of Atmospheric Composition Change (NDACC) durchgeführt.

Die erste Studie (Sussmann et al., 2013) vergleicht zeitlich quasi-koinzidente XCH_4-Daten, die nach NDACC- bzw. TCCON-spezifischen Verfahren aus den entsprechenden solaren Absorptionsspektren abgeleitet wurden. Dieser NDACC−TCCON-Vergleich wurde jeweils für die XCH_4-Daten der Standorte Garmisch (Deutschland) und Wollongong (Australien) ausgeführt. Insgesamt wurde eine nahezu perfekte Übereinstimmung in den XCH_4-Messungen aus NDACC und TCCON für beide Standorte festgestellt. Dem gegenüber stehen quasi-periodische Differenzen im Jahresgang der XCH_4-Daten aus NDACC und TCCON , die mit verbesserten, ACTM-modellierten Apriori-Informationen über die Vertikalverteilung der atmosphärischen Methankonzentration reduziert, jedoch nicht vollständig eliminiert werden konnten.

Die Ursachen dieser saisonalen XCH_4-Differenzen werden in der zweiten Studie (Ostler et al., 2014) mit zusätzlichen XCH_4-Daten der Stationen Karlsruhe (Deutschland), Izaña (Kanarische Inseln, Spanien) und Ny-Ålesund (Spitzbergen, Norwegen) erörtert. Zwei exemplarische Fallstudien zeigen, dass stratosphärische Absinkprozesse im Bereich des Polarwirbels oder Austauschprozesse zwischen Stratosphäre und Troposphäre als Auslöser für signifikante XCH_4-Änderungen von bis zu 1.7 % ($\sim$30 ppb) wirken. Diese dynamisch-induzierte Variabilität ist verbunden mit Variabilität in der Vertikalverteilung des Methangehalts, die von FTIR-Messungen mit eingeschränkter vertikaler Sensitivität und unrealistischer Apriori-Information nur bedingt in XCH_4 abgebildet werden kann. Ergo führt die unterschiedliche vertikale Sensitivität der NDACC- bzw. TCCON-Messungen in Gegenwart quasi-periodisch auftretender Ereignisse mit erhöhter atmosphärendynamischer Variabilität zu saisonal variierenden XCH_4-Unterschieden.Die hohe Genauigkeit der TCCON XCH_4-Messungen wird nur durch stratosphärische Absinkprozesse im Bereich der Arktis beeinträchtigt. Dagegen verlieren NDACC XCH_4-Daten hauptsächlich durch Austauschprozesse zwischen Stratosphäre und Troposphäre an Genauigkeit. Beide Problembereiche können durch verbesserte Apriori-Informationen umgangen werden.

Auf der Grundlage von 11 ausgewählten TCCON Messzeitserien aus dem Jahr 2010 analysiert die dritte Studie (Ostler et al., 2016), inwiefern die Übereinstimmung zwischen Modell und TCCON in XCH_4 von der Modellabbildung des stratosphärischen CH_4-Anteils abhängt. Dafür wurde ein Triplett von stratosphärischen CH_4 Modellfeldern – ein Datensatz aus Modellsimulationen und zwei Satelliten-basierte Datensätze – in Modell XCH_4-Daten umgewandelt. Der XCH_4 Modell−TCCON Vergleich wurde mit drei etablierten Chemie-Transport-Modellen durchgeführt: ACTM, TM5,(Tracer Model, version 5) und LMDz (Laboratoire de Météorologie Dynamique model with Zooming capability). Es wurde ersichtlich, dass eine große Bandbreite an stratosphärischen CH_4-Konzentrationen, abgeleitet aus verschiedenen Modellen und Satelliten, in eine signifikante Bandbreite an XCH_4-Werte übertragen wird. Besonders auffällig ist dabei der große systematische XCH_4-Modellfehler von 2.1 % ($\sim$38 ppb) für ACTM, welcher

wahrscheinlich durch Modellfehler in der Simulation des stratosphärischen Transports angetrieben wird und sich in gegenüber Satellitendaten überhöhten stratosphärischen CH_4 Konzentrationen zeigt. Die Verwendung der beiden Satellitendatensätze reduziert den ACTM XCH_4 Fehler auf 0.2 % (3.3 ppb), während ihr Effekt auf den XCH_4-Modellfehler von TM5 und LMDz zweideutig ist. D.h., dass die entsprechenden XCH_4-Modellfehler (0.5 % and 0.4 %) sowohl vergrößert (auf 0.6 % and 1.1 %), als auch verringert (auf 0.2 %) werden können. Das impliziert, dass die Unsicherheit der Satellitendaten eine noch genauere Evaluierung der modellierten stratosphärischen CH_4-Felder und deren Beitrag zu XCH_4-Daten verhindert. Gleichzeitig zeigt sich, dass die Ursachen für Unterschiede zwischen modellierten stratosphärischen CH_4 besser erfasst werden sollten, um den Wert von XCH_4-Daten für die inverse Modellierung von regionalen CH_4-Emissionen voll auszunutzen.

Acknowledgements

An erster Stelle möchte ich mich bei PD Dr. Ralf Sussmann sehr herzlich für die Gelegenheit bedanken, in seiner Arbeitsgruppe am KIT/IMK-IFU eine Dissertation zu der vorliegenden Thematik anzufertigen. Für sein enormes Engagement bei der Betreuung und Förderung dieser Arbeit durch Anregungen und kritische Diskussionen gebührt Ralf mein tiefster Dank. Mit seiner Klarheit und Kreativität beim Umgang mit komplexen Problemen hat Ralf meine Entwicklung als Wissenschaftler, aber auch als Mensch positiv beeinflusst. Als Teil seiner Arbeitsgruppe konnte ich von hervorragenden Arbeitsbedingungen mit optimalen technischen Voraussetzungen genauso profitieren, wie von seiner treibenden Kraft bei der Gestaltung eines fruchtbaren Arbeitsklimas im Team. Für die schöne Zeit in Garmisch und während diverser Dienstreisen bin ich sehr dankbar, ebenso wie für die Erstellung des Erstgutachtens.

Prof. Dr. Jucundus Jacobeit danke ich sehr herzlich für die freundliche Aufnahme an der Universität Augsburg und für die wohlwollende Unterstützung in allen akademischen Angelegenheiten im Zusammenhang mit meinem Promotionsverfahren an der Universität Augburg. Darüber hinaus bin ich Prof. Jacobeit außerordentlich dankbar für seine Bereitschaft das Zweitgutachten zu erstellen.

Prof. Dr. Hans Peter Schmid danke ich sehr für die herzliche Aufnahme am KIT/IMK-IFU in Garmisch-Partenkirchen, für sein stetiges Interesse an dieser Arbeit und die hervorragende Förderung. Am KIT/IMK-IFU in Garmisch-Partenkirchen arbeiten zu können war ein Privileg, nicht zuletzt aufgrund der perfekten Arbeitsbedingungen.

Für sein bereitwilliges Mitwirken bei der Zielvereinbarungskommission für diese kumulative Dissertation danke ich Prof. Dr. Harald Kunstmann sehr.

I am very grateful to Dr. Prabir K. Patra for his close collaboration which has been very beneficial for this dissertation. His efficiency in quickly providing model simulations was just as impressing as his scientific expertise. Moreover, this inspiring cooperation with Prabir was accompanied by a lot of fun.

Ein großer Dank gebührt der gesamten Arbeitsgruppe „Atmosphärische Variabilität und Trends“ am KIT/IMK-IFU, insbesondere für die angenehme Arbeitsatmosphäre und

kollegiale Zusammenarbeit. Mein besonderer Dank gilt Dipl.-Ing. Markus Rettinger für seinen unermüdlichen Einsatz bei der Betreuung und Auswertung der FTIR-Messungen in Garmisch. Dipl.-Phys. Frank Forster danke ich für sein großzügiges Entgegenkommen während meiner Einarbeitung. Meinem Zimmerkollegen Dipl.-Phys. Andreas Reichert danke ich für seine Hilfsbereitschaft bei technischen sowie fachlichen Fragen, die angenehme Arbeitsatmosphäre im Büro und natürlich für seine Freundschaft. Auch bei MSc Petra Hausmann möchte ich mich für ihre Unterstützung bedanken.

Ein spezieller Dank gilt meinen Eltern und meinen Großeltern für ihre ständige Unterstützung während meiner Promotionszeit.

List of figures

Abbreviations

ACE-FTS	Atmospheric Chemistry Experiment Fourier Transform Spectrometer
AGCM	Atmospheric General Circulation Model
CCSR/NIES/FRCGC	Center for Climate System Research/ National Institute for Environmental Studies/ Frontier Research Center for Global Change
CTM	Chemical Transport Model
ENVISAT	Environmental Satellite
FTIR	Fourier Transform Infrared
GHG	Greenhouse Gas
GOSAT	Greenhouse gases Observing Satellite
IR	Infrared
LMDz	Laboratoire de Météorologie Dynamique model with Zooming capability
MIPAS	Michelson Interferometer for Passive Atmospheric Sounding
MIR	Mid-Infrared
NIR	Near-Infrared
NDACC	Network for the Detection of Atmospheric Composition Change
OCO	Orbiting Carbon Observatory
RF	Radiative Forcing
SCIAMACHY	Scanning Imaging Absorption Spectrometer for Atmospheric Chartography
STE	Stratosphere-troposphere exchange
TANSO	Thermal and Near-infrared Sensor for Carbon Observation

TCCON	Total Carbon Column Observing Network
TM5	Transport Model, version 5
UTLS	Upper Troposphere-Lower Stratosphere
WACCM	Whole Atmosphere Chemistry Climate Model
WMO	World Meteorological Organization
XCH_4	Column-averaged dry-air mixing ratio of methane

Contents

Chapter 1

Introduction

1.1 Methane and climate change

The main driver of present global warming is the anthropogenic increase of greenhouse gas (GHG) emissions since pre-industrial times. Among the well-mixed GHGs including carbon dioxide (CO_2), methane (CH_4) has the second largest climate impact – quantified by a direct radiative forcing (RF) of 0.48 Wm^2 – due to a 150 % rise of CH_4 concentrations within the Industrial Era (Myhre et al., 2013). In addition, increased CH_4 emissions have produced indirect climate impacts from tropospheric ozone (O_3) and stratospheric water vapour (H_2O), since atmospheric CH_4 acts as a precursor for these forcing agents. Although the role of CH_4 in present climate warming is well determined, future projections for the climate impact of CH_4 can not be assigned with high confidence. A major reason for this uncertainty is limited understanding of interactions between the biogeochemical cycle of CH_4 and the climate system.

Climate-methane cycle feedbacks comprise changes in natural CH_4 emissions from wetlands and thawing permafrost regions on land and sea floor. Warmer temperatures, elevated CO_2 concentrations and land management are known as driving factors for an increase in wetland CH_4 emissions which is likely in a future climate (Ciais et al., 2013; Petrescu et al., 2015). However, large disagreements in wetland model simulations combined with a lack of observation data sets reflect current difficulties in assessing the climate sensitivity of wetlands (Melton et al., 2013; Sjögersten et al., 2014). Shortcomings in the understanding of methane-climate connections also exist for the permafrost

CH_4 feedback. Current model simulations and observations suggest that permafrost thaw will cause additional CH_4 emissions (Ciais et al., 2013; Schuur et al., 2015). This positive feedback is considered as a long-term process with a moderate magnitude similar to other climate–terrestrial ecosystem feedbacks (Ciais et al., 2013; Schuur et al., 2015). This implies that the awakening of sleeping giants such as CH_4 hydrates seems to be too slow to cause abrupt climate change. Good news also comes from observations in northeast Greenland indicating that certain ice-free areas will act as a net CH_4 sink in a warmer climate (Jørgensen et al., 2015).

Given the short lifetime of atmospheric CH_4 ($\sim$10 years; see Patra et al., 2011), the reduction of anthropogenic CH_4 emissions is an attractive goal for near-term climate change mitigation (Rogelj et al., 2014). At the same time, a regulation of CH_4 emissions provides benefits for air quality on the long term (Shindell et al., 2012). In order to meet future challenges in both the risk of climate-methane feedbacks and the potential of reduced CH_4 emissions for climate mitigation policies, an accurate knowledge of CH_4 sources and sinks is needed.

1.2 Monitoring methane emissions

Apart from distinct soils, CH_4 sources and sinks are spatially separated from each other. While CH_4 is emitted at the Earth's surface, the depletion of CH_4 takes place in the atmosphere, predominant by chemical reactions with very short-lived ($\sim$1 s) hydroxil free radicals (OH). This unique atmospheric sink is driven by ultraviolet sunlight and commonly regarded as stable over the long-term (Wennberg, 2006; Montzka et al., 2011; Patra et al., 2014). In contrast, CH_4 emission sources are various with almost equal contributions from human activities and natural processes (Fig. 1.1). The total amount of global and anthropogenic CH_4 emissions is constrained reasonably well, whereas the assignment of CH_4 emissions according to source type and region remains uncertain (Dlugokencky et al., 2011; Kirschke et al., 2013).

Currently, the quantification of CH_4 emissions is based on two methodologies known as "bottom-up" and "top-down" approach. In a simplified view, bottom-up estimates correspond to statistical datasets, that are created from local information such as number of cars or cows complemented by process-based estimates for natural CH_4 emissions. By

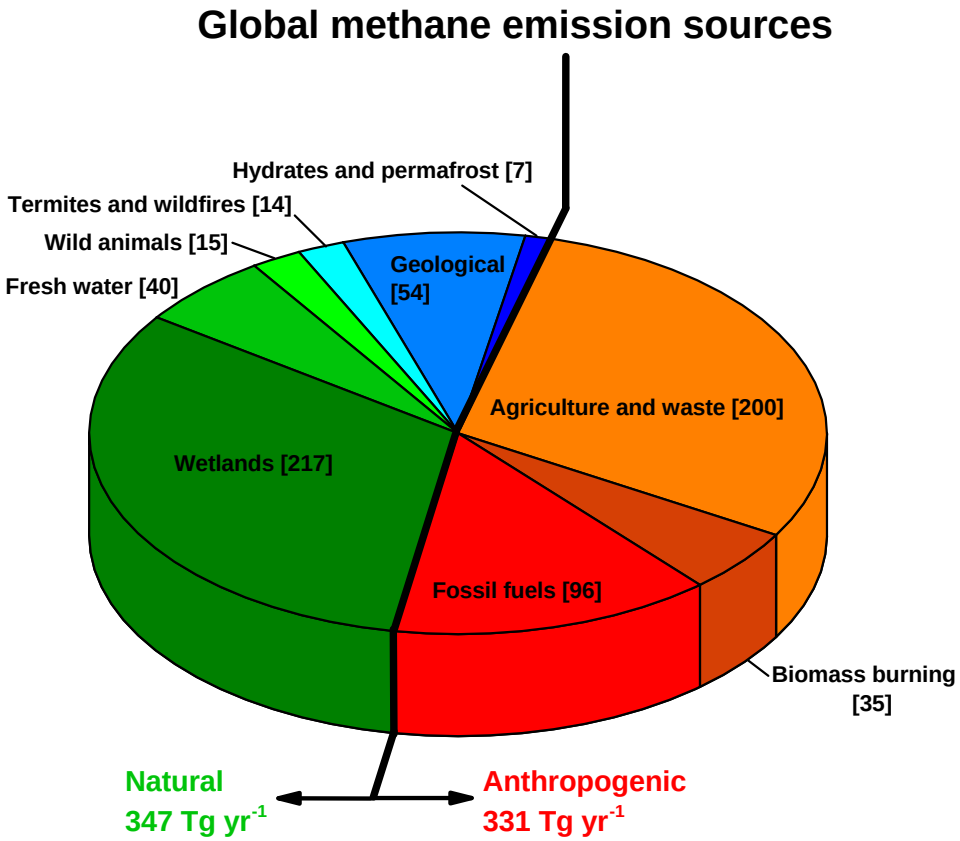

Figure 1.1: Mean CH_4 emission estimates calculated from an ensemble of bottom-up estimates for the period 2000−2009, see Table 1 in Kirschke et al. (2013).

contrast, top-down methods use atmospheric measurements in order to reconstruct the strength of emission sources. A crucial requirement for this attribution is the simulation of mixing and transport processes in the atmosphere via a chemical transport model (CTM) in combination with an inverse approach. Such atmospheric inversion models provide top-down estimates in terms of optimized emission fluxes. Both bottom-up and top-down methods have strengths and weaknesses, but top-down approaches have increasingly been established for the evaluation of bottom-up emission inventories on a global to regional scale (Nisbet and Weiss, 2010). Results from several atmospheric inversions suggest that regional to national CH_4 emissions are underestimated by official inventories (Miller et al., 2013; Brandt et al., 2014; McKain et al., 2015; Bergamaschi et al., 2015). Nevertheless, inversion-based estimates still contain uncertainties limiting the attribution of decadal variability in atmospheric CH_4 concentrations – such as the surprising stabilization period from 1999 to 2006 – to changes in CH_4 emissions (Kirschke

et al., 2013; Nisbet et al., 2014).

In order to reduce this level of uncertainty in top-down estimates, large scientific efforts have been made to improve measurement networks and atmospheric modeling. This development includes the increasing use of satellite observations within atmospheric inversions (Frankenberg et al., 2005, 2008; Meirink et al., 2008; Bergamaschi et al., 2009; Frankenberg et al., 2011; Beck et al., 2012; Bergamaschi et al., 2013; Fraser et al., 2013; Monteil et al., 2013; Cressot et al., 2014; Houweling et al., 2014; Wecht et al., 2014; Alexe et al., 2015; Turner et al., 2015). Remote-sensing measurements from the Scanning Imaging Absorption Spectrometer for Atmospheric Chartography (SCIAMACHY) aboard the Environmental Satellite (Envisat) and from the Thermal and Near-infrared Sensor for Carbon Observation (TANSO) on the Greenhouse gases Observing Satellite (GOSAT) provide great potential due to their large spatiotemporal sampling resolution. Quasi-global coverage involves, that these satellite observations reach key regions where surface measurement networks lack in density such as tropical lands – the major domain of wetland emissions. Satellite-based CH_4 measurements need to be calibrated by ground-based high-precision CH_4 measurements. This goal is achieved by soundings from the Network for the Detection of Atmospheric Composition Change (NDACC) and from the Total Carbon Column Observing Network (TCCON) (Sussmann et al., 2005; Morino et al., 2011; Schneising et al., 2012; Schepers et al., 2012; Yoshida et al., 2013; Dils et al., 2014). Ground- and satellite-based remote-sensing platforms are in close collaboration and provide a special type of CH_4 measure that accounts for the entire vertical distribution of atmospheric CH_4 concentrations – the dry-air column-averaged CH_4 mixing ratio – abbreviated by XCH_4.

1.3 Characteristics of column-averaged methane

Figure 1.2 illustrates that XCH_4 is obtained by remote sensing observations, whereas in situ CH_4 mixing ratios result from direct measurements mostly performed near the surface – the upstream portal of tropospheric CH_4. Given the large spatial variability of atmospheric processes (transport, mixing and chemical removal), surface in situ CH_4 and XCH_4 display different sensitivity to surface fluxes. Compared to surface in situ measurements, total column observations have a large spatial footprint and are

almost independent from vertical mixing rates in the lowermost troposphere (Keppel-Aleks et al., 2011). These properties make inversion-based emission estimates from total column observations far less sensitive to erroneous model representations of vertical mixing. However, these benefits are confronted by strict requirements for XCH_4 observations regarding accuracy and precision (Olsen and Randerson, 2004).

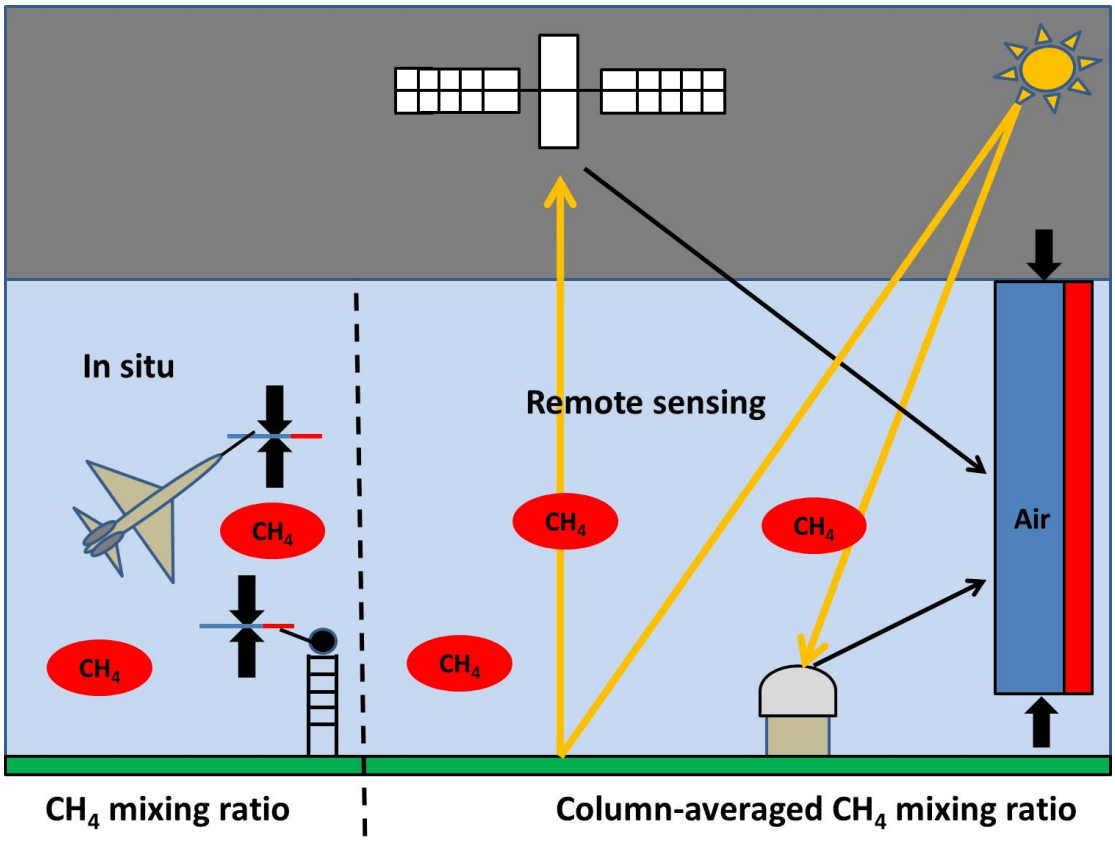

Figure 1.2: Atmospheric observations of CH_4 concentrations. The left part illustrates the measurement principle of in situ observations performed by airborne and surface-based instruments. The right part shows the methodology of remote sounding measurements with space- and ground-based instruments collecting sunlight which was transmitted through the atmosphere. These indirect measurements provide information about the column-averaged CH_4 mixing ratio (XCH_4).

TCCON XCH_4 measurements are obtained with high precision and achieve high accuracy by calibration to airborne in situ measurements (Wunch et al., 2010; Geibel et al., 2012). Methane total column observations conducted with NDACC instrumentation are not calibrated against the World Meteorological Organization (WMO) in situ trace gas measurement scales by contrast to TCCON retrievals. However, NDACC observations have been performed since two decades, whereas the first TCCON site has been established in 2004. Therefore, a joint NDACC-TCCON XCH_4 dataset – with

more measurement sites and longer observation coverage – would be favorable for trend studies, satellite validation, and constraining sources and sinks via inverse modeling.

Column-averaged CH_4 is a complex atmospheric quantity because it integrates information from the entire CH_4 vertical distribution, which is a result of dynamical and chemical processes on various spatial as well as temporal scales. Due to turbulence on local- to synoptic-scale, tropospheric CH_4 mixing ratios are quite homogenous looking at a vertical cross section, i.e. there virtually is no vertical CH_4 gradient in the free troposphere. A small part of the global tropospheric CH_4 is carried into the stratosphere via vertical motion through the tropical tropopause and subsequently distributed around the globe. This stratospheric transport is a steady process, consisting of a slow meridional circulation and a more rapid component with quasi-horizontal mixing (Waugh and Hall, 2002). Hence, the size of the CH_4 source region for stratospheric CH_4 concentrations is limited to the tropical upper troposphere, whereas tropospheric CH_4 is a result of various surface emissions distributed around the globe. Moreover, the transport of CH_4 from the tropical tropopause to the stratospheric location takes much longer time ($\sim 1-6$ years) compared to transport from the Earth's surface to the tropical tropopause (~ 0.5 years). In addition to these differences between tropospheric and stratospheric dynamics, there are differences in tropospheric and stratospheric chemistry. Although depletion of atmospheric CH_4 takes place in both atmospheric layers, the most prominent difference is the dominant role of O_3 in the chemical composition of the stratosphere with O_3 concentrations increasing up to ~ 12 parts per million (ppm) according to the 1976 U.S. Standard Atmosphere (NOAA et al., 1976). Finally, these troposphere-stratosphere differences in CH_4 source/sink regions, in atmospheric transport and chemistry contribute to a strong troposphere-stratosphere gradient in CH_4 mixing ratios. As a result, CH_4 mixing ratios typically are decreasing from the tropopause towards higher atmospheric altitudes (see Fig. 1.3).

Although the dynamics in the extratropical troposphere and stratosphere are basically separated from each other by the tropopause, there are various exchange processes across the tropopause acting on synoptic scales (Stohl et al., 2003). Thus, the vertical CH_4 distribution is expected to reflect variability induced by such dynamical events. To meet the requirements on precision and accuracy, XCH_4 measurements should reflect the variability in CH_4 concentrations at different height layers. Up to now, it has not

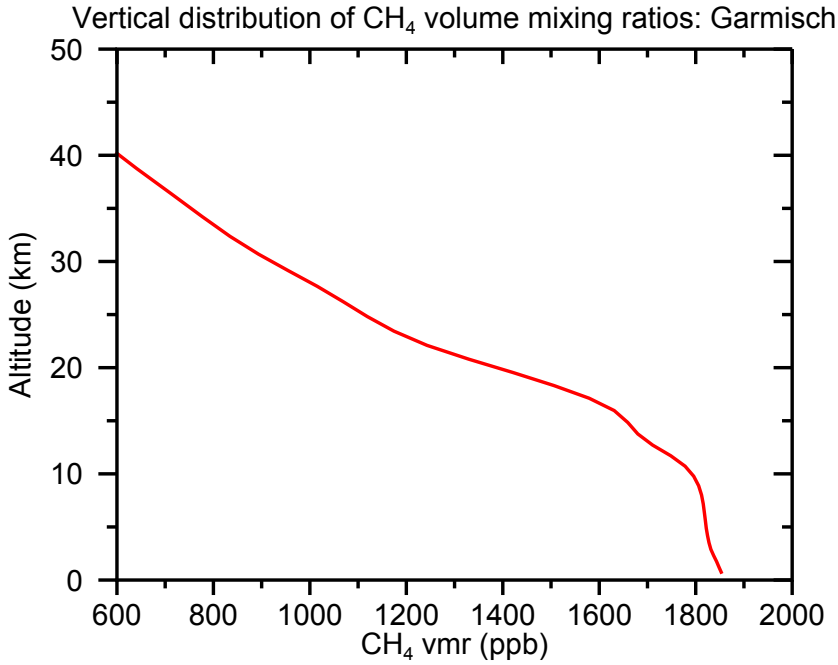

Figure 1.3: Vertical profile of CH_4 volume mixing ratios (vmr), derived from the Whole Atmosphere Chemistry Climate Model for the site Garmisch (WACCM, version 5, 40-year run; see Garcia et al. (2007)).

been investigated in detail to what extent indirect observations from NDACC and TCCON are sensitive to dynamical variability in the upper troposphere-lower stratosphere region. Previous studies have rather pursued the strategy to separate the tropospheric part from the total column CH_4, considering that a variable stratospheric contribution to XCH_4 may obscure tropospheric signals (Washenfelder et al., 2003; Angelbratt et al., 2011; Sepúlveda et al., 2012, 2014; Wang et al., 2014; Saad et al., 2014). This unwanted stratospheric variability has primarily been associated with shifts in the tropopause position – with variations on synoptical and seasonal timescales – controlling the relative contribution of the stratosphere to the vertically integrated airmass. However, the relative contribution of stratospheric CH_4 to XCH_4 also depends on the exact vertical gradient of CH_4 in the stratosphere, which is determined by a complex interplay of chemistry and transport. Consequently, simulating and observing XCH_4 requires an accurate representation of the stratospheric CH_4 distribution by models and observations. Although it is known, that model simulations of stratospheric CH_4 show large inter-model differences (Patra et al., 2011), the impact of model stratospheric CH_4 fields on XCH_4 data has not been evaluated in detail u to now.

Finally, all these aspects suggest, that there are major shortcomings in our present

knowledge of how XCH_4 is controlled by H_4 variations in the free atmosphere. Benefits of XCH_4 observations for the assessment of CH_4 emissions can only be exploited entirely, if present knowledge gaps are to be closed. Therefore, this work investigates the sensitivity of XCH_4 to atmospheric dynamics, in order to improve the current understanding on the factors controlling XCH_4.

1.4 Outline of the Dissertation

This dissertation investigates the dependence of the atmospheric quantity XCH_4 on upper troposheric and stratospheric CH_4 distributions. As a first goal this thesis analyzes the agreement between NDACC and TCCON observations of XCH_4 with an overall and a seasonal point of view. The second goal is to analyze to what extent NDACC and TCCON XCH_4 observations reflect atmospheric variability that is induced by dynamical processes in the upper troposphere and lower stratosphere (UTLS) region. The third goal of this dissertation is to quantify the sensitivity of XCH_4 to stratospheric CH_4 distributions. In order to examine these goals, this dissertation consists of three articles with a causal connection between each individual scientific study:

1. Sussmann et al. (2013)
2. Ostler et al. (2014)
3. Ostler et al. (2016)

The starting point is the comparison between ground-based FTIR observations of XCH_4 conducted under the framework of NDACC, and TCCON, respectively (Sussmann et al., 2013). Both networks obtain information about the total column of CH_4 from IR absorption measurements at several (joint) stations (see 1.5.2), but they observe different spectral regions and apply different retrieval strategies to produce XCH_4 data. As the consistency of both data sets in terms of accuracy cannot be granted at first place, the focus of the first article is on analyzing the overall and seasonal agreement between quasi-coincident XCH_4 retrievals from NDACC and TCCON. Consequently, the title of the first study is *First intercalibration of column-averaged methane from the Total Carbon Column Observing Network and the Network for the Detection of Atmospheric Composition Change*. Based on same-day coincidence between NDACC and TCCON

measurements, the first study uses multiannual datasets of XCH_4 monthly means from the stations Garmisch, Germany (47.48° N, 11.06° E, 743 m a.s.l.), and Wollongong, Australia (34.41° S, 150.88° E, 30 m a.s.l.). The overall agreement between NDACC and TCCON XCH_4 is investigated by using linear regression, trend analysis, and correlation analysis via t-test. The seasonal agreement is evaluated by statistical analysis of the XCH_4 residual time series (NDACC−TCCON) in terms of residual standard deviation, auto- and cross-correlation. Moreover, the study applies a special approach to reduce the a priori impact – a priori profiles of CH_4 mixing ratio and vertical sensitivity are different for NDACC and TCCON standard XCH_4 retrieval – on the comparison between NDACC and TCCON retrievals of XCH_4: site- and time-specific model profiles of CH_4 mixing ratios are used as a common prior for both NDACC and TCCON retrievals. The article Sussmann et al. (2013) thus provides the basis for answering the general question if NDACC XCH_4 retrievals achieve the high accuracy standards that are mandatory for TCCON. At the same time, the article discusses the requirements for a joint use of NDACC and TCCON XCH_4 data and possible applications of this combined dataset in satellite validations or flux inversions.

The findings of the first article about the behavior of these two different XCH_4 retrievals suggest a refined intercomparison with additional data sets from FTIR sites covering geophysical conditions other than those for Garmisch and Wollongong. For this reason, the second article Ostler et al. (2014) expands the NDACC−TCCON comparison with XCH_4 observations from Ny-Ålesund (78.92° N, 11.93° E, 20 m a.s.l.), Karlsruhe (49.08° N, 8.43° E, 110 m a.s.l.), and Izaña (28.31° N, 16.45° W, 2.370 m a.s.l.). The second study takes a step forward as it investigates how the differing retrieval characteristics depend on atmospheric situations with elevated dynamical variability, such as stratospheric subsidence or STE processes. Consequently, the title of the second study reads as *Multistation intercomparison of column-averaged methane from NDACC and TCCON: impact of dynamical variability.* Two representative case studies (stratospheric subsidence and intrusion) are accompanied by meteorological detection methods in order to estimate the relative fraction of FTIR measurement days affected by high dynamical variability in the UTLS region. Excluding these flagged observations from the XCH_4 intercomparison allows to quantify the impact of dynamical varibility on the agreement between NDACC and TCCON retrievals of XCH_4. Finally, the second article discusses the findings in relation to current strategies established for mitigating the impact of

stratospheric variability on XCH_4. In summary, the second article (Ostler et al., 2014) is a direct consequence of the first study (Sussmann et al., 2013) as it provides a closer look to unresolved questions of the first study and, thereby, specifies the characteristics of NDACC and TCCON XCH_4 retrievals.

The findings of the second article reveal the importance of the stratospheric contribution as a controlling factor for the CH_4 total column, thereby motivating the third article Ostler et al. (2016) entitled *Model−TCCON comparisons of column-averaged methane with a focus on the stratosphere*. The third article is complementary to the second article (Ostler et al., 2014) insofar as it deals with the sensitivity of XCH_4 to the stratospheric CH_4 distribution. The latter mainly is driven by stratospheric transport, a dynamical process acting on much longer timescales than subsidence or STE-processes which were investigated in the second paper. The basic concept of this third study is to use a triplet of model CH_4 fields differing in stratospheric CH_4 mixing ratios:

a) Modeled CH_4 fields

b) Modeled CH_4 fields corrected by MIPAS-based CH_4

c) Modeled CH_4 fields corrected by MIPAS-based CH_4 adjusted to ACE-FTS observations

The model correction is equivalent to a substitution of model stratospheric CH_4 fields by satellite-inferred CH_4 data, which are based on retrievals of MIPAS (Michelson Interferometer for Passive Atmospheric Sounding; Fischer et al., 2008) aboard ENVISAT, and retrievals of ACE-FTS (Atmospheric Chemistry Experiment Fourier Transform Spectrometer; Bernath et al., 2005) aboard the Canadian satellite SciSat-1, respectively. The triplet of differing model CH_4 fields then is converted to a triplet of XCH_4 data sets. This allows to quantify the dependence of XCH_4 data on the model stratospheric CH_4 distribution. In order to evaluate the impact of model stratospheric CH_4 fields on XCH_4, accurate XCH_4 observations are applied as reference. This observational XCH_4 data set consists of TCCON XCH_4 retrievals from 11 selected sites covering measurements in the year 2010. The whole XCH_4 model−TCCON comparison is performed with three well-established CTMs: ACTM (Patra et al., 2016), TM5 (the Tracer Model, version 5; Pandey et al., 2016), and LMDz (Laboratoire de Météorologie Dynamique model

with Zooming capability; Locatelli et al., 2015) The results of the model−TCCON comparison are presented and discussed with an emphasis on model-to-model differences in the simulation of stratospheric CH_4. In this context, model transport characteristics are tested using a well-known transport diagnostic – the mean age of stratospheric air. In the third study, mean age data was derived from both model simulations and MIPAS observations of sulfur hexafluoride (SF_6). Besides that, the significance of the findings on the sensitivity of XCH_4 to stratospheric CH_4 is also discussed relating to the satellite data range.

1.5 Ground-based FTIR observations of column-averaged methane

This section gives a short insight into the physical and methodological concepts required for ground-based solar Fourier Tranform Infrared (FTIR) observations and includes a brief introduction of the two FTIR networks. Following explanations refer to Liou (2002) and Zdunkowski et al. (2007). More details to FTIR spectrometry can be found in Griffiths and de Haseth (2007).

1.5.1 Basic concept of FTIR spectrometry

Ground-based Fourier Tranform Infrared (FTIR) spectrometry is a passive remote sensing technique using direct sunlight as information carrier for physical properties of the atmosphere, such as the CH_4 concentration profile. A typical FTIR observation of XCH_4 is the result of a measured signal – the infrared (IR) absorption spectrum – and a retrieval process consisting of a forward and an inverse problem.

Measured signal

After collecting solar radiation with the spectrometer, the measured signal is converted into an absorption spectrum via the principle of Fourier Transformation. The absorption spectrum contains so-called molecular fingerprints in terms of spectral absorption lines, reflecting that, during traveling through the atmosphere, the intensity of solar radiation has been attenuated by molecular absorption. In order to interact with IR radiation, the vibrations of atmospheric molecules need to cause a change of the electric dipole

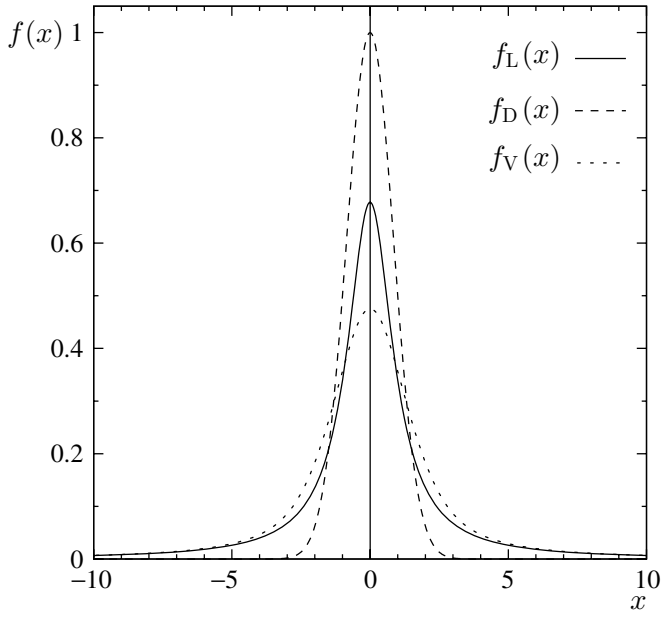

Figure 1.4: Comparison of the Lorentz, the Doppler and the Voigt line-shape factors with x = $(\nu - \nu_0)/\alpha$, where ν_0 is the wavenumber of an ideal, monochromatic line and α is the half-width of the line at the half-maximum. Taken from Zdunkowski et al. (2007).

moment. For a CH_4 molecule, there are two vibration modes that are producing an oscillating electric dipole moment and, thereby, allowing an interaction between molecule and electromagnetic radiation.

The absorption of radiation then is equivalent to a change in the internal energy of a molecule. In the IR range, vibrational transitions are coupled with relatively small rotational energy changes, therefore leading to vibrational-rotational absorption lines. Despite the quantized structure of such energy transitions, the observed absorption lines are not monochromatic, but appear with finite width.

In the atmosphere, this line broadening is caused by external influences on the molecule during the absorption process. Collisions with other molecules – collision broadening – and thermal motion of the molecule – Doppler broadening – yield the line shape. In the infrared collision (or pressure) broadening is dominant typically at altitudes below 20 km and produces spectral lines that are characterized by a Lorentz profile. Doppler broadening dominates at higher altitudes with spectral lines described by the Doppler line shape. At an altitude region between $\sim$20 km and $\sim$50 km both broadening processes take place involving a combined line shape described by the Voigt profile. Figure 1.4 illustrates the individual line shapes and, thereby, reveals that collisional

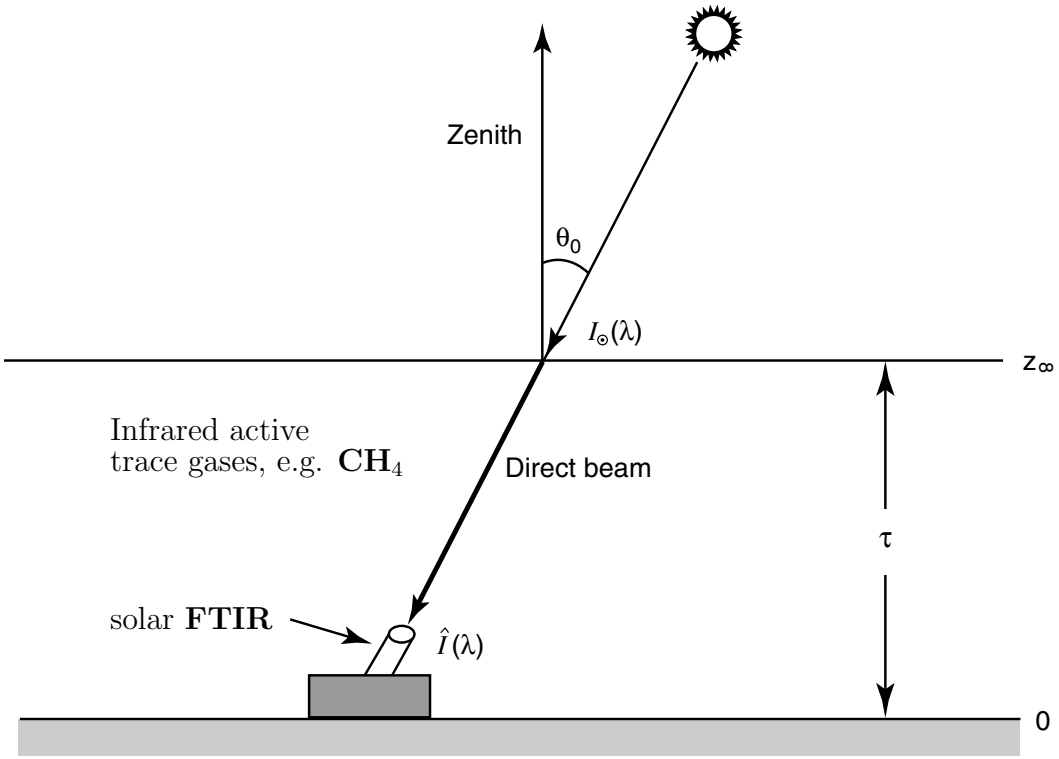

Figure 1.5: Geometry of a ground-based solar FTIR spectrometer for the measurement of a direct solar beam. The solar zenith angle is defined by θ_0, the optical depth is denoted by τ, and the solar intensity and measured intensity are given by $I_{\odot}$ and $\hat{I}$, respectively. Adopted from Liou (2002).

line broadening is dominant in the line wings, whereas Doppler broadening controls the line center. This for example implies that a absorption line with fully saturated center can only receive additional absorption at the line wings in terms of collision broadening. As contributions from both collision and Doppler broadening to the line shape depend on atmospheric pressure and temperature, the spectral line shape typically retains information on the absorption at different altitudes. Therefore, the observed spectral absorption characteristics of CH_4 are connected with the altitude, the amount of CH_4, and the observed intensity.

Retrieval process

The forward problem is the simulation of the detected radiance signal, the IR spectrum with the characteristic absorption lines. In order to fulfill this task, a forward model has to simulate the radiative transfer considering the geophysical and optical composition of the local Earth-atmosphere system (see Fig. 1.5) as well as the instrumental properties. For ground-based FTIR observations, radiative transfer is simplified, since

thermal emission and solar scattering processes can be neglected in the spectral region from about 0.2 to 5 μm. Hence, the radiative transfer equation to be solved by the forward model is the Beer–Bouguer–Lambert law:

$$\hat{I}\left(\lambda\right) = I_{\odot}\left(\lambda\right) \exp\left[-\int_{z_0}^{z_\infty} \tau\left(\lambda, z\right) dz\right] \tag{1.1}$$

While traversing the atmosphere, the incoming intensity of solar radiation at the top of the atmosphere $I_{\odot}$ is decreased to $\hat{I}$ at the ground (see Fig. 1.5). For a given wavelength λ, the attenuation of solar sun light along its way from the top of the atmosphere (z_∞) to the FTIR spectrometer at the ground (z_0) depends on the optical depth $\tau(\lambda, z)$ of the atmosphere. The optical depth $\tau(\lambda, z)$ consists of N components from N absorbing molecules:

$$\tau\left(\lambda, z\right) = \sum_{i=1}^{N} \sigma_i\left(\lambda,\, T(z), p(z)\right) \cdot \frac{n_i(z)}{\cos\left(\theta(\lambda, z)\right)} \tag{1.2}$$

The contribution of an absorbing trace gas i to $\tau(\lambda, z)$ is determined by the molecular absorption cross section $\sigma_i(\lambda,\, T(z), p(z))$ and the trace gas concentration $n_i(z)$, weighted by the cosine of the apparent zenith angle $\theta(\lambda, z)$. The absorption cross section $\sigma_i(\lambda,\, T(z)p(z))$ depends on the vertical profile of temperature $T(z)$ and pressure $p(z)$ which yield the characteristic absorption line shape. Hence, all parameters in Eq. (1.2) are continuous functions of the altitude z. However, for the computation of $\hat{I}$, the integral in the exponent of Eq. (1.1) is approximated by a summation of discrete atmospheric layers.

The forward simulation also depends on the quantity of interest, e.g. the vertical profile of CH_4 concentrations. This means, that the forward model F attributes a state vector $\boldsymbol{x}$, containing the quantity of interest, to a vector of measurements $\boldsymbol{y}$. Consequently, this functional relationship has to be inverted in order to retrieve the atmospheric target (illustrated in Fig. 1.6). However, finding the inverse of F is not trivial, because the inverse problem for FTIR observations is ill-posed with more unknowns than independent measurements, i.e., various parameters (concentration of several GHGs, temperature and pressure profile, etc.) have an impact on the detected radiation in addition to the atmospheric target. A common approach for solving this inverse problem is to iteratively

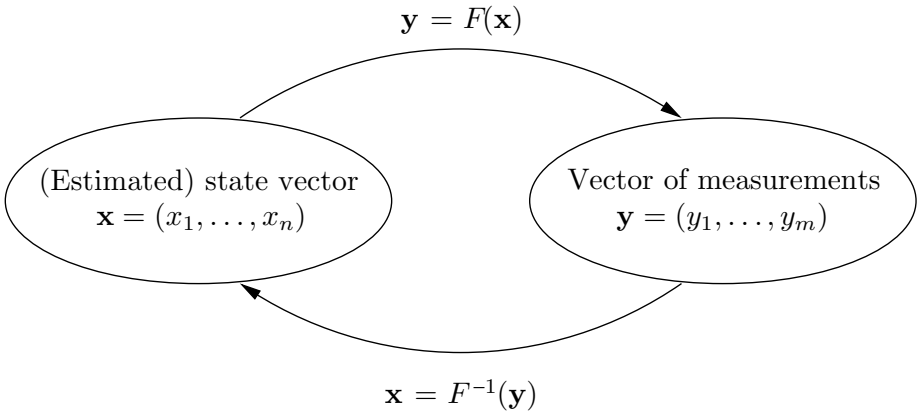

Figure 1.6: Forward and inverse problem in remote sensing applications. Note that the solution to the inverse problem in general provides only an estimate for the true state of the atmosphere. Taken from Zdunkowski et al. (2007).

minimize the following cost function:

$$[\boldsymbol{y} - F(\boldsymbol{x})]^T \mathbf{S}_\epsilon^{-1} [\boldsymbol{y} - F(\boldsymbol{x})] + [\boldsymbol{x} - \boldsymbol{x}_a]^T \mathbf{R} [\boldsymbol{x} - \boldsymbol{x}_a] \tag{1.3}$$

The covariance matrix $\mathbf{S}_\epsilon$ describes the statistics of the measured signal error. The regularization matrix $\mathbf{R}$, also known as smoothing-constraint, defines distinct mathematical conditions to the solution. Both $\mathbf{S}_\epsilon$ and $\mathbf{R}$ are part of the prior knowledge, which also includes a best estimate of the atmospheric composition before the measurement in terms of an a priori profile of CH_4 concentrations $\boldsymbol{x}_a$. Due to the non-linearity of the forward model F, the cost function (Eq. 1.3) is minimized by Newton's iterative method.

Finally, the inverse model provides a best estimate of the atmospheric state given the measurement, the prior knowledge of the atmospheric composition and the mathematical regularization. Integrating the retrieved CH_4 profile yields the total column of CH_4 molecules, which is weighted by the dry-air pressure column to produce the final product of the retrieval process – the dry-air column-averaged CH_4 mixing ratio (XCH_4).

1.5.2 Networks: NDACC and TCCON

Ground-based FTIR observations are performed at various sites, distributed around the globe (Fig. 1.7), under the framework of TCCON (https://tccon-wiki.caltech.edu/) and the Infrared Working Group (IRWG) within NDACC (http://www.acd.ucar.edu/irwg/).

Starting in 1991 with a main focus on the stratosphere, NDACC priorities have broad-

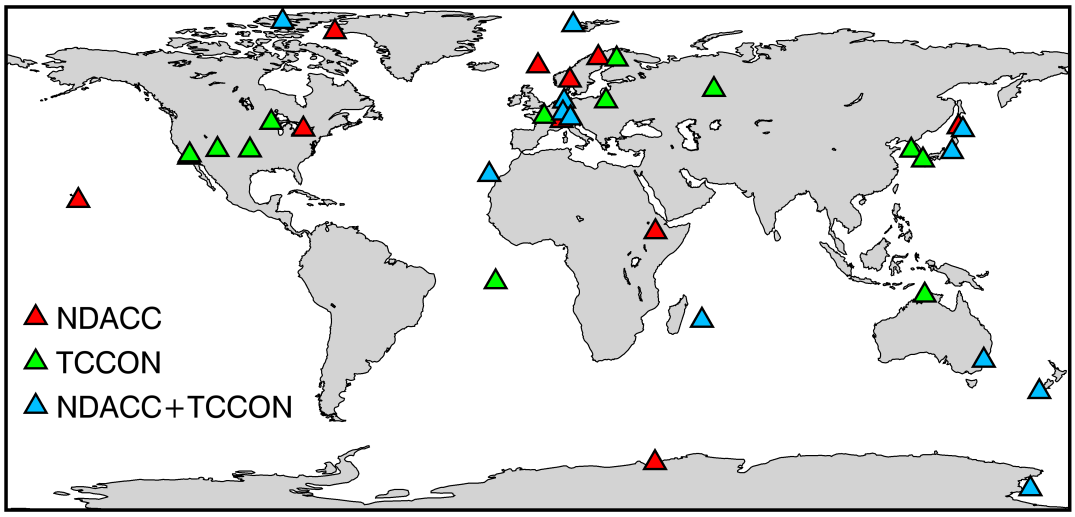

Figure 1.7: Global map with NDACC and TCCON sites

ened to the entire atmosphere and its interaction with the climate system. The first TCCON observations were conducted in 2004 and the following construction of the network was intended for validation of satellite observations from the Orbiting Carbon Observatory (OCO). After the launch of OCO in 2009 had failed, a second Orbiting Carbon Observatory (OCO-2) was successfully launched in July 2014. Thus, TCCON has yet began to serve its initial purpose considering that TCCON observations have already been used for the evaluation of other satellite-based remote sensing projects. Besides satellite validation, the greater goal of TCCON is to better understand the sources and sinks of CO_2 and CH_4.

A close partnership between NDACC and TCCON also arises from the fact that several operational FTIR sites are part of both NDACC and TCCON. In practice, this means that the FTIR spectrometer has to be equipped with two specific detectors, because NDACC and TCCON measurements analyze different spectral regions of the transmitted sunlight: NDACC-type observations use the mid-infrared (MIR) spectral region, whereas TCCON-type measurements rely on the intensity of absorption in the near-infrared (NIR) spectrum. Characteristic CH_4 absorption features can be found in the MIR around 2800 cm^{-1} (3.6 μm) and in the NIR around 6000 cm^{-1} (1.7 μm).

The TCCON data are archived at http://tccon.ornl.gov/, NDACC data are available at ftp://ftp.cpc.ncep.noaa.gov/ndacc/station/. TCCON ensures a high level of standardization regarding instrumentation and retrieval process (Wunch et al., 2011), including a common data processing and analysis software. In contrast, NDACC recommends certain fixed retrieval parameters, but also allows for some flexibility by site.

Chapter 2

Summary and synthesis

2.1 Article I

The first article *First intercalibration of column-averaged methane from the Total Carbon Column Observing Network and the Network for the Detection of Atmospheric Composition Change* (Sussmann et al., 2013) compares quasi-coincident XCH_4 retrievals derived from NDACC- and TCCON-type ground-based FTIR soundings. In the following, NDACC-type retrievals, a priori profiles, or averaging kernels are denoted by MIR according to the spectral region where the FTIR measurement has recorded an absorption spectrum. In analogy to this nomenclature, NIR is equivalent to TCCON specifications. The NDACC/TCCON (MIR/NIR) data set from the site Garmisch comprises monthly means of XCH_4 for the period from July 2007 until the end of 2011, data sets from the site Wollongong cover the period from June 2008 until the end of 2011. The comparison of XCH_4 retrievals was evaluated by a linear fit in order to determine an XCH_4 calibration factor between NDACC and TCCON. For the direct comparison of XCH_4 monthly means, the fitted linear regression produced a MIR/NIR slope of 0.9996 for Garmisch and a MIR/NIR slope of 0.9987 for Wollongong. Given the 2-σ slope uncertainties of 0.0011 (Garmisch) and 0.0016 (Wollongong), the fitted slopes are not different from 1 for both sites. Moreover, the linear fits did not yield a significant y-intercept for the individual sites. These statistical parameters suggest that, overall, there is no systematic XCH_4 difference between NDACC and TCCON retrievals for both sites. This finding is supported by the fact that the time series of XCH_4 residual differences (NDACC$-$TCCON) did not show any trend for Garmisch, and Wollongong,

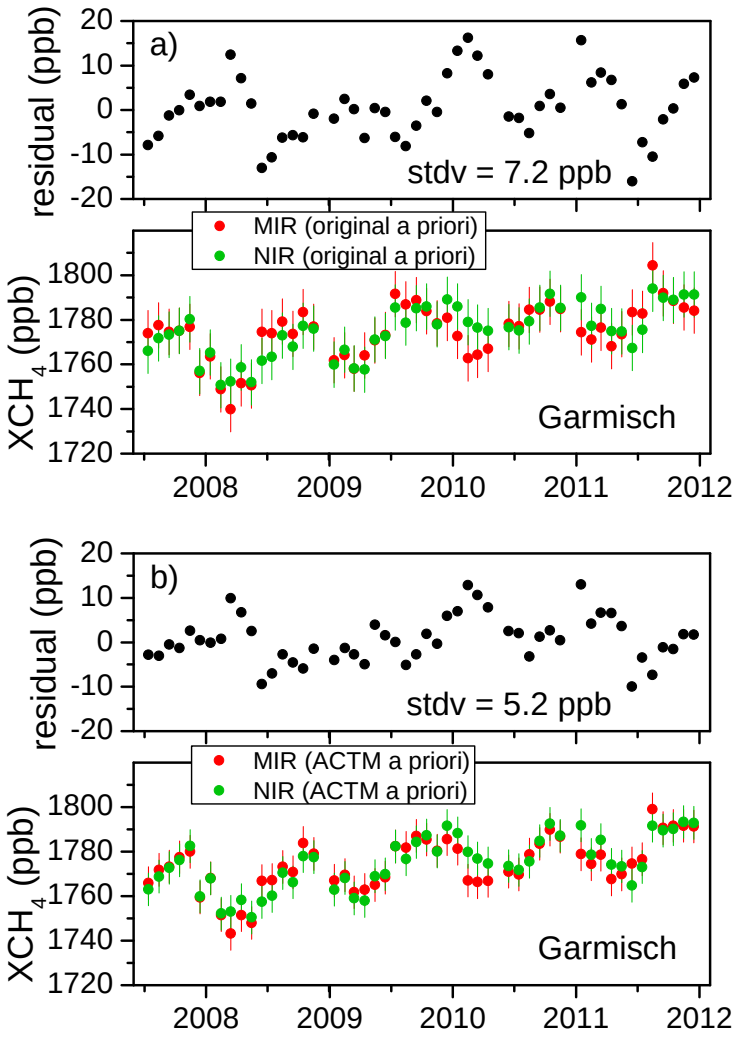

Figure 2.1: (a) Lower trace: monthly mean MIR (NDACC) and NIR (TCCON) time series for Garmisch. Both column series are plotted as retrieved. Error bars are 2-σ uncertainites derived from the standard deviation (stdv) of the linear slope fit (2 stdv/$\sqrt{2}$). Upper trace: residual time series, i.e. difference time series of the NIR and MIR data shown in the lower trace. (**b**) Same as (**a**) but using ACTM profiles as common prior.

respectively. However, the XCH_4 residual time series displays a quasi-periodic seasonal bias between NDACC and TCCON data, which is quantified by the residual standard deviation (RSD). Most of these seasonal XCH_4 differences are caused by two basically different characteristics of NDACC and TCCON retrievals: (i) different a priori information about atmospheric CH_4 concentrations and (ii) different vertical sensitivity (smoothing). By using a common prior the first main retrieval difference is eliminated easily, but the second difference component as a result of the retrieval processes cannot be compensated in such a simple way. Therefore, the common prior was based on site- and time-specific ACTM model profiles reflecting realistic CH_4 distributions in order to

avoid different smoothing errors – the direct consequence of different vertical sensitivities. After applying this refined mitigation strategy, the RSD is reduced from 7.2 ppb to 5.2 ppb for Garmisch, and from 7.1 ppb to 6.6 ppb for Wollongong (see Fig. 2.1). This corresponds to an improved seasonal agreement between NDACC and TCCON retrievals of XCH_4.

Finally, the first study shows that there is no need for an overall NDACC/TCCON intercalibration factor, but the seasonal XCH_4 variations can be different for NDACC observations compared to TCCON observations. The main drivers for this quasi-periodic seasonal bias between NDACC and TCCON data are differences in retrieval a priori CH_4 mixing ratio profiles and different retrieval vertical sensitivities. The first article also discusses the implications of these findings for a joint use of NDACC and TCCON XCH_4 data within satellite validation and inversion studies. One conclusion is that an accurate validation of satellite XCH_4 retrievals with NDACC and TCCON observations requires the use of a common prior of CH_4 mixing ratios for all retrievals involved. In order to reduce seasonal biases, the best choice for such a common prior is to use realistic site- and time-dependent CH_4 distributions. As TCCON a priori profiles are steadily improved, they could be suitable for the use as common prior. In practice, this approach can be implemented by reprocessing retrieval data (NDACC, TCCON, satellite) with the common prior or by an a posteriori adjustment of the retrievals taking into account the retrieval vertical sensitivity (averaging kernel).

2.2 Article II

The second article *Multistation intercomparison of column-averaged methane from NDACC and TCCON: impact of dynamical variability* (Ostler et al., 2014) continues the NDACC−TCCON comparison with a significantly enlarged XCH_4 dataset. In addition to Garmisch and Wollongong data, the second study is based on long-term XCH_4 observations from the high arctic site Ny-Ålesund, the mid-latitude site Karlsruhe, and the subtropical high-altitude station Izaña. Analysis methodology is analogous to Sussmann et al. (2013) including the strategy of using ACTM-simulated CH_4 mixing ratio profiles as a common prior. For each site, the direct comparison of NDACC and TCCON XCH_4 monthly means produced a interval of intercalibration factors (linear fit slope ± corresponding slope uncertainty). Given that the fitted slope interval (2-σ uncertainty)

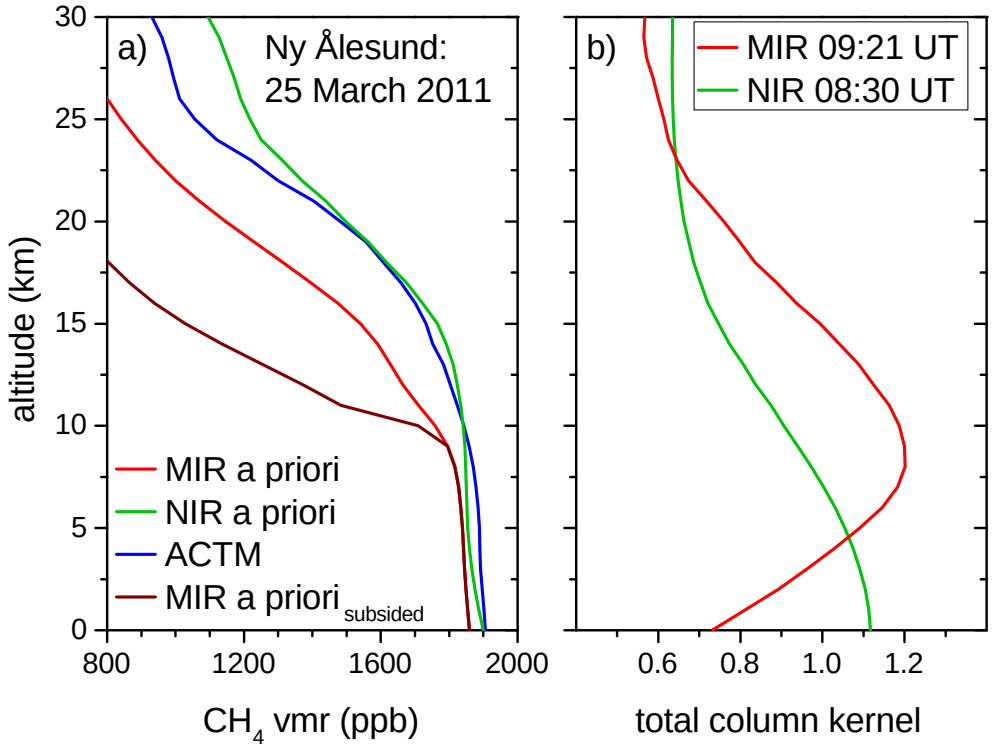

Figure 2.2: **(a)** A priori profiles used for analysis of Ny-Ålesund spectra recorded on 25 March 2011. MIR a priori is the standard a priori profile from WACCM for Ny-Ålesund. NIR a priori is the TCCON standard a priori profile (release ggg_2012_July_Update) for Ny-Ålesund. ACTM is the actual ACTM profile for 25 March 2011 used as a common prior for standard intercomparison of the NIR and MIR retrievals. MIR a priori$_{\text{subsided}}$ is a strongly subsided profile typical for intravortex conditions used for recorrection of the NIR and MIR retrievals in a more realistic intercomparison. **(b)** Averaging kernels for MIR and NIR retrievals using Ny-Ålesund spectra recorded on 25 March 2011.

included the value 1.0, the agreement of NDACC and TCCON XCH_4 was graded as perfect. According to this criteria, the NDACC−TCCON agreement for Garmisch, Wollongong, and Karlsruhe XCH_4 data was evaluated as perfect. A very good overall agreement was also found for Izaña XCH_4 data sets, but could not be classified as perfect given the small 2-σ slope uncertainty of 0.0006 for a slope of 0.9986. For Ny-Ålesund data, a slope of 0.9909 with a 2-σ uncertainty of 0.0022 indicated a systematic XCH_4 difference between NDACC and TCCON retrievals by contrast to the results for the remaining sites. Besides this exceptional overall bias, the Ny-Ålesund data sets also showed an above-average seasonal bias with a large RSD of 13.0 ppb compared to RSD values of 8.6 ppb (Garmisch), 7.4 ppb (Wollongong), and 6.1 ppb (Karlsruhe). In contrast to these significant seasonal differences, the Izaña XCH_4 data sets show

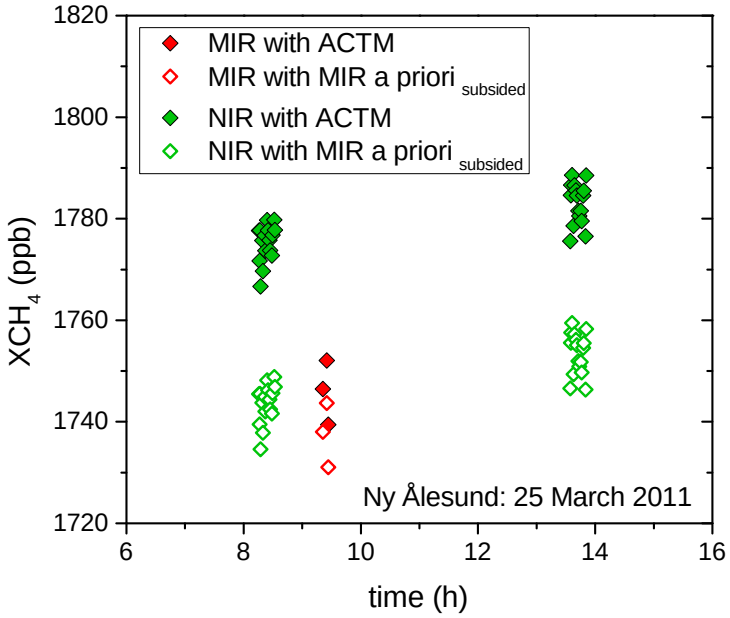

Figure 2.3: Ny-Ålesund XCH_4 on 25 March 2011 retrieved from FTIR data. MIR and NIR retrievals are corrected to the common ACTM prior (filled squares) and are corrected to a strongly subsided MIR a priori profile (open squares) as shown in 2.2a.

a nearly perfect seasonal agreement (RSD = 2.5 ppb). This can be attributed to the favorable measurement conditions with a high number of unperturbed clear-sky observations. Again, seasonal XCH_4 differences are reduced for all sites by using ACTM-based common priors, but remaining maximum XCH_4 residuals (12−30 ppb) still occur periodically. These residual differences indicate the presence of different smoothing effects, hence the common prior strategy has only been successful to some extent. Knowing that smoothing effects are dominant when atmospheric CH_4 concentrations significantly deviate from the retrieval a priori profile of CH_4 concentrations, the second study further investigates the retrieval characteristics at situations with high atmosphere dynamical variability.

For two case studies, we showed that the XCH_4 difference between NDACC and TCCON almost disappears if the common prior is further improved in order to reflect the actual atmospheric state of high variability. The first case study for Ny-Ålesund illustrates that the TCCON retrieval overestimates XCH_4 if the retrieval a priori does not account for polar vortex-induced stratospheric subsidence. In the case of strong stratospheric subsidence, the standard retrieval a priori and the ACTM-simulated profile of CH_4 mixing ratios differ from the actual distribution of CH_4 mixing ratios (see Fig.

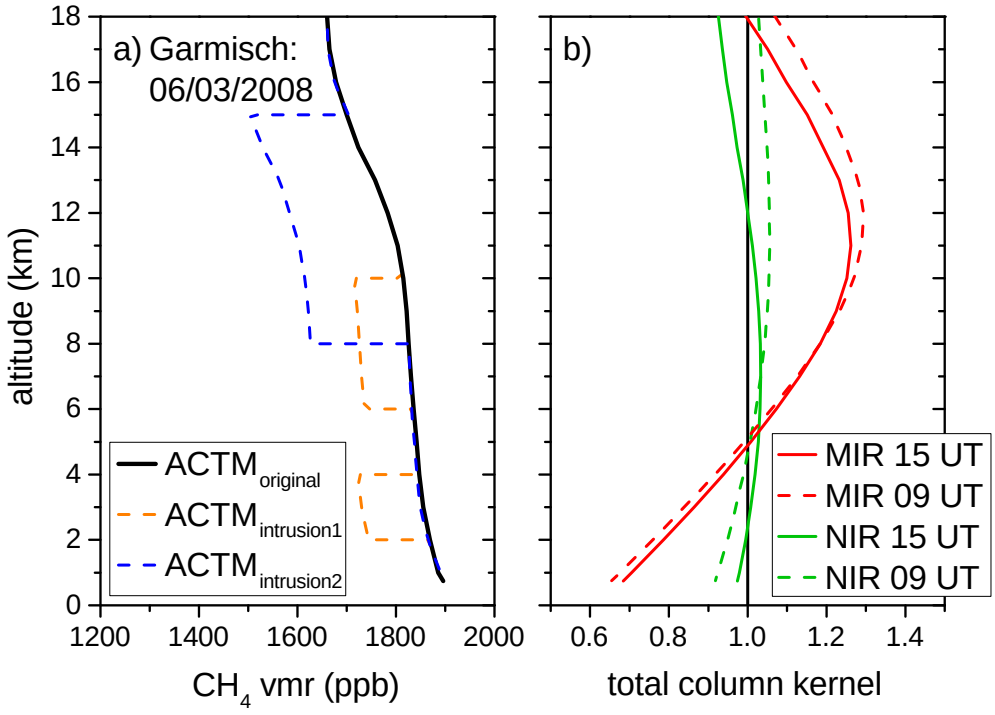

Figure 2.4: **(a)** ACTM profiles used for the a posteriori correction of MIR and NIR retrievals of Garmisch spectra recorded on 6 March 2008: $\mathrm{ACTM_{original}}$ is the original ACTM profile used in the correction. $\mathrm{ACTM_{intrusion1}}$ and $\mathrm{ACTM_{intrusion2}}$ are the original ACTM profiles which were modified due to a deep stratospheric intrusion event on this day. $\mathrm{ACTM_{intrusion1}}$ is used for the recorrection of retrievals before 11:00 UTC, $\mathrm{ACTM_{intrusion2}}$ is used for the recorrection of retrievals after 11:00 UTC. **(b)** Averaging kernels for MIR and NIR retrievals of Garmisch spectra recorded on 6 March 2008.

2.2a). Deviations of the a priori profile from the real vertical profile of CH_4 concentrations are smoothed by the retrieval wherever the retrieval vertical sensitivity is not perfect and, accordingly, the respective total column averaging kernel is different from 1. Indeed, the retrieval vertical sensitivity is limited for the situation on 25 March 2011 with total column kernels differing from one (see Fig. 2.2b). In particular, the TCCON total column kernel is less than 1 in the lower stratosphere, meaning that the TCCON retrieval underestimates the perturbation of the vertical distribution of CH_4 concentrations. Consequently, the retrieved XCH_4 is $\sim$29 ppb greater for TCCON compared to NDACC observations when using the unrealistic CH_4 a priori profile (see Fig. 2.3). By contrast, the use of a realistic CH_4 a priori profile prevents different smoothing effects and thereby reduces the XCH_4 NDACC$-$TCCON difference.

The second case study demonstrates that a deep stratospheric intrusion at Garmisch creates residual XCH_4 differences of $\sim$15 ppb due to an underestimation of XCH_4 by

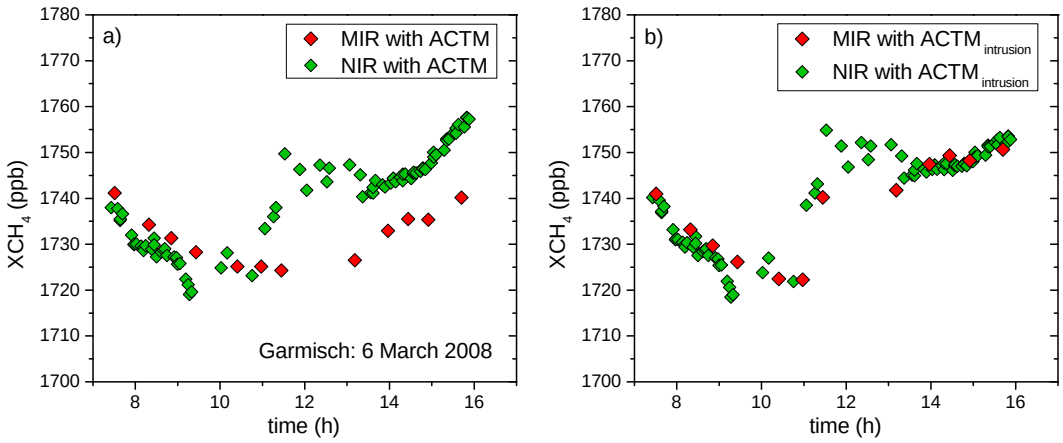

Figure 2.5: Garmisch XCH_4 on 6 March 2008 retrieved from FTIR data. **(a)** MIR and NIR retrievals are corrected to a common ACTM a priori. **(b)** MIR and NIR retrievals are corrected to the modified ACTM profiles shown in Fig. 2.4a.

the NDACC retrieval. As for the case of stratospheric subsidence, an unrealistic a priori profile of CH_4 concentrations (Fig. 2.4a) combined with different retrieval vertical sensitivities (Fig. 2.4b) leads to different smoothing effects, and XCH_4 NDACC−TCCON differences (Fig. 2.5a), respectively. Due to limited retrieval vertical sensitivity in the UTLS region the NDACC retrievals do not reflect the significant 25 ppb increase in XCH_4 within one hour, which is connected with the disappearance of a stratospheric intrusion. Applying an improved CH_4 a priori profile to the NDACC and TCCON retrievals yields a nearly perfect agreement between NDACC and TCCON observations (Fig. 2.5b).

Moreover, we find that such dynamical events (subsidence and STE-processes) are not individual cases, but have an impact on the complete time series of XCH_4 observations, e.g., $\sim$23 % of the FTIR measurement days at Ny-Ålesund were affected by polar vortex conditions and $\sim$35 % of Garmisch measurement days are influenced by STE processes. After excluding the flagged data from the intercomparison, the seasonal agreement is significantly improved for Garmisch data (RSD reduced by 1.5 ppb). For the Ny-Ålesund data sets the exclusion results only in a small improvement relating to seasonality (RSD reduced by 0.5 ppb), and the overall bias (fit slope improved from 0.909 to 0.9922).

Finally, these findings quantitatively confirm that the accuracy of NDACC−TCCON XCH_4 retrievals is impacted by variability originating from the stratosphere. The alternative for mitigating this stratospheric variability is to separate a tropospheric part

from the retrieved XCH_4. This can be achieved via so-called proxy methods – stratospheric CH_4 is substituted by a FTIR retrieval of a correlated stratospheric tracer – or by directly retrieving accurate CH_4 profiles. The fact, that smoothing effects are different for NDACC and TCCON XCH_4 retrievals, has several implications for the practical applications of these data sets: First, for validation of satellite XCH_4 retrievals from GOSAT and SCIAMACHY, the use of TCCON retrievals should be preferred because of the similar vertical sensitivity of these ground- and satellite-based remote sounding systems, i.e., systematic retrieval errors can be identified from remaining satellite−TCCON differences. Second, based on the different retrieval vertical sensitivities a combined NDACC-TCCON retrieval setup could increase the information content and produce more accurate XCH_4 data. Third, if a high level of seasonal accuracy is required for the use of XCH_4 data within inversion or trend studies, then NDACC and TCCON XCH_4 retrievals should be filtered with regard to high atmosphere dynamical variability. New instructions for this task have been presented in this work, along with already recommended strategies like refined fitting methods for the determination of tropospheric trends.

2.3 Article III

The third article *Model−TCCON comparisons of column-averaged methane with a focus on the stratosphere* (Ostler et al., 2016) complements the second article (Ostler et al., 2014) in improving the knowledge about the sensitivity of XCH_4 to the distribution of stratospheric CH_4. To do this, a triplet of model CH_4 fields with different stratospheric CH_4 distributions is validated against XCH_4 observations from 11 selected TCCON sites. The triplet of model stratospheric CH_4 fields comprises the simulated stratospheric CH_4 distribution, the MIPAS-retrieved stratospheric CH_4 data set, and the MIPAS-retrieved stratospheric CH_4 data set being adjusted to ACE-FTS observations (abbreviated as MIPAS_ACE). Given the sparse data coverage of ACE-FTS measurements, these observations were not used directly. Instead, the MIPAS CH_4 data set was adjusted by latitudinal offsets derived from collocated CH_4 to ACE-FTS observations. Those three model CH_4 fields (original, MIPAS, MIPAS_ACE) were then used to extract model CH_4 profiles according to the location and time of TCCON measurements performed in the year 2010. Subsequently, model CH_4 vertical profiles, differing in the

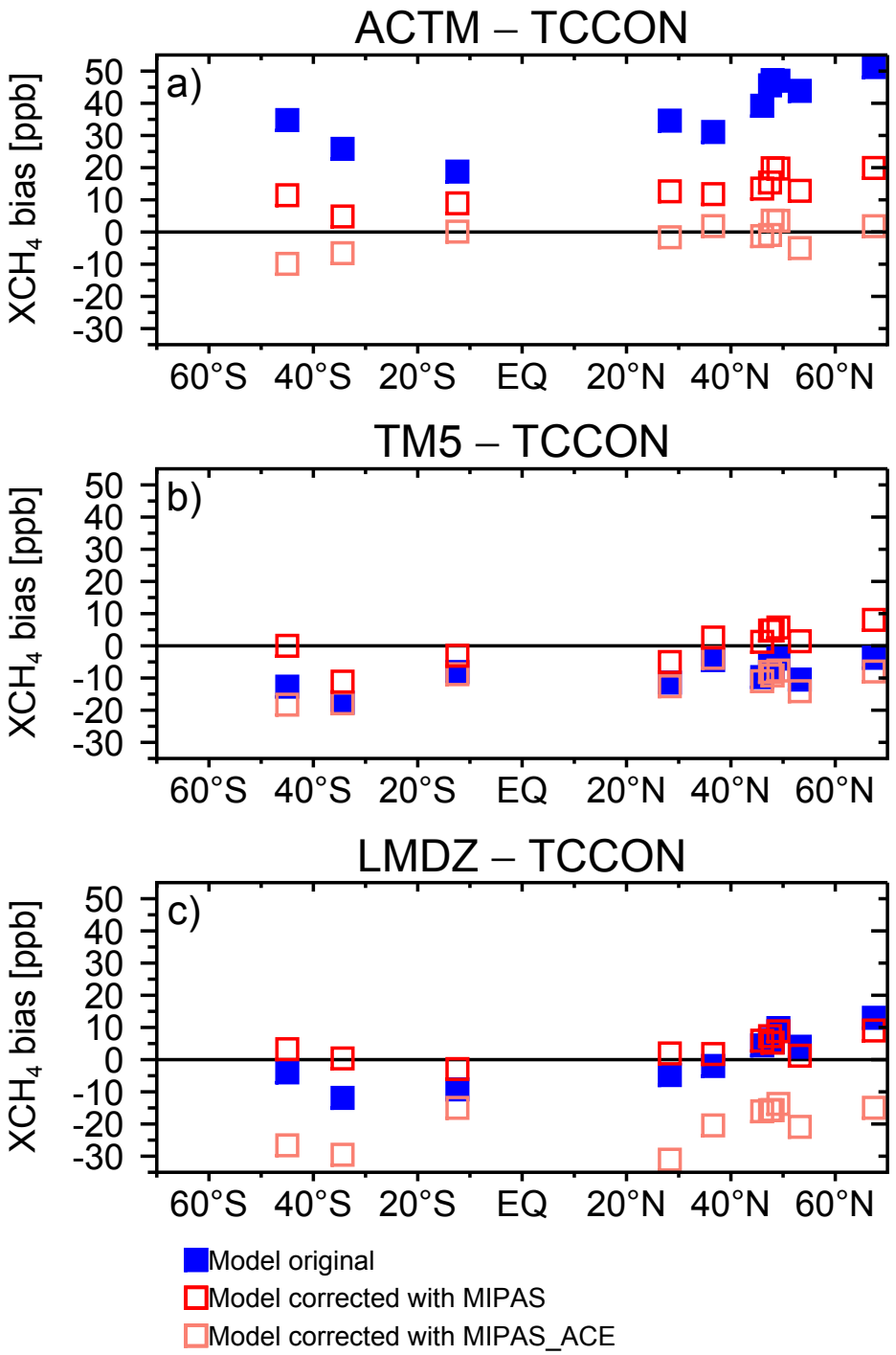

Figure 2.6: Site-specific model XCH_4 biases with respect to TCCON observations in parts per billion (ppb) for the year 2010. Different colors indicate different stratospheric CH_4 fields used for the calculation of model XCH_4.

stratospheric CH_4 distribution, have been converted to XCH_4 accounting for TCCON retrieval a priori profiles and averaging kernels. TCCON data retrieved with the software package GGG2014 was obtained from the TCCON Data Archive, hosted by the Carbon Dioxide Information Analysis Center (CDIAC: http://cdiac.ornl.gov/). The XCH_4

model−TCCON comparison was performed with three CTMs (ACTM, TM5, LMDz) that have already been used to invert CH_4 emission fluxes from atmospheric CH_4 observations. The mean difference between model and TCCON XCH_4 daily mean time series yields a site-specific model XCH_4 bias for each TCCON site. Averaging the absolute site-specific XCH_4 biases produces the average model XCH_4 bias.

The site-specific model XCH_4 biases are shown in Fig. 2.6, where the individual TCCON sites are represented by their geographical latitude. Figure 2.6 illustrates that the average model XCH_4 bias (blue squares) is significantly larger for ACTM (38.1 ppb, Fig. 2.6a) than for TM5 (8.7 ppb, Fig. 2.6b), and LMDz (6.8 ppb, Fig. 2.6c), respectively. For ACTM the site-specific model XCH_4 biases result in a min−max range of 32.5 ppb with biases increasing towards higher latitudes. Such a latitudinal latitudinal dependence is not visible for TM5 XCH_4 biases with a min−max range of 13.9 ppb. A noticeable latitudinal dependence also is not detected for LMDz with XCH_4 biases providing a min−max range of 24.9 ppb.

Using MIPAS data for stratospheric model CH_4 fields reduces the average model XCH_4 bias for all models (see red open squares in Fig. 2.6). The improvement is significant for ACTM, where the average XCH_4 bias is reduced from 38.1 ppb to 13.7 ppb accompanied by a reduction of the min−max range from 32.5 ppb to 15.1 ppb. The reduction of the average XCH_4 bias is small for the low-biased models TM5 (from 8.7 ppb to 4.3 ppb) and LMDz (from 6.8 ppb to 4.3 ppb). At the same time, the min−max range of site-specific XCH_4 biases is increased from 13.9 ppb to 19.2 ppb for TM5, and decreased from 24.9 ppb to 12.0 ppb for LMDz. The best agreement between ACTM and TCCON XCH_4 is found when applying MIPAS data adjusted to ACE-FTS observations for stratospheric model CH_4 fields (light red open squares in Fig. 2.6). ACTM average XCH_4 bias then is 3.3 ppb with a min−max range of 13.4 ppb. In contrast to that, the use of MIPAS_ACE stratospheric CH_4 increases the average XCH_4 model bias for TM5 (from 8.7 ppb to 10.8 ppb; min−max range = 14.6 ppb) and for LMDz (from 6.8 ppb to 20.0 ppb; min−max range = 17.3 ppb).

The results of the XCH_4 model−TCCON comparison reveal that the impact of the stratospheric model correction on XCH_4 is diverse for the models and depends on the satellite data set. In order to understand this, the CH_4 mixing ratio differences between simulated and satellite CH_4 data are presented in terms of zonally-averaged vertical

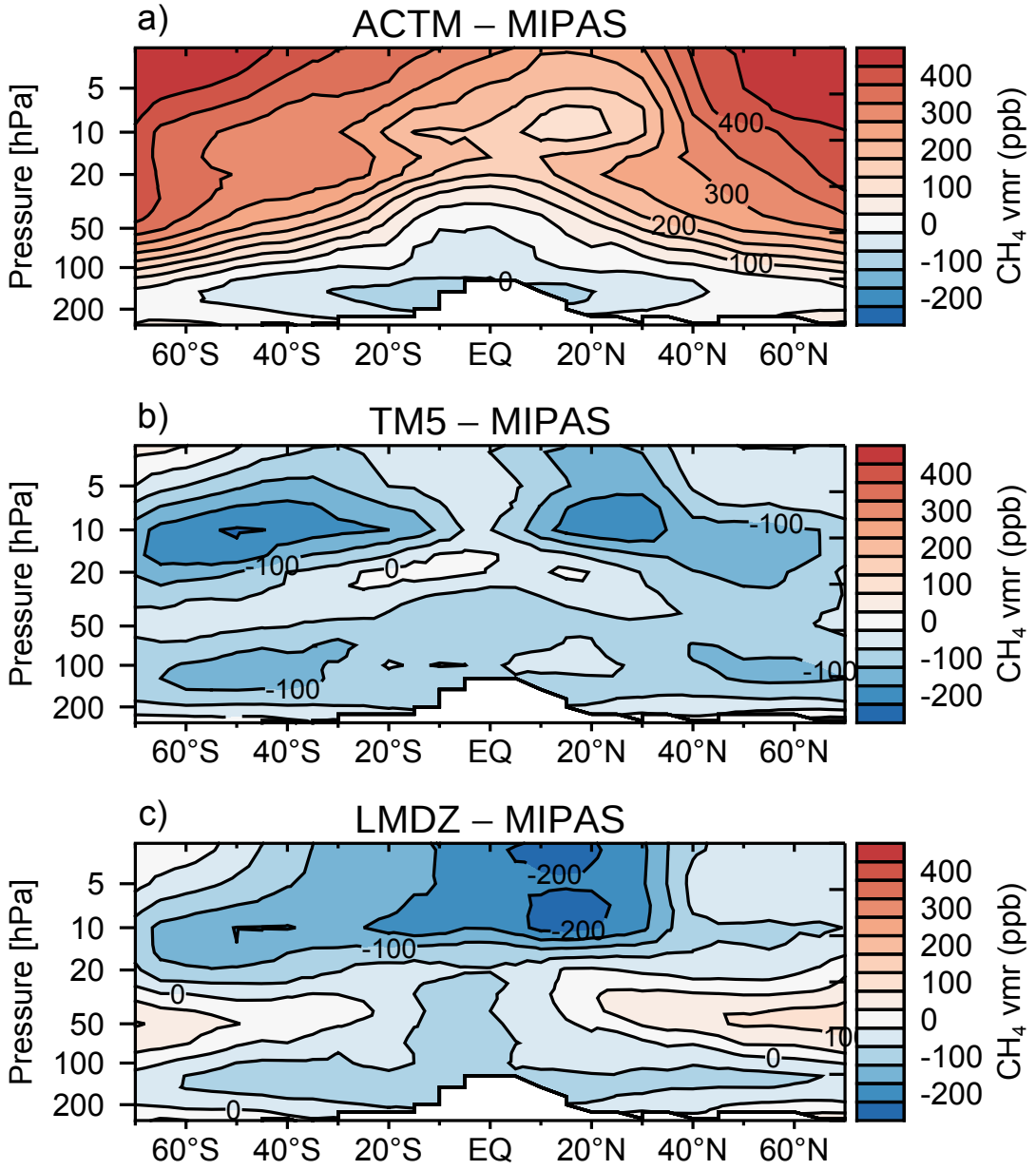

Figure 2.7: Model−MIPAS differences of stratospheric CH_4 volume mixing ratios (vmr) in parts per billion (ppb). Zonally-averaged CH_4 vmr differences are annual means for the year 2010.

distributions in Fig. 2.7 (MIPAS), and Fig. 2.8 (MIPAS_ACE), respectively. The comparison of ACTM stratospheric CH_4 against both satellite data sets suggests a large positive ACTM CH_4 bias increasing from negligible values at the tropopause up to 450 ppb at upper stratospheric altitudes (see Figs. 2.7a and 2.8a). However, the ACTM CH_4 bias with respect to MIPAS_ACE particularly is larger within the lower stratosphere by up to 200 ppb than with respect to MIPAS. Therefore, the model correction with MIPAS_ACE data has a larger impact on the ACTM XCH_4 than the MIPAS-based

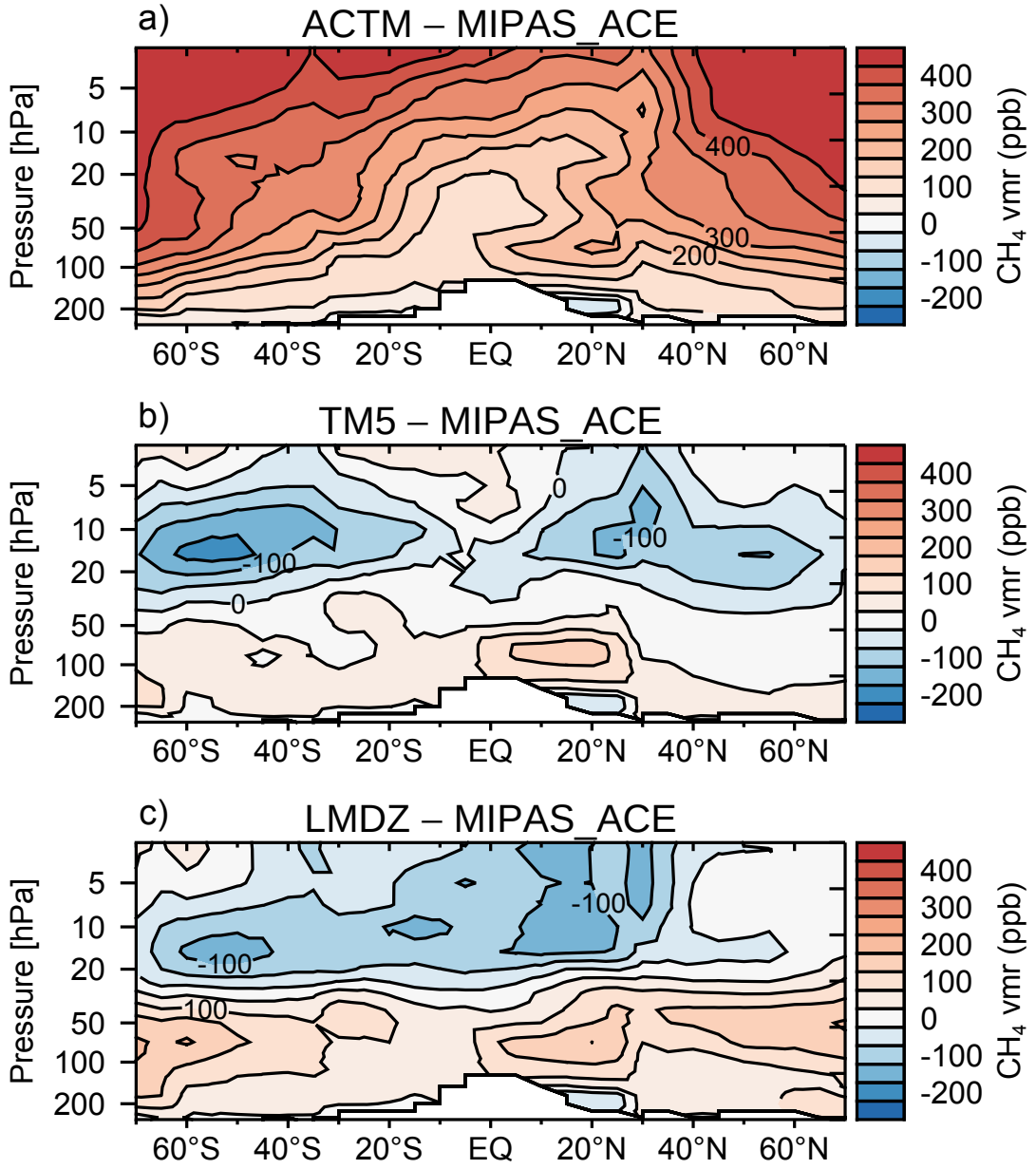

Figure 2.8: Model−ACE-FTS differences of stratospheric CH_4 volume mixing ratios (vmr) in parts per billion (ppb). Zonally-averaged CH_4 vmr differences are annual means for the year 2010.

model correction. Figure 2.7b indicates that TM5 modeled CH_4 mixing ratios appear to be too small (by up to 150 ppb) compared to MIPAS data. This negative TM5 CH_4 bias is partially alleviated or even changed into a small positive CH_4 bias of $\sim$ 50 ppb within the lower stratosphere when using MIPAS_ACE as reference (see Fig. 2.8b). This explains why the model correction with two differing satellite CH_4 data sets has an ambiguous impact on the XCH_4 model−TCCON agreement for TM5. For LMDz the situation is similar to TM5, i.e. negative model CH_4 biases can disappear or even

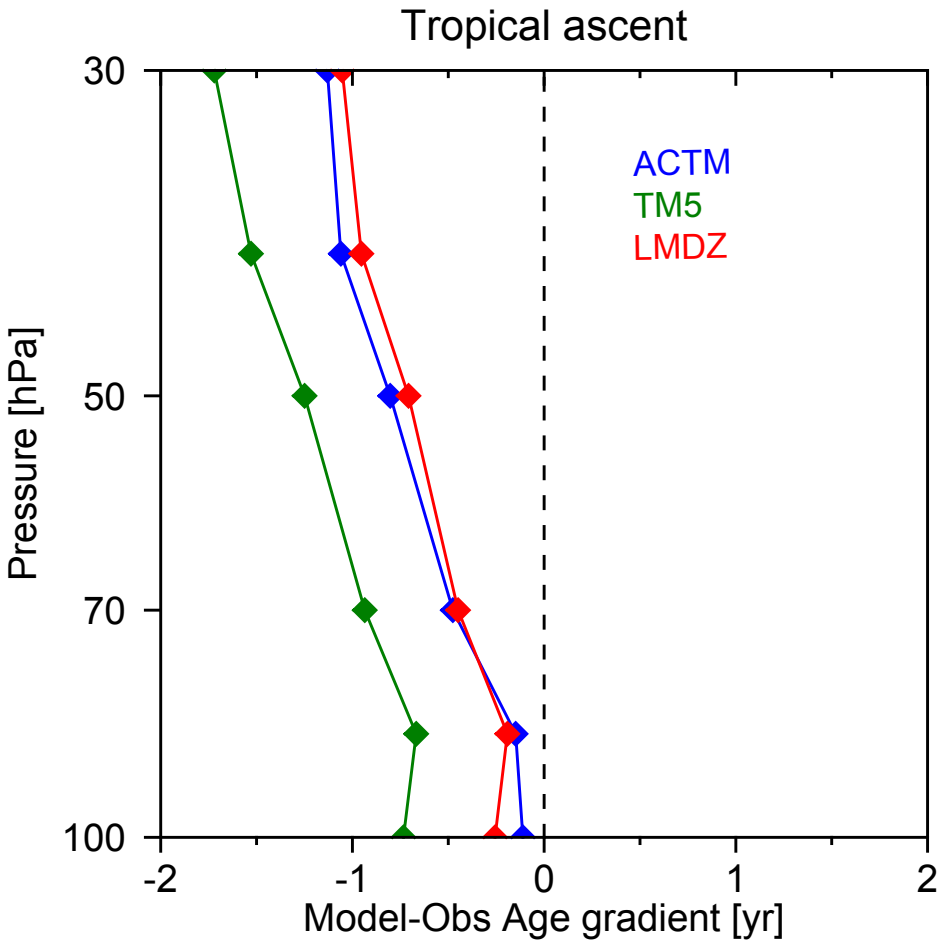

Figure 2.9: Model−MIPAS differences of the mean age gradient as a transport diagnostics for tropical ascent. The mean age gradient was calculated as difference between the lower stratospheric mean ages averaged over 35°N–50°N and 10°S–10°N. Mean age data in years (yr) are calculated as annual means on the MIPAS pressure-latitude grid.

change into positive values when using MIPAS_ACE data as reference instead of MIPAS data. This effect again is most noticeable for lower stratospheric CH_4 mixing ratios that are shifted into the positive direction with values up to 150 ppb. The findings for TM5 and LMDz imply that these models, in contrast to ACTM, represent stratospheric CH_4 within the range established by the observational data sets MIPAS and MIPAS_ACE. Consequently, this satellite data range limits a more accurate evaluation of modeled stratospheric CH_4 fields and the corresponding XCH_4 data.

The analysis of the model and satellite stratospheric CH_4 fields leads to the major finding that the inter-model spread in XCH_4 data mainly is caused by an inter-model spread

in stratospheric CH_4 fields. Most prominent is the problem of ACTM simulations producing significantly higher stratospheric CH_4 mixing ratios compared to those simulated by TM5 or LMDz. The inter-model spread in stratospheric CH_4 very likely originates from model-to-model differences in the simulation of transport and chemical CH_4 loss. Indeed, the CTMs used in the third study differ in several aspects that are known to cause model errors (Locatelli et al., 2015): vertical/horizontal resolution, meteorological fields used to nudge horizontal winds, sub-grid-scale physical parameterizations, advection schemes, numerical methods, etc. Furthermore, the models also differ in the chemical fields being relevant for stratospheric CH_4 loss. However, Patra et al. (2011) also have identified a significant inter-model spread in stratospheric CH_4 despite applying uniform fields of OH, Cl, and O^1D for all models of the TransCom-CH_4 experiment. They, therefore, suggested a predominant role of transport in the simulation of CH_4 vertical distributions. For this reason, the models of the third study were tested for their simulation of stratospheric transport by applying transport diagnostics introduced by Strahan et al. (2011). One model transport diagnostic examines model-to-model differences in the simulation of the tropical ascent rate, which is assessed by the horizontal mean age gradient between mid-latitude (35°N−50°N) and tropical (10°S−10°N) lower stratosphere (30−100 hPa). Using MIPAS mean age data as reference, Fig. 2.9 clearly shows very similar mean age gradients for ACTM and LMDz that are shifted by $\sim$ 0.5 years from the TM5-modeled mean age gradient. This means that the tropical ascent rate is stronger in TM5 simulations compared to ACTM, and LMDz simulations, respectively.

Another transport diagnostics analyzes CH_4 mixing ratios of the tropical lower stratosphere indicating the strength of (cumulative) horizontal mixing. Using MIPAS CH_4 as reference, Figure 2.10 reveals model-to-model differences in simulation of horizontal mixing: the ACTM−MIPAS differences are offset by up to $\sim$ 50 ppb from the model−MIPAS differences for TM5 and LMDz being almost identical to each other. This suggests that horizontal mixing is weaker for ACTM simulations compared to TM5, and LMDz simulations, respectively.

Finally, the results of the third study confirm that the XCH_4 model−observation agreement significantly depends on the model representation of stratospheric CH_4. Inter-model differences in XCH_4 data are a consequence of an inter-model spread in stratospheric CH_4 fields, which in turn very likely originates from model-to-model differences

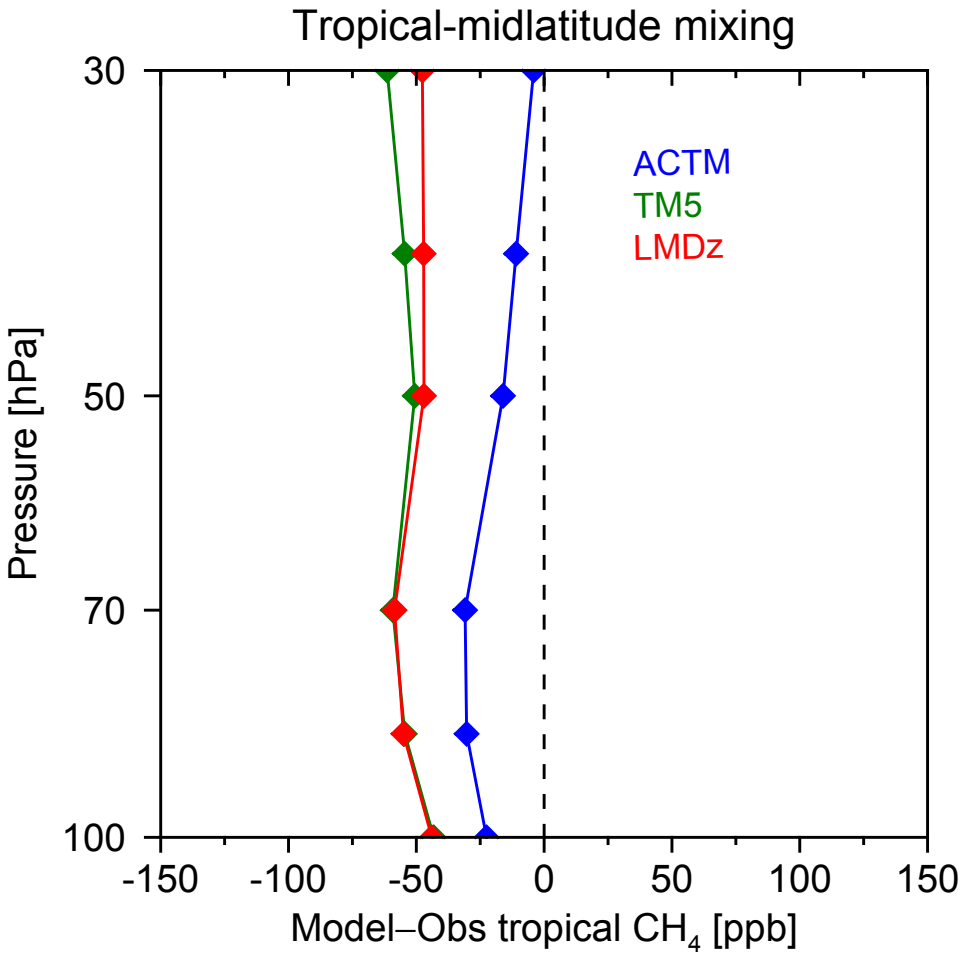

Figure 2.10: Model−MIPAS differences of tropical CH_4 mixing ratios as a transport diagnostics for horizontal mixing. The CH_4 differences are calculated as annual means on the MIPAS pressure-latitude grid.

in the simulation of stratospheric transport. In order to better understand the impact of individual model transport components on the simulation of stratospheric CH_4, a refined model intercomparison with more process-oriented model tests would be needed. I.e., different input parameters (e.g., physical parameterizations, advection schemes, reanalysis data) could be used to provide an ensemble of stratospheric CH_4 distributions for each CTM. In a second step, the stratospheric CH_4 fields of such model-ensembles should be evaluated with an accurate observational data set of stratospheric CH_4. However, an extensive in situ data set of stratospheric CH_4 is not available in the medium term and the existing satellite data, as used in the third study, show significant differences within the lower stratosphere. Hence, a better assessment of the satellite data quality is desirable for an accurate model evaluation. In this context, it is important

to note that the results of a recent inter-satellite comparison by Plieninger et al. (2016) indicate a high bias for MIPAS-retrieved lower stratospheric CH_4. This implies that ACE-FTS data seems to be more reliable than MIPAS data and, thus, preferable for an evaluation of model stratospheric CH_4 fields as done in the third study. Consequently, the model correction with MIPAS data adjusted to ACE-FTS observations may produce more reasonable results in the third study.

2.4 Synthesis of the three articles

The analysis of the first article reveals a very good overall agreement between NDACC and TCCON observations of XCH_4. This finding suggests that NDACC XCH_4 retrievals are able to meet the accuracy standards of TCCON observations on a overall point of view. However, the first study also shows that the seasonal NDACC−TCCON agreement in XCH_4 is not perfect and depends on the a priori profile of CH_4 concentrations that is used by the retrievals. I.e., a better seasonal agreement between NDACC and TCCON XCH_4 requires that both retrievals apply a common prior instead of their specific standard retrieval a priori profile. The success of this approach depends on how realistically the common prior reflects the atmospheric CH_4 concentrations at the time and location of measurement. If the common prior fails to reproduce the vertical distribution of CH_4 concentrations, then the NDACC and TCCON retrievals can be affected by smoothing effects. Moreover, such smoothing effects are different for NDACC and TCCON observations because of differing retrieval vertical sensitivity.

This diagnosis is verified by the results of the second article, where situations with dynamically induced variability are identified as driver for significant differences between NDACC and TCCON observations of XCH_4. The second study shows that TCCON observations at high latitudes can be affected by significant smoothing effects if the retrieval a priori profile does not account for stratospheric subsidence within the polar vortex. In contrast, NDACC retrievals are more affected by smoothing effects arising from STE processes like deep stratospheric intrusions. As STE processes can occur throughout the year at all latitudes, they have an impact on the XCH_4 seasonal cycle retrieved by NDACC observations. In addition to STE events, stratospheric subsidence has an impact on the accuracy of FTIR observations at high altitudes within the early spring period. The findings of the second study suggest, that the accuracy of the seasonal

XCH_4 variations retrieved from NDACC and TCCON observations can be improved, if retrieval a priori profiles of CH_4 concentrations realistically reflect short-term variability of atmosphere dynamical processes in the UTLS region.

As confirmed in the second study, a lot of atmospheric variability originates from the stratospheric contribution and (in part) reduces the accuracy of FTIR total column retrievals. The second article only examined the impact of dynamical events with exceeding atmospheric variability, but did not attend to the overall distribution of stratospheric CH_4. For this reason, the third study investigated the sensitivity of XCH_4 to stratospheric CH_4 distributions using simulated and satellite-retrieved CH_4 fields. The third study clearly showed that there is a remarkable diversity in both model and satellite stratospheric CH_4 fields, i.e. there is a inter-model spread in stratospheric CH_4 and a large satellite data range. This range of stratospheric CH_4 fields translates into different XCH_4 data involving different latitudinal biases with regard to TCCON observations. The findings of the third study suggest that the inter-model spread in stratospheric CH_4 is driven by model-to-model differences in the simulation of stratospheric transport. At the same time, the findings of recent inter-satellite comparison by Plieninger et al. (2016) suggest a high bias in MIPAS lower stratospheric CH_4. These conclusions require more verification in order to understand and to reduce the inconsistencies in model simulations and satellite observations of stratospheric CH_4.

Finally, this dissertation shows that atmospheric dynamics in the UTLS region as well as the overall distribution of stratospheric CH_4 produce a significant imprint on XCH_4. This imprint can be very strong on short-term scales when regional events like stratospheric subsidence or STE processes induce high dynamical variability, thereby disturbing the vertical distribution of CH_4 concentrations. At the same time, the stratospheric contribution creates a significant imprint on the global XCH_4 distribution in the long term. In summary, the findings of the three articles imply that the accuracy of XCH_4 observations and model simulations very much depends on how well atmosphere dynamical variability can be observed and simulated. The results of this thesis demonstrate that both sides – observations and simulations – can improve on this, in order to enhance the benefit of XCH_4 data for assessing CH_4 emissions.

Chapter 3

Conclusions and outlook

The assessment of global to regional CH_4 budgets is a major objective of climate research and provides a wide-ranging field of activity for scientists. One approach to estimate CH_4 emissions uses process-based models in combination with emission inventories, but does not care about real atmospheric CH_4 concentrations. Nisbet and Weiss (2010) state that in the context of designing emission regulations this shortcoming of bottom-up estimates is equivalent to the situation of "dieting without weighing oneself". For this reason, observations of atmospheric CH_4 concentrations are needed to complement the bottom-up approach with top-down estimates of CH_4 emissions. However, inferring emission fluxes from atmospheric concentrations is complicated, because CH_4 emissions only produce a small relative change with respect to the atmospheric CH_4 background concentrations. In particular for the quantity XCH_4, seasonal deviations from the background level (1780 ppb) are typically smaller than 1 % and a growth rate of 6 ppb yr^{-1} only corresponds to ~ 0.3 % of the background signal. Consequently, the benefit of XCH_4 observations for top-down estimates depends on the precision and accuracy of these measurements, but also on how accurate atmospheric tansport and chemistry can be simulated.

In this context, this dissertation thesis highlights the role of atmospheric dynamics in understanding XCH_4 observations and simulations. The first article (Sussmann et al., 2013) and the second one (Ostler et al., 2014) confirm that the overall accuracy of ground-based XCH_4 observations from NDACC and TCCON is reasonable. Since NDACC as well as TCCON retrievals are indirect measurements, the accuracy of these observations

is connected to the respective vertical sensitivity, which is not ideal for both retrieval methods. Limited retrieval vertical sensitivity combined with extreme variability in the vertical distribution of CH_4 concentrations confines the accuracy of current XCH_4 retrievals. This diagnosis is trivial and not novel, but the impact of dynamical events like stratospheric subsidence or stratosphere-troposphere exchange on the accuracy of XCH_4 observations has been investigated in the second article for the first time. The findings in Ostler et al. (2014) demonstrate that realistic a priori knowledge of the vertical distribution of CH_4 concentrations is essential for a high level of accuracy in XCH_4 observations, especially if the atmosphere is disturbed by dynamical events. Seasonal differences between NDACC and TCCON XCH_4 data were found and attributed, in part, to dynamical variability.

Seasonal variations in XCH_4 are a result of a complex interplay between emissions, atmospheric transport and chemistry (OH sink). The results of the third article confirm the findings from earlier studies (e.g., Washenfelder et al., 2003) that the stratospheric contribution is an important controlling factor for the integrated quantity XCH_4. The disagreement between model representations of stratospheric CH_4 reflects current deficiencies in the modeling of stratospheric transport and chemistry, which are hindering the potential of XCH_4 observations to be fully exploited for the inverse modeling of regional CH_4 emissions. Therefore, a conclusion of the third study is that the modeling of stratospheric CH_4 requires improvements, i.e. the impact of model-to-model differences in the simulation of stratospheric transport and chemistry needs to be investigated in detail. At the same time, the third study reveals that stratospheric satellite data require a better quality assessment in order to be used for a robust evaluation of CTMs. Validation of satellite data is a steady process requiring more in situ observations of stratospheric CH_4 as reference. Beyond that, the finding of the third study, that the ACTM simulations of stratospheric CH_4 are largely biased, has implications for the first and the second article using ACTM-modeled CH_4 profiles as common prior for NDACC and TCCON retrievals: it is likely that a certain part of the different smoothing effects for NDACC and TCCON retrievals are driven by the high-biased ACTM stratospheric CH_4 distributions. Therefore, it can be concluded that the remaining seasonal bias between NDACC and TCCON XCH_4 data may be reduced by using a common prior with more accurate stratospheric CH_4 distributions than provided by ACTM.

Overall, this thesis has contributed to a better knowledge of the atmospheric quantity XCH_4, but room for improvement on either the observation or the simulation side is still left. The quality of ground-based FTIR retrievals from NDACC and TCCON has been continuously improved from the network starting time until now. This process of development is going to be sustained in the future with improvements in spectroscopy, line shape parameterizations and a priori information about the atmospheric composition. A new, refined spectroscopy, for example, is in preparation and will be applied in the near future. However, using this new spectroscopy for NDACC retrievals requires that the current retrieval strategy, which was optimized with the old spectroscopy (see Sussmann et al., 2011), has to be carefully tested again in order to avoid H_2O interference errors. Furthermore, there are ongoing efforts in developing an improved CH_4 profile retrieval strategy for NDACC as well as TCCON retrievals. Such a profile retrieval strategy should ideally mitigate problems with stratospheric variability.

Raising the level of accuracy for ground-based XCH_4 observations also requires extended validation with balloon- and air-borne in situ measurements in addition to the small number of validation campaigns performed yet within TCCON. Although the first study (Sussmann et al., 2013) and the second one (Ostler et al., 2014) provide a seasonal validation of NDACC XCH_4 retrievals against TCCON observations, they do not achieve a long-term validation of ground-based XCH_4 observations against WMO standards of in situ measurements. In this context, it is highly desirable to obtain an in situ validation data set including a full seasonal cycle and also covering the stratospheric layer. For the future, aircore observations can act as a cost-efficient possibility to perform in situ measurements covering the stratosphere more regularly. Aircore observation use a long tube with one open end to collect ambient air while descending through the atmosphere (Karion et al., 2010). After arriving at the ground, the aircore is sealed upon recovery until it is analyzed for trace gas concentrations according to WMO in situ trace gas measurement scales. Using a balloon-borne platform, the aircore observation can reach high altitudes ($\sim$ 30 km). In particular for TCCON data, such a long-term validation with aircore in situ measurements will strengthen the reliability of the retrieval accuracy once more.

Although we have shown that NDACC XCH_4 retrievals have the potential to reach the accuracy level of TCCON XCH_4 observations, there is little application of NDACC XCH_4 data by the scientific community compared to TCCON. Given our experience

in working with both NDACC and TCCON data, this shortcoming mainly is due to practical issues like data processing. I.e., TCCON XCH_4 data are easily applicable and ensure high accuracy because of strict regulation in retrieval strategy and data processing. In contrast, there is no strict regulation for NDACC XCH_4 retrievals: the retrieval strategy is recommended, but not definite and XCH_4 is not available as retrieval output (the NDACC end product is the retrieved CH_4 total column). This also means that the NDACC data user has to convert the retrieved CH_4 total column into XCH_4 by oneself. Such a conversion is based on the calculation of the dry pressure column which in turn requires pressure and water vapor profiles. This extra work maybe prevents scientist to use NDACC data. Therefore, it can be expected that providing XCH_4 as one end product amongst others with a fixed retrieval strategy and common quality control could help to make NDACC XCH_4 data more attractive to climate scientists. At the same time NDACC retrievals should not loose their experimental character, whereas TCCON retrievals could benefit from a more experimental, site-specific mode of operation alongside the common validated retrieval strategy.

Improving the quality of XCH_4 observations and simulations is beneficial for top-down estimates, but is not the unique solution to current shortcomings in the assessment of the CH_4 budget. As proposed by Kirschke et al. (2013), the partitioning of CH_4 emissions by region and process is not possible with the use of XCH_4 data alone, but needs a synergistic combination of surface in situ observations and satellite-derived total column retrievals. However, there is also the possibility to acquire knowledge about sectoral emission contingents from simultaneous observations of XCH_4 and other atmospheric trace gas total columns like ethane (C_2H_6). Under the assumption that the predominant part of atmospheric C_2H_6 originates from fugitive emissions of the fossil fuel sector, the ratio of XC_2H_6 and XCH_4 observations could be used as constraint on inventory-based estimates of fugitive emissions from natural gas production and use. Such an approach refers to the study of Wennberg et al. (2012), which was based on an analysis of aircraft in situ measurements of C_2H_6 and CH_4. Simpson et al. (2012) already showed that the prominent CH_4 stagnation period from 1999 to 2006 is accompanied by a decline in C_2H_6 concentrations. Furthermore, Franco et al. (2015) recently found out that the atmospheric burden of C_2H_6 has increased since 2009. Another recent study by Hausmann et al. (2016) analyzed the relationship between NDACC-type retrievals of XCH_4 and XC_2H_6 for two sites representing northern and southern hemisphere. For the

time period of renewed CH_4 increase (2007−2014), they found a significant correlation between the northern-hemispheric time series of XCH_4 and XC_2H_6. By using a two-box model (representative for two hemispheres) in combination with the observation-based ethane-to-methane ratios, Hausmann et al. (2016) were able to optimize both CH_4 and C_2H_6 emissions. Their results suggested that the oil and natural gas emission contribution to the renewed methane increase ranges between 18% and 73% with a most plausible contribution being at least 39%. Finally, these correlations between spatiotemporal distributions of atmospheric CH_4 and C_2H_6 concentrations suggest that fugitive emissions are an important driver for the long-term trend in atmospheric CH_4 levels. This implies that, in the near future with increasing exploitation of natural gas in the norther hemisphere, fugitive CH_4 emissions are not expected to be reduced.

In addition to the scientific interest in CH_4 emission fluxes, there are many open questions on the role of CH_4 in atmospheric chemistry. At the moment, it is not clear if the increase in atmospheric CH_4 concentrations has already caused a reduction in global OH concentrations and an increase in stratospheric H_2O concentrations. Another contemporary issue is the question to what extent the renewed increase in atmospheric CH_4 levels has contributed to the recent NH increase in hydrogen chloride (HCl). Stratospheric HCl as the main stratospheric chlorine reservoir is able to release the depletion of stratospheric O_3. Though the role of stratospheric CH_4 as precursor of stratospheric HCl is well-known, Mahieu et al. (2014) have not investigated the impact of increasing CH_4 levels, but have attributed the renewed HCl increase to changes in the stratospheric circulation. Finally, this shows that atmospheric CH_4 concerns various areas of climate research with a lot of remaining challenges for scientists – there is still a lot to be done.

Appendix A:

Publications comprising this dissertation thesis

A.1 Article I

Ralf Sussmann, Andreas Ostler, Frank Forster, Markus Rettinger, Nicholas M. Deutscher, David W. T. Griffith, James W. Hannigan, Nicholas Jones, and Prabir K. Patra: First intercalibration of column-averaged methane from the Total Carbon Column Observing Network and the Network for the Detection of Atmospheric Composition Change, Atmos. Meas. Tech., 6, 397-418, doi:10.5194/amt-6-397-2013, 2013.

Atmos. Meas. Tech., 6, 397–418, 2013
www.atmos-meas-tech.net/6/397/2013/
doi:10.5194/amt-6-397-2013

Atmospheric Measurement Techniques
Open Access

First intercalibration of column-averaged methane from the Total Carbon Column Observing Network and the Network for the Detection of Atmospheric Composition Change

R. Sussmann[1], A. Ostler[1], F. Forster[1], M. Rettinger[1], N. M. Deutscher[2,3], D. W. T. Griffith[2], J. W. Hannigan[4], N. Jones[2], and P. K. Patra[5]

[1]Karlsruhe Institute of Technology, IMK-IFU, Garmisch-Partenkirchen, Germany
[2]School of Chemistry, University of Wollongong, Wollongong, New South Wales, Australia
[3]Institute of Environmental Physics, University of Bremen, Bremen, Germany
[4]Atmospheric Chemistry Division, National Center for Atmospheric Research, Boulder, Colorado, USA
[5]Research Institute for Global Change, JAMSTEC, Yokohama, 236-0001, Japan

Correspondence to: R. Sussmann (ralf.sussmann@kit.edu)

Received: 15 January 2012 – Published in Atmos. Meas. Tech. Discuss.: 13 February 2012
Revised: 29 January 2013 – Accepted: 31 January 2013 – Published: 20 February 2013

Abstract. We present the first intercalibration of dry-air column-averaged mole fractions of methane (XCH_4) retrieved from solar Fourier transform infrared (FTIR) measurements of the Network for the Detection of Atmospheric Composition Change (NDACC) in the mid-infrared (MIR) versus near-infrared (NIR) soundings from the Total Carbon Column Observing Network (TCCON). The study uses multi-annual quasi-coincident MIR and NIR measurements from the stations Garmisch, Germany (47.48° N, 11.06° E, 743 m a.s.l.), and Wollongong, Australia (34.41° S, 150.88° E, 30 m a.s.l.).

Direct comparison of the retrieved MIR and NIR XCH_4 time series for Garmisch shows a quasi-periodic seasonal bias leading to a standard deviation (stdv) of the difference time series (NIR–MIR) of 7.2 ppb. After reducing time-dependent a priori impact by using realistic site- and time-dependent ACTM-simulated profiles as a common prior, the seasonal bias is reduced (stdv = 5.2 ppb). A linear fit to the MIR/NIR scatter plot of monthly means based on same-day coincidences does not show a y-intercept that is statistically different from zero, and the MIR/NIR intercalibration factor is found to be close to ideal within 2-σ uncertainty, i.e. 0.9996(8). The difference time series (NIR–MIR) do not show a significant trend. The same basic findings hold for Wollongong. In particular an overall MIR/NIR intercalibration factor close to the ideal 1 is found within 2-σ uncertainty. At Wollongong the seasonal cycle of methane is less pronounced and corresponding smoothing errors are not as significant, enabling standard MIR and NIR retrievals to be used directly, without correction to a common a priori.

Our results suggest that it is possible to set up a harmonized NDACC and TCCON XCH_4 data set which can be exploited for joint trend studies, satellite validation, or the inverse modeling of sources and sinks.

1 Introduction

Atmospheric methane has become one of the so-called Kyoto gases since it causes a considerable contribution ($0.48\,W\,m^{-2}$) to the total anthropogenic radiative forcing of $2.43\,W\,m^{-2}$ (Forster et al., 2007). In addition, CH_4 has an indirect greenhouse effect of $0.13\,W\,m^{-2}$ by forming tropospheric ozone, stratospheric water vapor, and other infrared-active trace gases (Lelieveld et al., 1998). The main methane sources are natural wetlands, biomass burning and anthropogenic activities like livestock breeding, rice cultivation, or usage of fossil fuels. Global emissions are about 515 Tg per year (Patra et al., 2011), of which 60–70 % are anthropogenic (Denman et al., 2007). The major sink of methane is the destruction by hydroxyl radicals (OH), which contributes to about 90 % of the methane loss in the atmosphere. Other

sinks are the uptake of methane by soils or the reaction with chlorine radicals (Denman et al., 2007).

Since the beginning of industrialization, methane concentrations in the atmosphere have more than doubled (e.g., Etheridge et al., 1998). However, there was a period of near-zero growth at the beginning of this century (Dlugokencky et al., 2003; Bousquet et al., 2006), and after 2006 the atmospheric methane concentration started to increase again (Rigby et al., 2008; Dlugokencky et al., 2009). The increase for the years 2007–2008 has been quantified, and possible causes discussed (e.g. Bousquet et al., 2011; Frankenberg et al., 2011). More recently, it has been shown via ground-based FTIR (Fourier transform infrared) methane column measurements that the renewed increase after 2006 has been ongoing for about ≈ 5 yr until the present (end of 2011) with a rate of $\approx 5\,\mathrm{ppb\,yr^{-1}}$ above northern mid-latitudes (Sussmann et al., 2012).

Ground-based column measurements of methane are complementary to in situ measurements in many respects; e.g. column measurements are representative of a larger geographical region (e.g. Keppel-Aleks et al., 2011), while in situ measurements can represent a specific location or biome. Measured methane columns are impacted by the varying stratospheric contribution, while the interpretation of surface measurements to infer sources and sinks can be impacted by so-called rectifier effects resulting from errors in the transport modeling. Rectifier effects can be avoided if column measurements are used, because these are insensitive to vertical mixing (Gloor et al., 2000). In situ measurements are directly traceable to calibration standards, while ground-based column measurements can be traced back to such standards via aircraft calibration campaigns. Column measurements are preferred for satellite validation since they provide the same quantity as satellites measure.

There are two established global networks performing ground-based remote sensing measurements of column-integrated methane. Within the Network for the Detection of Atmospheric Composition Change (NDACC , http://www.ndacc.org) solar FTIR measurements in the mid-infrared (MIR) have been performed for about two decades (currently 22 stations). Retrievals of methane from NDACC-MIR spectra have been used for trend studies (Angelbratt et al., 2011; Sussmann et al., 2012) and satellite validation (e.g. Sussmann et al., 2005). Since 2004 the NDACC has been complemented by the Total Carbon Column Observing Network (TCCON, http://www.tccon.caltech.edu/), which is dedicated to high-precision retrievals of climate gases (e.g. CO_2, CH_4, N_2O) from solar absorption spectra in the near-infrared (NIR) spectral region (Wunch et al., 2011a). TCCON has been used for the validation of models (Houweling et al., 2010) and satellite measurements of methane (e.g. Morino et al., 2011; Schneising et al., 2012), but also for deriving information on sources and sinks of greenhouse gases (e.g. Wunch et al., 2009; Chevallier et al., 2011; Keppel-Aleks et al., 2012). The TCCON measurements are calibrated against the World Meteorological Organization (WMO) in situ trace gas measurement scales, using profiles obtained by aircraft in situ measurements flown over TCCON sites (Washenfelder et al., 2006; Deutscher et al., 2010; Wunch et al., 2010; Messerschmidt et al., 2011; Geibel et al., 2012). Currently, there are 18 operational TCCON stations, most of which have been established during the last couple of years.

If a sufficiently precise and accurate relationship can be established between the NDACC and TCCON column-averaged dry-air mole fractions of methane, then data from the two networks could be combined to provide wider spatial and temporal coverage than either network individually. This is not only an advantage for satellite validation but also provides the opportunity for trend analysis dating back 15 yr before TCCON operations began. It is, therefore, the goal of this study to establish the NDACC–TCCON intercalibration for XCH_4. An important question in this context is whether or not one overall intercalibration factor for all stations can be found and quantified, or whether a site- and time-dependent intercalibration parameterization, with a significant linear and/or seasonal component, is necessary.

Our paper is structured as follows: After introducing the participating FTIR sites and their measurement settings in Sect. 2 along with the MIR and NIR retrieval strategies, we describe our intercomparison method (Sect. 3). The results are shown in Sect. 4. Section 5 gives a summary and Sect. 6 the conclusions with recommendations on the joint use of the MIR and NIR data along with an outlook.

2 Ground-based sounding of columnar methane in the MIR and NIR

2.1 Garmisch FTIR soundings

The Garmisch solar FTIR system (47.48° N, 11.06° E, 743 m a.s.l.) is operated by the group "Variability and Trends" at the Institute for Meteorology and Climate Research, Karlsruhe Institute of Technology, Germany. Operation of a Bruker IFS125HR interferometer was initiated in 2004 as part of TCCON, and the system took part in the aircraft calibration campaign of the EU project IMECC (Infrastructure for Measurement of the European Carbon Cycle) (Messerschmidt et al., 2011; Geibel et al., 2012). Column-averaged methane is retrieved from single-scan measurements in the NIR (see Table 1 for the spectral micro windows) recorded with an InGaAs diode using a maximum optical path difference of 45 cm. The FTIR system also performs NDACC-type measurements in the MIR (Table 1) in alternating mode with the NIR measurements. The interferograms for the MIR methane retrievals are recorded with an InSb detector using an optical path difference of typically 175 cm. Six scans are averaged with an integration time of approximately seven minutes. Data obtained with the

Table 1. Strategies for retrieval of column-averaged methane from MIR and NIR solar spectra.

	MIR	NIR
micro windows[a] (interfering species fitted)	2613.70–2615.40 (HDO, CO_2) 2835.50–2835.80 (HDO) 2921.00–2921.60 (HDO, H_2O, NO_2)	5880.00–5996.00 (CO_2, H_2O, HDO) 5996.45–6007.55 (CO_2, H_2O, HDO) 6007.00–6145.00 (CO_2, H_2O, HDO)
line list	HITRAN 2000 including 2001 update release (Rothman et al., 2003)	HITRAN 2008 (Rothman et al., 2009) including update by Frankenberg et al. (2008)
calibration	no	XCH_4 calibration factor from Wunch et al. (2010): TCCON/aircraft (WMO) = 0.978
retrieval constraint	Tikhonov L_1, regularization strength α optimized via L-curve/minimum diurnal variation ($\approx$ 2 dofs[b]); altitude constant on per-cent-vmr[c] scale	scaling of a methane a priori profile
a priori vmr profiles	WACCM[d] (1 fixed profile)	generated from MkIV FTS balloon profiles (1 fixed profile)
background fit	linear slope	linear slope
retrieval quality selection	threshold (0.15 %) for rms-noise/dofs[b]	fractional var. in solar intensity (0.0–5.0 %) XCH_4 ($0.0–2.0 \times 10^{-6}$) XCH_4 error ($0.0–1.0 \times 10^{-7}$) SZA[e] (0.0–82°)
calculation of column-averaged dry-air mole fractions	use 4-times-daily-NCEP[f] PTU profiles for calculating the air column and water vapor column	use simultaneously measured O_2 column
precision (1-σ diurnal variation)	< 0.3 %	< 0.3 %
seasonal bias (H_2O/HDO-CH_4 interference error[g])	< 0.14 %	hitherto undetermined
references	Sussmann et al. (2011)	Wunch et al. (2011a)

[a] units are cm^{-1}; [b] dofs – degrees of freedom for signal; [c] vmr – volume mixing ratio; [d] WACCM – Whole Atmosphere Chemistry Climate Model; [e] SZA – solar zenith angle; [f] NCEP – National Center for Environmental Prediction; [g] see Sussmann and Borsdorff (2007) for a definition.

Garmisch FTIR have been used for satellite validation (de Laat et al., 2010; Morino et al., 2011; Wunch et al., 2011b), carbon cycle research (Chevallier et al., 2011), and studies of atmospheric variability and trends (e.g., Borsdorff and Sussmann, 2009; Sussmann et al., 2011). The intercalibration uses the Garmisch time series of July 2007–December 2011 which comprises 3403 MIR spectra and 35 171 NIR spectra.

2.2 Wollongong FTIR soundings

The Wollongong solar FTIR system (34.41° S, 150.88° E, 30 m a.s.l.) was set up in 1995 as part of the NDACC network. It is operated by the Center for Atmospheric Chemistry at the University of Wollongong, Australia. From 1995 to 2007 a Bomem DA8 FTIR system was operated (Griffith et al., 1998). It was replaced in 2007 with a Bruker IFS 125HR instrument set up for measurements in both the MIR and the NIR spectral ranges (Jones et al., 2013; Wunch et al., 2011a). For this study only the Bruker data were used. Spectra in the MIR range are recorded with an InSb detector, using an optical path difference of 257 cm and averaging two successive scans with an integration time of approximately four minutes. The settings for the NIR measurements are identical to those at Garmisch. The intercalibration uses the Wollongong time series of June 2008–December 2011 which comprises 1405 MIR spectra and 15 787 NIR spectra.

2.3 MIR and NIR retrieval strategies

The codes SFIT (MIR) and GFIT (NIR) have common roots as to the ray tracing and forward model; however, the inverse models are different.

For the retrieval of XCH_4 from NDACC-type MIR measurements the retrieval strategy MIR-GBM v1.1 (Sussmann et al., 2011) is used in this study along with the spectral-fitting software SFIT2 ver. 3.94 (Pougatchev et al., 1995). The basic features of MIR-GBM v1.1 are given in Table 1. SFIT is set up for a full profile retrieval via the use of a climatological covariance ("optimal estimation") or an inverse covariance, i.e. an ad hoc regularization matrix. The a priori volume mixing ratio (vmr) profiles used for SFIT, i.e. one fixed profile per site have, been derived from the Whole Atmosphere Chemistry Climate Model (WACCM; Garcia et al., 2007); see Fig. 1 and Appendix B for details. For SFIT methane retrievals we found a Tikhonov-L1 regularization scheme to be favorable, with the regularization applied to an a priori profile given in relative units (per cent scale) and with an altitude-constant regularization strength (Sussmann et al., 2011). This is what we call the MIR-GBM v.1.1 retrieval strategy, and it includes the use of 4-times daily NCEP pressure/temperature/humidity profiles to calculate the dry-air column, and 3 MIR spectral micro windows along with HITRAN 2000. The MIR retrievals are used as retrieved, i.e. they are not calibrated, e.g. to WMO/GAW trace gas measurement scales.

TCCON-type NIR measurements are analyzed with the spectral fitting software GFIT ver. 4.4.10 (release ggg_20091107) referred to as "GFIT" hereafter. The basic features of GFIT are given in Table 1, while more details can be found in Wunch et al. (2011a). GFIT uses an a priori profile derived from mid-latitude FTIR balloon measurements (Fig. 1a). Note there has been a recent GFIT update, i.e. ver. 4.8.6 (release ggg_2012_July_Update) using site- and time-dependent a priori profiles (see Fig. 1b and "Note: impact of GFIT 2012 update"). Column-averaged dry-air mole fractions are retrieved by scaling an a priori profile to provide the best fit to the measured spectra and, finally, by dividing these columns by the dry-air column. The dry-air column is directly derived from the simultaneously retrieved O_2 column. GFIT uses a broad spectral window including full bands in

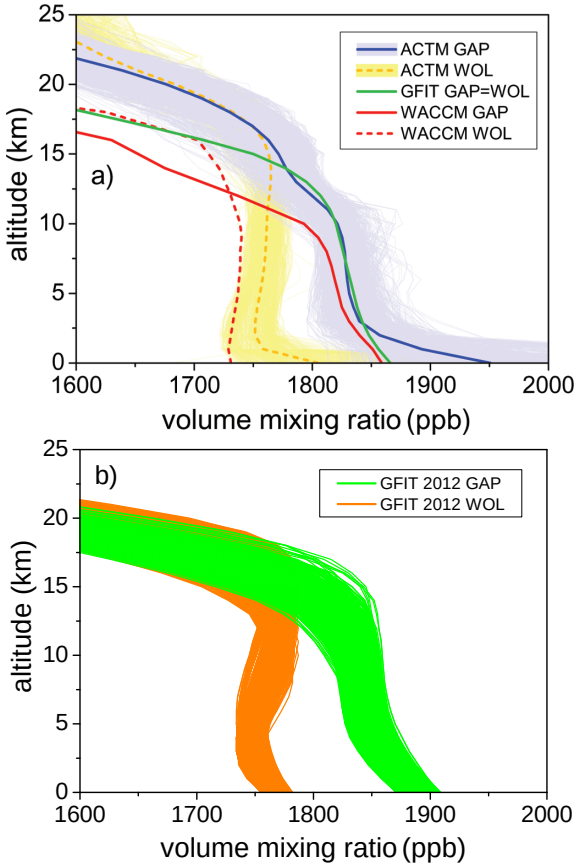

Fig. 1. A priori profiles used in this work. **(a)** GFIT is the standard a priori profile of the NIR retrievals using GFIT ver. 4.4.10 (release ggg_20091107, one fixed profile for all stations) and WACCM for the MIR retrievals (one per station). The ACTM model profiles (3-hourly model) are suggested as a common prior. **(b)** A priori profiles used in the recent GFIT 2012 update, i.e. ver. 4.8.6 (release ggg_2012_July_Update). See "Note" for an investigation of the impact of this GFIT update.

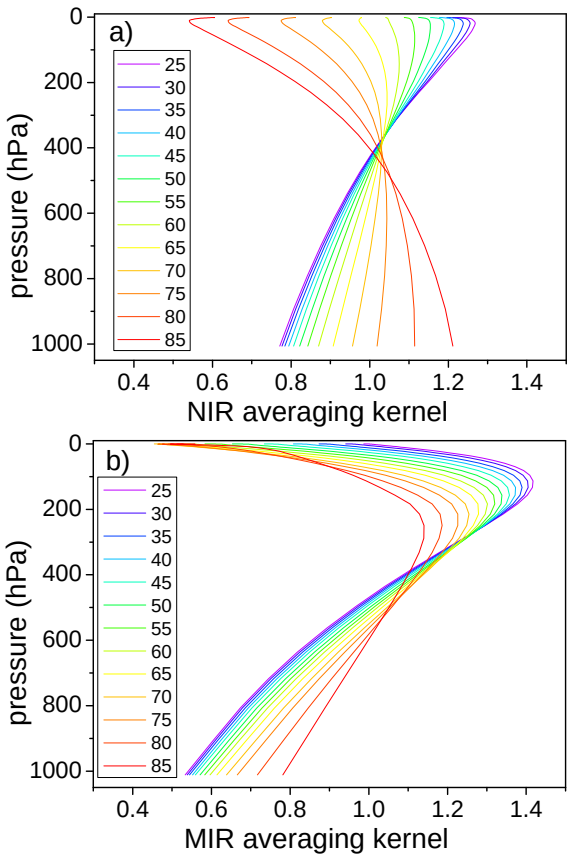

Fig. 2. Averaging kernels **(a)** for the NIR retrievals and **(b)** the MIR retrievals. Solar zenith angles (in deg) are color coded.

the NIR. The GFIT XCH_4 results are scaled by a calibration factor of 0.978 that has been obtained from coincident measurements with aircraft equipped with WMO-scale in situ instrumentation, and this bias is attributed to spectroscopy uncertainties (Wunch et al., 2010). Note that a recent European aircraft campaign provided another calibration factor for XCH_4; see Geibel et al. (2012) for details. We use the Wunch et al. (2010) factor for this paper because it is the official factor used within TCCON for the time being. The averaging kernels for the NIR and MIR retrievals are given in Fig. 2.

3 Intercomparison method

Any direct comparison of two different remote sounders is potentially complicated because in general they contain a differing a priori impact, i.e. effects from (i) differing a priori profiles and (ii) differing smoothing effects because of differing averaging kernels influencing the retrieved trace gas column amounts. Therefore, our intercomparison strategy comprises (i) an approach for eliminating the impact from differing a priori profiles (Sect. 3.1) and (ii) a strategy for optimum selection of a common a priori profile model in order to minimize smoothing errors (Sect. 3.2). Finally, we investigate the impact from applying the strategies (i) and (ii) upon the time series (Sect. 3.3).

3.1 Eliminating the impact from differing a priori profiles

According to Rodgers (2000) the impact from differing a priori profiles can be taken into account by an a posteriori adjustment of the soundings for a common a priori profile $\boldsymbol{x}_{\text{common}}$. This approach has been applied recently for the comparison of carbon dioxide and methane columns measured by SCIAMACHY to ground-based FTIR measurements and to model results (Reuter et al., 2011; Schneising et al., 2012). In our case we obtain corrected column-averaged mole fractions c_{cor} for the MIR or NIR soundings which can be directly compared:

$$c_{\mathrm{cor}} = \hat{c} + \frac{1}{p_0} \sum_l (1 - \boldsymbol{a}^l)(\boldsymbol{x}^l_{\mathrm{common}} - \boldsymbol{x}^l_a)\Delta p^l \quad (1)$$

Here c represents the column-averaged mole fraction of methane retrieved from MIR or NIR spectra. For every model layer l the difference between 1 (i.e. the ideal averaging kernel) and the vector component $\boldsymbol{a}^l$ of the total column averaging kernel in this layer is multiplied with the difference between the common a priori mole fraction $\boldsymbol{x}^l_{\mathrm{common}}$ and the FTIR (MIR or NIR) a priori mole fraction $\boldsymbol{x}^l_a$ as well as with the pressure difference between the lower and upper boundaries of layer l; p_0 denotes the surface pressure.

Obviously, this correction can be neglected in cases of the averaging kernel being close to ideal or the a priori profile $\boldsymbol{x}_a$ being close to $\boldsymbol{x}_{\mathrm{common}}$. However, this is not the case in our application since the MIR and NIR a prioris and the MIR and NIR averaging kernels differ; see Figs. 1 and 2, respectively.

Equation (1) has been designed for post-retrieval exchange of an a priori profile. Therefore, in the ideal case, it should yield the same results as performing a retrieval after exchanging the a priori beforehand. However, Eq. (1) uses averaging kernels which are linear approximations of the retrieval which is non-linear in $\boldsymbol{x}$. We show in Appendix A that this non-linearity is small and negligible within the context of this paper. Therefore, we will be able to use in this paper retrievals re-run after exchanging the a priori beforehand, along with retrievals corrected a posteriori via Eq. (1). If the latter are exploited, the reason has been to save computation efforts.

3.2 Strategy for selecting a common a priori

After correction to a common a priori $\boldsymbol{x}_{\mathrm{common}}$, there is still the smoothing term $(1 - \boldsymbol{a}^l)$ $(\boldsymbol{x}^l_{\mathrm{common}} - \boldsymbol{x}^l_{\mathrm{true}})$. This smoothing term varies seasonally because of the zenith angle dependency of the averaging kernels (Fig. 2). Also the magnitude of the smoothing term is different for MIR and NIR because of the differing averaging kernels. Our strategy to minimize this difference is to use time-dependent and site-dependent profiles $\boldsymbol{x}_{\mathrm{common}}(t, \mathrm{lat},\ \mathrm{lon})$ that are as close as possible to $\boldsymbol{x}_{\mathrm{true}}(t, \mathrm{lat},\ \mathrm{lon})$ at a site at the moment of observation.

Therefore, we favor the use of ACTM CH_4 model profiles for each site as common a priori; see Fig. 1 and Appendix B for details. Briefly, ACTM-simulated vertical profiles of dry-air mole fractions on the native model vertical grid and nearest horizontal grid of the FTIR sites are sampled at 3-hourly intervals for use as a priori in this study. We interpolated the model profiles for each measurement time on the model pressure grid and applied this interpolated profile. Another favorable choice (especially for Wollongong) is the use of the MIR retrieval a priori which is a time-constant but site-dependent prior $\boldsymbol{x}_{\mathrm{common}}(\mathrm{lat},\ \mathrm{lon})$ derived from the WACCM model. See also Appendix B for a description of how the WACCM-based prior has been set up.

The benefit of using ACTM will be demonstrated later in quantitative terms; i.e. we will find a smaller seasonal bias between MIR and NIR retrievals using ACTM profiles as $\boldsymbol{x}_{\mathrm{common}}$ compared to two possible other ad hoc choices for $\boldsymbol{x}_{\mathrm{common}}$, namely using the time-constant (MIR or NIR) retrieval a prioris. To show this, the following 4 cases will be investigated in parallel: (i) using the original MIR and NIR aprioris, (ii) using time-dependent ACTM profiles as common prior $\boldsymbol{x}_{\mathrm{common}}$, (iii) using the constant MIR retrieval a priori as $\boldsymbol{x}_{\mathrm{common}}$, and (iv) using the constant NIR retrieval a priori as $\boldsymbol{x}_{\mathrm{common}}$.

3.3 Impact of varied a priori profiles on the time series

For the intercomparisons we use monthly means calculated from individual MIR and NIR measurements recorded on the same days. Only months with > 5 measurements have been included.

An example for the bias and the seasonal variation induced by changing an a priori profile is visualized in Fig. 3. It shows the impact on the Garmisch NIR time series from changing the standard GFIT a priori profile to ACTM profiles (Fig. 3a). An insignificant bias results (-0.27 ± 0.58 ppb) along with a significant change of the seasonal cycle (difference time series with stdv = 2.1 ppb). The analogous plot for Wollongong (Fig. 3b) shows a similar change in seasonality (stdv = 2.8 ppb) along with a larger, significant bias (-5.04 ± 1.07 ppb). The latter may be understood by the larger overall discrepancy between the GFIT a priori profile and the ACTM profiles at Wollongong compared to the Garmisch case; see Fig. 1. Figure C1 shows analogous plots for all the other cases with exchanged prior for Garmisch and Wollongong. Numbers are listed in Table 2. Each exchange causes a bias and a change in seasonality. The impact on seasonality tends to be larger for the cases where the original a priori profile is replaced by time-dependent ACTM profiles compared to the other cases. This is because in the cases where one of the two constant retrieval a priori profiles is used as common prior, the seasonal variation of the correction term is only driven by changes in the averaging kernels as a function of zenith angle. This can be seen from Table 2, e.g. stdv = 1.7 ppb for Garmisch MIR retrieved with GFIT a priori compared to stdv = 4.7 ppb for the retrieval based on ACTM, or stdv = 0.9 ppb for Wollongong NIR retrieved with WACCM a priori compared to stdv = 2.8 ppb for the retrieval based on ACTM.

4 Intercomparison results

4.1 Direct comparison

Figure 4a shows a scatter plot of the NIR and MIR monthly means as retrieved with the original a prioris for Garmisch and Wollongong, respectively. Error bars on data points are 2-σ uncertainties derived from the stdv of the linear slope fit

Table 2. Impact of varied a priori profiles on mean XCH_4 level retrieved in the NIR and MIR, and stdv of differences (retrieval with new a priori – retrieval with original a priori). Numbers are for monthly means constructed from same-day measurement coincidences. Uncertainties are 2 times the standard errors of the mean (2-σ/sqrt(n)).

data set	new a priori	n, number of coincident monthly means	mean difference (retrieved with new a priori – retrieved with original a priori) (ppb)	stdv of differences (retrieved with new a priori – retrieved with original a priori) (ppb)
Garmisch	NIR retrieved with ACTM a priori	51	−0.27 (±0.58)	2.1
	NIR retrieved with WACCM a priori	51	+0.75 (±0.44)	1.6
	MIR retrieved with ACTM a priori	51	−0.55 (±1.3)	4.7
	MIR retrieved with GFIT a priori	51	−3.19 (±0.48)	1.7
Wollongong	NIR corrected to ACTM a priori	27	−5.04 (±1.07)	2.8
	NIR retrieved with WACCM a priori	27	−1.65 (±0.35)	0.9
	MIR corrected to ACTM a priori	27	+1.75 (±1.25)	3.3
	MIR retrieved with GFIT a priori	26	+5.36 (±0.37)	1.0

(2 stdv/$\sqrt{2}$). (Remark: we used this way of obtaining error bars because they reflect both the statistical uncertainty of the individual monthly means originating from the scatter of the retrievals and systematic errors of the monthly means due to errors in the seasonality. We found that the latter (systematic) error contribution is the dominant one: calculating the stdv of the monthly means directly from the retrievals gave significantly smaller numbers; i.e. retrieval scatter is not the dominant source of uncertainty. Furthermore, this (insignificant) uncertainty of the monthly means from the retrieval scatter changes strongly from month to month, because of the varying number of available measurements. Therefore, we did not use the scatter of the retrievals for weighting the individual monthly means during the slope fits.) Uncertainties for the slopes are derived from the fit and are at 2-σ.

The linear MIR/NIR slopes (obtained from linear fits forced through zero) are not significantly different from 1 for both stations, i.e. 0.9998(11) for Garmisch and 0.9987(16) for Wollongong. In other words, there is no evidence from the direct comparison that an intercalibration of the MIR and NIR data sets would be required before using them together. This will be shown and discussed in more detail in the correlation analysis of Sect. 4.3 (along with the other cases where common a prioris are used for the NIR and MIR data).

Figure 5a shows the same MIR and NIR monthly mean data as time series. It can be seen that the MIR and NIR seasonalities differ significantly (stdv = 7.2 ppb for the difference time series shown in the upper trace). An analogous plot for Wollongong can be found in Appendix C (Fig. C2c).

4.2 Comparison with common a priori: analysis of seasonality

Figure 5b show both NIR and MIR time series, but now retrieved using ACTM profiles as common a priori as described in Sect. 3. By comparison to the original time series (Fig. 5a) it can be seen that the exchange of the a priori profiles affects the MIR retrievals in a different way than the NIR retrievals. This is because of the differing original a priori profiles (Fig. 1) and the differing averaging kernels (Fig. 2).

4.2.1 Stdv of NIR–MIR difference time series

The effect of using the common ACTM a priori is that the seasonality of the MIR and NIR XCH_4 time series are in better agreement: the stdv of the difference time series NIR–MIR has been 7.2 ppb for the original time series (Fig. 5a). After using the common ACTM a priori (Fig. 5b) the stdv of the difference time series is reduced to 5.2 ppb. Analogous plots for Wollongong can be found in Appendix C: here, the original stdv of 7.1 ppb (Fig. C2c) is reduced to stdv = 6.6 ppb (Fig. C2d) if ACTM profiles are used. Obviously, the reduction of stdv's by use of the time-dependent ACTM prior is smaller for Wollongong than for Garmisch. This may be understood by the fact that the Southern Hemisphere seasonal cycle (Wollongong) is less pronounced compared to the Northern Hemisphere cycle at Garmisch – and because of this reason the use of the time-constant original prior is a better approximation for Wollongong than for Garmisch. Figure C2 also shows the cases where, rather than

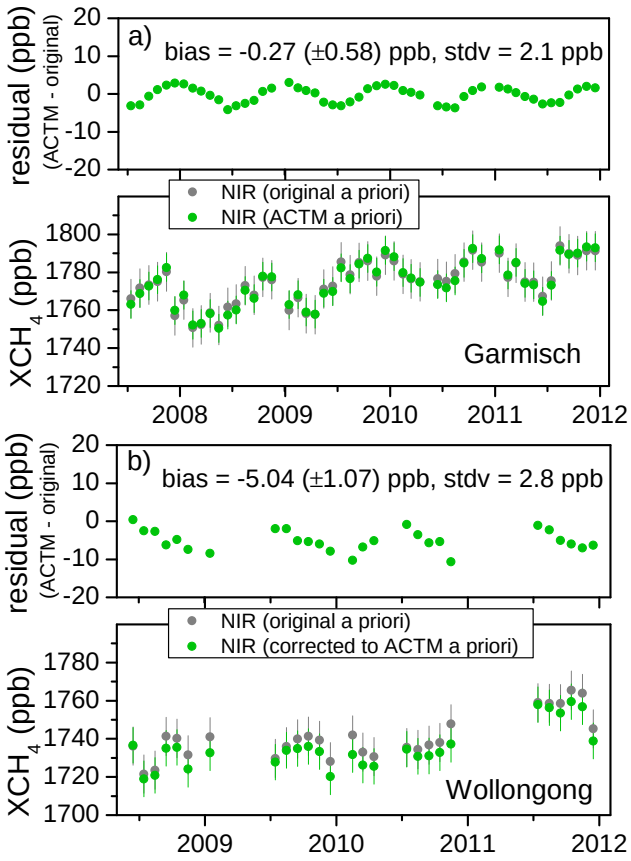

Fig. 3. (a) Lower trace: monthly mean time series of column-averaged methane retrieved from NIR spectral measurements at Garmisch – retrieved using the original (GFIT) a priori profile (grey) as well as the ACTM a priori profiles. The impact from changing the a priori profile is shown in the upper trace. Error bars are 2-σ uncertainites as explained in Fig. 4. Bias uncertainty is 2 stdv/$\sqrt{n}$ of the residuals. **(b)** Same as **(a)** but for Wollongong; green points: data corrected to ACTM prior using Eq. (1). (2008 stands for 1 January 2008; the minor tic is 1 July).

using ACTM, one of the two retrieval a prioris (WACCM or GFIT) has been used as common a priori profile: e.g. the original stdv of 7.2 ppb for Garmisch (Fig. 5a) is only reduced to stdv = 6.5 ppb (Fig. C2a) if the WACCM a priori profile is used, and it is reduced to 6.2 ppb if the GFIT a priori is used as a common prior (Fig. C2b). Obviously, the reduction of stdv's is smaller for the cases using one of the constant retrieval a prioris as common prior compared to the ACTM cases. This confirms what has been postulated in Sect. 3.2, namely that the seasonally varying smoothing term can be minimized by using the more realistic ACTM model as common prior.

4.2.2 NIR–MIR cross-correlation

Now we use the concept of cross-correlation to characterize and quantify the difference in NIR and MIR seasonalities shown in Fig. 5a as well as the reduction of this difference by using a common prior; see Fig. 6. In a strict mathematical sense, the seasonalities of the NIR and MIR data retrieved with the original a priori (blue line in Fig. 6) cannot be described by a simple phase shift because (i) the maximum of the cross-correlation is at zero time delay, (ii) the recurrences are weaker than the central maximum, and (iii) both the central maximum and the maxima of the recurrences are altogether < 1. However, the cross-correlation does show periodic recurrences, and the wings of the maxima are asymmetric towards negative time delays of about 1 month at half maximum. This behavior can be interpreted as being similar to a phase shift, and we will use the term "seasonal bias" for this behavior in the following discussion. For the data based on the common ACTM a priori (red line in Fig. 6) two things have changed: (i) the asymmetry of the maximum is reduced, and (ii) the maximum cross-correlation has increased and is closer to 1. This means that the seasonal bias is reduced by the use of ACTM. Figure C3a and b show similar but weaker effects for the cases where either of the two retrieval a prioris is used as common prior: the increase of the maxima towards 1 is less pronounced.

Figure C3c–e show the analogous cases for Wollongong. Obviously, compared to Garmisch there are nearly no recurrences, and in the cases with common a prioris (red lines) the value of the maximum cross-correlation is similar to the reference cases with original a priori (blue lines). This can be understood by the fact that the seasonal cycle of the Southern Hemisphere site Wollongong is much less pronounced compared to the Northern Hemisphere site Garmisch, and this is in line with the findings from our analysis of stdv's in the previous section.

4.2.3 Autocorrelation of NIR–MIR difference time series

Now we investigate the residual in Fig. 5b (stdv = 5.2 ppb) in more detail. An autocorrelation of this residual indicates that it is no white-noise residual but still contains some seasonality (blue line in Fig. 7). However, this seasonality has been reduced by the use of the common ACTM prior compared to the case with original a prioris. This can be seen via the larger-amplitude recurrences of the black line in Fig. 7 compared to the blue line. Figure 7 also shows that, for cases using either of the constant retrieval a prioris as common prior, the maxima of the recurrences are in between the original and the ACTM case (red and green lines in Fig. 7). This confirms once more that the ACTM prior does the best job in reducing the seasonal bias.

Next we investigate the reason for the residual seasonality in Fig. 5b (stdv = 5.2 ppb). The question is whether one can understand the maxima of the corrected NIR–MIR differences (March 2008, March 2010, and March 2011) to be due to an SZA (airmass) dependency. We prepared coincidences now on a 10-min scale (our initial coincidences had been

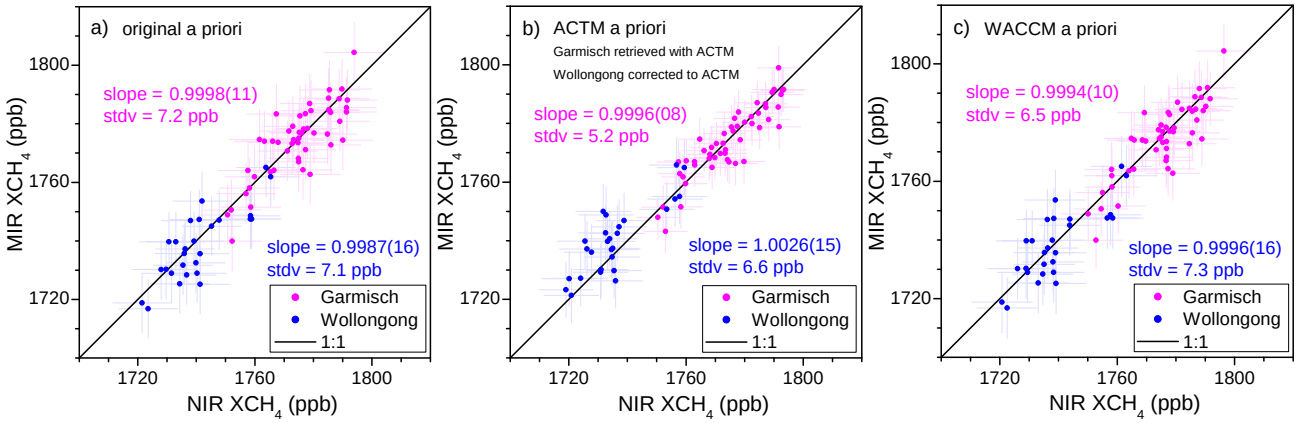

Fig. 4. (a) Scatter plot of MIR and NIR monthly means, both series retrieved with the standard retrieval a priori profile. Error bars on data points are 2-σ uncertainties derived from the stdv of the linear slope fit ($2\,\mathrm{stdv}/\sqrt{2}$). Uncertainties for the slopes are derived from the fit and are at 2-σ. **(b)** Same as **(a)** but using ACTM profiles as common prior. **(c)** Same as **(a)** but using WACCM profiles as common prior.

Table 3. Trend analysis of the XCH_4 difference time series (NIR–MIR).

data set	a priori	time period	trend NIR–MIR (ppb yr^{-1})	2-σ trend uncertainty (ppb yr^{-1})	significant trend (95 % confidence)?
Garmisch	NIR & MIR retrieved with original a priori	07/2007–12/2011	+0.91	±1.51	no
	NIR & MIR retrieved with ACTM a priori	07/2007–12/2011	+0.66	±1.11	no
	NIR & MIR retrieved with ACTM a priori	06/2008–12/2011	+1.32	±1.73	no
	NIR retrieved with WACCM apriori[a]	07/2007–12/2011	+0.88	±1.37	no
	MIR retrieved with GFIT a priori[b]	07/2007–12/2011	+0.87	±1.31	no
Wollongong	NIR & MIR retrieved with original a priori	06/2008–12/2011	+0.44	±2.52	no
	NIR & MIR corrected to ACTM a priori	06/2008–12/2011	+0.26	±2.35	no
	NIR retrieved with WACCM a priori[1]	06/2008–12/2011	+0.31	±2.61	no
	MIR retrieved with GFIT a priori[2]	06/2008–12/2011	+0.47	±2.68	no

[a] MIR retrieved with original (WACCM) a priori; [b] NIR retrieved with original (GFIT) a priori; [c] trend obtained by linear fit to the monthly mean difference time series (NIR–MIR).

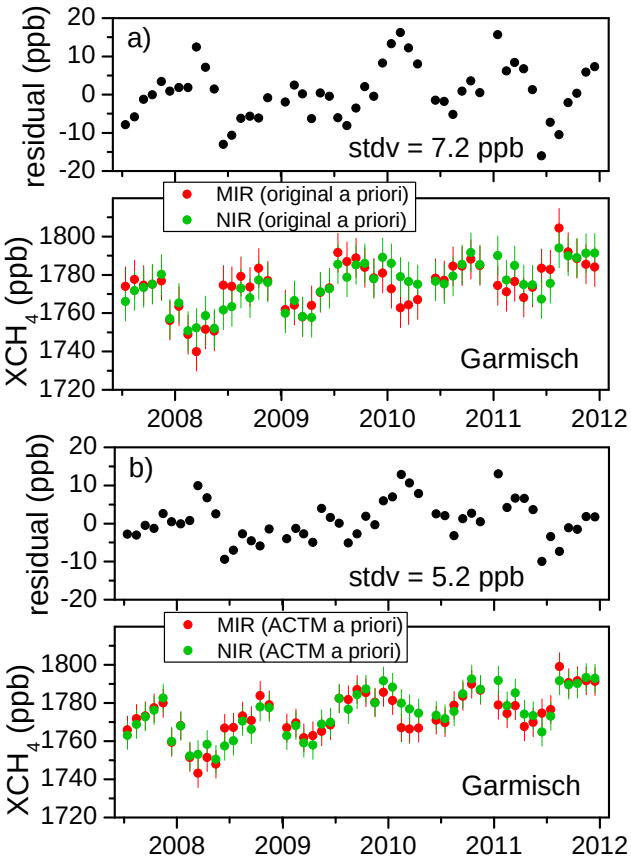

Fig. 5. (a) Lower trace: monthly mean MIR and NIR time series for Garmisch. Both column series are plotted as retrieved; i.e. no correction for a priori impact according to Eq. (1) has been performed. Error bars are 2-σ uncertainites as explained in Fig. 4. Upper trace: residual time series, i.e. difference time series of the NIR and MIR data shown in the lower trace. **(b)** Same as **(a)** but using ACTM profiles as common prior.

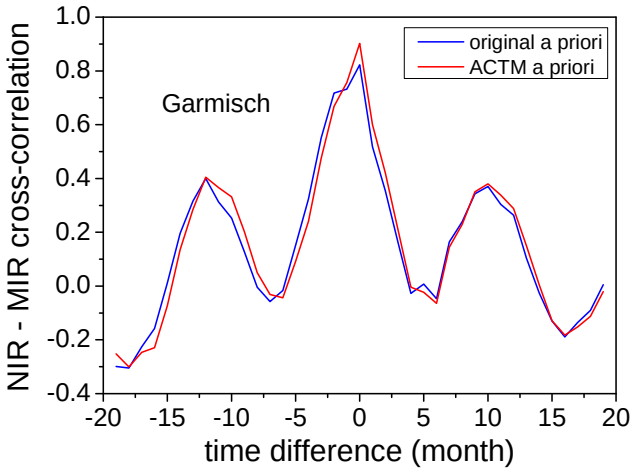

Fig. 6. Cross-correlation of Garmisch NIR and MIR monthly mean time series. Blue: retrievals with original a priori profiles. Red: retrievals with ACTM profiles as common a priori.

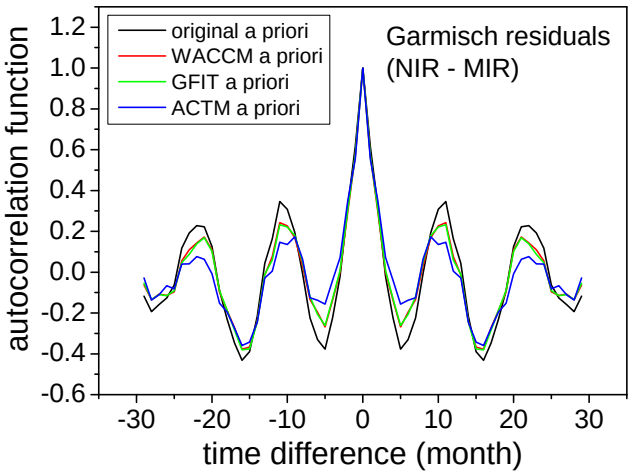

Fig. 7. Autocorrelation of Garmisch residuals, i.e. NIR–MIR difference time series (see e.g., Fig. 5). Retrievals with original a priori profiles (black), and retrievals with WACCM (red), GFIT (green), and ACTM (blue) as common a priori profiles.

"same day") from the ACTM-based MIR and NIR Garmisch series and plotted the resulting NIR–MIR differences month-by-month as a function of solar zenith angle (SZA); see Fig. C4. The resulting SZA dependency of the NIR–MIR differences is about (-0.25) ppb deg^{-1} for the interval 25–60 deg and it is about $(+0.1)$ ppb deg^{-1} for the interval 60–82 deg. From this, together with the fact that the average SZA of the March data is about 60 deg, one would predict that the NIR–MIR differences should show a minimum for March. This contradicts our finding of March maxima in Fig. 5b. We conclude that the observed small airmass dependency of the corrected NIR–MIR differences is not the dominant driver of their observed residual seasonality of Fig. 5b. From this we conjecture that the origin of this residual seasonality may be due to differences in the smoothing of $\boldsymbol{x}^l_{\mathrm{ACTM}} - \boldsymbol{x}^l_{\mathrm{true}}$ for MIR and NIR retrievals (see Sect. 3.2 for a discussion of this smoothing term).

4.2.4 Trend of the NIR–MIR difference time series

Another finding from analyzing the difference time series NIR–MIR is that they do not show a significant trend; this is important for trend studies based on joint use of MIR and NIR data. The trends have been obtained by a linear fit to the monthly mean difference time series. See Table 3 for derived numbers on trends and uncertainties for both stations and all cases with different a prioris.

Table 4. Significance of correlation between multi-annual data sets of NIR and MIR XCH_4 retrievals using varied a priori profiles. Significant correlation is achieved if the quality measure (5th column) exceeds the t-value. Data are monthly means constructed from same-day measurement coincidences.

data set	a priori	n, number of coincident monthly means	r, Pearson coefficient	quality measure $r \cdot \sqrt{\frac{n-2}{1-r^2}}$	t-value for 99 % confidence	significant correlation (99 % confidence)?
Garmisch	NIR & MIR retrieved with original a priori	51	0.82	10.12	2.68	yes
	NIR & MIR retrieved with ACTM a priori	51	0.91	15.27	2.68	yes
	NIR retrieved with WACCM a priori[a]	51	0.85	11.51	2.68	yes
	MIR retrieved with GFIT a priori[b]	51	0.86	11.87	2.68	yes
Wollongong	NIR & MIR retrieved with original a priori	27	0.82	7.17	2.79	yes
	NIR & MIR corrected to ACTM a priori	27	0.84	7.75	2.79	yes
	NIR retrieved with WACCM a priori[a]	27	0.80	6.78	2.79	yes
	MIR retrieved with GFIT a priori[b]	26	0.79	6.33	2.80	yes

[a] MIR retrieved with original (WACCM) a priori; [b] NIR retrieved with original (GFIT) a priori.

4.3 Comparison with common a priori: correlation analysis

The data sets for our correlation analysis are displayed via scatter plots of MIR and NIR monthly means: Fig. 4a shows the Garmisch and Wollongong case retrieved with the original retrieval a prioris, Fig. 4b with common ACTM prior, and Fig. 4c with common WACCM prior. Another case using the constant NIR (GFIT) retrieval a priori as common prior is given in Appendix C (Fig. C5).

4.3.1 Correlation analysis via t-test

Table 4 gives an analysis of correlation significance via a t-test. The table shows numbers of Pearson's correlation coefficient r and the derived quality measure $r\sqrt{((n-2)/(1-r^2))}$, where n is the number of coincident monthly means. Significant correlation is achieved if the quality measure exceeds the t-value. The numbers show for both Garmisch and Wollongong data a significant MIR–NIR correlation with $> 99\,\%$ probability for all cases, even for the cases where the retrievals are based on the original a priori. However, the benefit of using the ACTM model as common prior can be seen via a significantly enlarged quality measure: for Garmisch, the quality measure increases from 10.12 to 15.27 if the ACTM is used instead of the original a priori; for Wollongong the quality measure is increased from 7.17 to 7.75. Obviously, the improvement of using ACTM is more pronounced for Garmisch compared to Wollongong. As discussed before, this can be interpreted as a more pronounced seasonal cycle at Garmisch. The other cases, using either of the two retrieval a prioris as common prior, only show weaker effects upon the quality measure compared to the reference case with original a prioris. This once more confirms the advantage of using ACTM as a common prior in terms of bringing the (pronounced Northern Hemisphere) seasonality into agreement.

4.3.2 Significance of intercept and slope

The NIR and MIR retrieval methods are predicted to be both linear and have no intercept. If we apply least squares

Table 5. Intercept and slope of linear scatter plot fits between multi-annual data sets of NIR and MIR XCH_4 retrievals using varied a priori profiles. Data are monthly means constructed from same-day measurement coincidences.

		fit $y = a + bx$		fit $y = bx$		
data set	a priori	intercept a and 2-σ uncertainty (ppb)	statistically significant intercept on 2-σ level?	slope b and 2-σ uncertainty	slope different from 1 on 2-σ level?	stdv (ppb)
Garmisch	NIR & MIR retrieved with original a priori	209(310)	no	0.9998(11)	no	7.2
	NIR & MIR retrieved with ACTM a priori	183(217)	no	0.9996(8)	no	5.2
	NIR retrieved with WACCM a priori[a]	127(286)	no	0.9994(10)	no	6.5
	MIR retrieved with GFIT a priori[b]	170(239)	no	0.9980(10)	yes	6.2
Wollongong	NIR & MIR retrieved with original a priori	265(411)	no	0.9987(16)	no	7.1
	MIR & NIR corrected to ACTM a priori	250(385)	no	1.0026(15)	yes	6.6
	NIR retrieved with WACCM a priori[a]	271(433)	no	0.9996(16)	no	7.3
	MIR retrieved with GFIT a priori[b]	316(452)	no	1.0019(17)	yes	7.5

[a] MIR retrieved with original (WACCM) a priori; [b] NIR retrieved with original (GFIT) a priori.

fits allowing for nonzero intercepts to the Wollongong and Garmisch data sets, the fits yield intercepts that are relatively large (typically 200 ppb or ≈ 10 % of the XCH_4 values), but these are for all cases not significant within 2-σ uncertainty; see Table 5. This is a direct consequence of the relatively small dynamical range of XCH_4 of ≈ 3 % (Fig. 4). Because of this situation we decided to perform fits with zero intercept, as concluded earlier by Wunch et al. (2010) in an analogous case.

The slopes obtained from fits forced through zero are given in Table 5 as well. For the majority of cases (5 out of 8) the XCH_4 intercalibration factors (i.e. slopes MIR/NIR) do not differ significantly from 1 within 2-σ uncertainty. This holds for both Garmisch and Wollongong MIR and NIR data retrieved with the original a prioris (slope 0.9998(11) or 0.2 per mille relative difference for Garmisch, slope 0.9987(16) or 1.3 per mille rel. difference for Wollongong), as well as for Garmisch and Wollongong data retrieved with the common WACCM prior (slope 0.9994(10) or 0.6 per mille rel. difference, and slope 0.9996(16) or 0.4 per mille rel. difference, respectively), and also for Garmisch data retrieved with common ACTM prior (slope 0.996(8) or 0.4 per mille rel. difference). There are 3 cases where we also find slopes close to 1, however, with small deviations from 1 just above (2-σ) significance level (Table 5): for Garmisch data retrieved with common GFIT a priori we find a slope of 0.9980(10), for Wollongong data corrected to the common ACTM prior 1.0026(15), and for Wollongong data retrieved with common GFIT prior we find a slope of 1.0019(17). The slopes of these 3 cases correspond to differences in XCH_4 of 3.6–4.8 ppb or 1.9–2.6 per mille. Although these NDACC–TCCON differences are significant within 2-σ, we want to note that they are relatively small, i.e. even smaller than the TCCON target accuracy of 3 per mille.

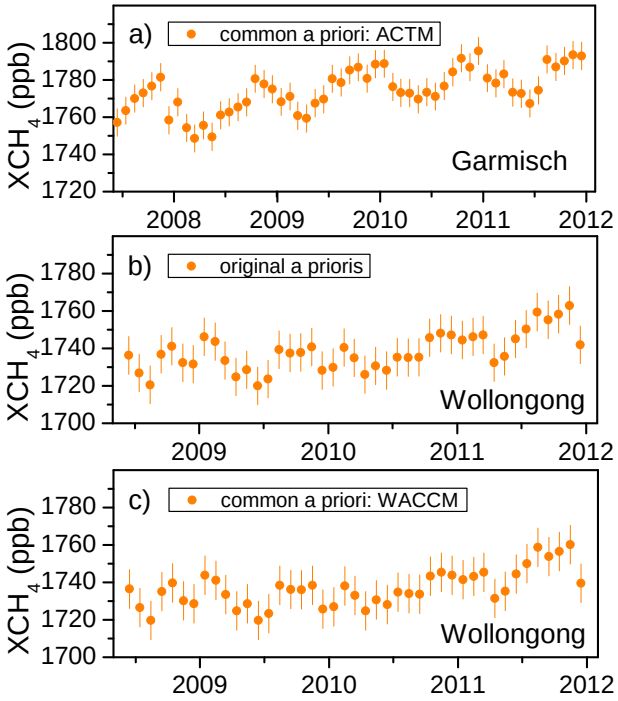

Fig. 8. Joint NIR and MIR time series, **(a)** for Garmisch (ACTM based), **(b)** for Wollongong based on original a prioris, and **(c)** for Wollongong using WACCM as common prior. Error bars are 2-σ uncertainites as explained in Fig. 4.

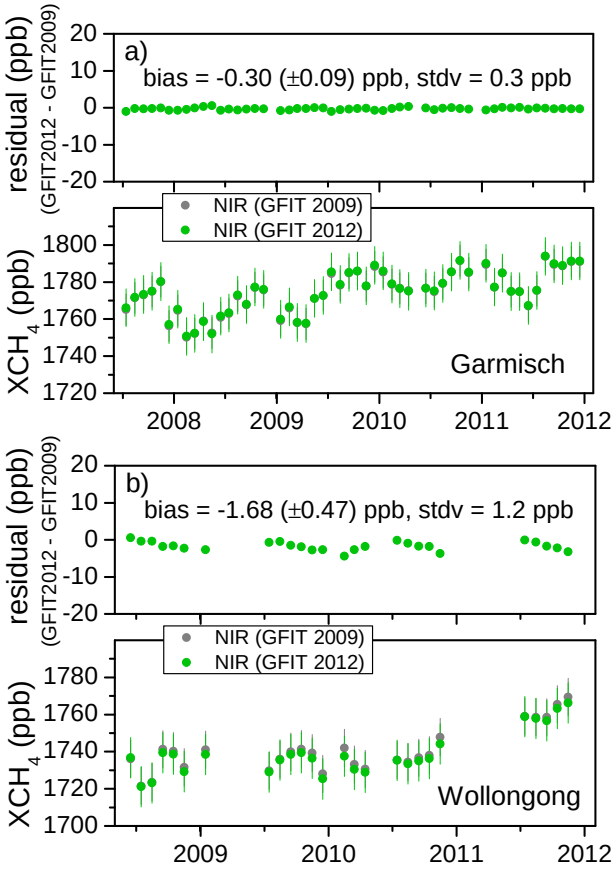

Fig. 9. (a) Lower trace: monthly mean time series of column-averaged methane retrieved from NIR spectral measurements at Garmisch – retrieved using both GFIT ver. 4.4.10 (release ggg_20091107) used throughout this paper (grey) and the very recent update GFIT ver. 4.8.6 (release ggg_2012_July_Update) (green). The (negligible) impact from this GFIT update is shown in the upper trace. **(b)** Same as **(a)** but for Wollongong.

5 Summary on the intercalibration of NDACC and TCCON XCH_4 data

We conclude from the previous sections (in particular, Table 5) that the direct comparison of the original Garmisch and Wollongong MIR and NIR data sets as retrieved shows a very good overall agreement within the error bars: slope 0.9998(11) or relative difference 0.2 per mille for Garmisch, and slope 0.9987(16) or relative difference 1.3 per mille for Wollongong. That is, we do not find the need for applying an overall MIR/NIR intercalibration factor.

However, the Garmisch MIR and NIR time series based upon the original retrieval a prioris do contain a significant seasonal bias, which appears to be dominated by the differing a priori profiles and averaging kernels of the MIR and NIR retrievals. It was shown that this seasonal bias can be significantly reduced by implementing the same a priori for the MIR and NIR data sets. This common a priori should ideally be based on a realistic site-specific and time-dependent model. This approach allows for the reduction of the differing smoothing errors due to the differing averaging kernels leading to better agreement of the MIR and NIR seasonal cycles. The impact of this is stronger for Garmisch with its more pronounced (Northern Hemisphere) seasonal cycle compared to Wollongong. As outlined in the previous chapters the best choice for Garmisch is the one with ACTM as common prior (MIR/NIR slope = 0.9996(8), stdv = 5.2 ppb). In Fig. 8a such a joint (NIR plus MIR) data set is shown for Garmisch; the monthly means have been constructed from the columns retrieved from the individual MIR and NIR spectra recorded within this month, each column weighted by the number of scans per spectrum.

For Wollongong, MIR and NIR data agree well with original a prioris (slope = 0.9987(16), stdv = 7.1 ppb); see Fig. 8b for the joint (MIR plus NIR) data set. The advantage of using the common ACTM prior is less prominent in terms of MIR/NIR stdv (i.e. 6.6 ppb) due to the weaker seasonal cycle (compared to Garmisch). Another fact is that for the Wollongong ACTM case there is this small but significant deviation from the ideal intercalibration factor 1, i.e. 1.0026(15). Therefore, a recommended alternative for Wollongong would be to use the common WACCM prior leading to a close-to-ideal slope of 0.9996(16), although the stdv is slightly increased (7.3 ppb). The joint data set based on the WACCM option is displayed in Fig. 8c. Note that there are practically no differences between Fig. 8b and c.

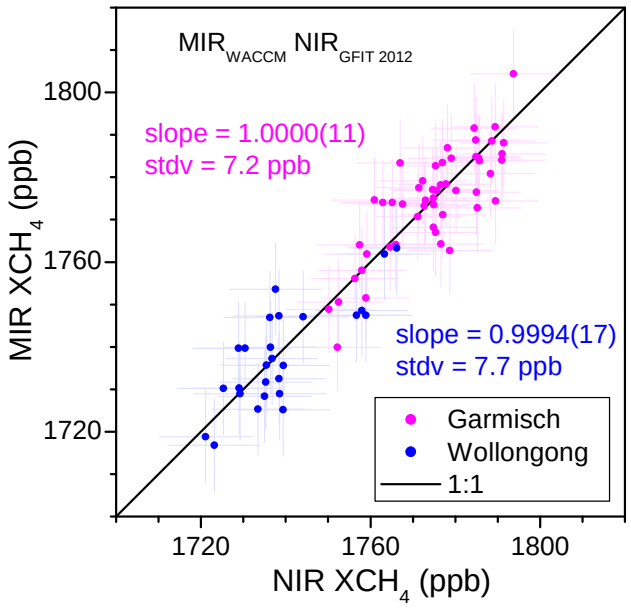

Fig. 10. Scatter plot of MIR and NIR monthly means, both series retrieved with the standard retrieval a prioris (similar to Fig. 4a) but using the recent update GFIT ver. 4.8.6 (release ggg_2012_July_Update).

6 Conclusions on joint use of NDACC and TCCON XCH_4 data

It has been shown recently that the MIR XCH_4 data can be used as retrieved for trend studies, if such studies are based on de-seasonalized data (Sussmann et al., 2012). On the other hand we have shown in this paper that in general the information content and smoothing errors of the NIR and MIR retrievals can be significantly different, leading to differing seasonalities. Therefore, the use of these data sets for satellite validation or flux inversions would need to take the a priori profiles and averaging kernels of the retrievals into account.

The use of a joint NDACC and TCCON data set for satellite validation would ideally be performed using satellite data based on the same common realistic (model) a priori as used for the NIR and MIR ground FTIR data. This can either be done by reprocessing the satellite data with the common a priori or, with less effort, by using Eq. (1).

In future work we will apply the concepts introduced in this study to all other existing stations that perform coincident MIR and NIR soundings of column-averaged methane. The goal is to further confirm or refine the intercalibration behavior found in this work.

Finally, we investigated the recent MIR retrieval update (GFIT ver. 4.8.6, release ggg_2012_July_Update; see "Note: impact of GFIT 2012 update"). We found that, using GFIT 2012, the slopes for the direct NIR–MIR comparison are again not significantly different from 1, as found previously using GFIT 2009. However, GFIT 2012 is based upon a more realistic (i.e. site- and time-dependent) set of a priori profiles. Figure 1b shows that these are quite similar to the ACTM profiles (Fig. 1a). We conjecture that the new GFIT 2012 a priori profiles should be a good choice for use as a common priori in order to minimize the impact from differing a priori profiles and smoothing errors for the purpose of joint NDACC and TCCON studies and satellite validation.

Note: impact of GFIT 2012 update

After completion of this work a new official release of the GFIT (NIR) retrieval software has become available and been released (GFIT ver. 4.8.6, release ggg_2012_July_Update). The main change relative to the GFIT version used in our paper (GFIT ver. 4.4.10, release ggg_20091107) has been that the (one) a priori profile used for all sites is now being corrected for the actual tropopause altitude on a per-day and a per-site basis; see Fig. 1b. Figure 9a shows that the impact of this update is negligible in terms of the questions investigated in our paper; i.e. the bias (GFIT 2012 minus GFIT 2009) is only $-0.3\,(\pm 0.09)$ ppb for Garmisch and no significant additional seasonality is introduced (difference time series with stdv = 0.3 ppb). Also for Wollongong only a small impact is found in the bias (-1.68 ± 0.47 ppb) and seasonality (stdv = 1.2 ppb); see Fig. 9b. This means that the basic findings and conclusions from our paper should hold for retrievals with the new GFIT version as well. For example, Fig. 10 also shows that, using the GFIT 2012 version, the slopes for the direct NIR–MIR comparison are again not significantly different from 1, as found previously using GFIT 2009 (Fig. 4a).

Appendix A

Validity of the linear approximation of Eq. (1)

Equation (1) contains an approximation as it uses averaging kernels which are linear approximations of the true retrieval which is non-linear in the state vector $\boldsymbol{x}$. To investigate the validity of this approximation within the context of our paper, we performed new retrievals of the full Garmisch MIR and NIR time series using 3-hourly ACTM model profile as prior and compared this to the alternative way of replacing the original a priori by ACTM, namely via Eq. (1). These two different versions of ACTM-based time series were compared to the time series retrieved with original a priori using 10-min coincidences. The results are shown in Fig. A1a. Here, the differences of the retrievals using ACTM prior and the retrievals using the original prior are displayed via red crosses. The black crosses are the differences of the retrievals (based on the original a priori) corrected to ACMT prior via Eq. (1) and the retrieval with the original a priori. It can be seen in Fig. A1a that there are only small differences between the red and black crosses, and this is visualized via green

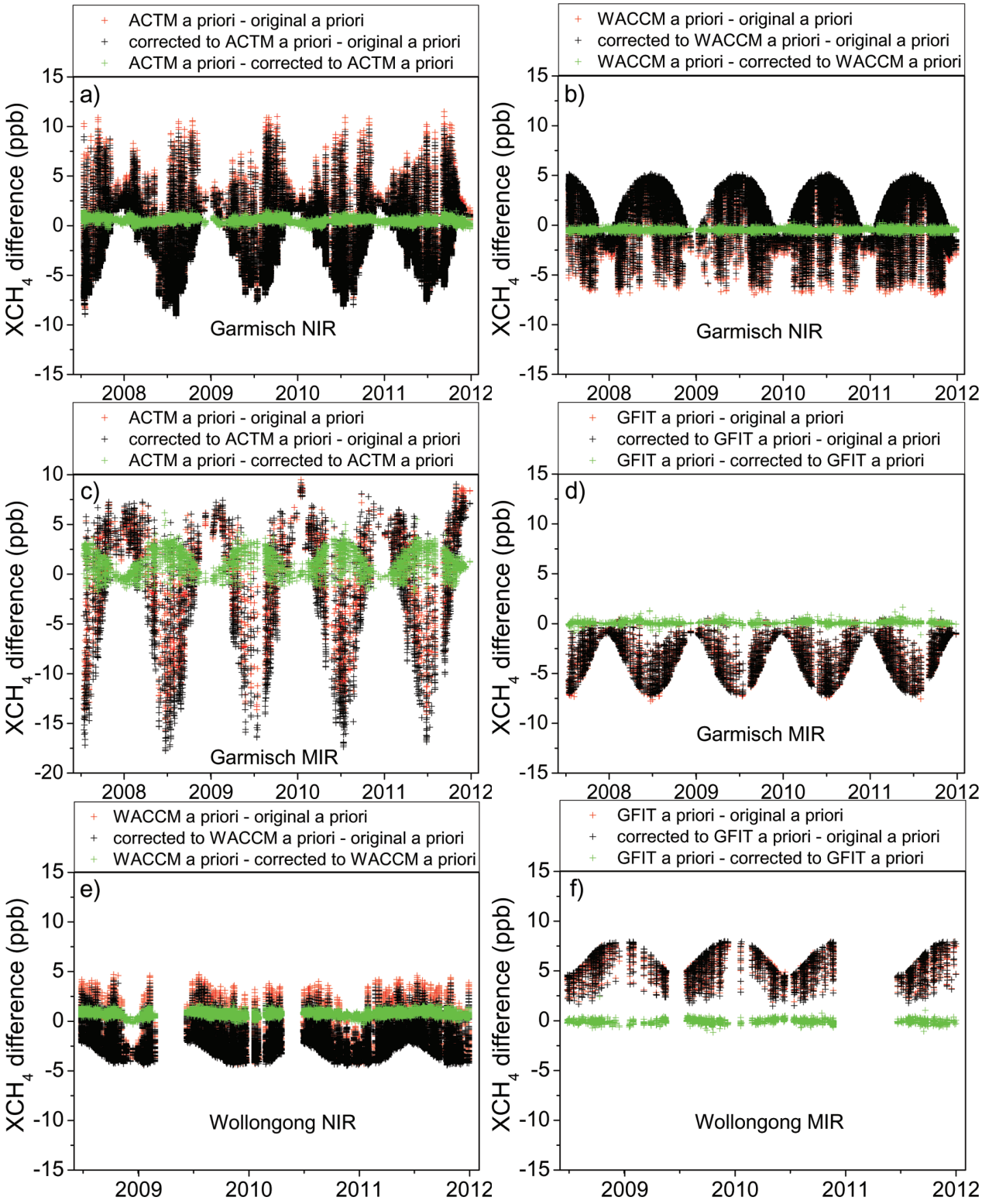

Fig. A1. Investigation of the validity of the linear approximation within Eq. (1). **(a)** Red: XCH_4 from Garmisch NIR measurements retrieved with 3-hourly ACTM profiles minus retrievals using the original (GFIT) prior. Black: same as red but using Eq. (1) for a posteriori exchange of the a priori profile. Green: difference between red and black – deviations from zero are due to non-linearity of the retrieval. Data basis is retrievals from individual NIR and MIR spectra constructed from same-day NIR–MIR coincidences. **(b)** Same as **(a)** but for Garmisch NIR retrievals using the WACCM a priori profile (i.e., the prior of the MIR retrievals), **(c)** Garmisch MIR retrievals using the 3-hourly ACTM profiles, **(d)** Garmisch MIR retrievals using the GFIT a priori, **(e)** Wollongong NIR retrievals using the WACCM a priori, and **(f)** Wollongong MIR retrievals using the GFIT a priori.

Table A1. Impact of non-linearity on XCH_4 from using Eq. (1) for a posteriori exchange of an a priori profile versus performing a retrieval with exchanged a priori. Data basis is retrievals from individual MIR and NIR spectra, from same-day NIR–MIR coincidences. Uncertainties are 2 times the standard errors of the mean (2-σ/sqrt (n)).

data set	a priori	mean bias from non-linearity (XCH_4 retrieved with exchanged a priori minus XCH_4 from use of Eq. 1) (ppb)	stdv from non-linearity (XCH_4 retrieved with exchanged a priori minus XCH_4 from use of Eq. 1) (ppb)
Garmisch	NIR ACTM	0.57 (±0.001)	0.24
	NIR WACCM	−0.50 (±0.001)	0.12
	MIR ACTM	1.19 (±0.012)	1.19
	MIR GFIT	0.10 (±0.003)	0.16
Wollongong	NIR WACCM	0.67 (±0.002)	0.24
	MIR GFIT	−0.08 (±0.005)	0.23

crosses. Figure A1b–f show analogous plots of the effects on MIR and NIR retrieval differences by exchanging their original a prioris with ACTM (MIR and NIR), GFIT (MIR), and WACCM (NIR) a prioris for both stations. We derived from Fig. A1 numbers on the mean bias and the seasonality of the bias introduced by the use of Eq. (1). These are summarized in Table A1. The general finding from Fig. A1 and Table A1 is that the non-linearity introduces significant but very small mean biases in both MIR and NIR cases at Wollongong and Garmisch, and also the seasonality of these biases is negligible or small. Only in the case of Garmisch data based upon ACTM a priori were non-linearity errors of > 1 ppb (bias and seasonal/zenith angle dependent stdv) found.

Appendix B

Description of the a priori models

B1 ACTM-based prior

The model used for obtaining a common a priori profile of the MIR and NIR retrievals is the CCSR/NIES/FRCGC AGCM-based chemistry transport model (i.e., ACTM), which has been developed for simulating the major long-lived greenhouse gases (Patra et al., 2009). The ACTM simulations are conducted at T42 spectral truncations in the horizontal ($\approx 2.8 \times \approx 2.8$ degrees latitude/longitude) and 67 vertical levels covering the height range from the earth's surface to the mesosphere ($\approx 1.3 \times 10^{-5}$ σ pressure or ≈ 80 km). The emissions and loss of methane in ACTM are adopted from the TransCom-CH_4 simulation protocol (Patra et al., 2011). Comparisons showed that forward ACTM simulations of annual-mean methane are in close agreement (within 1 ppb) with measurements from surface sites as to inter-hemispheric gradients (Patra et al., 2011). ACTM-simulated vertical profiles of dry-air mole fractions on the native model vertical grid and nearest horizontal grid of the FTIR sites are sampled at 3-hourly intervals for use as a priori in this study. We interpolated the model profiles for each measurement time on the model pressure grid and applied this interpolated profile.

B2 WACCM-based prior

Chemical profiles for all targeted NDACC and many background species have been generated for all NDACC, TCCON and other sites for use as a priori. These a priori profiles have several advantages over other sources of a priori information. The modeled data employs surface emission data that can provide more accurate low-altitude mixing ratios that the FTIR retrieval may not be sensitive to and may not be included in other a priori sources, e.g. satellite profiles. By deriving a mean a priori from a long-term model run, the variability of the mean is also determined and is a sole source variability and a valuable component for understanding smoothing by the retrieval. To the accuracy of the model the interspecies correlations are self-consistent. The global surface-to-mesosphere model provides consistency for all sites in the altitude of interest for the FTIR retrievals. The WACCM model is described in Garcia et al. (2007).

To provide a priori that are as unbiased as possible, the a priori are an average from monthly sampling of the 40-yr portion from 1980 to 2020 of a 75-yr CCMVal model intercomparison. The CCMVal project is described in Eyring et al. (2007) and compares several models under specific IPCC scenarios for ozone recovery. In particular we use a moderate set of scenarios following REF2 and IPCC scenarios A1B for greenhouse gas emissions, AR4 for sea surface temperatures and surface halogen as prescribed by WMO/UNEP. Details can be found in Eyring et al. (2007). These a priori provide a reasonable mean from which observations will vary. The a priori were tested for applicability at all sites before adoption as an NDACC a priori standard.

Appendix C

Supplementary figures

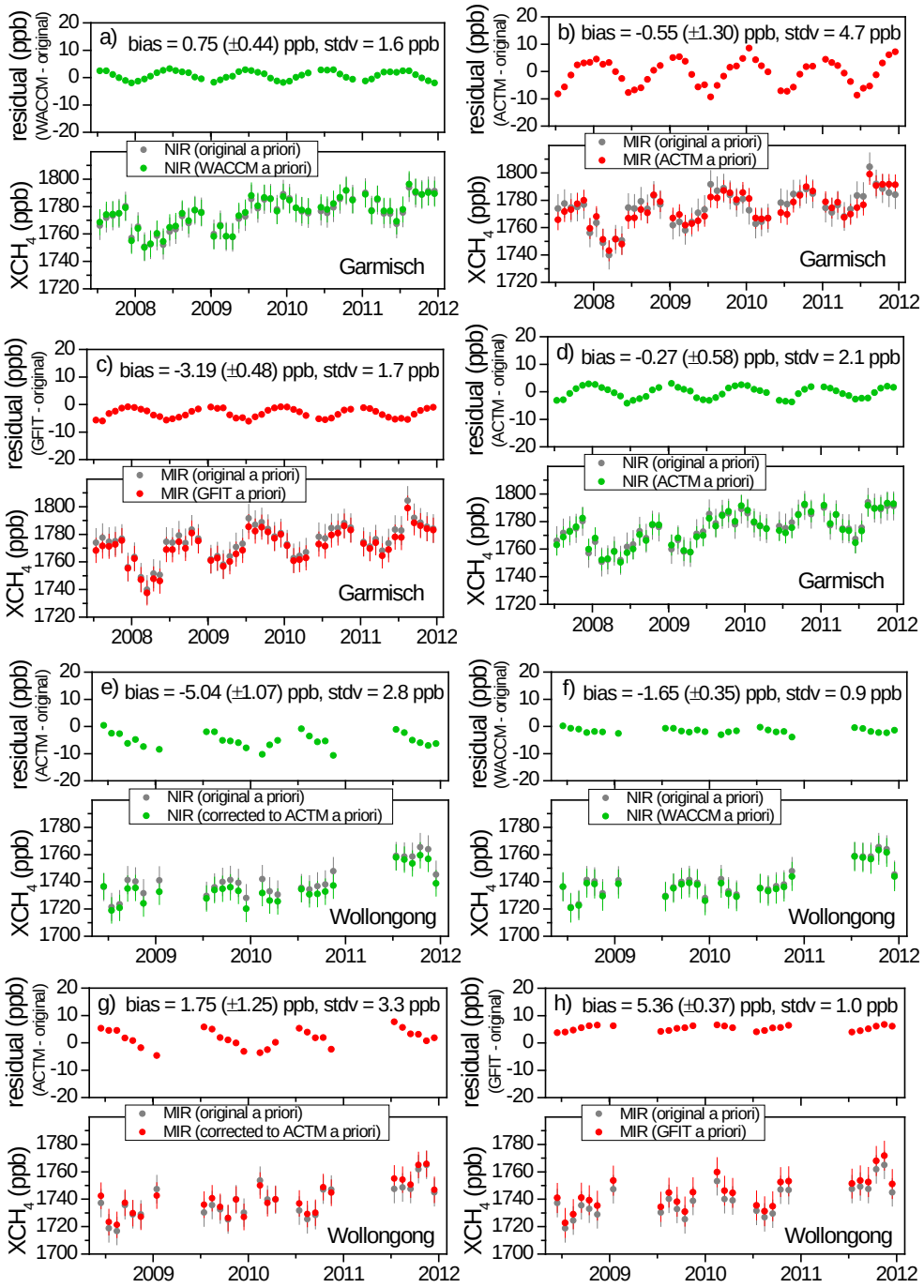

Fig. C1. Same as Fig. 3 but showing the impact on **(a)** Garmisch NIR retrievals using the Garmisch WACCM a priori profile (i.e. the standard prior of the Garmisch MIR retrievals) as prior, **(b)** Garmisch MIR retrievals using 3-hourly ACTM profiles, **(c)** Garmisch MIR retrievals using the GFIT a priori profile (i.e. the standard prior of the NIR retrievals), **(d)** Wollongong NIR retrievals using 3-hourly ACTM profiles, **(e)** Wollongong NIR retrievals using the WACCM a priori profile, **(f)** Wollongong MIR retrievals with the a priori profile corrected to 3-hourly ACTM profiles via Eq. (1), and **(g)** Wollongong MIR retrievals using the GFIT a priori profile.

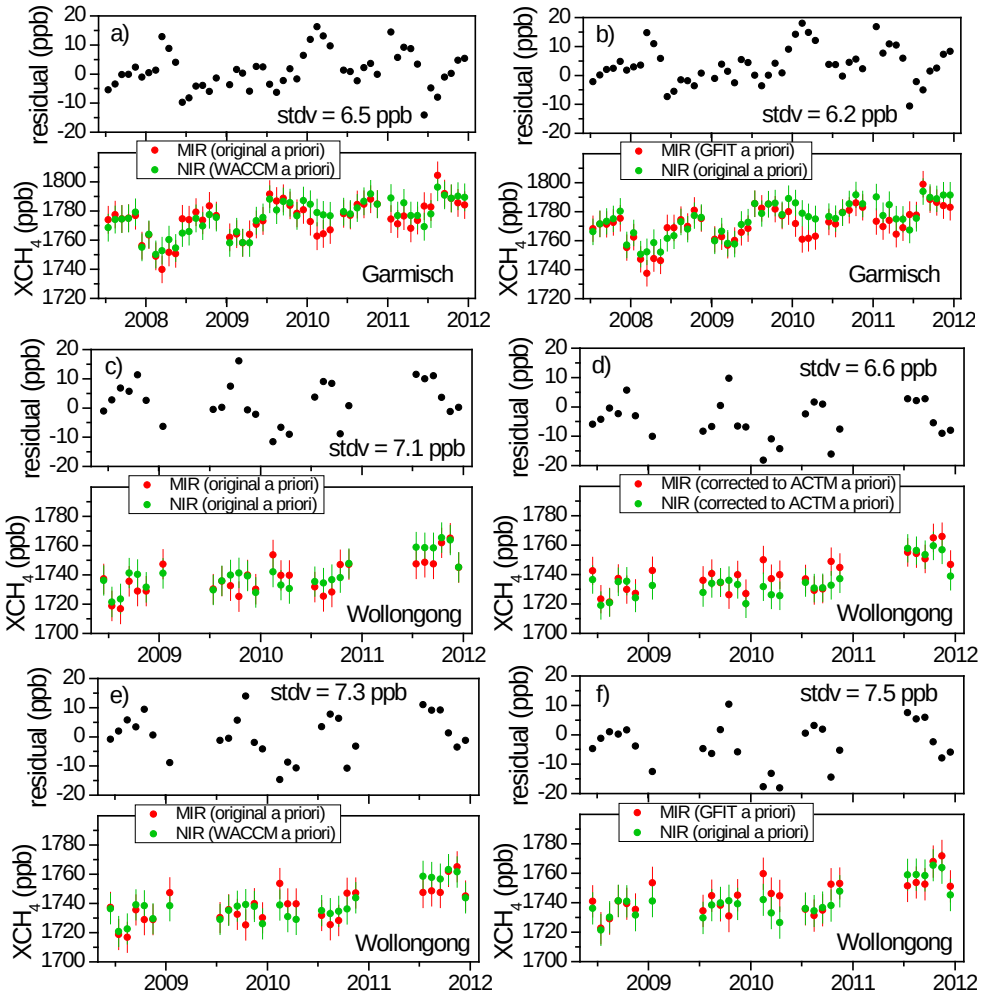

Fig. C2. Same as Fig. 5 but using **(a)** for Garmisch the WACCM a priori profile as common prior (i.e. the standard prior of the Garmisch MIR retrievals), **(b)** for Garmisch the GFIT a priori profile (i.e. the standard prior of the NIR retrievals), **(c)** for Wollongong the original a prioris, **(d)** for Wollongong a correction to 3-hourly ACTM profiles as common prior, **(e)** for Wollongong the WACCM a priori profile, and **(f)** for Wollongong the GFIT a priori profile.

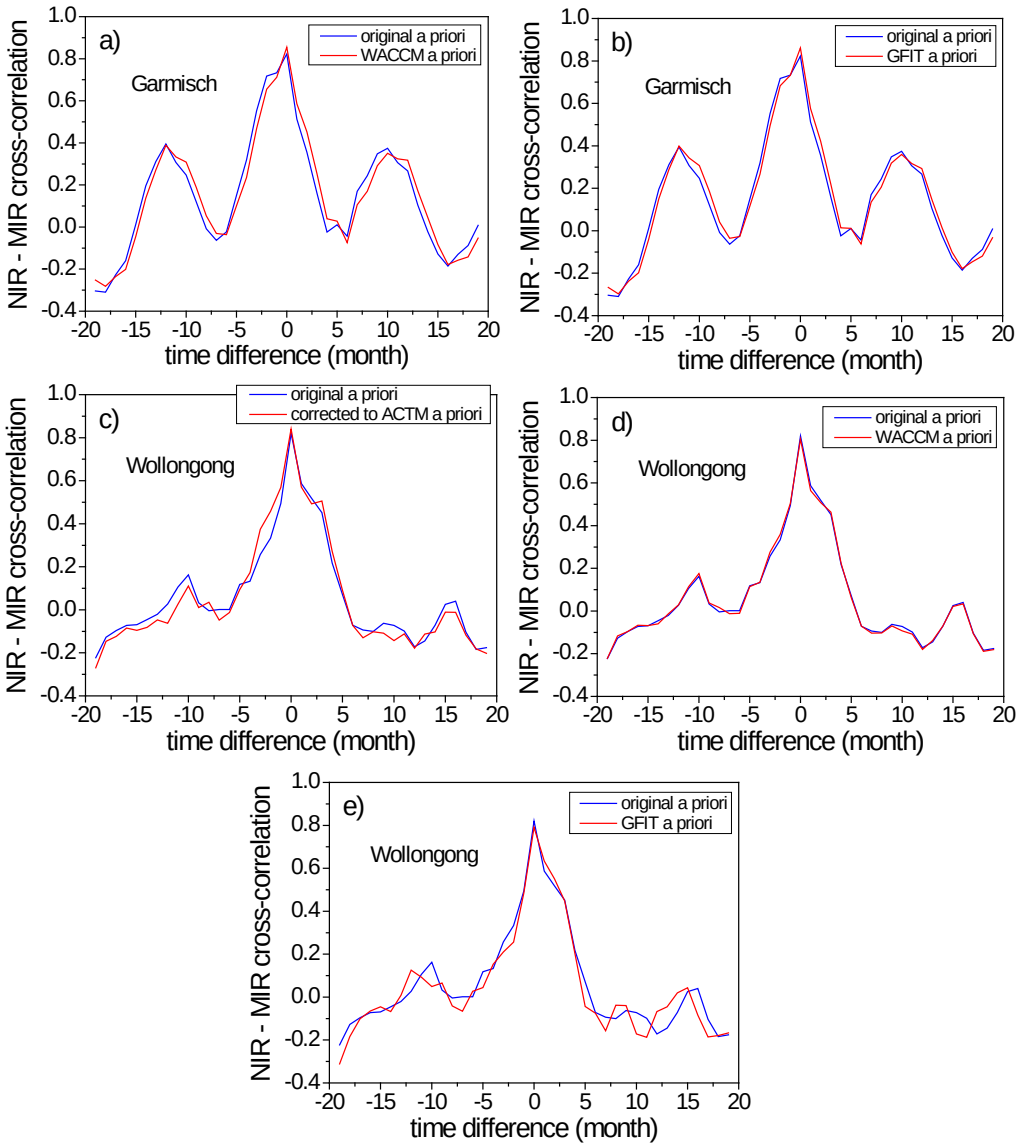

Fig. C3. Same as Fig. 6, i.e. cross-correlations using original priors (blue) compared to cases with varied common a priori profiles (red): **(a)** Garmisch with WACCM prior, **(b)** Garmisch with GFIT prior, **(c)** Wollongong with ACTM prior, **(d)** Wollongong with WACCM prior, and **(e)** Wollongong with GFIT prior.

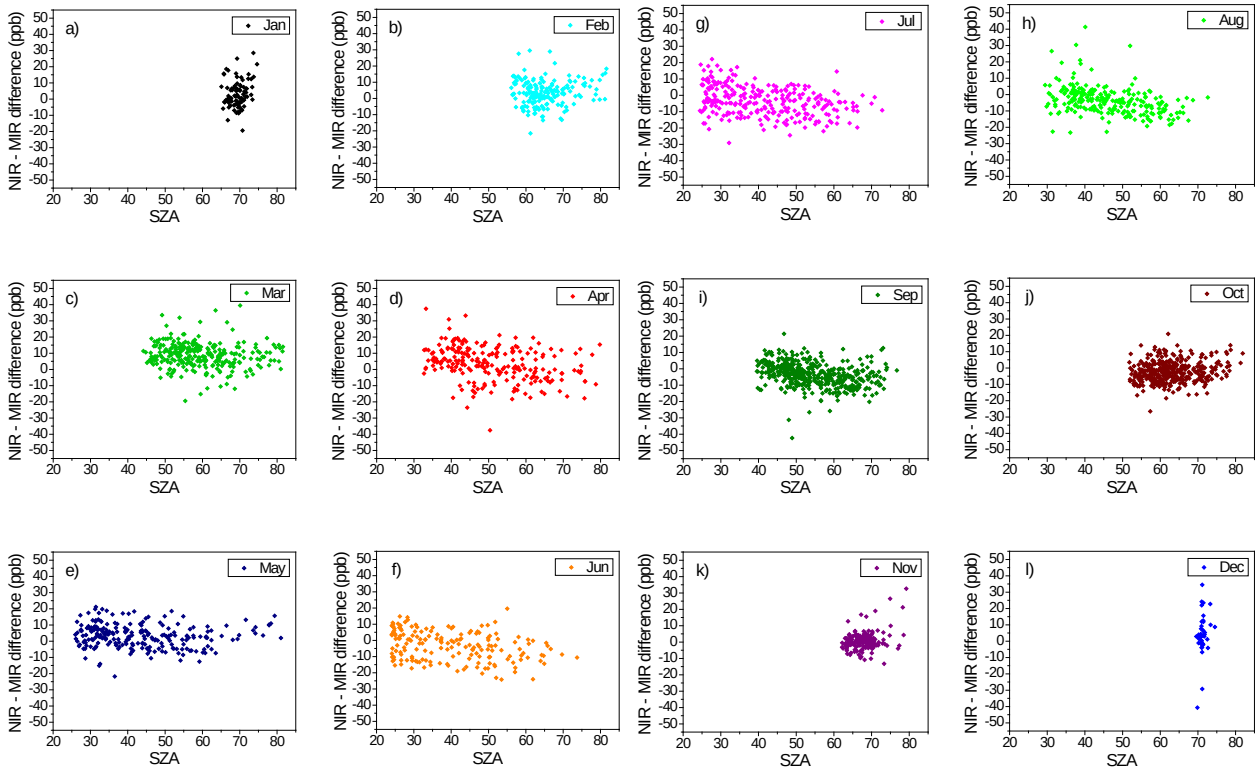

Fig. C4. Monthly mean NIR–MIR differences (10-min coincidences) for Garmisch retrievals with common ACTM a priori profiles as a function of solar zenith angle (SZA).

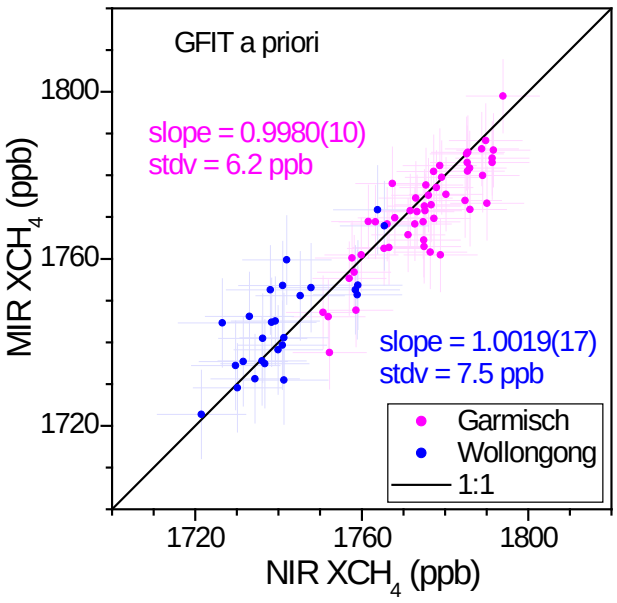

Fig. C5. Same as Fig. 4 but using the GFIT 2009 a priori profile as a common prior for the MIR and NIR retrievals.

Acknowledgements. We thank H. P. Schmid (IMK-IFU) for his continual interest in this work. It is a pleasure to thank both the referee Vanessa Sherlock and the Anonymous Referee for very sound and helpful comments. Provision of the GFIT code by G. Toon (JPL) is gratefully acknowledged. Our work has been performed as part of the ESA GHG-cci project via subcontract with the University of Bremen. In addition we acknowledge funding by the EC within the INGOS project. We thank for support by the Deutsche Forschungsgemeinschaft and Open Access Publishing Fund of the Karlsruhe Institute of Technology. The Wollongong work was funded through the Australian International Science Linkage grant CG130014 and the Australian Research Council, grants DP0879468 and DP110103118.

Edited by: A. J. M. Piters

References

Angelbratt, J., Mellqvist, J., Blumenstock, T., Borsdorff, T., Brohede, S., Duchatelet, P., Forster, F., Hase, F., Mahieu, E., Murtagh, D., Petersen, A. K., Schneider, M., Sussmann, R., and Urban, J.: A new method to detect long term trends of methane (CH_4) and nitrous oxide (N_2O) total columns measured within the NDACC ground-based high resolution solar FTIR network, Atmos. Chem. Phys., 11, 6167–6183, doi:10.5194/acp-11-6167-2011, 2011.

Borsdorff, T. and Sussmann, R.: On seasonality of stratomesospheric CO above midlatitudes: New insight from solar FTIR spectrometry at Zugspitze and Garmisch, Geophys. Res. Lett., 36, L21804, doi:10.1029/2009GL040056, 2009.

Bousquet, P., Ciais, P., Miller, J. B., Dlugokencky, E. J., Hauglustaine, D. A., Prigent, C., Van der Werf, G. R., Peylin, P., Brunke, E. G., Carouge, C., Langenfels, R. L., Lathiere, J., Papa, F., Ramonet, M., Schmidt, M., Steele, L. P., Tyler, S. C., and White, J.: Contribution of anthropogenic and natural sources to atmospheric methane variability, Nature, 443, 439–443, 2006.

Bousquet, P., Ringeval, B., Pison, I., Dlugokencky, E. J., Brunke, E.-G., Carouge, C., Chevallier, F., Fortems-Cheiney, A., Frankenberg, C., Hauglustaine, D. A., Krummel, P. B., Langenfelds, R. L., Ramonet, M., Schmidt, M., Steele, L. P., Szopa, S., Yver, C., Viovy, N., and Ciais, P.: Source attribution of the changes in atmospheric methane for 2006–2008, Atmos. Chem. Phys., 11, 3689–3700, doi:10.5194/acp-11-3689-2011, 2011.

Chevallier, F., Deutscher, N., Conway, C. J., Ciais, P., Ciattaglia, L., Dohe, S., Fröhlich, M., Gomez-Pelaez, A. J., Griffith, D., Hase, F., Haszpra, L., Krummel, P., Kyrö, E., Labuschagne, C., Langenfelds, R., Machida, T., Maignan, F., Matsueda, H., Morino, I., Notholt, J., Ramonet, M., Sawa, Y., Schmidt, M., Sherlock, V., Steele, P., Strong, K., Sussmann, R., Wennberg, P., Wofsy, S., Worthy, D., Wunch, D., and Zimnoch, M.: Global CO_2 surface fluxes inferred from surface air-sample measurements and from surface retrievals of the CO_2 total column, Geophys. Res. Lett., 38, L24810, doi:10.1029/2011GL049899, 2011.

de Laat, A. T. J., Gloudemans, A. M. S., Schrijver, H., Aben, I., Nagahama, Y., Suzuki, K., Mahieu, E., Jones, N. B., Paton-Walsh, C., Deutscher, N. M., Griffith, D. W. T., De Mazière, M., Mittermeier, R. L., Fast, H., Notholt, J., Palm, M., Hawat, T., Blumenstock, T., Hase, F., Schneider, M., Rinsland, C., Dzhola, A. V., Grechko, E. I., Poberovskii, A. M., Makarova, M. V., Mellqvist, J., Strandberg, A., Sussmann, R., Borsdorff, T., and Rettinger, M.: Validation of five years (2003–2007) of SCIAMACHY CO total column measurements using ground-based spectrometer observations, Atmos. Meas. Tech., 3, 1457–1471, doi:10.5194/amt-3-1457-2010, 2010.

Denman, K. L., Brasseur, G., Chidthaisong, A., Ciais, P., Cox, P. M., Dickinson, R. E., Hauglustaine, D., Heinze, C., Holland, E., Jacob, D., Lohmann, U., Ramachandran, S., da Silva Dias, P. L., Wofsy, S. C., and Zhang, X.: Couplings Between Changes in the Climate System and Biogeochemistry, in: Climate Change 2007: The Physical Science Basis. Contribution of Working Group I to the Fourth Assessment Report of the Intergovernmental Panel on Climate Change, edited by: Solomon, S., Qin, D., Manning, M., Chen, Z., Marquis, M., Averyt, K. B., Tignor, M., and Miller, H. L., Cambridge University Press, Cambridge, UK and New York, NY, USA, 2007.

Deutscher, N. M., Griffith, D. W. T., Bryant, G. W., Wennberg, P. O., Toon, G. C., Washenfelder, R. A., Keppel-Aleks, G., Wunch, D., Yavin, Y., Allen, N. T., Blavier, J.-F., Jiménez, R., Daube, B. C., Bright, A. V., Matross, D. M., Wofsy, S. C., and Park, S.: Total column CO_2 measurements at Darwin, Australia – site description and calibration against in situ aircraft profiles, Atmos. Meas. Tech., 3, 947–958, doi:10.5194/amt-3-947-2010, 2010.

Dlugokencky, E. J., Houweling, S., Bruhwiler, L., Masarie, K. A., Lang, P. M., Miller, J. B., and Tans, P. P.: Atmospheric methane levels off: Temporary pause or a new steady-state?, Geophys. Res. Lett., 30, 1992, doi:10.1029/2003GL018126, 2003.

Dlugokencky, E. J., Bruhwiler, L., White, J. W. C., Emmons, L. K., Novelli, P. C., Montzka, S. A., Masarie, K. A., Lang, P. M., Crotwell, A. M., Miller, J. B., and Gatti, L. V.: Observational constraints on recent increases in the atmospheric CH_4 burden, Geophys. Res. Lett., 36, L18803, doi:10.1029/2009GL039780, 2009.

Etheridge, D., Steele, L., Francey, R., and Langenfelds, R.: Atmospheric methane between 1000 A.D. and present: Evidence of anthropogenic emissions and climatic variability, J. Geophys. Res., 103, 15979–15993, 1998.

Eyring, V., Waugh, D. W., Bodeker, G. E., Cordero, E., Akiyoshi, H., Austin, J., Beagley, S. R., Boville, B., Braesicke, P., Brühl, C., Butchart, N., Chipperfield, M. P., Dameris, M., Deckert, R., Deushi, M., Frith, S. M., Garcia, R. R., Gettelman, A., Giorgetta, M., Kinnison, D. E., Mancini, E., Manzini, E., Marsh, D. R., Matthes, S., Nagashima T., Newman, P. A., Nielsen, J. E., Pawson, S., Pitari, G., Plummer, D. A., Rozanov, E., Schraner, M., Scinocca, J. F., Semeniuk, K., Shepherd, T. G., Shibata, K., Steil, B., Stolarski, R., Tian, W., and Yoshiki, M.: Multimodel projections of stratospheric ozone in the 21st century, J. Geophys. Res., 112, D16303, doi:10.1029/2006JD008332, 2007.

Forster, P., Ramaswamy, V., Artaxo, P., Berntsen, T., Betts, R., Fahey, D., Haywood, J., Lean, J., Lowe, D., Myhre, G., Nganga, J., R. Prinn, G. Raga, M. S., and Dorland, R. V.: Changes in Atmospheric Constituents and in Radiative Forcing, Climate Change 2007: The Physical Science Basis, Contribution of Working Group I to the Fourth Assessment Report of the Intergovernmental Panel on Climate Change (IPCC), 2007.

Frankenberg, C., Warneke, T., Butz, A., Aben, I., Hase, F., Spietz, P., and Brown, L. R.: Pressure broadening in the $2\nu_3$ band of methane and its implication on atmospheric retrievals, At-

mos. Chem. Phys., 8, 5061–5075, doi:10.5194/acp-8-5061-2008, 2008.

Frankenberg, C., Aben, I., Bergamaschi, P., Dlugokencky, E. J., van Hees, R., Houweling, S., van der Meer, P., Snel, R., and Tol, P.: Global column-averaged methane mixing ratios from 2003 to 2009 as derived from SCIAMACHY: Trends and variability, J. Geophys. Res., 116, D04302, doi:10.1029/2010JD014849, 2011.

Garcia, R. R., Marsh, D. R., Kinnison, D. E., Boville, B. A., and Sassi, F.: Simulation of secular trends in the middle atmosphere, 1950–2003, J. Geophys. Res., 112, D09301, doi:10.1029/2006JD007485, 2007.

Geibel, M. C., Messerschmidt, J., Gerbig, C., Blumenstock, T., Chen, H., Hase, F., Kolle, O., Lavrič, J. V., Notholt, J., Palm, M., Rettinger, M., Schmidt, M., Sussmann, R., Warneke, T., and Feist, D. G.: Calibration of column-averaged CH_4 over European TCCON FTS sites with airborne in-situ measurements, Atmos. Chem. Phys., 12, 8763–8775, doi:10.5194/acp-12-8763-2012, 2012.

Gloor, M., Fan, S. M., Pacala, S., and Sarmiento, J.: Optimal sampling of the atmosphere for purpose of inverse modeling: A model study, Global Biogeochem. Cy., 14, 407–428, 2000.

Griffith, D. W. T., Jones, N. B., and Matthews, W. A.: Interhemispheric ratio and Annual Cycle of Carbonyl Sulphide (OCS) Total Column from Ground-Based FTIR Spectra, J. Geophys. Res., 103, 8447–8454, 1998.

Houweling, S., Aben, I., Breon, F.-M., Chevallier, F., Deutscher, N., Engelen, R., Gerbig, C., Griffith, D., Hungershoefer, K., Macatangay, R., Marshall, J., Notholt, J., Peters, W., and Serrar, S.: The importance of transport model uncertainties for the estimation of CO_2 sources and sinks using satellite measurements, Atmos. Chem. Phys., 10, 9981–9992, doi:10.5194/acp-10-9981-2010, 2010.

Jones, N. B., Griffith, D. W. T., Murphy, C., Wilson, S., Deutscher, N. M., and Macatangay, R.: The Australian NDACC long term ground based measurements: site description and analysis methods, Atmos. Meas. Tech. Discuss., in preparation, 2013.

Keppel-Aleks, G., Wennberg, P. O., and Schneider, T.: Sources of variations in total column carbon dioxide, Atmos. Chem. Phys., 11, 3581–3593, doi:10.5194/acp-11-3581-2011, 2011.

Keppel-Aleks, G., Wennberg, P. O., Washenfelder, R. A., Wunch, D., Schneider, T., Toon, G. C., Andres, R. J., Blavier, J.-F., Connor, B., Davis, K. J., Desai, A. R., Messerschmidt, J., Notholt, J., Roehl, C. M., Sherlock, V., Stephens, B. B., Vay, S. A., and Wofsy, S. C.: The imprint of surface fluxes and transport on variations in total column carbon dioxide, Biogeosciences, 9, 875–891, doi:10.5194/bg-9-875-2012, 2012.

Lelieveld, J., Crutzen, P. J., and Dentener, F. J.: Changing concentration, lifetime and climate forcing of atmospheric methane, Tellus B, 50, 128–150, 1998.

Messerschmidt, J., Geibel, M. C., Blumenstock, T., Chen, H., Deutscher, N. M., Engel, A., Feist, D. G., Gerbig, C., Gisi, M., Hase, F., Katrynski, K., Kolle, O., Lavrič, J. V., Notholt, J., Palm, M., Ramonet, M., Rettinger, M., Schmidt, M., Sussmann, R., Toon, G. C., Truong, F., Warneke, T., Wennberg, P. O., Wunch, D., and Xueref-Remy, I.: Calibration of TCCON column-averaged CO_2: the first aircraft campaign over European TCCON sites, Atmos. Chem. Phys., 11, 10765–10777, doi:10.5194/acp-11-10765-2011, 2011.

Morino, I., Uchino, O., Inoue, M., Yoshida, Y., Yokota, T., Wennberg, P. O., Toon, G. C., Wunch, D., Roehl, C. M., Notholt, J., Warneke, T., Messerschmidt, J., Griffith, D. W. T., Deutscher, N. M., Sherlock, V., Connor, B., Robinson, J., Sussmann, R., and Rettinger, M.: Preliminary validation of column-averaged volume mixing ratios of carbon dioxide and methane retrieved from GOSAT short-wavelength infrared spectra, Atmos. Meas. Tech., 4, 1061–1076, doi:10.5194/amt-4-1061-2011, 2011.

Patra, P. K., Takigawa, M., Dutton, G. S., Uhse, K., Ishijima, K., Lintner, B. R., Miyazaki, K., and Elkins, J. W.: Transport mechanisms for synoptic, seasonal and interannual SF6 variations and "age" of air in troposphere, Atmos. Chem. Phys., 9, 1209–1225, doi:10.5194/acp-9-1209-2009, 2009.

Patra, P. K., Houweling, S., Krol, M., Bousquet, P., Belikov, D., Bergmann, D., Bian, H., Cameron-Smith, P., Chipperfield, M. P., Corbin, K., Fortems-Cheiney, A., Fraser, A., Gloor, E., Hess, P., Ito, A., Kawa, S. R., Law, R. M., Loh, Z., Maksyutov, S., Meng, L., Palmer, P. I., Prinn, R. G., Rigby, M., Saito, R., and Wilson, C.: TransCom model simulations of CH_4 and related species: linking transport, surface flux and chemical loss with CH_4 variability in the troposphere and lower stratosphere, Atmos. Chem. Phys., 11, 12813–12837, doi:10.5194/acp-11-12813-2011, 2011.

Pougatchev, N. S., Connor, B. J., and Rinsland, C. P.: Infrared measurements of the ozone vertical distribution above Kitt Peak, J. Geophys. Res., 100, 16689–16697, 1995.

Reuter, M., Bovensmann, H., Buchwitz, M., Burrows, J., Connor, B. J., Deutscher, N. M., Griffith, D. W. T., Heymann, J., Keppel-Aleks, G., Messerschmidt, J., Notholt, J., Petri, C., Robinson, J., Schneising, O., Sherlock, V., Velazco, V., Warneke, T., Wennberg, P. O., and Wunch, D.: Retrieval of atmospheric CO_2 with enhanced accuracy and precision from SCIAMACHY: Validation with FTS measurements and comparison with model results, J. Geophys. Res., 116, D04301, doi:10.1029/2010JD015047, 2011.

Rigby, M., Prinn, R. G., Fraser, P. J., Simmonds, P. G., Langenfelds, R. L., Huang, J., Cunnold, D. M., Steele, L. P., Krummel, P. B., Weiss, R. F., O'Doherty, S., Salameh, P. K., Wang, H. J., Harth, C. M., Mühle, J., and Porter, L. W.: Renewed growth of atmospheric methane, Geophys. Res. Lett., 35, L22805, doi:10.1029/2008GL036037, 2008.

Rodgers, C. D.: Inverse Methods for Atmospheric Sounding: Theory and Practice, Oceanic and Planetary Physics, edited by: Taylor, F. W., World Scientific, 2000.

Rothman, L. S., Barbe, A., Benner, D. C., Brown, L. R., Camy-Peyret, C., Carleer, M. R., Chance, K., Clerbaux, C., Dana, V., Devi, V. M., Fayt, A., Flaud, J. M., Gamache, R. R., Goldman, A., Jacquemart, D., Jucks, K. W., Lafferty, W. J., Mandin, J. Y., Massie, S. T., Nemtchinov, V., Newnham, D. A., Perrin, A., Rinsland, C. P., Schroeder, J., Smith, K. M., Smith, M. A. H., Tang, K., Toth, R. A., Vander Auwera, J., Varanasi, P., and Yoshino, K.: The HITRAN molecular spectroscopic database: edition of 2000 including updates through 2001, J. Quant. Spectrosc. Ra., 82, 5–44, 2003.

Rothman, L. S., Gordon, I. E., Barbe, A., Benner, D. C., Bernath, P. F., Birk, M., Boudon, V., Brown, L. R., Campargue, A., Champion, J., Chance, K., Coudert, L. H., Dana, V., Devi, V. M., Fally, S., Flaud, J. M., Gamache, R. R., Goldman, A., Jacquemart, D., Kleiner, I., Lacome, N., Lafferty, W. J., Mandin, J., Massie, S. T., Mikhailenko, S. N., Miller, C. E., Moazzen-Ahmadi, N., Nau-

menko, O. V., Nikitin, A. V., Orphal, J., Perevalov, V. I., Perrin, A., Predoi-Cross, A., Rinsland, C. P., Rotger, M., Šimečková, M., Smith, M. A. H., Sung, K., Tashkun, S. A., Tennyson, J., Toth, R. A., Vandaele, A. C., and Vander Auwera, J.: The HITRAN 2008 molecular spectroscopic database, J. Quant. Spectrosc. Ra., 110, 533–572, 2009.

Schneising, O., Bergamaschi, P., Bovensmann, H., Buchwitz, M., Burrows, J. P., Deutscher, N. M., Griffith, D. W. T., Heymann, J., Macatangay, R., Messerschmidt, J., Notholt, J., Rettinger, M., Reuter, M., Sussmann, R., Velazco, V. A., Warneke, T., Wennberg, P. O., and Wunch, D.: Atmospheric greenhouse gases retrieved from SCIAMACHY: comparison to ground-based FTS measurements and model results, Atmos. Chem. Phys., 12, 1527–1540, doi:10.5194/acp-12-1527-2012, 2012.

Sussmann, R. and Borsdorff, T.: Technical Note: Interference errors in infrared remote sounding of the atmosphere, Atmos. Chem. Phys., 7, 3537–3557, doi:10.5194/acp-7-3537-2007, 2007.

Sussmann, R., Stremme, W., Buchwitz, M., and de Beek, R.: Validation of ENVISAT/SCIAMACHY columnar methane by solar FTIR spectrometry at the Ground-Truthing Station Zugspitze, Atmos. Chem. Phys., 5, 2419–2429, doi:10.5194/acp-5-2419-2005, 2005.

Sussmann, R., Forster, F., Rettinger, M., and Jones, N.: Strategy for high-accuracy-and-precision retrieval of atmospheric methane from the mid-infrared FTIR network, Atmos. Meas. Tech., 4, 1943–1964, doi:10.5194/amt-4-1943-2011, 2011.

Sussmann, R., Forster, F., Rettinger, M., and Bousquet, P.: Renewed methane increase for five years (2007–2011) observed by solar FTIR spectrometry, Atmos. Chem. Phys., 12, 4885–4891, doi:10.5194/acp-12-4885-2012, 2012.

Washenfelder, R. A., Toon, G. C., Blavier, J.-F. L., Yang, Z., Allen, N. T., Wennberg, P. O., Vay, S. A., Matross, D. M., and Daube, B. C.: Carbon dioxide column abundances at the Wisconsin Tall Tower site, J. Geophys. Res., 111, 1–11, doi:10.1029/2006JD007154, 2006.

Wunch, D., Wennberg, P., Toon, G., Keppel-Aleks, G., and Yavin, Y.: Emissions of greenhouse gases from a North American megacity, Geophys. Res. Lett., 36, L15810, doi:10.1029/2009GL039825, 2009.

Wunch, D., Toon, G. C., Wennberg, P. O., Wofsy, S. C., Stephens, B. B., Fischer, M. L., Uchino, O., Abshire, J. B., Bernath, P., Biraud, S. C., Blavier, J.-F. L., Boone, C., Bowman, K. P., Browell, E. V., Campos, T., Connor, B. J., Daube, B. C., Deutscher, N. M., Diao, M., Elkins, J. W., Gerbig, C., Gottlieb, E., Griffith, D. W. T., Hurst, D. F., Jiménez, R., Keppel-Aleks, G., Kort, E. A., Macatangay, R., Machida, T., Matsueda, H., Moore, F., Morino, I., Park, S., Robinson, J., Roehl, C. M., Sawa, Y., Sherlock, V., Sweeney, C., Tanaka, T., and Zondlo, M. A.: Calibration of the Total Carbon Column Observing Network using aircraft profile data, Atmos. Meas. Tech., 3, 1351–1362, doi:10.5194/amt-3-1351-2010, 2010.

Wunch, D., Toon, G. C., Blavier, J.-F. L., Washenfelder, R. A., Notholt, J., Connor, B. J., Griffith, D. W. T., Sherlock, V., and Wennberg, P. O.: The Total Carbon Column Observing Network, Philos. T. Roy. Soc. A, 369, 2087–2112, doi:10.1098/rsta.2010.0240, 2011a.

Wunch, D., Wennberg, P. O., Toon, G. C., Connor, B. J., Fisher, B., Osterman, G. B., Frankenberg, C., Mandrake, L., O'Dell, C., Ahonen, P., Biraud, S. C., Castano, R., Cressie, N., Crisp, D., Deutscher, N. M., Eldering, A., Fisher, M. L., Griffith, D. W. T., Gunson, M., Heikkinen, P., Keppel-Aleks, G., Kyrö, E., Lindenmaier, R., Macatangay, R., Mendonca, J., Messerschmidt, J., Miller, C. E., Morino, I., Notholt, J., Oyafuso, F. A., Rettinger, M., Robinson, J., Roehl, C. M., Salawitch, R. J., Sherlock, V., Strong, K., Sussmann, R., Tanaka, T., Thompson, D. R., Uchino, O., Warneke, T., and Wofsy, S. C.: A method for evaluating bias in global measurements of CO_2 total columns from space, Atmos. Chem. Phys., 11, 12317–12337, doi:10.5194/acp-11-12317-2011, 2011b.

A.2 Article II

Andreas Ostler, Ralf Sussmann, Markus Rettinger, Nicholas M. Deutscher, Susanne Dohe, Frank Hase, Nicholas Jones, Mathias Palm, and Björn-Martin Sinnhuber: Multistation intercomparison of column-averaged methane from NDACC and TCCON: impact of dynamical variability, Atmos. Meas. Tech., 7, 4081-4101, doi:10.5194/amt-7-4081-2014, 2014.

Atmos. Meas. Tech., 7, 4081–4101, 2014
www.atmos-meas-tech.net/7/4081/2014/
doi:10.5194/amt-7-4081-2014

Atmospheric Measurement Techniques
Open Access

Multistation intercomparison of column-averaged methane from NDACC and TCCON: impact of dynamical variability

A. Ostler[1], R. Sussmann[1], M. Rettinger[1], N. M. Deutscher[3,4], S. Dohe[2], F. Hase[2], N. Jones[3], M. Palm[4], and B.-M. Sinnhuber[2]

[1]Karlsruhe Institute of Technology, IMK-IFU, Garmisch-Partenkirchen, Germany
[2]Karlsruhe Institute of Technology, IMK-ASF, Karlsruhe, Germany
[3]University of Wollongong, New South Wales, Wollongong, Australia
[4]Institute of Environmental Physics, University of Bremen, Bremen, Germany

Correspondence to: A. Ostler (andreas.ostler@kit.edu)

Received: 10 April 2014 – Published in Atmos. Meas. Tech. Discuss.: 10 July 2014
Revised: 6 October 2014 – Accepted: 21 October 2014 – Published: 3 December 2014

Abstract. Dry-air column-averaged mole fractions of methane (XCH_4) retrieved from ground-based solar Fourier transform infrared (FTIR) measurements provide valuable information for satellite validation, evaluation of chemical-transport models, and source-sink-inversions. In this context, Sussmann et al. (2013) have shown that midinfrared (MIR) soundings from the Network for the Detection of Atmospheric Composition Change (NDACC) can be combined with near-infrared (NIR) soundings from the Total Carbon Column Observing Network (TCCON) without the need to apply an overall intercalibration factor. However, in spite of efforts to reduce a priori impact, some residual seasonal biases were identified, and the reasons behind remained unclear. In extension to this previous work, which was based on multiannual quasi-coincident MIR and NIR measurements from the stations Garmisch (47.48° N, 11.06° E, 743 m a.s.l.) and Wollongong (34.41° S, 150.88° E, 30 m a.s.l.), we now investigate upgraded retrievals with longer temporal coverage and include three additional stations (Ny-Ålesund, 78.92° N, 11.93° E, 20 m a.s.l.; Karlsruhe, 49.08° N, 8.43° E, 110 m a.s.l.; Izaña, 28.31° N, 16.45° W, 2.370 m a.s.l.). Our intercomparison results (except for Ny-Ålesund) confirm that there is no overall bias between MIR and NIR XCH_4 retrievals, and all MIR and NIR time series reveal a quasi-periodic seasonal bias for all stations, except for Izaña.

We find that dynamical variability causes MIR–NIR differences of up to ∼ 30 ppb (parts per billion) for Ny-Ålesund, ∼ 20 ppb for Wollongong, ∼ 18 ppb for Garmisch, and ∼ 12 ppb for Karlsruhe. The mechanisms behind this variability are elaborated via two case studies, one dealing with stratospheric subsidence induced by the polar vortex at Ny-Ålesund and the other with a deep stratospheric intrusion event at Garmisch. Smoothing effects caused by the dynamical variability during these events are different for MIR and NIR retrievals depending on the altitude of the perturbation area. MIR retrievals appear to be more realistic in the case of stratospheric subsidence, while NIR retrievals are more accurate in the case of stratosphere–troposphere exchange (STE) in the upper troposphere/lower stratosphere (UTLS) region. About 35 % of the FTIR measurement days at Garmisch are impacted by STE, and about 23 % of the measurement days at Ny-Ålesund are influenced by polar vortex subsidence. The exclusion of data affected by these dynamical situations resulted in improved agreement of MIR and NIR seasonal cycles for Ny-Ålesund and Garmisch.

We found that dynamical variability is a key factor in constraining the accuracy of MIR and NIR seasonal cycles. To mitigate this impact it is necessary to use more realistic a priori profiles that take these dynamical events into account (e.g., via improved models), and/or to improve the FTIR retrievals to achieve a more uniform sensitivity at all altitudes (possibly including profile retrievals for the TCCON data).

Published by Copernicus Publications on behalf of the European Geosciences Union.

1 Introduction

Atmospheric methane (CH_4) is the most important anthropogenic greenhouse gas after carbon dioxide. The radiative forcing (RF) from emissions of CH_4 for 2011 relative to the preindustrial time (1750) is $0.97\,W\,m^{-2}$ reflecting a significant contribution to the total anthropogenic RF of $2.29\,W\,m^{-2}$ (Stocker et al., 2013). There is a diverse range of sources of CH_4 emissions from the Earth, coming from biogenic, thermogenic, and pyrogenic formation processes. Among these three groups there are several sources that are driven by anthropogenic activities (livestock breeding, rice cultivation, and exploitation of fossil fuels), whereas other main sources of CH_4 are not directly influenced by humans (natural wetlands, biomass burning, termites). However, there are large positive CH_4 feedbacks on climate warming such as increased emissions from wetlands and melting hydrates (Dlugokencky et al., 2011). The latter process has attracted special interest because a fast CH_4 release from the insulated hydrate reservoir would cause a massive warming effect within a few years (Archer, 2007).

Oxidation of atmospheric CH_4 by hydroxyl radicals (OH) is responsible for about 90 % of the global CH_4 sink. The remainder is absorbed by soils and by reactions with atomic and chlorine radicals in the stratosphere (Cicerone and Oremland, 1988). Another minor oxidation sink is the reaction with chlorine radicals in the marine boundary layer (Allan et al., 2007).

As a consequence of an imbalance between CH_4 sources and sinks, the global CH_4 surface concentration has increased to ~ 1803 ppb (parts per billion) in 2011, thereby exceeding the preindustrial levels by about 150 % (Stocker et al., 2013). Attributing the changes of atmospheric CH_4 to source variations on historical timescales (Houweling et al., 2008; Sapart et al., 2012) as well as in the recent past (Bousquet et al., 2006, 2011; Kirschke et al., 2013) has been the subject of extensive research, but is still associated with uncertainties. The ability to locate CH_4 emissions (anthropogenic and natural) on regional scales will be essential for future climate policy with regard to emission trading schemes. For this purpose, it is necessary to reduce the transport uncertainties of inversions. Furthermore, it is mandatory to increase the network of CH_4 observations and to improve the accuracy of CH_4 measurements. Indeed, the spatiotemporal coverage of atmospheric CH_4 measurements has been consistently improved since the early 1980s (Kirschke et al., 2013). Global networks for surface-based in situ measurements (i.e., Advanced Global Atmospheric Gases Experiment, AGAGE, and network of National Oceanic and Atmospheric Administration, Earth System Research Laboratory, Global Monitoring Division, NOAA ESRL GMD) have been developed and airborne measurements in the free troposphere have been performed (e.g., Wofsy et al., 2011). Furthermore, remote-sensing measurements of CH_4 columns have been achieved by satellite instruments such as SCIAMACHY (Scanning Imaging Absorption Spectrometer for Atmospheric Cartography) aboard Envisat (Environmental Satellite) and TANSO (Thermal And Near-infrared Sensor for carbon Observation) on GOSAT (Greenhouse Gases Observing Satellite). The ground-based equivalents of the satellite observations are represented by the high-precision Fourier-transform infrared (FTIR) measurements of the two established networks NDACC (Network for the Detection of Atmospheric Composition Change, http://www.ndacc.org/) and TCCON (Total Carbon Column Observing Network, http://www.tccon.caltech.edu/; Wunch et al., 2011a), since both measure the same quantity as satellites.

Because of their high accuracy for column-integrated CH_4 measurements, both TCCON (Butz et al., 2011; Schneising et al., 2012; Yoshida et al., 2013; Fraser et al., 2013) and NDACC (Sussmann et al., 2005; De Mazière et al., 2008) data have been used for satellite validation. Satellite retrievals are used extensively in top-down estimates of CH_4 emissions (Bergamaschi et al., 2009, 2013; Fraser et al., 2013; Monteil et al., 2013; Houweling et al., 2014), therefore, NDACC/TCCON FTIR retrievals have a strong indirect influence on the accuracy of inversions. In addition, ground-based FTIR measurements can be directly utilized for validation of models (Houweling et al., 2010; Saito et al., 2012; Belikow et al., 2013) and inversions (Fraser et al., 2013). Thus, it is obvious that ground-based FTIR retrievals of column-averaged CH_4 are a cornerstone for satellite retrievals, chemical transport models and inverse models.

By comparing column-averaged dry-air mole fractions of methane (XCH_4) from NDACC and TCCON retrieved at the sites Garmisch (47.5° N) and Wollongong (34.5° S), Sussmann et al. (2013) showed that the data from both networks can be directly combined without performing an intercalibration. Because of its wider spatial and temporal coverage such a joint data set can provide major benefits for validation as well as for long-term trend analysis. However, the agreement obtained between NDACC and TCCON retrievals was not perfect despite applying a refined intercomparison strategy accounting for differing a priori profiles and averaging kernels. The reasons for these residual differences remained unexplained from this previous study.

In this paper we extend the previous work by Sussmann et al. (2013) by updating the FTIR time series and including three additional stations (Ny-Ålesund, 78.9° N, Karlsruhe, 49.1° N, and Izaña, 28.3° N), thereby covering diverse geophysical conditions. Besides the intercomparison of NDACC and TCCON measurements, the main focus of this study is understanding the impact of dynamical effects such as stratospheric subsidence and stratosphere–troposphere exchange (STE) processes on the residual differences observed between NDACC and TCCON retrievals of CH_4.

Our paper is structured as follows: the participating FTIR sites and their measurement settings are introduced in Sect. 2 along with the MIR (midinfrared) and NIR (near-infrared) retrieval strategies. After explaining the intercomparison strat-

Table 1. The FTIR stations of this NDACC versus TCCON intercomparison of XCH_4, along with geographical coordinates and the time period of FTIR measurements used.

Site	latitude	longitude	altitude	time period
Garmisch	47.48° N	11.06° E	0.743 km	07/2007–12/2012
Wollongong	34.41° S	150.88° E	0.030 km	06/2008–12/2012
Izaña	28.31° N	16.45° W	2.370 km	12/2010–12/2012
Karlsruhe	49.08° N	8.43° E	0.110 km	04/2010–12/2012
Ny-Ålesund	78.92° N	11.93° E	0.020 km	03/2005–08/2012

egy the corresponding results are shown in Sect. 3. Section 4 investigates in quantitative terms the impact of dynamical variability on residual differences between MIR and NIR retrievals. This is performed via analysis of one case study showing strong stratospheric subsidence induced by the polar vortex at Ny-Ålesund and another case study for a deep stratospheric intrusion event above Garmisch. Section 5 discusses what can be done to mitigate the impact of stratospheric variability. Finally, Sect. 5 gives a summary and conclusions.

2 Ground-based soundings of columnar methane in the MIR and NIR

The NDACC Infrared Working Group currently consists of 22 sites with measurements dating back up to 2 decades. The NDACC retrievals are obtained from solar absorption spectra recorded in the MIR spectral range. Since the establishment of TCCON in 2004, solar absorption measurements in the NIR have started to provide high-precision retrievals of climate gases, such as CO_2, CH_4, and N_2O (Wunch et al., 2011a). Today, there are around 20 operational TCCON sites.

The observational data set obtained from ground-based solar absorption measurements at Garmisch and Wollongong is extended by 1 year from the previous study of Sussmann et al. (2013), until the end of 2012. Additionally, the intercomparison data set is supplemented by FTIR measurements from three further sites (Ny-Ålesund, Karlsruhe, Izaña), thereby covering diverse geophysical conditions (Table 1). The solar FTIR systems of the individual sites are described in Appendix A. The intercomparison of MIR and NIR measurements requires that both MIR and NIR observations are performed in alternating mode.

For the analysis of NDACC- and TCCON-type measurements we used the spectral fitting software SFIT (or PROFFIT) and GFIT, respectively (Pougatchev et al., 1995; Hase et al., 2004; Wunch et al., 2011a). The MIR and NIR retrieval strategies are identical to the strategies used in Sussmann et al. (2013), with the exception of the update from GFIT v.4.4.10 to GFIT v.4.8.6 (GGG2012) which now includes the use of site- and time-dependent a priori profiles. The retrieval strategy MIR-GBM v1.1 (Sussmann et al., 2011) is used for retrieving XCH_4 from measurements in the midinfrared spectral region (2613–2921 cm^{-1}). Within SFIT (or PROFFIT) a full profile retrieval is set up using a Tikhonov L1 regularization with an altitude-constant regularization strength applied to an a priori profile given in relative units (percent scale). One fixed a priori volume mixing ratio (vmr) profile is used per site, derived from the Whole Atmosphere Chemistry Climate Model (WACCM, version 5, 40-year run; Garcia et al., 2007). The MIR XCH_4 is calculated by dividing the retrieved total column by the corresponding dry pressure column. To obtain the daily dry pressure column we used the NCEP (National Center for Environmental Prediction) pressure–temperature–humidity profile from 12:00 UT (universal time) for calculating the air column and water vapor column.

For the NIR retrievals GFIT uses an iterative method of scaling the a priori profile to provide the best fit to the measured spectrum in the near-infrared spectral region (5938–6076 cm^{-1}). The retrieved total column is divided by the dry pressure column derived from the simultaneously measured oxygen column (Wunch et al., 2011a) and subsequently scaled by the calibration factor 0.976. This calibration is used to account for spectroscopic uncertainties and was determined from various campaigns using coincident airborne in situ measurements calibrated to the WMO scale (Wunch et al., 2010; Geibel et al., 2012). The 2σ uncertainty of the calibration factor is $\sim 0.2\,\%$ and can be regarded as the accuracy of TCCON XCH_4. In contrast to that, MIR retrievals are used without calibration, but are optimized to reduce the seasonal bias due to H_2O dependence to $< 0.14\,\%$. The precision of MIR and NIR retrievals estimated on 1σ diurnal variation is $< 0.3\,\%$.

For the MIR retrievals we used HITRAN (HIgh-resolution TRANsmission molecular absorption database) 2000 including the 2001 update release (Rothman et al., 2003). For the NIR retrievals GFIT uses line lists which are based on HITRAN 2004 (Rothman et al., 2004), and HITRAN 2008 (Rothman et al., 2009) including an update by Frankenberg et al. (2008). Further details of the retrieval strategies can be found in Sussmann et al. (2013).

Note that the MIR measurements of Karlsruhe and Izaña were analyzed with the retrieval code PROFFIT instead of SFIT. Differences in these codes are not expected to have an impact on the MIR retrievals as shown by Hase et al. (2004).

3 Intercomparison

3.1 Method

In addition to the direct intercomparison of MIR and NIR retrievals obtained with their individual retrieval a priori profiles, we will also investigate the intercomparison results after reducing the impact of differing a priori profiles of the MIR versus NIR retrievals. This is achieved by the intercomparison strategy proposed by Sussmann et al. (2013);

see Eq. (1) therein. This strategy applies two crucial benefits: (i) effects from differing a priori profiles are eliminated by an a posteriori adjustment of the soundings to a common a priori profile $\boldsymbol{x}_{\text{common}}$; and (ii) differing smoothing terms caused by the differing averaging kernels are minimized by using time-dependent and site-dependent profiles $\boldsymbol{x}_{\text{common}}$ that are as close as possible to the true profile $\boldsymbol{x}_{\text{true}}$ at a site at the moment of observation. As in Sussmann et al. (2013) we use 3-hourly sampled CH_4 model profiles for $\boldsymbol{x}_{\text{common}}$. The model profiles are provided by the Center for Climate System Research/National Institute for Environmental Studies/Frontier Research Center for Global Change (CCSR/NIES/FRCGC) atmospheric general circulation model (AGCM) based chemical transport model (CTM) (hereafter, ACTM; Patra et al., 2009, 2011). The ACTM simulations are operated at T42 spectral truncation in the horizontal and 67 vertical levels reaching from Earth's surface to the mesosphere (80 km). See Appendix B in Sussmann et al. (2013) for more details on the ACTM profiles.

Although the use of Eq. (1) in Sussmann et al. (2013) eliminates the impact of differing a priori profiles, differences (MIR–NIR) can still arise because of different vertical sensitivities for both retrievals. The smoothing term for the MIR retrieval is $(1-\boldsymbol{a}^l_{\text{MIR}})\ (\boldsymbol{x}^l_{\text{common}}-\boldsymbol{x}^l_{\text{true}})$, where $\boldsymbol{a}^l_{\text{MIR}}$ is the total column averaging kernel of the MIR retrieval for model layer l. The analogous smoothing term for the NIR retrieval $(1-\boldsymbol{a}^l_{\text{NIR}})\ (\boldsymbol{x}^l_{\text{common}}-\boldsymbol{x}^l_{\text{true}})$ is different because in general it holds that $\boldsymbol{a}^l_{\text{MIR}} \neq \boldsymbol{a}^l_{\text{NIR}}$. This aspect is crucial for understanding the origin of possible residual XCH_4 differences (NIR–MIR). The magnitude of such residual XCH_4 differences (MIR–NIR) depends on the season because the averaging kernels show zenith angle dependence and, therefore, a seasonal behavior, shown in Fig. 2 in Sussmann et al. (2013). This seasonality of residuals will be discussed in Sect. 3.2 below. The differences are largest when the model differs the most from the true atmospheric profile, which is most likely to occur in special atmospheric situations. Examples for this can be cases with strong stratospheric subsidence or stratospheric intrusions. Case studies that illustrate this effect will be discussed in quantitative terms in Sect. 4.

The intercomparison is based on monthly means calculated from individual MIR and NIR measurements recorded on the same day. Only months with >5 MIR and >5 NIR measurements have been included. The criterion of daily coincidence ensures that the results of the monthly mean intercomparison will also reflect the agreement between NIR and MIR retrievals on daily and shorter timescales.

3.2 Results

Figure 1a shows a scatter plot of the MIR and NIR monthly means containing data from all five FTIR sites as retrieved with their original retrieval a priori profiles. Error bars on data points are 2σ uncertainties derived from the standard deviation (SD) of the linear slope fit ($2\ \text{SD}/\sqrt{2}$) determined

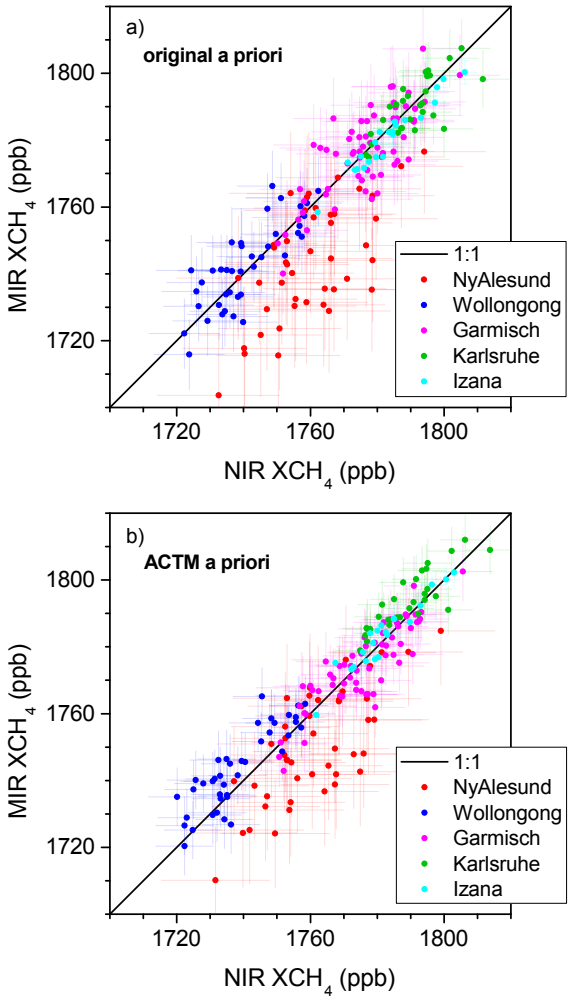

Figure 1. (a) Scatter plot of MIR and NIR monthly means, both series retrieved with the standard retrieval a priori profiles. Error bars on data points are 2σ uncertainties derived from the SD of the linear slope fit ($2\ \text{SD}/\sqrt{2}$). **(b)** Same as **(a)** but for using ACTM profiles as common prior.

separately for each site, see Sussmann et al. (2013) for a discussion of this error characterization. The linear MIR/NIR slopes and their corresponding 2σ uncertainties are obtained from linear fits forced through zero. Consecutively, the slope uncertainty is illustrated behind the slope value in brackets corresponding to the third and fourth decimal place of the slope value. The linear MIR/NIR slopes (obtained from linear fits forced through zero) are not significantly different from 1 for three stations; i.e., 1.0002(12) for Garmisch, 1.0010(13) for Wollongong and 0.9996(13) for Karlsruhe, see Table 2. However, they are significantly different from 1 for Izaña (0.9986(06)) and for Ny-Ålesund (0.9909(22)). The slope for Izaña corresponds to a small bias in XCH_4 (1.4 ‰) whereas there is a relatively big bias for Ny-Ålesund of 9.1 ‰. This means that the results of the direct intercomparison confirm the conclusion of Sussmann et al. (2013), that

the MIR and NIR data sets could be used together without the need of an intercalibration (except for Ny-Ålesund; possible reasons will be discussed in Sect. 4).

Figure 1b is the same as Fig. 1a but using ACTM profiles as common prior. The linear MIR/NIR slopes (obtained from linear fits forced through zero) are not significantly different from 1 for Garmisch (0.9994(09)) and Izaña (1.0007(07)). However, the MIR/NIR slopes are different from 1 for Karlsruhe (1.0024(11)), Wollongong (1.0030(11)), and Ny-Ålesund (0.9940(19)). It is not obvious that there is a significant improvement in the overall agreement of the MIR and NIR XCH_4 monthly means after the adjustment to the common prior, except at Ny-Ålesund, where the difference of the linear slope from 1 is reduced (from 0.9909(22) to 0.9940(19)) corresponding to a bias of 6 ‰. However, as explained in Sussmann et al. (2013) the main benefit of using the common ACTM a priori is that the seasonalities of the MIR and NIR XCH_4 time series are in a better agreement.

The MIR and NIR monthly mean time series for all stations are shown in Fig. 2a–j, retrieved with both their original retrieval a priori profiles and with the common ACTM prior profile. It can be seen that for all stations except Izaña the SD of the difference time series (Fig. 2a–j, upper trace) is reduced by using the ACTM profiles as common prior. For Izaña there is no reduction of the SD (Fig. 2j) because the MIR and NIR time series are already in very good agreement (SD = 2.5 ppb) without applying the a posteriori adjustment to a common a priori profile (Fig. 2i). This is probably due to generally favorable measurement conditions at Izaña with a high fraction of days with unperturbed clear sky conditions. An overview of all SDs and MIR/NIR slopes is given in Table 2.

Although the use of ACTM as a common prior leads to an improved agreement between MIR and NIR XCH_4, there are still differences which can reach levels of up to 30 ppb for Ny-Ålesund (Fig. 2b), 20 ppb for Wollongong (Fig. 2d), 18 ppb for Garmisch (Fig. 2f), and 12 ppb for Karlsruhe (Fig. 2h). Furthermore, Fig. 2 shows a periodicity in the occurrence of the maximum differences at all stations except Izaña.

A principal explanation for such seasonal differences (MIR–NIR) has been given in Sect. 3.1; i.e., ACTM profiles cannot completely resolve the local dynamical variability caused by atmospheric processes such as stratospheric subsidence or stratosphere–troposphere exchange processes. In order to investigate this effect in quantitative terms, in the following section we present a case study of stratospheric subsidence induced by the polar vortex at Ny-Ålesund and another case study of a deep stratospheric intrusion event at Garmisch. In addition to that, in Sect. 5 we discuss the potential of different methods to mitigate the impact caused by stratospheric variability.

4 Effects of dynamical variability

4.1 Impact of subsidence

The motivation for this case study is to demonstrate and explain the effects of polar subsidence on the MIR and NIR retrievals (Sect. 4.1.1). Furthermore, the total impact on the intercalibration results for Ny-Ålesund is inferred by excluding FTIR measurements that are affected by polar vortex subsidence (Sect. 4.1.2).

4.1.1 Case study I: Ny-Ålesund on 25 March 2011

As shown by Lindenmaier et al. (2012) and Sinnhuber et al. (2011) the meteorological conditions during winter/spring 2011 formed a strong polar vortex that persisted into April. Besides that, high potential vorticity (PV) values of 46 PVU (potential vorticity unit) on the 450 K potential temperature (PT) surface (ECMWF reanalysis, European Centre for Medium-Range Weather Forecasts) strongly indicate that Ny-Ålesund was underneath the area of the polar vortex on 25 March 2011.

Therefore, we investigate the impact of replacing the ACTM-based a priori profile with a strongly subsided CH_4 profile, which is typical for intravortex conditions and may be more realistic for 25 March 2011 above Ny-Ålesund. Such a profile (labeled MIR a $priori_{subsided}$) is given in Fig. 3a along with the ACTM profile for 25 March 2011 and the standard retrieval a priori profiles. This subsided profile corresponds to the MIR standard retrieval a priori from WACCM, which has been modified to account for subsidence according to Toon et al. (1992), see Appendix B for details.

Figure 4 shows the MIR and NIR XCH_4 as computed using the original ACTM as common prior along with the case using MIR a $priori_{subsided}$. It can be seen that in the case of using the original ACTM as a common prior, there is a significant difference between the NIR and MIR retrievals ($\sim$ 29 ppb for the time period 08:00–10:00 UT), while there is good agreement if using the subsided profile MIR a $priori_{subsided}$ (mean difference of $\sim$ 6 ppb for the time period 08:00–10:00 UT). Most of the difference arises from the fact that the NIR data based on the ACTM prior profile are reduced by $\sim$ 31 ppb (for the time interval 08:00–10:00 UT) if MIR a $priori_{subsided}$ is used instead. For the MIR data the reduction due to the use of MIR a $priori_{subsided}$ is only $\sim$ 8 ppb. This is due to the fact that the NIR total column kernels are not as sensitive as the MIR total column kernels in the lower stratosphere (see Fig. 3b). Figure C1 shows an analogous plot with the MIR and NIR retrievals based on their original standard a priori profiles. The effect of using the subsided profile (MIR a $priori_{subsided}$) instead of the original standard retrieval a priori profiles is very similar to the effect described with regard to Fig. 4; i.e., the difference between the NIR and MIR retrievals is reduced from $\sim$ 37 to $\sim$ 6 ppb (for the time period 08:00–10:00 UT). Furthermore, MIR and NIR retrievals

Table 2. Slope of linear scatter plot fits between multiannual data sets of NIR and MIR XCH_4 retrievals using varied a priori profiles. Slope uncertainties are derived from the fit and are at 2σ. The slope uncertainty is illustrated in brackets corresponding to the third and fourth decimal place of the slope value; i.e., (12) implies a slope uncertainty of ± 0.0012. Standard deviations of NIR–MIR differences are provided as SD. Data are monthly means constructed from same-day measurement coincidences.

		fit $y = bx$		
Data set	a priori	slope b and 2σ uncertainty	slope different from 1 on 2σ level?	SD (ppb)
Garmisch	NIR & MIR retrieved with original a priori	1.0002(12)	no	8.6
	NIR & MIR corrected to ACTM a priori	0.9994(09)	no	6.3
Wollongong	NIR & MIR retrieved with original a priori	1.0010(13)	no	7.4
	NIR & MIR corrected to ACTM a priori	1.0030(11)	yes	6.1
Izaña	NIR & MIR retrieved with original a priori	0.9986(06)	yes	2.5
	NIR & MIR corrected to ACTM a priori	1.0007(07)	no	3.0
Karlsruhe	NIR & MIR retrieved with original a priori	0.9996(13)	no	6.1
	NIR & MIR corrected to ACTM a priori	1.0024(11)	yes	5.1
Ny-Ålesund	NIR & MIR retrieved with original a priori	0.9909(22)	yes	13.0
	NIR & MIR corrected to ACTM a priori	0.9940(19)	yes	11.5

are reduced by 4 and 35 ppb, respectively, compared to the standard a priori profiles.

Our case study for Ny-Ålesund shows in quantitative terms that the effect of polar subsidence on $(\boldsymbol{x}^l_{\text{common}} - \boldsymbol{x}^l_{\text{true}})$ can be high enough to significantly impact the accuracy of the MIR and NIR retrievals in a different way. Especially, the NIR retrievals are significantly affected when using a priori profiles which do not account for stratospheric subsidence, because their averaging kernels are less sensitive in the stratosphere.

4.1.2 Exclusion of subsidence events

While the case study in Sect. 4.1.1 was focused on the different impacts of stratospheric subsidence on the MIR and NIR retrievals for a single day, we now investigate the overall impact of subsidence on the full Ny-Ålesund time series used for the intercomparison of MIR and NIR XCH_4 retrievals.

To identify the location of the polar vortex and the onset and breakup dates of the vortex, we used the criteria from Nash et al. (1996). Thereby, we determined if Ny-Ålesund was inside the vortex or not at the 450 K potential temperature level (about 18 km altitude). Figure 5 shows the number of FTIR measurement days at Ny-Ålesund that were influenced by the polar vortex together with the total number of FTIR measurement days, separated by year. As FTIR measurements (MIR and NIR) at Ny-Ålesund are typically performed from the middle of March until the end of September, the overlap time with the polar vortex period is limited to early spring. We found that the relative fraction of FTIR measurement days influenced by the polar vortex is $\sim 63\,\%$ in March and $\sim 57\,\%$ in April (averaged for the time period 2005–2012).

All in all, 23 % of the FTIR measurement days were influenced by the polar vortex. These days were excluded from the MIR/NIR intercomparison and monthly mean scatter plots (MIR versus NIR) were analyzed via linear fits. The parameters from these fits are listed in Table 3. The linear MIR/NIR slope of the data set that is corrected to ACTM as common prior is improved slightly from 0.9940(19) to 0.9950(20) and the SD is further reduced from 11.5 to 11.0 ppb.

Despite these slightly positive effects of the exclusion of polar vortex situations on the overall intercomparison, there are still significant residual XCH_4 differences (MIR–NIR) for Ny-Ålesund, which vary temporally (see Fig. C2). Hence, we speculate that deviations of the ACTM profiles from the true profiles in the stratosphere also occur outside the early spring period. Indeed, besides subsidence, there are further dynamical processes in the UTLS (upper troposphere/lower stratosphere) region that may contribute to a variability of the CH_4 profile not captured by ACTM. This assumption is supported by the fact that the residual XCH_4 differences from the stations Garmisch, Wollongong, and Karlsruhe cannot be linked to the polar vortex subsidence because of their geographical position. Therefore, the emphasis of Sect. 4.2 lies on the impact of dynamical variability caused by STE processes. Moreover, systematic deviations of the a priori profiles in the stratospheric CH_4 could also act as a source for smoothing effects.

4.2 Impact of stratosphere–troposphere exchange processes

STE processes cause the transport of air-masses across the tropopause. For a detailed overview of the extensive research

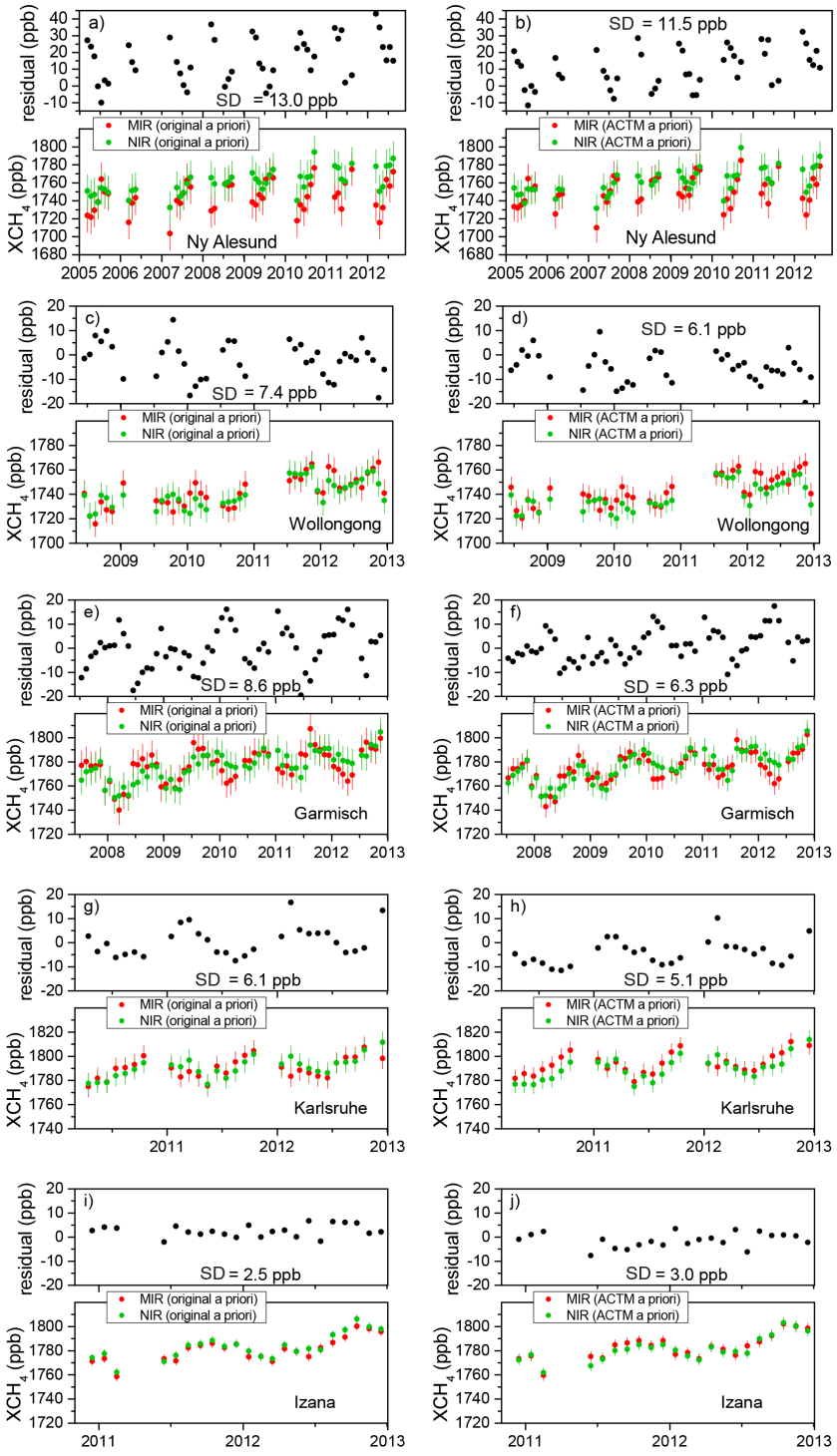

Figure 2. (a) Lower trace: monthly-mean MIR and NIR time series for Ny-Ålesund. Both column series are plotted as retrieved with their original retrieval a priori profiles. Error bars are 2σ uncertainties as explained in Fig. 1. Upper trace: residual time series; i.e., difference time series of the NIR and MIR data shown in the lower trace. **(b)** Same as **(a)** but using for Ny-Ålesund a correction to 3-hourly ACTM profiles as common prior, **(c)** for Wollongong the original retrieval a priori profiles, **(d)** for Wollongong a correction to ACTM, **(e)** for Garmisch the original retrieval a priori profiles, **(f)** for Garmisch a correction to ACTM, **(g)** for Karlsruhe the original retrieval a priori profiles, **(h)** for Garmisch a correction to ACTM, **(i)** for Izaña the original retrieval a priori profiles, and **(j)** for Izaña a correction to ACTM.

Table 3. As Table 2, but only for Ny-Ålesund. The data set "Ny-Ålesund PV filter" corresponds to MIR and NIR retrievals that are not influenced by the polar vortex.

Data set	a priori	fit $y = bx$		
		slope b and 2σ uncertainty	slope different from 1 on 2σ level?	SD (ppb)
Ny-Ålesund	NIR & MIR retrieved with original a priori	0.9909(22)	yes	13.0
Ny-Ålesund PV filter	NIR & MIR retrieved with original a priori	0.9922(23)	yes	12.4
Ny-Ålesund	NIR & MIR corrected to ACTM a priori	0.9940(19)	yes	11.5
Ny-Ålesund PV filter	NIR & MIR corrected to ACTM a priori	0.9950(20)	yes	11.0

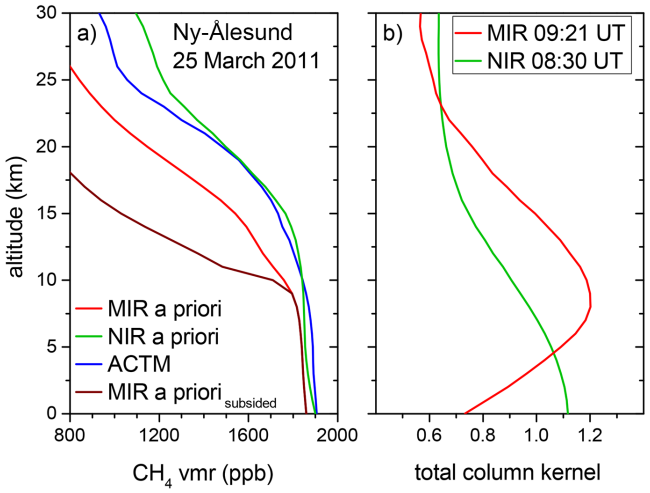

Figure 3. (a) A priori profiles used for analysis of Ny-Ålesund spectra recorded on 25 March 2011. MIR a priori is the standard a priori profile from WACCM for Ny-Ålesund used in SFIT. NIR a priori is the current a priori profile of GFIT (release ggg_2012_July_Update) for Ny-Ålesund. ACTM is the actual ACTM profile for 25 March 2011 used as a common prior for standard intercomparison of the NIR and MIR retrievals. MIR a $\text{priori}_{\text{subsided}}$ is a strongly subsided profile typical for intravortex conditions as explained in Appendix B used for recorrection of the NIR and MIR retrievals in a more realistic intercomparison. **(b)** Averaging kernels for MIR and NIR retrievals using Ny-Ålesund spectra recorded on 25 March 2011.

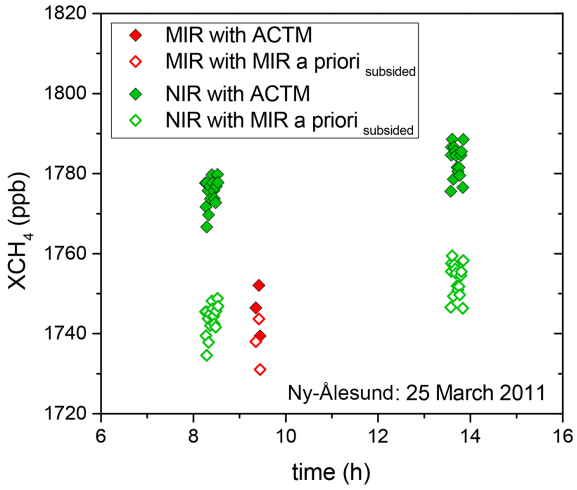

Figure 4. Ny-Ålesund XCH_4 on 25 March 2011 retrieved from FTIR data. MIR and NIR retrievals are corrected to the common ACTM prior (filled squares) and are corrected to a strongly subsided MIR a priori profile (open squares) as shown in Fig. 3a.

related to STE processes with some focus on processes in the extratropics we refer to Stohl et al. (2003). A considerable part of STE research dealt with the impacts of STE on the tropospheric ozone (O_3) budget due to its relevance to air quality (Stohl and Trickl, 1999; Stohl et al., 2000; Trickl et al., 2003, 2010). Recently, by using a high-resolution chemical transport model Lin et al. (2012) were able to show that stratospheric intrusions in springtime of 2010 significantly increased surface ozone at high-elevation western US sites.

Whereas ozone-related STE processes have been well studied, the impact of STE processes on the CH_4 budget has not been investigated very much. Nevertheless, by observing a stratospheric intrusion event on 27 March 2010, Xiong et al. (2013) revealed that areas with depleted CH_4 are collocated with enhanced O_3 and low tropopause. They analyzed data from Atmospheric Infrared Sounder (AIRS) retrievals and used aircraft in situ measurements that confirmed that CH_4 depletion occurred down to 550 hPa with a decrease in mixing ratios of up to 100 ppb.

In order to investigate the (possibly differing) impact of STE processes on MIR and NIR retrievals of XCH_4, Sect. 4.2.1 deals with a stratospheric intrusion event on 6 March 2008 at Garmisch. After that, the aim of Sect. 4.2.2 is to estimate the percentage of FTIR measurements that are affected by STE processes, and to identify the consequences for the intercomparison of MIR and NIR retrievals at Garmisch.

4.2.1 Case study II: Garmisch on 6 March 2008

Figure 6a shows the single MIR and NIR XCH_4 values on 6 March 2008 as computed with the a posteriori adjustment to the common ACTM prior. It is obvious that the agreement

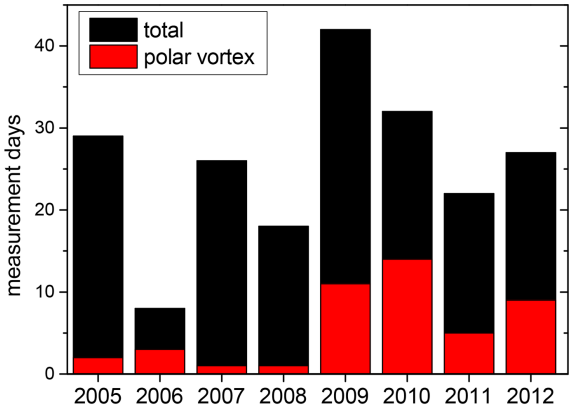

Figure 5. Number of days with coincident MIR and NIR FTIR measurements at Ny-Ålesund. Black: total number; red: only measurement days when the station has been inside the polar vortex.

between MIR and NIR XCH_4 is very good until 11:00 UTC (universal time coordinated), but then the NIR XCH_4 increases by about 25 ppb within 1 h. In contrast to that, the MIR XCH_4 increases only slightly, and this results in high XCH_4 residuals (NIR–MIR $\sim$ 15 ppb).

We will show in the following that this significant increase in XCH_4 differences within a short timescale of 1 h is caused by a deep stratospheric intrusion event that was observed by the tropospheric ozone lidar at Garmisch. Details and illustrations of lidar sounding series detecting stratospheric intrusions very similar to our 6 March 2008 case can be found, e.g., in Trickl et al. (2010). The lidar sounding series of 6 March 2008 (Trickl et al., 2014) points to the occurrence of various layers with elevated ozone levels generated by a stratospheric intrusion. Until 11:00 UTC, there is one layer existing approximately in the altitude range of 2–4 km and a second layer in the range of 6–10 km. Both regions are characterized by enhanced O_3 volume mixing ratios (typically up to 125 ppb). These layers with elevated ozone concentrations correspond to areas of depleted CH_4 volume mixing ratios. According to the lidar sounding, after 11:00 UTC there remains only one layer with ozone-rich air masses, i.e., CH_4-depleted air masses in the UTLS region (8–15 km).

To respond to the dynamical variability induced by the stratospheric intrusion the MIR and NIR retrievals were recorrected (Fig. 6b). The ACTM profiles were modified in a simple manner to represent the depletion of CH_4 before 11:00 UTC ($ACTM_{intrusion1}$) and after 11:00 UTC ($ACTM_{intrusion2}$). The magnitudes of the CH_4 depletions used in Fig. 7a correspond to typical values reported in the study by Xiong et al. (2013).

The transformation of O_3 lidar soundings into CH_4 profiles is just a semiquantitative approach. However, the recorrection of the MIR and NIR retrievals to the modified ACTM a priori profiles of Fig. 7a results in a nearly perfect agreement between MIR and NIR XCH_4 as shown

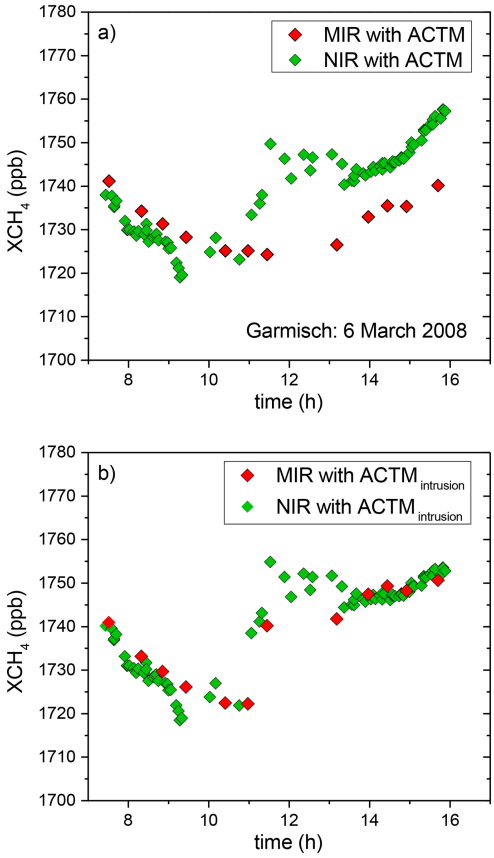

Figure 6. Garmisch XCH_4 on 6 March 2008 retrieved from FTIR data. **(a)** MIR and NIR retrievals are corrected to a common ACTM a priori. **(b)** MIR and NIR retrievals are corrected to the modified ACTM profiles shown in Fig. 7a.

in Fig. 6b. The recorrection effect on the NIR retrievals is small (< 5 ppb) because the NIR total column retrievals shows high sensitivity in the troposphere and the lowest stratosphere (see Fig. 7b). The effect on the MIR retrievals, however, is twofold: Although the MIR total column kernels are not perfectly sensitive in the troposphere (Fig. 7b) there is almost no recorrection effect on the MIR retrievals until 11:00 UTC. This is because of two smoothing effects, which compensated each other before the recorrection was applied. The lower-layer CH_4 depletion (Fig. 7a, $ACTM_{intrusion1}$, 2–4 km) was underestimated (see MIR averaging kernel in Fig. 7b) while the upper-layer CH_4 depletion (Fig. 7a, $ACTM_{intrusion1}$, 6–10 km) was overestimated (see MIR averaging kernel in Fig. 7b). Therefore, there was no net effect on the MIR retrievals before 11:00 UTC. However, after 11:00 UTC, MIR XCH_4 was significantly lower than NIR XCH_4 because of an overestimation of the CH_4 depletion in the UTLS region (Fig. 7a, $ACTM_{intrusion2}$, 8–15 km; see MIR averaging kernel in Fig. 7b). The recorrection effect on MIR retrievals after 11:00 UTC corresponds to an increase in XCH_4 of up to 15 ppb. All together, we are able to explain

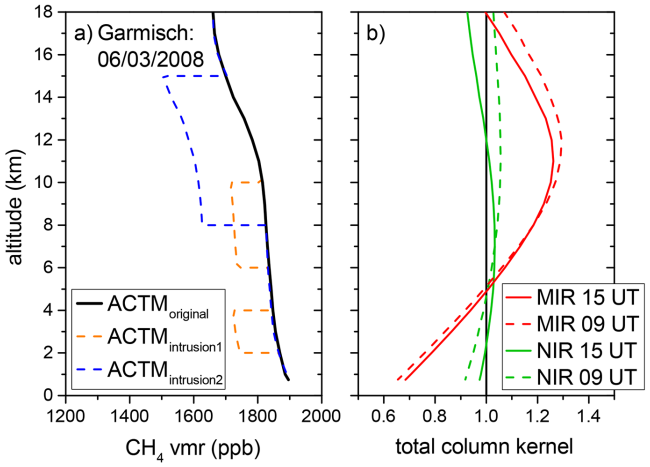

Figure 7. (a) ACTM profiles used for the a posteriori correction of MIR and NIR retrievals of Garmisch spectra recorded on 6 March 2008: $ACTM_{original}$ is the original ACTM profile used in the correction. $ACTM_{intrusion1}$ and $ACTM_{intrusion2}$ are the original ACTM profiles which were modified due to a deep stratospheric intrusion event on this day. $ACTM_{intrusion1}$ is used for the recorrection of retrievals before 11:00 UTC, $ACTM_{intrusion2}$ is used for the recorrection of retrievals after 11:00 UTC. **(b)** Averaging kernels for MIR and NIR retrievals of Garmisch spectra recorded on 6 March 2008.

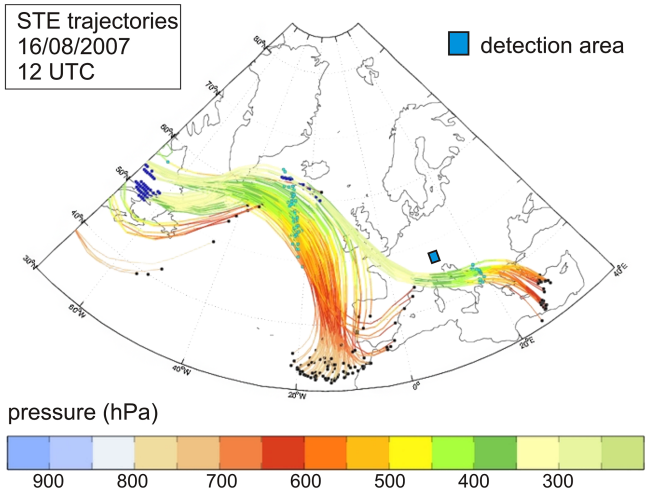

Figure 8. STE trajectories calculated with the tool of ETH Zürich, based on ECMWF data. The trajectories were initiated on 16 August 2007 at $t_0 = 12{:}00$ UTC. The time positions on the trajectories for t_0, $t_0 + 2$ d and $t_0 + 4$ d are marked by azure, cyan, and black dots, respectively.The frame of the detection area ($2° \times 2°$) around Garmisch is marked by the blue square.

the diurnal variation of the recorrected MIR and NIR XCH_4 (Fig. 6b) in relation to the basic features of the stratospheric intrusion above Garmisch.

Finally, we can understand the significant step in both MIR and NIR XCH_4 which can be seen after 11:00 UTC. The two tropospheric layers of CH_4-depleted air in the time period until their dissipation at 11:00 UTC have a bigger impact on XCH_4 compared to the CH_4 depletion in the UTLS after 11:00 UTC because the relative fraction of air mass is higher in the troposphere. Therefore, the mean XCH_4 (NIR, MIR) before 11:00 UTC is about 20 ppb lower than for the time period after 11:00 UTC. This is the first time that such a significant intraday increase in XCH_4 (1.15 %) could be detected from ground-based FTIR retrievals and explained by the dynamical variability of a stratospheric intrusion event.

4.2.2 Exclusion of STE events

For the detection of stratospheric intrusions coincident with FTIR measurements at Garmisch we adapted an approach for the analysis of stratospheric intrusions that was introduced by Trickl et al. (2010). This strategy uses STE trajectories based on ECMWF data. These STE trajectories represent a small subset of 4-day forward trajectories calculated with the Lagrangian analysis tool (LAGRANTO; Wernli and Davies, 1997) and are defined through two requirements: they are (i) initially residing in the stratosphere and then (ii) during the following 4 days are descending by more than 300 hPa into the troposphere.

For each day, STE trajectories have been calculated for the start times 00:00 and 12:00 UTC, and distributed by automated electronic mail by ETH Zürich (Swiss Federal Institute of Technology). As an example, Fig. 8 shows the intrusion trajectories initiated on 16 August 2007 at 12:00 UTC. For the identification of the stratospheric intrusions at Garmisch we defined a detection area of $\pm 1°$ (latitude and longitude) around Garmisch (see Fig. 8 blue square). The trajectories in Fig. 8 do not touch or pass through the detection area because, most likely, there will not be a STE event at Garmisch for the next 4 days. As a further requirement for counting a stratospheric intrusion, at least five trajectories should touch or hit the detection area.

In addition, trajectory calculations were carried out with the HYSPLIT (Hybrid Single Particle Lagrangian Integrated Trajectory) model. The HYSPLIT trajectories were evaluated according to the approach by Trickl et al. (2010, Sect. 2.3 therein) for identifying stratospheric intrusions at Garmisch. (Note that the detection analysis of stratospheric intrusions could not be made for the complete FTIR data set because of some missing trajectories. Nevertheless, the analysis covers the majority of the FTIR measurements.)

Our analysis reveals that ~ 35 % of the FTIR measurement days at Garmisch are influenced by STE processes. When excluding the affected XCH_4 data the agreement is improved significantly for the original a priori case with regard to the SD of difference time series NIR–MIR: using the original and common ACTM priors (see Fig. C3) it is reduced from 8.2 to 6.5 ppb and from 6.2 to 4.7 ppb, respectively. The MIR/NIR slope from the intercomparison with original prior (Fig. 9a) is not improved, but is still in the range of TCCON

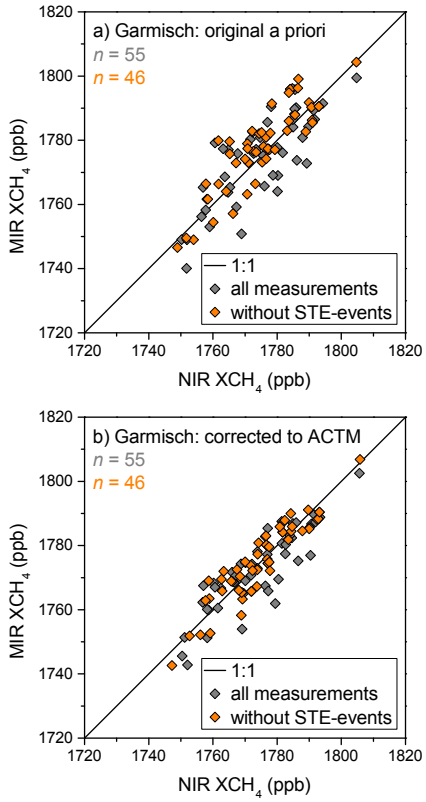

Figure 9. Scatter plot of MIR and NIR monthly means for Garmisch XCH_4 obtained from all FTIR measurements (black diamonds) and FTIR measurements which are not affected by STE events (red diamonds), respectively. **(a)** MIR and NIR XCH_4 retrieved with their original retrieval a priori profiles and **(b)** a posteriori corrected to common ACTM profiles. Note: the data set is not identical to that in Sect. 3 because STE trajectories are not available for the complete time series.

accuracy. In the case of the common prior profile (Fig. 9b), the MIR/NIR slope is slightly improved by the exclusion of affected data. All fit parameters for the data sets of the STE analysis at Garmisch are given in Table 4.

The improved agreement is achieved by the fact that measurement days with high residual XCH_4 differences, caused by different smoothing terms related to STE, are filtered out. Winter months are particularly affected by this extra filter criterion. This is in accordance with Sprenger and Wernli (2003), who showed that STE in the Northern Hemisphere has a distinct seasonal cycle with a flat maximum from December to April and a pronounced minimum in August and September.

Another outcome from Sprenger and Wernli (2003) is that at a subtropical site like Izaña, the frequency of STE events is much lower than at midlatitude sites like Garmisch, Karlsruhe, or Wollongong. Hence, the overall impact of STE processes on Izaña MIR and NIR retrievals is small compared to the other sites. This is confirmed by the very good agreement between MIR and NIR seasonalities at Izaña. Also, the polar site Ny-Ålesund is more influenced by STE processes than Izaña and thereby the MIR and NIR retrievals at Ny-Ålesund are affected by a second mechanism of dynamical variability in addition to polar subsidence. Besides that, we expect that remaining XCH_4 differences (NIR – MIR) are caused by near-surface CH_4 variations in combination with different MIR and NIR retrieval sensitivities. As the high mountain site Izaña is usually located above the planetary boundary layer (PBL), there should not be an impact on MIR and NIR retrievals. In contrast to that, Garmisch is located inside the PBL and therefore MIR and NIR retrievals are affected by this CH_4 variability. For this reason, MIR and NIR retrievals at Izaña are expected to be in better agreement compared to Garmisch (and this is in line with our results), although retrievals affected by STE processes have been excluded for Garmisch.

Finally, the qualitative findings from the STE analysis of MIR and NIR retrievals at Garmisch can be transferred directly to the sites Karlsruhe, Wollongong, and Ny-Ålesund. As explained above, they are consistent with the site-specific characteristics at Izaña.

5 Mitigation strategies for the stratospheric impact

The stratospheric part of CH_4 is defined by the position of the tropopause and the CH_4 vmr gradient in the UTLS. Whereas the CH_4 vmr gradient in the UTLS is the result of large-scale vertical transport (Brewer–Dobson circulation), the position of the tropopause depends on synoptic (e.g., polar vortex, STE) as well as seasonal variations (except for the tropics). Due to these facts the stratospheric part of CH_4 can produce a lot of variability and uncertainty (smoothing effects) in the total column CH_4 and, consequently, in XCH_4. This variability can be misleading within the analysis of trends with regard to tropospheric emissions. Therefore, methods have been developed to overcome this problem of stratospheric variability by separating the tropospheric part of CH_4 from the total column

First of all, Washenfelder et al. (2003) showed that stratospheric tracer–tracer relationships can be used to approximate the stratospheric CH_4 in order to subtract it from the total column CH_4 to get a tropospheric CH_4 with a theoretical precision of $\sim 0.5\,\%$. Their study was based on simultaneous NIR retrievals of CH_4 and hydrogen fluoride (HF) that is strongly anticorrelated with stratospheric CH_4. This method has been refined by Saad et al. (2014) by explicitly accounting for averaging kernels. As a result the mean precision of tropospheric CH_4 was improved to $\sim 0.1\,\%$. At the same time, Wang et al. (2014) showed that nitrous oxide (N_2O) can also be an appropriate proxy for stratospheric CH_4 with less H_2O dependence compared to HF. In contrast to NIR, the proxy retrieval is not applicable for MIR measurements, as shown by Sepúlveda et al. (2012). However,

Table 4. As Table 2, but only for Garmisch using MIR and NIR retrievals which are coincident to the STE trajectory data set. Data sets are divided into monthly means using measurements from all days (Garmisch complete) or only days without STE events at Garmisch (Garmisch without STE).

Data set	a priori	fit $y = bx$		
		slope b and 2σ uncertainty	slope different from 1 on 2σ level?	SD (ppb)
Garmisch complete	NIR & MIR retrieved with original a priori	1.0001(12)	no	8.2
Garmisch without STE	NIR & MIR retrieved with original a priori	1.0015(11)	yes	6.5
Garmisch complete	NIR & MIR corrected to ACTM a priori	0.9993(09)	no	6.2
Garmisch without STE	NIR & MIR corrected to ACTM a priori	1.0002(08)	no	4.7

the latter extracted tropospheric CH_4 directly from optimized profile retrievals in the MIR.

Nevertheless, all methods mentioned have their limitations, e.g., Sepúlveda et al. (2014) found that their tropospheric CH_4 product can be affected significantly by variations in the UTLS. They emphasize that tropospheric CH_4 with a precision of $\sim 0.5\,\%$ can be derived only by means of an a posteriori correction of the MIR retrievals. The results of the proxy methods in the NIR achieve high theoretical precision indeed, but their accuracy directly depends on the accuracy of the total column CH_4 which is linked to the quality of a priori profiles. For example, especially in polar vortex conditions, NIR proxy retrievals are limited due to smoothing effects (Saad et al., 2014). In the end the smoothing effect described in Sect. 4.1.1 directly affects the accuracy of the tropospheric CH_4 which points to the importance of realistic a priori profiles for scaling retrievals. One further problem is introduced by the complex structure of STE events because they do not only affect the stratosphere, but also the troposphere, as shown in Sect. 2.2.1.

Due to these reasons and the fact that our MIR retrieval strategy is optimized with regard to total columns, we decided to focus on total XCH_4. However, a comparison of tropospheric NIR and MIR retrievals is certainly interesting. It is obvious that such an intercomparison should be performed with retrieval methods dedicated to tropospheric columns, and improved a priori profiles that are able to reproduce the polar vortex subsidence in a realistic way. The NIR proxy retrievals (Saad et al., 2014; Wang et al., 2014) will benefit from these a priori profiles in the same way as the total column retrievals. In addition to that, these profiles could be used by tropospheric MIR profile retrievals (Sepúlveda et al., 2014), thereby acting as a common prior within an intercomparison study.

Attention should also be paid to the dependence of XCH_4 on stratospheric variability with regard to validation of satellite and model data. This means that the prior and the averaging kernels should be taken into account, particularly as satellites have their own vertical sensitivities. In the case of similar vertical sensitivities we can assume that the smoothing effects from satellite and ground-based retrievals are of nearly equal magnitude. Hence, remaining differences can be attributed to other error sources such as systematic errors. Thus, NIR TCCON retrievals may be more valuable than MIR NDACC retrievals if SWIR (shortwave infrared) sounders such as GOSAT or SCIAMACHY are concerned. Furthermore, it is important to be very careful with the interpretation of results when evaluating model data from arctic regions.

Instead of separating the stratospheric part from the total column, we tried to detect and exclude situations with high dynamical variability by analyzing meteorological parameters (Sects. 4.1.2 and 4.2.2). In future, these meteorological criteria for exclusion could be installed as additional information in the prior data (TCCON). Another possibility for the exclusion of affected data has been presented by Angelbratt et al. (2011). They used a multiple regression model with anomalies of HF, carbon monoxide (CO), and tropopause height to reduce the variability in total column CH_4. This concept of anomalies can also be transferred to the retrieval process. Certain threshold values of stratospheric tracers (HF, N_2O) can be implemented as filter criteria for XCH_4. In Appendix D we show that HF is suitable for detecting polar vortex subsidence. In contrast, the situation with STE is much more complex and HF cannot be recommended as an additional filter criterion.

Substantial progress could be achieved when combining the NIR and MIR measurements in a concurrent retrieval setup. In this approach the difference in averaging kernels is not considered as a problem but as an opportunity to differentiate more atmospheric layers. The synergetic potential of such an approach seems to be more promising in the case of polar vortex subsidence because the dynamics of subsidence are not as fine-structured compared to STE events. However, the main objective of combining both retrievals will be to determine the shape of the stratospheric CH_4 profile. Hence, reducing the uncertainty of the stratospheric CH_4 will be beneficial for models and retrievals. We want to construct such a combined method and also want to present the method in a subsequent study.

6 Summary and conclusions

We have compared MIR (NDACC) and NIR (TCCON) retrievals of XCH_4 obtained at the sites Garmisch, Karlsruhe, Izaña, Wollongong, and Ny-Ålesund. Our intercomparison results (Table 2) confirm the major findings from Sussmann et al. (2013). That is, there is no need to apply an MIR/NIR intercalibration factor due to very good overall agreement of the original MIR and NIR data sets as retrieved (except Ny-Ålesund). Furthermore, we showed that the remaining seasonal bias could be reduced by using a realistic site-specific and time-dependent common prior (ACTM). However, residual differences in Sussmann et al. (2013) and also in the present study reached significant levels (up to ~ 30 ppb for Ny-Ålesund), limiting the accuracy of the MIR and NIR seasonal cycles.

In this paper we were able to show that dynamical variability is the main source for these residual differences. Thereby, we complement the outcomes from Sussmann et al. (2013) with important additional findings about the characteristics of MIR and NIR retrievals of methane.

In extreme scenarios of atmospheric variability, i.e., stratospheric subsidence or deep STE events, the approach using a common model prior to reducing differing smoothing errors fails because the model profile is likely to deviate from the true atmospheric CH_4 profile. By means of a case study we showed that stratospheric subsidence at Ny-Ålesund is associated with large differences between MIR and NIR retrievals (~ 29 ppb for the time period 08:00–10:00 UT on 25 March 2011). Another case study indicated that a deep stratospheric intrusion at Garmisch gives rise to residual differences of up to ~ 15 ppb. Due to the different vertical sensitivities (averaging kernels), the smoothing effects of MIR and NIR retrievals are unequal for both case studies. While NIR retrievals are affected by stratospheric subsidence more than MIR retrievals, the situation is reversed for STE processes such as deep stratospheric intrusions. As a consequence, both the exclusion of Ny-Ålesund retrievals affected by stratospheric subsidence and the exclusion of Garmisch retrievals affected by STE processes resulted in improved agreement of MIR and NIR seasonal cycles (Tables 3, 4).

We found that 23 % of the FTIR measurement days at Ny-Ålesund are influenced by the polar vortex and 35 % of the FTIR measurement days at Garmisch are influenced by STE. Considering that the high increase in XCH_4 of ~ 25 ppb within 1 h at Garmisch is related to a deep stratospheric intrusion, it is obvious that such STE processes are able to introduce a remarkable variation in XCH_4. From the geographical and seasonal variability of STE presented in Sprenger and Wernli (2003) we conclude that, in contrast to Izaña, the other midlatitude sites (Karlsruhe, Wollongong) and the polar site (Ny-Ålesund) are also affected by STE processes. This is in line with the very good agreement of the MIR and NIR seasonal cycles for Izaña.

We conclude that atmospheric variability (subsidence, STE, and stratospheric variability in general) is a key factor in constraining the accuracy of MIR and NIR seasonal cycles. Different vertical sensitivities for both retrievals give rise to different smoothing effects. We showed that this impact can be mitigated by means of two basically different approaches. Either situations with high atmospheric variability are detected and excluded from further analysis or one has to focus on retrievals of tropospheric XCH_4 (Sect. 5). Nevertheless, NIR and MIR XCH_4 retrievals can be used in inversions without limitation of data. For example, inversions can explicitly account for averaging kernels and a priori profiles, thereby reducing the bias between MIR and NIR. At the same time, both measurements will be consistent with the model. In addition to that, inverse models are able to take the smoothing error directly into account.

One step forward would be to use models as a transfer standard between MIR and NIR column retrievals. Assuming that only the true CH_4 profile is able to harmonize NDACC and TCCON retrievals of XCH_4, it is possible to construct a concurrent retrieval setup. The synergetic potential of such a combined method is based on the different vertical sensitivities of the retrievals. A study on this subject has already been initiated and is subject of a subsequent publication.

However, NIR retrievals at polar sites may be improved by accounting for stratospheric subsidence in the standard retrieval a priori. Improving the quality of MIR retrievals affected by STE seems to be more complicated due to the diversity of STE processes. However, we conjecture that more realistic a priori profiles from high-resolution models reflecting small-scale processes could help to reduce MIR smoothing effects. An alternative method to overcome this problem would be to further improve the FTIR retrievals with the target to achieve a more uniform sensitivity at all altitudes; i.e., if the MIR averaging kernel was more evenly weighted with altitude then the MIR dependence on STE should be reduced. Also, using a formal optimal estimation (OE) inverse technique in GFIT could foreseeably help to improve the sensitivity of NIR retrievals to subsidence.

When using NDACC and/or TCCON XCH_4 data, it is critical to be aware of the effects of dynamic events on the accuracy of the relevant data set. Depending on the requirements on data accuracy, NDACC and/or TCCON XCH_4 data can be used with or without the exclusion of dynamical events. Methods to detect these events have been presented in this study. Given a proper data use based on the findings in this paper, a joint NDACC and TCCON data set will result in wider spatial and longer temporal coverage of XCH_4 data for the validation of top-down estimates, satellite validation, and trend studies.

Appendix A: Description of FTIR sounding sites

A1 Garmisch

The Garmisch solar FTIR system (47.48° N, 11.06° E, 743 m a.s.l.) is operated by the group Atmospheric Variability and Trends at the Institute of Meteorology and Climate Research – Atmospheric Environmental Research (IMK-IFU), Karlsruhe Institute of Technology (KIT). Column-averaged methane is retrieved from FTIR measurements performed with a Bruker IFS125HR interferometer. NIR forward and backward single-scan measurements are recorded with an InGaAs detector by using a maximum optical path difference of 45 cm. In the MIR spectral range the solar absorption spectra are detected with an InSb detector using a maximum optical path difference of 175 cm and averaging six scans with an integration time of approximately 7 min.

The Garmisch FTIR system took part in the aircraft calibration campaign of the EU project IMECC (Infrastructure for Measurement of the European Carbon Cycle) (Messerschmidt et al., 2011; Geibel et al., 2012). Garmisch FTIR measurements have been used for satellite validation (de Laat et al., 2010; Morino et al., 2011; Wunch et al., 2011b), carbon cycle research (Chevallier et al., 2011), and studies of atmospheric variability and trends (e.g., Borsdorff and Sussmann, 2009; Sussmann et al., 2009, 2012). The intercalibration of MIR and NIR measurements in this study covers the time period from July 2007 to December 2012.

A2 Wollongong

The Wollongong solar FTIR system (34.41° S, 150.88° E, 30 m a.s.l.) is operated by the Centre for Atmospheric Chemistry at the University of Wollongong, Australia. The intercomparison uses the Wollongong time series of June 2008–December 2012. In this time period the FTIR measurements were performed with a Bruker IFS125HR instrument. The settings for NIR measurements are identical to those at Garmisch. In the MIR spectral range solar absorption spectra were recorded with an InSb detector, using an optical path difference of 257 cm and averaging two scans with an integration time of approximately 4 min. Data obtained from Wollongong FTIR have contributed to a chemical-transport model validation by using MIR measurements of stratospheric tracer total column abundances (Kohlhepp et al., 2012).

A3 Karlsruhe

The Karlsruhe solar FTIR system (49.08° N, 8.43° E, 110 m a.s.l.) is operated by the group Ground-based remote-sensing at the Institute for Meteorology and Climate Research – Atmospheric Trace Gases (IMK-ASF), KIT, Germany. In 2009 a new FTIR container with a Bruker IFS125HR interferometer was set up for solar absorption measurements in the MIR and NIR.

The settings for NIR measurements are identical to those at Garmisch. MIR measurements are performed with an InSb detector using a maximum optical path difference of 180 cm. Four scans are averaged with an integration time of 9.5 min. This study uses MIR and NIR measurements out of the time period from March 2010 to December 2012. The Karlsruhe FTIR system participated in the aircraft calibration campaign of the EU project IMECC.

A4 Izaña

The Izaña solar FTIR system (28.31° N, 16.45° W, 2370 m a.s.l.) is located on the Canary Island of Tenerife and is part of a collaboration between the Meteorological State Agency of Spain (Spanish acronym: AEMET) and KIT. It is operated by the Izaña Atmospheric Research Center and the responsibility for the FTIR experiment lies with IMK-ASF of the Karlsruhe Institute for Technology.

Because measurements from 2007 to 2010 are affected by laser sampling ghosts, the intercalibration only uses FTIR data from December 2010 to December 2012 which have been recorded with a Bruker IFS125HR interferometer. The settings for NIR measurements are identical to those at Karlsruhe. The interferograms for the MIR retrievals are operated with an InSb detector using a maximum optical path difference of 180 cm before averaging six scans with an integration time of about 7 min. Izaña FTIR measurements have been used for a long-term validation of tropospheric column-averaged methane in the midinfrared spectral region (Sepúlveda et al., 2012) and have also been part of a technical study about a method for ghost correction in historic near-infrared FTIR measurements (Dohe et al., 2013).

A5 Ny-Ålesund

The Ny-Ålesund solar FTIR system (78.92° N, 11.93° E, 20 m a.s.l.) is part of the the joint French–German Arctic Research Base AWIPEV (Alfred Wegener Institute for Polar and Marine Research and the French Polar Institute Paul Emile Victor) on the Svalbard archipelago. The intercalibration contains FTIR measurements from March 2005 to August 2012 which have been performed with a Bruker 120HR interferometer by the AWI (Alfred Wegener Institute) Potsdam and the University of Bremen. Ground-based solar absorption measurements are operated from the end of March until the end of September when the polar night begins.

Column-averaged methane is retrieved from double-scan TCCON-type measurements recorded with an InGaAs diode using a maximum optical path difference of 30 cm. No DC/solar intensity variation correction was applied to Ny-Ålesund data. MIR retrievals are recorded with an InSb detector by using an optical path difference of 180 cm. Two scans are averaged with an integration time of approximately 2.5 min.

Appendix B: Derivation of a typical strongly subsided CH_4 profile for Ny-Ålesund

Inside the polar vortex, stratospheric subsidence leads to a depletion of the total columns of tropospheric source gases, whereas outside the polar vortex the columns of these gases remain unchanged. Based on the assumption that this variation of total columns is the result of vertical transport alone, Toon at al. (1992b) derived a mapping transformation which links points on the vmr profile outside the vortex to the same vmr inside according to the relation

$$\mathrm{vmr}_{\mathrm{subsided}}(z) = \mathrm{vmr}(z(1 + \mathrm{DOS})), \tag{B1}$$

where DOS is the degree of subsidence.

As explained in Sect. 4.1.1, Ny-Ålesund was affected by strong subsidence on 25 March 2011. Therefore, we decided to use a typical maximum DOS value of 0.44 to account for subsidence in the MIR and NIR retrievals on 25 March 2011. Equation (B1) was applied to the MIR original a priori profile (from WACCM) above the tropopause to get a subsided common prior (see Fig. 3a, MIR a $\mathrm{priori}_{\mathrm{subsided}}$).

Appendix C: Supplementary figures

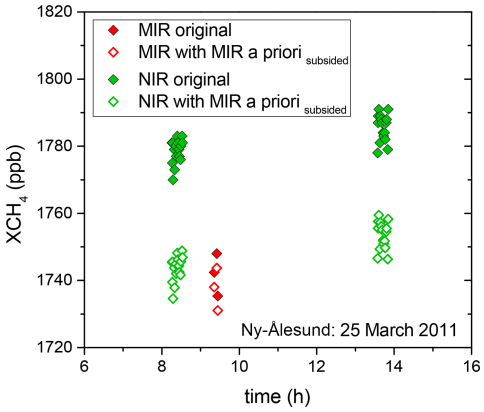

Figure C1. Same as Fig. 4 but MIR and NIR retrievals as computed with their standard (original) retrieval a priori profiles (filled squares) and as corrected to a strongly subsided MIR a priori profile (open squares) as shown in Fig. 3a.

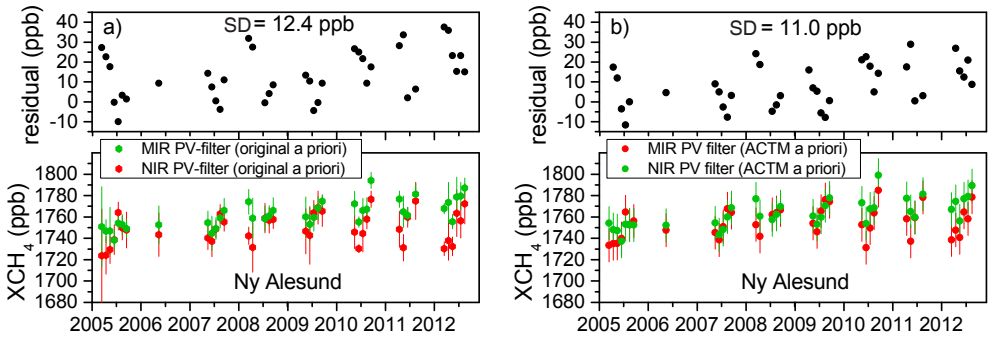

Figure C2. Same as Fig. 2 for Ny-Ålesund but excluding retrievals affected from stratospheric subsidence via PV as an extra filter criterion (see Sect. 4.1.2). **(a)** NIR and MIR retrievals with their original standard retrieval a priori profiles. **(b)** NIR and MIR retrievals corrected to the common ACTM a priori profile.

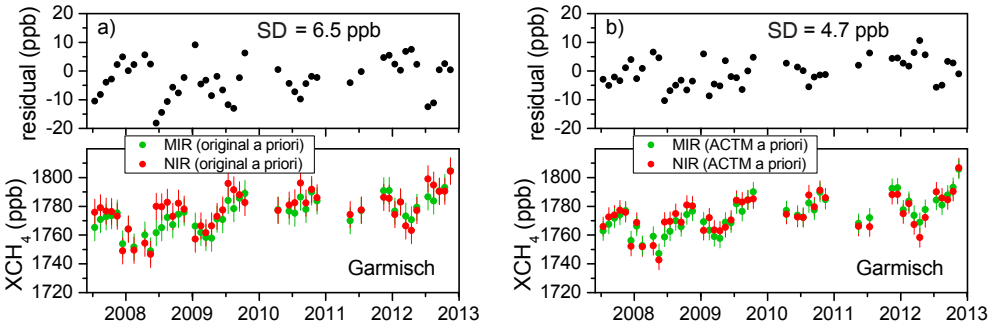

Figure C3. Same as Fig. 2 for Garmisch but excluding retrievals affected from STE events (see Sect. 4.2.2). **(a)** NIR and MIR retrievals with their original standard retrieval a priori profile. **(b)** NIR and MIR retrievals corrected to the common ACTM a priori profile.

Appendix D: Supplementary figures

In Sects. 4.1.2 and 4.2.2 we applied meteorological criteria for detecting situations with polar vortex subsidence, and STE, respectively. These methods are complex and not really practicable in the operational retrieval process. In contrast to that, it seems to be logical to use simultaneous measurements of stratospheric tracers (HF, N_2O) for detecting polar vortex subsidence and STE. The chemically inert trace gas HF appears to be an excellent candidate for such an intention since it is strongly anticorrelated with stratospheric CH_4.

In the case of polar vortex subsidence it can be expected that the stratospheric CH_4 depletion involves an enhancement in the HF total column. Figure D1 shows the NIR XHF daily mean time series of Ny-Ålesund. Measurement days with polar vortex subsidence were identified in Sect. 4.1.2 and are highlighted in Fig. D1. Indeed, it is clearly recognizable that the XHF values are significantly higher ($\sim$ factor 2) at the predominant part of polar vortex situations. Therefore, we conclude that it would be possible to exclude polar vortex situations at Ny-Ålesund with an XHF threshold of $\sim$ 100 ppt (parts per trillion).

In contrast to that, the situation is more difficult with regard to STE due to its complex nature. Thus, it is possible that both enhancements and depletions of CH_4 and consequently HF can occur. Figure D2 shows the NIR XHF daily mean time series of Garmisch. Days with and without STE were identified according to Sect. 4.2.2 and can be distinguished in Fig. D2. It is obvious that XHF is in same range of values in situations with STE as in situations without STE. Hence, XHF is not suitable for the detection of STE events.

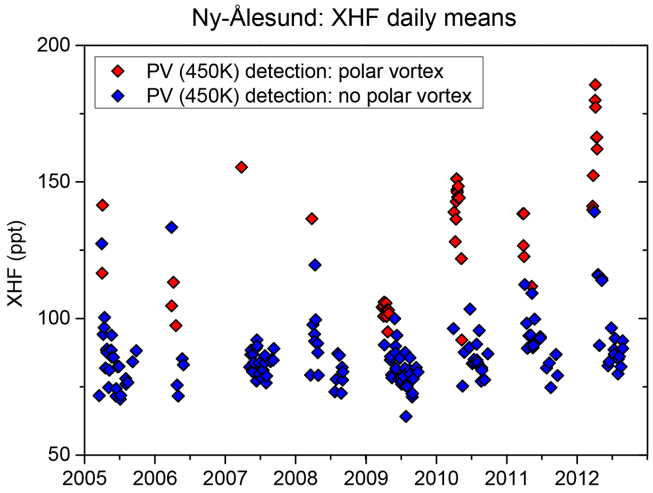

Figure D1. XHF daily mean time series for Ny-Ålesund obtained from NIR measurements (TCCON). Polar vortex days were detected by using the PV criterion by Nash et al. (1996).

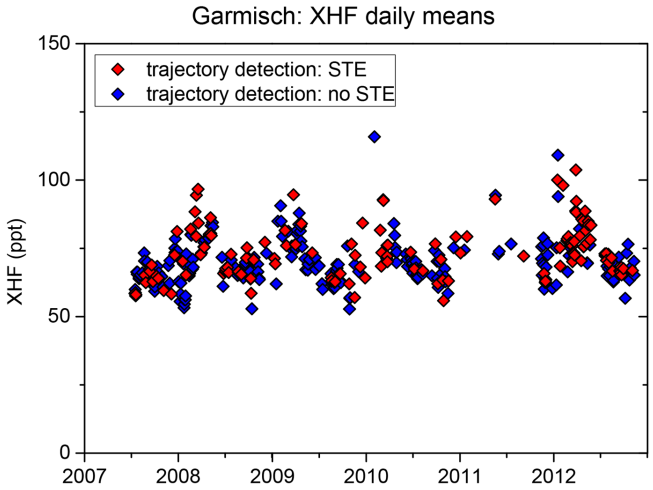

Figure D2. XHF daily mean time series for Garmisch obtained from NIR measurements (TCCON). The detection of measurement days affected by STE is described in Sect. 4.2.2.

Acknowledgements. We are indebted to P. K. Patra (JAMSTEC) for providing ACTM model data and thank T. Blumenstock (KIT) and O. E. García-Rodríguez (AEMET) for making Izaña FTIR data available. Furthermore, we thank D. W. T. Griffith (University of Wollongong) and J. Notholt (IUP) for providing FTIR data from Wollongong and Ny-Ålesund, respectively. We thank H. P. Schmid (IMK-IFU) for his continual interest in this work. Provision of the GFIT code by G. Toon (JPL) is gratefully acknowledged. Our work has been performed as part of the ESA GHG-cci project via subcontract with the University of Bremen. In addition we acknowledge funding by the EC within the INGOS project. We thank the ECMWF for providing access to the meteorological data. We thank the Deutsche Forschungsgemeinschaft and Open Access Publishing Fund of the Karlsruhe Institute of Technology for support. The Wollongong work was funded through the Australian International Science Linkage grant CG130014 and the Australian Research Council, grants DP0879468 and DP110103118.

The service charges for this open access publication have been covered by a Research Centre of the Helmholtz Association.

Edited by: J. Joiner

References

Angelbratt, J., Mellqvist, J., Blumenstock, T., Borsdorff, T., Brohede, S., Duchatelet, P., Forster, F., Hase, F., Mahieu, E., Murtagh, D., Petersen, A. K., Schneider, M., Sussmann, R., and Urban, J.: A new method to detect long term trends of methane (CH_4) and nitrous oxide (N_2O) total columns measured within the NDACC ground-based high resolution solar FTIR network, Atmos. Chem. Phys., 11, 6167–6183, doi:10.5194/acp-11-6167-2011, 2011.

Allan, W., Struthers, H., and Lowe, D. C.: Methane carbon isotope effects caused by atomic chlorine in the marine boundary layer: Global model results compared with Southern Hemisphere measurements, J. Geophys. Res., 112, D04306, doi:10.1029/2006JD007369, 2007.

Archer, D.: Methane hydrate stability and anthropogenic climate change, Global Biogeochem. Cy., 4, 521–544, doi:10.5194/bg-4-521-2007, 2007.

Belikov, D., Maksyutov, S., Miyasaka, T., Saeki, T., Zhuravlev, R., and Kiryushov, B.: Mass-conserving tracer transport modelling on a reduced latitude-longitude grid with NIES-TM, Geosci. Model Dev., 4, 207–222, doi:10.5194/gmd-4-207-2011, 2011.

Bergamaschi, P., Frankenberg, C., Meirink, J. F., Krol, M., Villani, M. G., Houweling, S., Dentener, F., Dlugokencky, E. J., Miller, J. B., Gatti, L. V., Engel, A., and Levin, I.: Inverse modeling of global and regional CH_4 emissions using SCIAMACHY satellite retrievals, J. Geophys. Res., 114, D22301, doi:10.1029/2009JD012287, 2009.

Bergamaschi, P., Houweling, S., Segers, A., Krol, M., Frankenberg, C., Scheepmaker, R. A., Dlugokencky, E., Wofsy, S. C., Kort, E. A., Sweeney, C., Schuck, T., Brenninkmeijer, C., Chen, H., Beck, V., and Gerbig, C.: Atmospheric CH_4 in the first decade of the 21st century: inverse modeling analysis using SCIAMACHY satellite retrievals and NOAA surface measurements, J. Geophys. Res., 118, 7350–7369, doi:10.1002/jgrd.50480, 2013.

Borsdorff, T. and Sussmann, R.: On seasonality of stratomesospheric CO above midlatitudes: New insight from solar FTIR spectrometry at Zugspitze and Garmisch, Geophys. Res. Lett., 36, L21804, doi:10.1029/2009GL040056, 2009.

Bousquet, P., Ciais, P., Miller, J. B., Dlugokencky, E. J., Hauglustaine, D. A., Prigent, C., Van der Werf, G. R., Peylin, P., Brunke, E. G., Carouge, C., Langenfels, R. L., Lathiere, J., Papa, F., Ramonet, M., Schmidt, M., Steele, L. P., Tyler, S. C., and White, J.: Contribution of anthropogenic and natural sources to atmospheric methane variability, Nature, 443, 439–443, 2006.

Bousquet, P., Ringeval, B., Pison, I., Dlugokencky, E. J., Brunke, E.-G., Carouge, C., Chevallier, F., Fortems-Cheiney, A., Frankenberg, C., Hauglustaine, D. A., Krummel, P. B., Langenfelds, R. L., Ramonet, M., Schmidt, M., Steele, L. P., Szopa, S., Yver, C., Viovy, N., and Ciais, P.: Source attribution of the changes in atmospheric methane for 2006–2008, Atmos. Chem. Phys., 11, 3689–3700, doi:10.5194/acp-11-3689-2011, 2011.

Butz, A., Guerlet, S., Hasekamp, O., Schepers, D., Galli, A., Aben, I., Frankenberg, C., Hartmann, J. M., Tran, H., Kuze, A., Keppel-Aleks, G., Toon, G., Wunch, D., Wennberg, P., Deutscher, N., Griffith, D., Macatangay, R., Messerschmidt, J., Notholt, J., and Warneke, T.: Toward accurate CO_2 and CH_4 observations from GOSAT, Geophys. Res. Lett., 38, L14812, doi:10.1029/2011GL047888, 2011.

Chevallier, F., Deutscher, N., Conway, C. J., Ciais, P., Ciattaglia, L., Dohe, S., Fröhlich, M., Gomez-Pelaez, A.J., Griffith, D., Hase, F., Haszpra, L., Krummel, P., Kyrö, E., Labuschagne, C., Langenfelds, R., Machida, T., Maignan, F., Matsueda, H., Morino, I., Notholt, J., Ramonet, M., Sawa, Y., Schmidt, M., Sherlock, V., Steele, P., Strong, K., Sussmann, R., Wennberg, P., Wofsy, S., Worthy, D., Wunch, D., and Zimnoch, M.: Global CO_2 surface fluxes inferred from surface air-sample measurements and from surface retrievals of the CO_2 total column, Geophys. Res. Lett., 38, L24810, doi:10.1029/2011GL049899, 2011.

Cicerone, R. J. and Oremland, R. S.: Biogeochemical aspects of atmospheric methane, Global Biogeochem. Cy., 2, 299–327, doi:10.1029/GB002i004p00299, 1988.

de Laat, A. T. J., Gloudemans, A. M. S., Schrijver, H., Aben, I., Nagahama, Y., Suzuki, K., Mahieu, E., Jones, N. B., Paton-Walsh, C., Deutscher, N. M., Griffith, D. W. T., De Mazière, M., Mittermeier, R. L., Fast, H., Notholt, J., Palm, M., Hawat, T., Blumenstock, T., Hase, F., Schneider, M., Rinsland, C., Dzhola, A. V., Grechko, E. I., Poberovskii, A. M., Makarova, M. V., Mellqvist, J., Strandberg, A., Sussmann, R., Borsdorff, T., and Rettinger, M.: Validation of five years (2003–2007) of SCIAMACHY CO total column measurements using ground-based spectrometer observations, Atmos. Meas. Tech., 3, 1457–1471, doi:10.5194/amt-3-1457-2010, 2010.

De Mazière, M., Vigouroux, C., Bernath, P. F., Baron, P., Blumenstock, T., Boone, C., Brogniez, C., Catoire, V., Coffey, M., Duchatelet, P., Griffith, D., Hannigan, J., Kasai, Y., Kramer, I., Jones, N., Mahieu, E., Manney, G. L., Piccolo, C., Randall, C., Robert, C., Senten, C., Strong, K., Taylor, J., Tétard, C., Walker, K. A., and Wood, S.: Validation of ACE-FTS v2.2 methane profiles from the upper troposphere to the lower mesosphere, Atmos. Chem. Phys., 8, 2421–2435, doi:10.5194/acp-8-2421-2008, 2008.

Dlugokencky, E. J., Nisbet E. G., Fisher R., and Lowry, D.: Global atmospheric methane: budget, changes and dangers, Phil. Trans. R. Soc. A, 369, 2058–2072, doi:10.1098/rsta.2010.0341, 2011.

Dohe, S., Sherlock, V., Hase, F., Gisi, M., Robinson, J., Sepúlveda, E., Schneider, M., and Blumenstock, T.: A method to correct sampling ghosts in historic near-infrared Fourier transform spectrometer (FTS) measurements, Atmos. Meas. Tech., 6, 1981–1992, doi:10.5194/amt-6-1981-2013, 2013.

Frankenberg, C., Warneke, T., Butz, A., Aben, I., Hase, F., Spietz, P., and Brown, L. R.: Pressure broadening in the $2\nu_3$ band of methane and its implication on atmospheric retrievals, Atmos. Chem. Phys., 8, 5061–5075, doi:10.5194/acp-8-5061-2008, 2008.

Fraser, A., Palmer, P. I., Feng, L., Boesch, H., Cogan, A., Parker, R., Dlugokencky, E. J., Fraser, P. J., Krummel, P. B., Langenfelds, R. L., O'Doherty, S., Prinn, R. G., Steele, L. P., van der Schoot, M., and Weiss, R. F.: Estimating regional methane surface fluxes: the relative importance of surface and GOSAT mole fraction measurements, Atmos. Chem. Phys., 13, 5697–5713, doi:10.5194/acp-13-5697-2013, 2013.

Garcia, R. R., Marsh, D. R., Kinnison, D. E., Boville, B. A., and Sassi, F.: Simulation of secular trends in the middle atmosphere, 1950–2003, J. Geophys. Res., 112, D09301, doi:10.1029/2006JD007485, 2007.

Geibel, M. C., Messerschmidt, J., Gerbig, C., Blumenstock, T., Chen, H., Hase, F., Kolle, O., Lavrič, J. V., Notholt, J., Palm, M., Rettinger, M., Schmidt, M., Sussmann, R., Warneke, T., and Feist, D. G.: Calibration of column-averaged CH_4 over European TCCON FTS sites with airborne in-situ measurements, Atmos. Chem. Phys., 12, 8763–8775, doi:10.5194/acp-12-8763-2012, 2012.

Hase, F., Hannigan, J. W., Coffey, M. T., Goldman, A., Höpfner, M., Jones, N. B., Rinsland, C. P., and Wood, S. W.: Intercomparison of retrieval codes used for the analysis of high-resolution, ground-based FTIR measurements, J. Quant. Spectrosc. Radiat. Transfer, 87, 25–52, 2004.

Houweling, S., van der Werf, G. R., Goldewijk, K. K., Roeckmann, T., and Aben, I.: Early anthropogenic CH_4 emissions and the variation of CH_4 and $^{13}CH_4$ over the last millennium, Global Biogeochem. Cy., 22, GB1002, doi:10.1029/2007GB002961, 2008.

Houweling, S., Aben, I., Breon, F.-M., Chevallier, F., Deutscher, N., Engelen, R., Gerbig, C., Griffith, D., Hungershoefer, K., Macatangay, R., Marshall, J., Notholt, J., Peters, W., and Serrar, S.: The importance of transport model uncertainties for the estimation of CO_2 sources and sinks using satellite measurements, Atmos. Chem. Phys., 10, 9981–9992, doi:10.5194/acp-10-9981-2010, 2010.

Houweling, S., Krol, M., Bergamaschi, P., Frankenberg, C., Dlugokencky, E. J., Morino, I., Notholt, J., Sherlock, V., Wunch, D., Beck, V., Gerbig, C., Chen, H., Kort, E. A., Röckmann, T., and Aben, I.: A multi-year methane inversion using SCIAMACHY, accounting for systematic errors using TCCON measurements, Atmos. Chem. Phys., 14, 3991–4012, doi:10.5194/acp-14-3991-2014, 2014.

Kirschke, S., Bousquet, P., Ciais, P., Saunois, M., Canadell, J. G., Dlugokencky, E. J., Bergamaschi, P., Bergmann, D., Blake, D. R., Bruhwiler, L., Cameron-Smith, P., Castaldi, S., Chevallier, F., Feng, L., Fraser, A., Heimann, M., Hodson, E. L., Houweling, S., Josse, B., Fraser, P. J., Krummel, P. B., Lamarque, J. F., Langenfelds, R. L., Le Quere, C., Naik, V., O'Doherty, S., Palmer, P. I., Pison, I., Plummer, D., Poulter, B., Prinn, R. G., Rigby, M., Ringeval, B., Santini, M., Schmidt, M., Shindell, D. T., Simpson, I., Spahni, R., Steele, L. P., Strode, S. A., Sudo, K., Szopa, S., van der Werf, G. R., Voulgarakis, A., van Weele, M., Weiss, R. F., Williams, J. E., and Zeng, G.: Three decades of global methane sources and sinks, Nat. Geosci., 6, 813–823, doi:10.1038/ngeo1955, 2013.

Kohlhepp, R., Ruhnke, R., Chipperfield, M. P., De Mazière, M., Notholt, J., Barthlott, S., Batchelor, R. L., Blatherwick, R. D., Blumenstock, Th., Coffey, M. T., Demoulin, P., Fast, H., Feng, W., Goldman, A., Griffith, D. W. T., Hamann, K., Hannigan, J. W., Hase, F., Jones, N. B., Kagawa, A., Kaiser, I., Kasai, Y., Kirner, O., Kouker, W., Lindenmaier, R., Mahieu, E., Mittermeier, R. L., Monge-Sanz, B., Morino, I., Murata, I., Nakajima, H., Palm, M., Paton-Walsh, C., Raffalski, U., Reddmann, Th., Rettinger, M., Rinsland, C. P., Rozanov, E., Schneider, M., Senten, C., Servais, C., Sinnhuber, B.-M., Smale, D., Strong, K., Sussmann, R., Taylor, J. R., Vanhaelewyn, G., Warneke, T., Whaley, C., Wiehle, M., and Wood, S. W.: Observed and simulated time evolution of HCl, $ClONO_2$, and HF total column abundances, Atmos. Chem. Phys., 12, 3527–3556, doi:10.5194/acp-12-3527-2012, 2012.

Lin, M., Fiore, A. M., Cooper, O. R., Horowitz, L. W., Langford, A. O., Levy II, H., Johnson, B. J., Naik, V., Oltmans, S. J., and Senff, C. J.: Springtime high surface ozone events over the western United States: Quantifying the role of stratospheric intrusions, J. Geophys. Res., 117, D00V22, doi:10.1029/2012JD018151, 2012.

Lindenmaier, R., Strong, K., Batchelor, R. L., Chipperfield, M. P., Daffer, W. H., Drummond, J. R., Duck, T. J., Fast, H., Feng, W., Fogal, P. F., Kolonjari, F., Manney, G. L., Manson, A., Meek, C., Mittermeier, R. L., Nott, G. J., Perro, C., and Walker, K. A.: Unusually low ozone, HCl, and HNO_3 column measurements at Eureka, Canada during winter/spring 2011, Atmos. Chem. Phys., 12, 3821–3835, doi:10.5194/acp-12-3821-2012, 2012.

Messerschmidt, J., Geibel, M. C., Blumenstock, T., Chen, H., Deutscher, N. M., Engel, A., Feist, D. G., Gerbig, C., Gisi, M., Hase, F., Katrynski, K., Kolle, O., Lavrič, J. V., Notholt, J., Palm, M., Ramonet, M., Rettinger, M., Schmidt, M., Sussmann, R., Toon, G. C., Truong, F., Warneke, T., Wennberg, P. O., Wunch, D., and Xueref-Remy, I.: Calibration of TCCON column-averaged CO2: the first aircraft campaign over European TCCON sites, Atmos. Chem. Phys., 11, 10765–10777, doi:10.5194/acp-11-10765-2011, 2011.

Monteil, G., Houweling, S., Butz, A., Guerlet, S., Schepers, D., Hasekamp, O., Frankenberg, C., Scheepmaker, R., Aben, I., and Röckmann, T.: Comparison of CH_4 inversions based on 15 months of GOSAT and SCIAMACHY observations, J. Geophys. Res. Atmos., 118, 11807–11823, doi:10.1002/2013JD019760, 2013.

Morino, I., Uchino, O., Inoue, M., Yoshida, Y., Yokota, T., Wennberg, P. O., Toon, G. C., Wunch, D., Roehl, C. M., Notholt, J., Warneke, T., Messerschmidt, J., Griffith, D. W. T., Deutscher, N. M., Sherlock, V., Connor, B., Robinson, J., Sussmann, R., and Rettinger, M.: Preliminary validation of column-averaged volume mixing ratios of carbon dioxide and methane retrieved from

GOSAT short-wavelength infrared spectra, Atmos. Meas. Tech., 4, 1061–1076, doi:10.5194/amt-4-1061-2011, 2011.

Nash, E. R., Newman, P. A., Rosenfield, J. E., and Schoeberl, M. R.: An objective determination of the polar vortex using Ertel's potential vorticity, J. Geophys. Res., 101, 9471–9478, 1996.

Patra, P. K., Takigawa, M., Ishijima, K., Choi, B.-C., Cunnold, D., Dlugokencky, E. J., Fraser, P., Gomez-Pelaez, A. J., Goo, T.-Y., Kim, J.-S., Krummel, P., Langenfelds, R., Meinhardt, F., Mukai, H., O'Doherty, S., Prinn, R. G., Simmonds, P., Steele, P., Tohjima, Y., Tsuboi, K., Uhse, K., Weiss, R., Worthy, D., and Nakazawa, T. : Growth rate, seasonal, synoptic, diurnal variations and budget of methane in lower atmosphere, J. Meteorol. Soc. Jpn., 87, 635–663, 2009.

Patra, P. K., Houweling, S., Krol, M., Bousquet, P., Belikov, D., Bergmann, D., Bian, H., Cameron-Smith, P., Chipperfield, M. P., Corbin, K., Fortems-Cheiney, A., Fraser, A., Gloor, E., Hess, P., Ito, A., Kawa, S. R., Law, R. M., Loh, Z., Maksyutov, S., Meng, L., Palmer, P. I., Prinn, R. G., Rigby, M., Saito, R., and Wilson, C.: TransCom model simulations of CH_4 and related species: linking transport, surface flux and chemical loss with CH_4 variability in the troposphere and lower stratosphere, Atmos. Chem. Phys., 11, 12813–12837, doi:10.5194/acp-11-12813-2011, 2011.

Pougatchev, N. S., Connor, B. J., and Rinsland, C. P.: Infrared measurements of the ozone vertical distribution above Kitt Peak, J. Geophys. Res., 100, 16689–16697, 1995.

Rothman, L. S., Barbe, A., Benner, D. C., Brown, L. R., Camy-Peyret, C., Carleer, M. R., Chance, K., Clerbaux, C., Dana, V., Devi, V. M., Fayt, A., Flaud, J. M., Gamache, R. R., Goldman, A., Jacquemart, D., Jucks, K. W., Lafferty, W. J., Mandin, J. Y., Massie, S. T., Nemtchinov, V., Newnham, D. A., Perrin, A., Rinsland, C. P., Schroeder, J., Smith, K. M., Smith, M. A. H., Tang, K., Toth, R. A., Vander Auwera, J., Varanasi, P., and Yoshino, K.: The HITRAN molecular spectroscopic database: edition of 2000 including updates through 2001, J. Quant. Spectrosc. Radiat. Transfer, 82, 5–44, 2003.

Rothman, L. S., Jacquemart, D., Barbe, A., Benner, D. C., Birk, M., Brown, L. R., Carleer, M. R., Chackerian, C., Chance, K., Coudert, L. H., Dana, V., Devi, V. M., Flaud, J. M., Gamache, R. R., Goldman, A., Hartmann, J. M., Jucks, K. W., Maki, A. G., Mandin, J. Y., Massie, S. T., Orphal, J., Perrin, A., Rinsland, C. P., Smith, M. A. H., Tennyson, J., Tolchenov, R. N., Toth, R. A., Vander Auwera, J., Varanasi, P., and Wagner, G.: The HITRAN 2004 molecular spectroscopic database, J. Quant. Spectrosc. Rad. Trans., 96, 139–204, doi:10.1016/j.jqsrt.2004.10.008, 2005.

Rothman, L. S., Gordon, I. E., Barbe, A., Benner, D. C., Bernath, P. F., Birk, M., Boudon, V., Brown, L. R., Campargue, A., Champion, J., Chance, K., Coudert, L. H., Dana, V., Devi, V. M., Fally, S., Flaud, J.M., Gamache, R. R., Goldman, A., Jacquemart, D., Kleiner, I., Lacome, N., Lafferty, W. J., Mandin, J., Massie, S. T., Mikhailenko, S. N., Miller, C. E., Moazzen-Ahmadi, N., Naumenko, O. V., Nikitin, A. V., Orphal, J., Perevalov, V. I., Perrin, A., Predoi-Cross, A., Rinsland, C. P., Rotger, M., Šimečková, M., Smith, M. A. H., Sung, K., Tashkun, S. A., Tennyson, J., Toth, R. A., Vandaele, A. C., and Vander Auwera, J.: The HITRAN 2008 molecular spectroscopic database, J. Quant. Spectrosc. Radiat. Transfer, 110, 533–572, 2009.

Saad, K. M., Wunch, D., Toon, G. C., Bernath, P., Boone, C., Connor, B., Deutscher, N. M., Griffith, D. W. T., Kivi, R., Notholt, J., Roehl, C., Schneider, M., Sherlock, V., and Wennberg, P. O.: Derivation of tropospheric methane from TCCON CH_4 and HF total column observations, Atmos. Meas. Tech., 7, 2907–2918, doi:10.5194/amt-7-2907-2014, 2014.

Saito, R., Patra, P. K., Deutscher, N., Wunch, D., Ishijima, K., Sherlock, V., Blumenstock, T., Dohe, S., Griffith, D., Hase, F., Heikkinen, P., Kyrö, E., Macatangay, R., Mendonca, J., Messerschmidt, J., Morino, I., Notholt, J., Rettinger, M., Strong, K., Sussmann, R., and Warneke, T.: Technical Note: Latitude-time variations of atmospheric column-average dry air mole fractions of CO_2, CH_4 and N_2O, Atmos. Chem. Phys., 12, 7767–7777, doi:10.5194/acp-12-7767-2012, 2012.

Sapart, S. J., Monteil, G., Prokopiou, M., van de Wal, R. S. W., Kaplan, J. O., Sperlich, P., Krumhardt, K. M., van der Veen, C., Houweling, S., Krol, M. C., Blunier, T., Sowers, T., Martinerie, P., Witrant, E., Dahl-Jensen, D., and Röckmann, T.: Natural and anthropogenic variations in methane sources during the past two millennia, Nature, 490, 85–88, doi:10.1038/nature11461, 2012.

Schneising, O., Bergamaschi, P., Bovensmann, H., Buchwitz, M., Burrows, J. P., Deutscher, N. M., Griffith, D. W. T., Heymann, J., Macatangay, R., Messerschmidt, J., Notholt, J., Rettinger, M., Reuter, M., Sussmann, R., Velazco, V. A., Warneke, T., Wennberg, P. O., and Wunch, D.: Atmospheric greenhouse gases retrieved from SCIAMACHY: comparison to ground-based FTS measurements and model results, Atmos. Chem. Phys., 12, 1527–1540, doi:10.5194/acp-12-1527-2012, 2012.

Sepúlveda, E., Schneider, M., Hase, F., García, O. E., Gomez-Pelaez, A., Dohe, S., Blumenstock, T., and Guerra, J. C.: Long-term validation of tropospheric column-averaged CH_4 mole fractions obtained by mid-infrared ground-based FTIR spectrometry, Atmos. Meas. Tech., 5, 1425–1441, doi:10.5194/amt-5-1425-2012, 2012.

Sepúlveda, E., Schneider, M., Hase, F., Barthlott, S., Dubravica, D., García, O. E., Gomez-Pelaez, A., González, Y., Guerra, J. C., Gisi, M., Kohlhepp, R., Dohe, S., Blumenstock, T., Strong, K., Weaver, D., Palm, M., Sadeghi, A., Deutscher, N. M., Warneke, T., Notholt, J., Jones, N., Griffith, D. W. T., Smale, D., Brailsford, G. W., Robinson, J., Meinhardt, F., Steinbacher, M., Aalto, T., and Worthy, D.: Tropospheric CH_4 signals as observed by NDACC FTIR at globally distributed sites and comparison to GAW surface in situ measurements, Atmos. Meas. Tech., 7, 2337–2360, doi:10.5194/amt-7-2337-2014, 2014.

Sinnhuber, B.-M., Stiller, G., Ruhnke, R., von Clarmann, T., Kellmann, S., and Aschmann, J.:, Arctic winter 2010/2011 at the brink of an ozone hole, Geophys. Res. Lett., 38, L24814, doi:10.1029/2011GL049784, 2011.

Sprenger, M. and Wernli, H.: A northern hemispheric climatology of crosstropopause exchange for the ERA15 time period (1979–1993), J. Geophys. Res., 108, 8521, doi:10.1029/2002JD002636, 2003.

Stocker, T., Qin, D., Plattner, G. K., Tignor, M., Allen, S. K., Boschung, J., Nauels, A., Xia, Y., Bex, V., and Midgley, P. M. (Eds.): Summary for Policymakers, Climate Change 2013: The Physical Science Basis. Contribution of Working Group I to the Fifth Assessment Report of the Intergovernmental Panel on Climate Change, Cambridge University Press, Cambridge, United Kingdom and New York, NY, USA, 2013.

Stohl, A. and Trickl, T.: A textbook example of long-range transport: Simultaneous observation of ozone maxima of stratospheric

and North American origin in the free troposphere over Europe, J. Geophys. Res., 104, 30445–30462, 1999.

Stohl, A., Spichtinger-Rakowsky, N., Bonasoni, P., Feldmann, H., Memmesheimer, M., Scheel, H. E., Trickl, T., Hübener, S. H., Ringer, W., and Mandl, M.: The influence of stratospheric intrusions on alpine ozone concentrations, Atmos. Environ., 34, 1323–1354, 2000.

Stohl, A., Bonasoni, P., Cristofanelli, P., Collins, W., Feichter, J., Frank, A., Forster, C., Gerasopoulos, E., Gäggeler, H., James, P., Kentarchos, T., Kromp-Kolb, H., Krüger, B., Land, C., Meloen, J., Papayannis, A., Priller, A., Seibert, P., Sprenger, M., Roelofs, G. J., Scheel, H. E., Schnabel, C., Siegmund, P., Tobler, L., Trickl, T., Wernli, H., Wirth, V., Zanis, P., and Zerefos, C.: Stratosphere-troposphere exchange: a review, and what we have learned from STACCATO, J. Geophys. Res., 108, 8516, doi:10.1029/2002JD002490, 2003.

Sussmann, R., Stremme, W., Buchwitz, M., and de Beek, R.: Validation of ENVISAT/SCIAMACHY columnar methane by solar FTIR spectrometry at the Ground-Truthing Station Zugspitze, Atmos. Chem. Phys., 5, 2419–2429, doi:10.5194/acp-5-2419-2005, 2005.

Sussmann, R., Borsdorff, T., Rettinger, M., Camy-Peyret, C., Demoulin, P., Duchatelet, P., Mahieu, E., and Servais, C.: Technical Note: Harmonized retrieval of column-integrated atmospheric water vapor from the FTIR network – first examples for long-term records and station trends, Atmos. Chem. Phys., 9, 8987–8999, doi:10.5194/acp-9-8987-2009, 2009.

Sussmann, R., Forster, F., Rettinger, M., and Jones, N.: Strategy for high-accuracy-and-precision retrieval of atmospheric methane from the mid-infrared FTIR network, Atmos. Meas. Tech., 4, 1943–1964, doi:10.5194/amt-4-1943-2011, 2011.

Sussmann, R., Forster, F., Rettinger, M., and Bousquet, P.: Renewed methane increase for five years (2007–2011) observed by solar FTIR spectrometry, Atmos. Chem. Phys., 12, 4885–4891, doi:10.5194/acp-12-4885-2012, 2012.

Sussmann, R., Ostler, A., Forster, F., Rettinger, M., Deutscher, N. M., Griffith, D. W. T., Hannigan, J. W., Jones, N., and Patra, P. K.: First intercalibration of column-averaged methane from the Total Carbon Column Observing Network and the Network for the Detection of Atmospheric Composition Change, Atmos. Meas. Tech., 6, 397–418, doi:10.5194/amt-6-397-2013, 2013.

Toon, G. C., Farmer, C. B., Schaper, P.W., Lowes, L. L., Norton, R. H., Schoeberl, M. R., Lait, L. R., and Newman, P. A.: Evidence for subsidence in the 1989 Polar winter stratosphere from airborne infrared composition measurements, J. Geophys. Res., 97, 7963–7970, 1992.

Trickl, T., Cooper, O. C., Eisele, H., James, P., Mücke, R., and Stohl, A.: Intercontinental transport and its influence on the ozone concentrations over central Europe: Three case studies, J. Geophys. Res., 108, 8530, doi:10.1029/2002JD002735, 2003.

Trickl, T., Feldmann, H., Kanter, H.-J., Scheel, H.-E., Sprenger, M., Stohl, A., and Wernli, H.: Forecasted deep stratospheric intrusions over Central Europe: case studies and climatologies, Atmos. Chem. Phys., 10, 499–524, doi:10.5194/acp-10-499-2010, 2010.

Trickl, T., Vogelmann, H., Giehl, H., Scheel, H.-E., Sprenger, M., and Stohl, A.: How stratospheric are deep stratospheric intrusions?, Atmos. Chem. Phys., 14, 9941–9961, doi:10.5194/acp-14-9941-2014, 2014.

Wang, Z., Deutscher, N. M., Warneke, T., Notholt, J., Dils, B., Griffith, D. W. T., Schmidt, M., Ramonet, M., and Gerbig, C.: Retrieval of tropospheric column-averaged CH_4 mole fraction by solar absorption FTIR-spectrometry using N_2O as a proxy, Atmos. Meas. Tech., 7, 3295–3305, doi:10.5194/amt-7-3295-2014, 2014.

Washenfelder, R. A., Wennberg, P. O., and Toon, G. C.: Tropospheric methane retrieved from ground-based near-IR solar absorption spectra, Geophys. Res. Lett., 30, 2226, doi:10.1029/2003GL017969, 2003.

Wernli, H. and Davies, H. C.: A Lagrangian-based analysis of extratropical cyclones, I, The method and some applications, Q. J. R. Meteorol. Soc., 123, 467–489, 1997.

Wofsy, S. C. and the HIPPO Science Team and Cooperating Modellers and Satellite Teams: TS6 HIAPER Pole-to-Pole Observations (HIPPO): fine-grained, global-scale measurements of climatically important atmospheric gases and aerosols, Philos. T. Roy. Soc. A, 369, 2073–2086, doi:10.1098/rsta.2010.0313, 2011.

Wunch, D., Toon, G. C., Wennberg, P. O., Wofsy, S. C., Stephens, B. B., Fischer, M. L., Uchino, O., Abshire, J. B., Bernath, P., Biraud, S. C., Blavier, J.-F. L., Boone, C., Bowman, K. P., Browell, E. V., Campos, T., Connor, B. J., Daube, B. C., Deutscher, N. M., Diao, M., Elkins, J. W., Gerbig, C., Gottlieb, E., Griffith, D. W. T., Hurst, D. F., Jiménez, R., Keppel-Aleks, G., Kort, E. A., Macatangay, R., Machida, T., Matsueda, H., Moore, F., Morino, I., Park, S., Robinson, J., Roehl, C. M., Sawa, Y., Sherlock, V., Sweeney, C., Tanaka, T., and Zondlo, M. A.: Calibration of the Total Carbon Column Observing Network using aircraft profile data, Atmos. Meas. Tech., 3, 1351–1362, doi:10.5194/amt-3-1351-2010, 2010.

Wunch, D., Toon, G. C., Blavier, J.-F. L., Washenfelder, R. A., Notholt, J., Connor, B. J., Griffith, D. W. T., Sherlock, V., and Wennberg, P. O.: The Total Carbon Column Observing Network, Phil. Trans. R. Soc. A, 369, 2087–2112, doi:10.1098/rsta.2010.0240, 2011a.

Wunch, D., Wennberg, P. O., Toon, G. C., Connor, B. J., Fisher, B., Osterman, G. B., Frankenberg, C., Mandrake, L., O'Dell, C., Ahonen, P., Biraud, S. C., Castano, R., Cressie, N., Crisp, D., Deutscher, N. M., Eldering, A., Fisher, M. L., Griffith, D. W. T., Gunson, M., Heikkinen, P., Keppel-Aleks, G., Kyrö, E., Lindenmaier, R., Macatangay, R., Mendonca, J., Messerschmidt, J., Miller, C. E., Morino, I., Notholt, J., Oyafuso, F. A., Rettinger, M., Robinson, J., Roehl, C. M., Salawitch, R. J., Sherlock, V., Strong, K., Sussmann, R., Tanaka, T., Thompson, D. R., Uchino, O., Warneke, T., and Wofsy, S. C.: A method for evaluating bias in global measurements of CO_2 total columns from space, Atmos. Chem. Phys., 11, 12317–12337, doi:10.5194/acp-11-12317-2011, 2011b.

Xiong, X., Barnet, C., Maddy, E., Wofsy, S. C., Chen, L., Karion, A., and Sweeney, C.: Detection of methane depletion associated with stratospheric intrusion by atmospheric infrared sounder (AIRS), Geophys. Res. Lett., 40, 2455–2459, doi:10.1002/grl.50476, 2013.

Yoshida, Y., Ota, Y., Eguchi, N., Kikuchi, N., Nobuta, K., Tran, H., Morino, I., and Yokota, T.: Retrieval algorithm for CO_2 and CH_4 column abundances from short-wavelength infrared spectral observations by the Greenhouse gases observing satellite, Atmos. Meas. Tech., 4, 717–734, doi:10.5194/amt-4-717-2011, 2011.

A.3 Article III

Andreas Ostler, Ralf Sussmann, Prabir K. Patra, Sander Houweling, Marko De Bruine, Gabriele P. Stiller, Florian J. Haenel, Johannes Plieninger, Philippe Bousquet, Yi Yin, Marielle Saunois, Kaley A. Walker, Nicholas M. Deutscher, David W. T. Griffith, Thomas Blumenstock, Frank Hase, Thorsten Warneke, Zhiting Wang, Rigel Kivi, and John Robinson: Model − TCCON comparisons of column-averaged methane with a focus on the stratosphere, submitted to Atmos. Meas. Tech., 2016.

Model – TCCON comparisons of column-averaged methane with a focus on the stratosphere

Andreas Ostler[1], Ralf Sussmann[1], Prabir K. Patra[2], Sander Houweling[3,4], Marko De Bruine[3], Gabriele P. Stiller[5], Florian J. Haenel[5], Johannes Plieninger[5], Philippe Bousquet[6,7], Yi Yin[6,7], Marielle Saunois[6,7], Kaley A. Walker[8], Nicholas M. Deutscher[9,10], David W. T. Griffith[9], Thomas Blumenstock[6], Frank Hase[6], Thorsten Warneke[10], ZhitingWang[10], Rigel Kivi[11], and John Robinson[12]

[1]Karlsruhe Institute of Technology, IMK-IFU, Garmisch-Partenkirchen, 82467, Germany
[2]Research Institute for Global Change, JAMSTEC, Yokohama, 236-0001, Japan
[3]Institute for Marine and Atmospheric Research Utrecht, Utrecht University, Utrecht, 3584 CC, the Netherlands
[4]SRON Netherlands Institute for Space Research, Utrecht, 3584 CA, the Netherlands
[5]Karlsruhe Institute of Technology, IMK-ASF, Karlsruhe, 76021, Germany
[6]Laboratoire des Sciences du Climat et de l'Environnement, IPSL-LSCE, CEA-CNRS-UVSQ, UMR8212 91191, France
[7]Universit´e de Versailles Saint Quentin en Yvelines, France
[8]Department of Physics, University of Toronto, Toronto, Ontario M5S 1A7, Canada
[9]School of Chemistry, University of Wollongong, Wollongong, NSW 2522, Australia
[10] Institute of Environmental Physics, University of Bremen, Bremen, 28334, Germany
[11] Finnish Meteorological Institute, Arctic Research Center,Sodankylä, 99600,Finland
[12]Department of Atmospheric Research, National Institute of Water and Atmospheric Research (NIWA) Ltd, Wellington 6021, New Zealand

Correspondence to: R. Sussmann (ralf.sussmann@kit.edu)

Abstract. The distribution of methane (CH_4) in the stratosphere can be a major driver of spatial variability in the dry-air column-averaged CH_4 mixing ratio (XCH_4), which is being measured increasingly for the assessment of CH_4 surface emissions. Chemistry-transport models (CTMs) therefore need to simulate the tropospheric and stratospheric fractional columns of XCH_4 accurately for estimating surface emissions from XCH_4. Simulations from three CTMs are tested against XCH_4 observations from the Total Carbon Column Network (TCCON). We analyze how the model-TCCON agreement in XCH_4 depends on the model representation of stratospheric CH_4 distributions. Model equivalents of TCCON XCH_4 are computed with stratospheric CH_4 fields from both the model simulations and from satellite-based CH_4 distributions from MIPAS (Michelson Interferometer for Passive Atmospheric Sounding) and MIPAS CH_4 fields adjusted to ACE-FTS (Atmospheric Chemistry Experiment Fourier Transform Spectrometer) observations. In comparison to simulated model fields we find an improved model-TCCON XCH_4 agreement for all models with MIPAS-based stratospheric CH_4 fields. For the Atmospheric Chemistry Transport Model (ACTM) the average XCH_4 bias is significantly reduced from 38.1 ppb to 13.7 ppb, whereas small improvements are found for the models TM5 (Transport Model, version 5; from 8.7 ppb to 4.3 ppb), and LMDz (Laboratoire de Météorologie Dynamique model with Zooming capability; from 6.8 ppb to 4.3 ppb), respectively. MIPAS stratospheric CH_4 fields adjusted to ACE-FTS reduce the average XCH_4 bias for ACTM (3.3 ppb), but increase the average XCH_4 bias for TM5 (10.8 ppb) and LMDz (20.0 ppb). These findings imply that the range of satellite-based

stratospheric CH_4 is insufficient to resolve a possible stratospheric contribution to differences in total column CH_4 between TCCON and TM5 or LMDz. Applying transport diagnostics to the models indicates that model-to-model differences in the simulation of stratospheric transport, notably the age of stratospheric air, can largely explain the inter-model spread in stratospheric CH_4 and, hence, its contribution to XCH_4. This implies that there is a need to better understand the impact of individual model transport components (e.g., physical parameterization, meteorological data sets, model horizontal/vertical resolution) on modeled stratospheric CH_4.

1 Introduction

The column-averaged dry-air mixing ratio of methane (CH_4), denoted as XCH_4, is an integrated measure of CH_4 with contributions from the troposphere and the stratosphere. Observations of XCH_4 contain source/sink information on a global to regional scale. They are provided by the ground-based networks NDACC (Network for the Detection of Atmospheric Composition Change, http://www.ndacc.org/; Kurylo, 1991) and TCCON (Total Carbon Column Observing Network, http://www.tccon.caltech.edu/; Wunch et al., 2011a), and also by satellite-based observation platforms like SCIAMACHY (Scanning Imaging Absorption Spectrometer for Atmospheric Cartography; Burrows et al., 1995; Frankenberg et al., 2011) and GOSAT (Greenhouse Gases Observing Satellite; Kuze et al., 2009; Yokota et al., 2009). Satellite-inferred XCH_4 observations are increasingly used in atmospheric inverse modelling because of their beneficial spatiotemporal data coverage (Bergamaschi et al., 2013; Fraser et al., 2013; Monteil et al., 2013; Fraser et al., 2014, Houweling et al., 2014; Wecht et al., 2014; Cressot et al., 2014; Alexe et al., 2015; Turner et al., 2015; Locatelli et al., 2015). Given the high accuracy of ground-based XCH_4 TCCON retrievals, these observations are typically used for the evaluation of both chemistry-transport model (CTM) simulations (Saito et al., 2012; Belikov et al., 2013; Monteil et al., 2013; Fraser et al., 2014; Alexe et al., 2015; Turner et al., 2015), and satellite-retrieved XCH_4 (Parker et al., 2011; Schepers et al., 2012; Dils et al., 2014; Houweling et al., 2014; Parker et al., 2015; Kulawik et al., 2015; Parker et al., 2015; Pandey et al., 2016; Inoue et al., 2016).

Because of the various influences on XCH_4, however, the interpretation of residual XCH_4 differences with TCCON may be difficult. For example, a good agreement between XCH_4 simulations and observations may suggest that a CTM is able to represent atmospheric conditions in a realistic way. However, it could also be that systematic model and satellite data errors in the troposphere and the stratosphere compensate each other. For this reason, it is necessary to extend model validations with additional atmospheric CH_4 observations that are complementary to XCH_4 observations, like surface or airborne in situ measurements, or balloon-based vertical profiles (Karion et al., 2010). In the context of a refined model comparison, it is also possible to separate ground-based XCH_4 observations into tropospheric and stratospheric partial columns (Washenfelder et al., 2003; Sepúlveda et al., 2012; 2014; Wang et al., 2014; Saad et al., 2014).

Model-measurement XCH_4 residuals are minimized by atmospheric inversions in order to constrain CH_4 emission fluxes. Inversion models are also able to make use of in situ measurements and XCH_4 observations at the same time in order to adjust prior emission fluxes. Nevertheless, such inverse models still have to deal with ill-defined XCH_4 residual biases,

which, in contrast to well-quantified biases, cannot be attributed to errors in the model or the observations without an unambiguous assignment (Houweling et al., 2014). Currently, there are various approaches to optimize bias functions within the inverse model or to construct bias corrections as ad hoc functions of latitude or air mass. Ad hoc bias corrections, like removing a latitudinal background pattern in XCH_4 model-observation differences, are common, even though they bear the risk of obscuring real signals from emissions on the Earth's surface. Given the fact that the stratospheric contribution relative to the CH_4 total column increases from ~5% at the tropics up to ~25% at mid- and high latitudes, model errors in the representation of stratospheric CH_4 mixing ratios are expected to give rise to a latitudinal varying bias (Turner et al., 2015). Although it is known that CTMs differ by up to ~50% in the simulation of lower stratospheric CH_4 distributions (Patra et al., 2011), an atmospheric region with a steep methane gradient of ~ -50 ppb/km, the impact of model errors in stratospheric CH_4 on XCH_4 has not been rigorously quantified up to now. In this context, the goal of this study is to better understand the sensitivity of XCH_4 model-observation differences to the model representation of stratospheric CH_4.

Our XCH_4 model-observation analysis is based on optimized model simulations from three well-established CTMs on the one side and accurate XCH_4 observations from TCCON on the other. The impact of model stratospheric CH_4 distributions on XCH_4 is estimated by replacing modeled stratospheric CH_4 fields with monthly mean CH_4 distributions observed by MIPAS (Michelson Interferometer for Passive Atmospheric Sounding), and by ACE-FTS (Atmospheric Chemistry Experiment Fourier Transform Spectrometer). In addition to this, we briefly evaluate the model characteristics of stratospheric transport in order to understand differences between simulated and observed CH_4 distributions. The paper has the following structure: After introducing the models (Sect. 2) and the observations (Sect. 3), we present both a direct model-TCCON comparison and a comparison with refined model data using satellite data products of stratospheric CH_4 in Sect. 4. The transport characteristics of the models are discussed in Sect. 5, followed by a summary and conclusions in Sect. 6.

2 Model simulations

The focus of this study is assessing the impact of stratospheric CH_4 on XCH_4. Therefore, we try to ensure that model simulations represent tropospheric CH_4 mixing ratios as well as possible. For this purpose, we use optimized CH_4 model simulations that have been constrained by surface observations. Our model analysis comprises simulations from three well-established CTMs that have already been part of the chemistry-transport model inter-comparison experiment TransCom-CH_4 (Patra et al., 2011) and used in inverse modelling of CH_4 emissions. Furthermore, we use model simulations of stratospheric mean age for an evaluation of model transport characteristics in Sect. 5. Basic model features are given in Table 1.

2.1 ACTM

The ACTM model (Patra et al., 2009a) is an atmospheric general circulation model (AGCM)-based CTM from the Center for Climate System Research/National Institute for Environmental Studies/Frontier Research Center for Global Change (CCSR/NIES/FRCGC). Here, we use optimized ACTM simulations presented in Patra et al. (2016) as inversion case 2

(CH_4ags). The ACTM horizontal resolution is ~ 2.8°×2.8° (T42 spectral truncations) with 67 sigma-pressure vertical levels. The meteorological fields of ACTM are nudged with reanalysis data from the Japan Meteorological Agency, version JRA-25 (Onogi et al., 2007). ACTM uses an optimized OH field (Patra et al., 2014) based on a scaled version of the seasonally varying OH field from Spivakovski et al. (2000). The concentration fields being relevant for stratospheric CH_4 loss − OH, $O(^1D)$, and chlorine (Cl) radicals – are based on simulations by the ACTM's stratospheric model run (Takigawa et al., 1999). ACTM mean age is derived from the simulation of an idealized transport tracer with uniform surface fluxes, linearly increasing trend, and no loss in the atmosphere (Patra et al., 2009b). The ACTM simulate the observed CH_4 inter-hemispheric gradient in the troposphere and individual in situ measurements generally within 10 ppb (Patra et al., 2016).

2.2 TM5

The global chemistry Tracer Model, version 5 (TM5) has been described in Krol et al. (2005) and used as an atmospheric inversion model for CH_4 emissions (Bergamaschi et al., 2005; Meirink et al., 2008, Houweling et al., 2014). Here, we use TM5 simulations of CH_4 optimized with surface measurements only (Pandey et al., 2016). TM5 is run with a horizontal resolution of 6°×4° and a vertical grid of 25 layers. TM5 meteorology is driven by the reanalysis data set ERA-interim (Dee et al., 2011) from the European Centre for Medium Range Weather Forecasts (ECMWF). The simulation of the chemical CH_4 sink uses OH fields from Spivakovski et al. (2000), which have been scaled to match methyl chloroform measurements. In addition to that, stratospheric CH_4 loss via Cl and $O(^1D)$ radicals is simulated using their concentration fields based on the 2-D photochemical Max-Planck-Institute (MPI) model (Bruehl and Crutzen, 1993). Known deficiencies in the TM5 simulation of inter-hemispheric mixing have been corrected by extending the model with a horizontal diffusion parameterization that is adjusted to match SF_6 simulations with SF_6 measurements (Monteil et al., 2013).

TM5 simulations of sulfur hexafluoride (SF_6) were used to derive stratospheric mean age data. SF_6 mixing ratios are monotonically increasing with time showing higher mixing ratios in the troposphere than in the stratosphere, given the transport time from SF_6 surface sources to higher altitudes. This implies that tropospheric and stratospheric SF_6 mixing ratios of equal size are separated from each other by a time lag which is commonly defined as mean age of air. In order to derive mean age from SF_6 model simulations, the same tropospheric SF_6 reference time series was used as for the derivation of MIPAS mean age data (see Stiller et al., 2012)

2.3 LMDz

The LMDz (Laboratoire de Météorologie Dynamique model with Zooming capability) is a general circulation model (Hourdin et al., 2006), that has been used to investigate the impact of transport model errors on inverted CH_4 emissions (Locatelli et al., 2013). Here, we use optimized LMDz simulations of CH_4, recently presented as LMDz-SP constrained by surface measurements from background sites (Locatelli et al., 2015). These model simulations are nudged with the ERA-Interim reanalysis data set for horizontal winds (u,v). LMDz has a horizontal resolution of 3.75°×1.875°, and 39 hybrid sigma-pressure layers. The chemical destruction of CH_4 by OH and $O(^1D)$ is based on prescribed concentration fields

simulated by the chemistry–climate model LMDz-INCA (Szopa et al., 2013). No Cl-based CH_4 destruction is prescribed in this version of the model. Besides CH_4, LMDz simulations of SF_6 were used to derive mean age data in analogy to the method used for TM5.

3 Intercomparison strategy and observations

3.1 Intercomparison strategy

We want to quantify the dependence of the XCH_4 model-observation agreement on the model representation of stratospheric CH_4 mixing ratios. For this purpose, we apply original CH_4 model fields and two corrected CH_4 model fields, where we have replaced the modeled stratospheric CH_4 by satellite data sets of stratospheric CH_4 mixing ratios. The first satellite data set consists of MIPAS CH_4 observations, whereas the second satellite data set contains MIPAS CH_4 observations that are adjusted to ACE-FTS-observed CH_4 levels. This allows us to represent an uncertainty range for the satellite-based model correction. Finally, our XCH_4 model-observation comparison deals with a triplet of model CH_4 fields for each CTM.

Using TCCON XCH_4 observations as validation reference, we evaluate the impact of correcting the modeled stratospheric CH_4 on XCH_4. Consequently, modeled vertical profiles of CH_4 were extracted for each TCCON site and subsequently converted to XCH_4 by accounting for the TCCON retrieval a priori and vertical sensitivity. This means that model CH_4 profiles are adjusted to the actual surface pressure measured at the time of a single TCCON observation. In addition to that, model profiles are convolved with the daily TCCON retrieval a priori profiles of CH_4, that have been converted from wet-air into dry-air units by subtracting a daily water vapour profile provided by NCEP (National Centers for Environmental Prediction).and the averaging kernel depending on the actual solar zenith angle. Thereby, monthly mean CH_4 profiles from LMDz also receive a daily component depending on the surface pressure, the TCCON a priori profiles and averaging kernels. The statistical analysis of XCH_4 model-TCCON differences then is based on the daily mean time series for the year 2010 and produces two site-specific parameters: the mean difference (bias) and the residual standard deviation (RSD).

3.2 TCCON observations of column-averaged methane

Solar absorption measurements in the near-infrared (NIR) are performed via ground-based Fourier Transform Spectrometers (FTS) at TCCON sites across the globe. TCCON-type measurements are analyzed with the GGG software package including the spectral fitting code GFIT to derive total column abundances of several trace gases (Wunch et al., 2011). The CH_4 total column is inverted from the spectra in three different spectral windows centered at 5938 cm^{-1}, 6002 cm^{-1}, and 6076 cm^{-1}. The spectral fitting method is based on iteratively scaling a priori profiles to provide the best fit to the measured spectrum. The general shape of the a priori profiles has been inferred from aircraft, balloon and satellite profiles (ACE-FTS profiles measured in the 30-40° N latitude range from 2003 to 2007). In addition, the shape of the daily a priori profile is vertically squeezed/stretched depending on tropopause altitude and the latitude of the measurement site. This means, that the tropopause altitude is used as a proxy for stratospheric ascent/descent to represent the origin of the airmass in the a priori

profile. XCH_4 is calculated by dividing the CH_4 number density by the simultaneously measured O_2 number density (a proxy for the dry-air pressure column).

These XCH_4 retrievals are a posteriori corrected for known airmass-dependent biases and calibrated to account for airmass-independent biases, which can, among other errors, arise from spectroscopic uncertainties (Wunch et al., 2011). The airmass-independent calibration factor, which is determined by comparisons with coincident airborne or balloon-borne in situ measurements over TCCON sites (Wunch et al., 2010; Messerschmidt et al., 2011; Geibel et al., 2012), allows for a calibration of TCCON XCH_4 retrievals to in situ measurements on the WMO scale. Furthermore, the quality of the retrievals is continuously improved by correcting the influence of systematic instrumental changes over time. As a result of these improvements there are different versions of the GGG software package. In this study we use TCCON retrievals performed with version GGG2014 (for details see https://tccon-wiki.caltech.edu/). The TCCON measurement precision (2-σ) for XCH_4 is <0.3% (< 5ppb) for single measurements. For the year 2010, XCH_4 observations are available from 11 TCCON sites, listed in Table 2. Knowing that TCCON XCH_4 accuracy can be affected by a strong polar vortex (Ostler et al., 2014), we exclude high-latitude observations at Sodankylä within the early spring period (March, April, May) from the analysis. TCCON data were obtained from the TCCON Data Archive, hosted by the Carbon Dioxide Information Analysis Center (CDIAC: http://cdiac.ornl.gov/). The individual data sets of the TCCON sites used in this study are available at this database.

3.3 Satellite-based data sets of stratospheric methane

In order to correct modeled stratospheric CH_4 fields, we use satellite-borne MIPAS measurements covering the stratosphere. As a Fourier-Transform Infrared Spectrometer aboard the Environmental Satellite (Envisat), MIPAS detected atmospheric emission spectra in the mid-infrared region via limb sounding (Fischer et al., 2008). Profiles of various atmospheric trace gas concentrations are derived by the research processor developed by the Karlsruhe Institute of Technology, Institute of Meteorology and Climate Research (KIT IMK) and the Instituto de Astrofísica de Andalucía (CSIC) (von Clarmann et al., 2003). The MIPAS CH_4 data set comprises zonal monthly means with a horizontal grid resolution of 5° latitude. In the vertical, the resolution of the MIPAS CH_4 fields range from 2.5 to 7 km, see Plieninger et al. (2015a) for more details. As an additional quality criterion, we only select MIPAS data points that are averaged over more than 300 profile measurements. As a result, our MIPAS CH_4 data set typically covers altitudes higher than ~10 km at mid latitudes and heights above ~15 km in the Tropics. This implies that we do not use a thermal or chemical tropopause definition, but use the MIPAS data where they are available. Therefore, we cannot exclude that our MIPAS-based CH_4 fields contain some upper tropospheric MIPAS values, i.e. our definition of stratospheric CH_4 is not strict from a meteorological point of view.

The corrected model CH_4 profiles rely on original model CH_4 fields that are merged with MIPAS-based zonal CH_4 fields (monthly means) interpolated to the model grid. Merging original model CH_4 fields/profiles with zonal monthly means implies that we lose some spatial and temporal variability in the corrected model CH_4 fields. However, for our aim ─ investigating the overall impact of model stratospheric CH_4 fields on the quantity XCH_4 ─ a monthly mean representation of stratospheric CH_4 in the corrected model fields is sufficient.

In our study we use the strongly revised MIPAS CH_4 data product for the MIPAS reduced-resolution period from January 2005 to April 2012. This new data set (version V5R_CH4_224/V5R_CH4_225) was recently introduced by Plieninger et al. (2015) with an emphasis on retrieval characteristics. Plieninger et al. (2015) showed that CH_4 mixing ratios are reduced in the lowermost stratosphere when using the new retrieval settings. This finding implies that the high bias of the older CH_4 data version in the lowermost stratosphere, which was determined by Laeng et al. (2015), has been partially alleviated. Nevertheless, a recent comparison study by Plieninger et al. (2016) suggests a remaining positive bias (100 – 200 ppb) relative to other satellite measurements such as ACE-FTS observations.

For this reason, a second satellite CH_4 data set was constructed by adjusting MIPAS stratospheric CH_4 mixing ratios to ACE-FTS measurements of CH_4. Given the sparse data coverage of ACE-FTS observations for the year 2010, we did not use ACE-FTS measurements directly. Instead, the MIPAS CH_4 fields were adjusted by offsets relative to ACE shown in Fig. 1, yielding the second satellite-based CH_4 data set abbreviated by MIPAS_ACE. We used collocated pairs of CH_4 profiles from MIPAS and ACE-FTS to derive a CH_4 offset as a function of altitude and latitude for the year 2010. The collocation criteria are based on a maximum radius of 500 km and a maximum temporal deviation of 5 hours, which is identical to Plieninger et al. (2016). Furthermore, the MIPAS averaging kernels were applied to ACE-FTS CH_4 profiles. ACE-FTS operates in solar occultation mode (Bernath et al., 2005) and also provides retrievals of several trace gases including CH_4. Here, we use ACE-FTS data from a research version of the 3.5 retrieval described in Buzan et al. (2015).

Figure 1 shows the CH_4 offset functions computed as mean differences between MIPAS and ACE-FTS for 30° latitudinal bands. Figure 1 confirms the findings by Plieninger et al. (2016) that MIPAS is biased positive by ~ 150 ppb relative to ACE-FTS within the lowermost stratosphere. For higher altitudes (> 25 km), mean differences between MIPAS and ACE-FTS are larger for the tropical domain (up to 100 ppb) compared to higher latitudes (up to 50 ppb).

3.4 MIPAS-observed mean age

Besides MIPAS CH_4 observations, we also use MIPAS data sets of stratospheric mean age inferred from SF_6 measurements. Here, we use the new MIPAS mean age data set presented by Haenel et al. (2015). This new mean age data set contains several improvements compared to the previous version introduced by Stiller et al. (2012). For MIPAS, the mean age is calculated as the average transport time from the tropical troposphere to a certain location in the stratosphere using NOAA (National Oceanic and Atmospheric Administration) observations as reference. The mean age of stratospheric air is of special interest for climate research because the distributions of greenhouse gases like ozone critically depend on possible changes in the stratospheric transport pathways (Engel et al., 2009). Mean age can be inferred from observations of clock-tracers (concentrations monotonically increasing with time) like SF_6 or CO_2, and can also be simulated by models. For this reason, it is a well-known diagnostic for stratospheric transport being very suitable for the evaluation of model transport characteristics (Waugh and Hall, 2002). The combined MIPAS data set of stratospheric CH_4 and mean age is used for the evaluation of model transport characteristics in Sect. 5.1.

4 Model-TCCON comparison of column-averaged methane

Figure 2 shows model biases in XCH_4 with respect to TCCON observations, where each TCCON site is represented by its geographical latitude. For each CTM a triplet of model CH_4 fields (uncorrected, MIPAS and MIPAS_ACE corrected) yields a triplet of model XCH_4 biases. All site-specific XCH_4 model biases are individually listed in Table 3. In addition, Table 4 provides an average XCH_4 bias for each model data set, computed as the mean of absolute site-specific biases.

The original XCH_4 bias for ACTM lies in between 18.8 ppb and 51.3 ppb (see Fig. 2a and Table 3). This high bias is significantly reduced when ACTM stratospheric CH_4 fields are replaced by satellite-based CH_4 fields. The model correction with MIPAS CH_4 reduces the average ACTM XCH_4 bias from 38.1 ppb to 13.7 ppb (see Table 4). Site-specific XCH_4 biases are ranging from 4.8 ppb to 19.9 ppb (see Table 3). The model correction with MIPAS_ACE reduces the average ACTM XCH_4 bias further from 38.1 ppb to 3.3 ppb (see Table 4) with values in an interval between –9.9 ppb and 3.5 ppb (see Table 3)), similar to that were expected from the comparison with ACTM simulations with tropospheric measurements (Patra et al., 2016).

For the original TM5 we detect negative site-specific XCH_4 biases with values between –17.6 ppb and –3.7 ppb (see Fig. 2b and Table 3). When TM5 CH_4 fields are corrected with MIPAS observations, this negative XCH_4 bias is reduced from -8.7 ppb to -4.3 ppb on average (see Table 3). The corresponding site-specific XCH_4 biases then are between –11.1 ppb and 8.1 ppb (Table 3). If the MIPAS_ACE is applied to TM5 then the site-specific TM5 XCH_4 biases are shifted further to the negative direction with values between –18.3 ppb and –3.7 ppb. In this case the average XCH_4 bias increased from 8.7 ppb to 10.8 ppb (Table 4).

With respect to TCCON observations LMDz produces both negative and positive XCH_4 biases ranging from –11.9 ppb (Wollongong) to 13.0 ppb (Sodankylä), see Fig. 2c and Table 3. The average LMDz XCH_4 bias is slightly reduced from 6.8 ppb to 4.3 ppb if LMDz is corrected with MIPAS CH_4 fields (see Table 4). After this correction, site-specific LMDz XCH_4 biases lie between −2.9 ppb and 9.1 ppb. Using MIPAS_ACE CH_4 fields for the LMDz model correction produces LMDz XCH_4 biases between −13.8 ppb and −31.1 ppb. At the same time, the average LMDz XCH_4 bias is increased from 6.8 ppb to 20.0 ppb (Table 4).

Overall, our results confirm that the model-TCCON agreement in XCH_4 depends very much on the model representation of stratospheric CH_4. It is obvious that the XCH_4 offset between ACTM and TCCON is significantly reduced with stratospheric CH_4 fields based on satellite data. By contrast, for TM5 and LMDz the impact of the model correction on the model-TCCON agreement is ambiguous. In that, the model-TCCON agreement can be improved (with MIPAS), but can also be reduced (with MIPAS_ACE). In order to understand this inter-model spread we look at the differences between modeled and satellite-retrieved CH_4 fields. Figure 3 shows zonal and annual averaged CH_4 mixing ratio differences between MIPAS and each CTM. Figure 3a illustrates that stratospheric CH_4 mixing ratios are generally much higher in ACTM than in MIPAS. The ACTM-MIPAS differences in CH_4 are increasing from negligible values within the lowermost stratosphere up to 450 ppb in the upper stratosphere. Furthermore, the ACTM-MIPAS difference in CH_4 also shows a latitudinal dependence, with

middle and upper stratospheric values increasing towards higher latitudes. The positive bias in stratospheric ACTM CH_4 mixing ratios causes a positive ACTM bias in XCH_4. In contrast to that, we find negative model-MIPAS differences in stratospheric CH_4 mixing ratios for TM5 (Fig. 3b) resulting in a small negative XCH_4 bias. We identify two altitude regions, where TM5 modeled CH_4 mixing ratios are smaller than MIPAS CH_4 mixing ratios: the lower stratosphere with differences in CH_4 mixing ratios of up to −100 ppb, and the upper stratosphere (> 30 hPa) with maximum CH_4 differences of ~ −150 ppb. Figure 3c shows the CH_4 mixing ratio differences between LMDz and MIPAS with noticeable negative CH_4 differences of up to −200 ppb within the tropical upper stratosphere. Negative CH_4 differences (~ −100 ppb) are also visible in the upper stratosphere of the mid- and high-latitude region. In contrast to this, we identify positive CH_4 differences of up to 100 ppb within the middle stratosphere (~ 50 hPa) of the mid and high latitudes. The negative and positive CH_4 differences partially cancel out in XCH_4. In analogy to Fig. 3, the CH_4 differences between model and MIPAS_ACE fields are illustrated in Fig. 4. Given the offset adjustment of MIPAS to ACE-FTS (see Fig. 1), the MIPAS_ACE CH_4 fields comprise lower CH_4 mixing ratios compared to MIPAS, mostly in the lower stratosphere. Hence, the ACTM-satellite CH_4 difference is larger for MIPAS_ACE fields than for MIPAS fields. For TM5 and LMDz model-satellite CH_4 differences are shifted into the positive direction (Figs. 4b and 4c). In other words, modeled stratospheric CH_4 mixing ratios appear to be too high when compared to MIPAS and too low in comparison to MIPAS_ACE.

5 Discussion

Our analysis shows that the model-TCCON agreement in XCH_4 critically depends on the model representation of stratospheric CH_4, which is diverse for the presented CTMs. In the following we discuss possible causes for the inter-model spread in stratospheric CH_4. In addition to that, we evaluate the findings of our XCH_4 model-TCCON comparison with respect to satellite data uncertainty.

5.1 Model transport characteristics as possible cause for inter-model spread in stratospheric methane

An inter-model spread in stratospheric CH_4 fields has already been detected by Patra et al. (2011) despite applying uniform fields of OH, Cl, and O^1D for all models. Their findings, therefore, suggested a predominant role of transport in the simulation of CH_4 vertical distributions. For this reason, we tested here whether differences in the modeling of stratospheric transport are noticeable. To do this, we follow the approach of Strahan et al. (2011) who sought to understand chemistry climate model ozone simulations using transport diagnostics. This method is based on the compact relationship between a long-lived stratospheric tracer and mean age in the lower stratosphere. In their work, they compared simulations and air-borne observations of N_2O/mean age correlations, in order to evaluate the model transport characteristics. Here, we use the MIPAS data of CH_4 and mean age as a reference to identify model-to-model differences in the simulation of stratospheric transport. The MIPAS data are not used to evaluate, whether modeled stratospheric circulations are realistic or not, given the uncertainties of MIPAS CH_4 and mean age data. For example, the MIPAS mean age range may be too large, because MIPAS

mean age can be up to 0.8 years too old due to the impact of mesospheric SF_6 loss (Stiller et al., 2012). This loss process was not included in the models used for this study. Moreover, the MIPAS CH_4 data significantly differs from ACE-FTS CH_4 data within the lower stratosphere (see Fig. 1).

In analogy to Strahan et al. (2011) we focus our model transport diagnostics on the tropical domain because tropical diagnostics quantities allow a better assessment of the individual transport processes ascent and mixing. Annual means of age and CH_4 mixing ratios for modeled as well as MIPAS-observed fields were calculated for the lower stratosphere (30−100 hPa) of the tropical domain (10°S−10°N), and of the northern-hemispheric mid-latitude region (35°N−50°N), respectively. Subsequently, vertical profiles of mean model-MIPAS differences were calculated to provide insight into the tropical transport characteristics.

Figure 5 illustrates that the model-MIPAS difference of tropical mean age is almost identical for all models. I.e. the model simulations produce similar mean ages that are younger than MIPAS-observed mean ages. Knowing that mean age only represents the combined effects of ascent and mixing, we separately look at those two processes being relevant for stratospheric transport. According to Strahan et al. (2011), the tropical ascent rate is assessed by the horizontal mean age gradient, calculated as the difference between mid-latitude and tropical mean ages. The model-MIPAS difference of the tropical ascent rate is shown in Fig. 6, indicating that ACTM and LMDz simulate tropical ascent in similar way. The TM5-modeled tropical ascent is faster compared to ACTM and LMDz. Next, we look at the tropical model-MIPAS CH_4 difference, which is used as a measure for (cumulative) horizontal mixing. Figure 7 reveals that horizontal mixing is different for ACTM compared to TM5 and LMDz looking very similar. I.e. the horizontal mixing appears to be weaker for ACTM compared to the other models. Finally, these model transport diagnostics indicate model-to-model differences in the simulation of tropical ascent and horizontal mixing, which are likely to cause an inter-model spread in model stratospheric CH_4 fields.

Indeed, model-to-model differences affecting the simulation of stratospheric transport are present in the vertical/horizontal resolution, sub-grid-scale physical parameterizations, advection schemes, numerical methods, etc. Furthermore, the simulation of stratospheric transport depends on the reanalysis data used to drive the model meteorology,. e.g. the ECMWF reanalysis data set ERA-Interim leads to an improved representation of the stratospheric circulation in comparison to the older ERA-40 reanalysis data (Monge-Sanz et al., 2007, 2011; Diallo et al., 2012). The ERA-Interim data are used by TM5 and LMDz, whereas ACTM applies the JRA-25 reanalysis data (Onogi et al., 2007), which is known to have several deficiencies compared to the newer JRA-55 data (Ebita et al., 2011). However, testing ACTM with both ERA-interim/40 and JRA-25/55 has not produced significant differences in CH_4 simulations (P. Patra, personal communication, 2016). Besides that, we do not expect that the poor representation of stratospheric CH_4 by ACTM (with 67 vertical levels) is impacted by a coarse vertical model grid resolution, as seen for an older version of LMDz (Locatelli et al., 2015).

5.2 Significance of satellite data range

The model correction with satellite-based CH_4 fields has an impact on the XCH_4 model-TCCON agreement, but the significance of this impact is diverse for the models. For ACTM both satellite-based CH_4 fields, in particular MIPAS_ACE, clearly yield an improved model-TCCON agreement. For TM5 and LMDz, the model-TCCON agreement can be slightly improved (with MIPAS), but also reduced (with MIPAS_ACE). Thereby, we assert, that original XCH_4 simulations from TM5 and LMDz lie inside the range that is spanned by the two satellite-based CH_4 fields. The most prominent feature of the satellite data range lies within the lower stratosphere where MIPAS-retrieved CH_4 mixing ratios are up to 200 ppb higher than ACE-FTS-retrieved CH_4 mixing ratios. Plieninger et al. (2016) also found a similar high bias for MIPAS CH_4 data in comparison to satellite-based CH_4 observations from SCIAMACHY or HALOE (HALogen Occultation Experiment). Furthermore, they showed that surface measurements provide CH_4 mixing ratios with slightly lower values than MIPAS-retrieved CH_4 mixing ratios of the upper troposphere, a finding that is against expectation. For these reasons, it is likely that our satellite data range is dominated by high biased lower stratospheric MIPAS CH_4 data. Thus, the model correction with ACE-FTS-based CH_4 fields seems more reliable. However, a definite assessment of the satellite data accuracies is not possible yet due to the lack of an extensive observational data set based on stratospheric in situ measurements.

6 Summary and conclusions

This study analyzed the importance of uncertainties in stratospheric CH_4 in comparisons of modeled and TCCON observed XCH_4. Modeled stratospheric CH_4 fields were substituted by satellite-retrieved CH_4 fields from MIPAS and ACE-FTS. Original and satellite-corrected model CH_4 fields were converted to XCH_4 and subsequently evaluated by comparison to TCCON XCH_4 observations from 11 sites. This approach and the statistical analysis of XCH_4 model-TCCON residuals were conducted with three well-established CTMs: ACTM, TM5 and LMDz.

Our model-TCCON XCH_4 intercomparison reveals an inter-model spread in XCH_4 bias caused by an inter-model spread in stratospheric CH_4. For ACTM we find a large average XCH_4 bias of 38.1 ppb, in contrast to small average XCH_4 biases of 8.7 ppb for TM5 and 6.8 ppb for LMDz. The ACTM XCH_4 bias is reduced by the model correction to 13.7 ppb with MIPAS, and to 3.3 ppb with MIPAS adjusted to ACE-FTS, respectively. For TM5 and LMDz the impact of the model correction with satellite-based CH_4 fields is ambiguous. In that. the model XCH_4 bias can be slightly reduced to 4.3 ppb with MIPAS, but can also be increased to 10.8 ppb for TM5 and 20.0 ppb for LMDz with MIPAS adjusted to ACE-FTS. This implies that for TM5 and LMDz the model representation of stratospheric CH_4 is located within the satellite data range mapped by MIPAS and ACE-FTS observations.

Possible causes for the inter-model spread in stratospheric CH_4 have been discussed with an emphasis on model transport characteristics. Applying tropical transport diagnostics suggests that the poor representation of stratospheric CH_4 by ACTM originates from errors in the simulation of transport pathways into and within the stratosphere. However, this only is an interpretation based on a diagnostic and requires more process-oriented model evaluation of stratospheric transport. The

inter-model spread in stratospheric CH_4 could be quantitatively investigated with a main focus on model-to-model differences in the simulation of stratospheric transport (physical parameterizations, reanalysis data sets, vertical/horizontal resolution), e.g., model simulations could be performed with different reanalysis data sets, and/or different physical parameterizations resulting in a model ensemble for each CTM or a multi-model ensemble consisting of multiple CTM data sets. This would allow the individual model errors in stratospheric CH_4 to be assessed more precisely.

Overall we state that there is a need for improvement in modeling of stratospheric CH_4 and, thus, XCH_4. At the same time, a better quantification of model errors in stratospheric CH_4 is limited by the uncertainty of satellite data products as used in this study. This implies that more stratospheric CH_4 in situ observations are required to validate both satellite-retrieved and modeled CH_4 data. A more accurate evaluation of modeled stratospheric CH_4 fields is particularly reasonable as these CTMs are used to invert CH_4 emissions from XCH_4 data. As surface emission signals in XCH_4 are small compared to co-resident XCH_4 atmospheric background levels, it is necessary to identify minor XCH_4 biases in the model as done in this study. Of course, an analogous quality requirement also is needed for ground-based and satellite-borne XCH_4 data. Indeed, as long as unallocated and poorly understood differences of several ppb remain between satellite-borne XCH_4 data and optimized model fields, it is difficult to take a full benefit of satellite XCH_4 data to robustly retrieve regional methane emissions.

Acknowledgements

We thank H. P. Schmid (KIT/IMK-IFU) for his continual interest in this work. Our work has been performed as part of the ESA GHG-cci project via subcontract with the University of Bremen. In addition we acknowledge funding by the EC within the InGOS project. A part of work at JAXA was supported by the Environment Research and Technology Development Fund (A-1102) of the Ministry of the Environment, Japan. From 2004 to 2011 the Lauder TCCON program was funded by the New Zealand Foundation of Research Science and Technology contracts CO1X0204, CO1X0703 and CO1X0406. Since 2011 the program has been funded by NIWA's Atmosphere Research Program 3 (2011/13 Statement of Corporate Intent). The Darwin and Wollongong TCCON sites are funded by NASA grants NAG5-12247 and NNG05-GD07G, and Australian Research Council grants DP140101552, DP110103118, DP0879468, LE0668470, and LP0562346. We are grateful to the DOE ARM program for technical support at the Darwin TCCON site. The Białystok and Orléans TCCON sites are funded by the EU projects InGOS and ICOS-INWIRE, and by the Senate of Bremen. Nicholas Deutscher was supported by an Australian Research Council fellowship, DE140100178. We also are grateful to P. O. Wennberg for providing TCCON data. The Atmospheric Chemistry Experiment (ACE), also known as SCISAT, is a Canadian-led mission mainly supported by the Canadian Space Agency and the Natural Sciences and Engineering Research Council of Canada.

References

Alexe, M., Bergamaschi, P., Segers, A., Detmers, R., Butz, A., Hasekamp, O., Guerlet, S., Parker, R., Boesch, H., Frankenberg, C., Scheepmaker, R. A., Dlugokencky, E., Sweeney, C., Wofsy, S. C., and Kort, E. A.: Inverse modelling of CH_4 emissions for 2010–2011 using different satellite retrieval products from GOSAT and SCIAMACHY, Atmos. Chem. Phys., 15, 113-133, doi:10.5194/acp-15-113-2015, 2015.

Belikov, D. A., Maksyutov, S., Sherlock, V., Aoki, S., Deutscher, N. M., Dohe, S., Griffith, D., Kyro, E., Morino, I., Nakazawa, T., Notholt, J., Rettinger, M., Schneider, M., Sussmann, R., Toon, G. C., Wennberg, P. O., and Wunch, D.: Simulations of column-averaged CO_2 and CH_4 using the NIES TM with a hybrid sigma-isentropic (σ-θ) vertical coordinate, Atmos. Chem. Phys., 13, 1713-1732, doi:10.5194/acp-13-1713-2013, 2013.

Bergamaschi, P., Krol, M., Dentener, F., Vermeulen, A., Meinhardt, F., Graul, R., Ramonet, M., Peters, W., and Dlugokencky, E. J.: Inverse modelling of national and European CH_4 emissions using the atmospheric zoom model TM5, Atmos. Chem. Phys., 5, 2431-2460, doi:10.5194/acp-5-2431-2005, 2005.

Bergamaschi, P., Houweling, S., Segers, A., Krol, M., Frankenberg, C., Scheepmaker, R. A., Dlugokencky, E.,Wofsy, S. C., Kort, E. A., Sweeney, C., Schuck, T., Brenninkmeijer, C., Chen, H., Beck, V., and Gerbig, C.: Atmospheric CH_4 in the first decade of the 21st century: inverse modeling analysis using SCIAMACHY satellite retrievals and NOAA surface measurements, J. Geophys. Res., 118, 7350–7369, doi:10.1002/jgrd.50480, 2013.

Bernath, P. F., McElroy, C. T., Abrams, M. C., Boone, C. D., Butler, M., Camy-Peyret, C., Carleer, M., Clerbaux, C., Coheur, P., Colin, R., DeCola, P., De Mazière, M., Drummond, J. R., Dufour, D., Evans, W. F. J., Fast, H., Fussen, D., Gilbert, K., Jennings, D. E., Llewellyn, E. J., Lowe, R. P., Mahieu, E., McConnell, J. C., McHugh, M., McLeod, S. D., Michaud, R., Midwinter, C., Nassar, R., Nichitiu, F., Nowlan, C., Rinsland, C. P., Rochon, Y. J., Rowlands, N., Semeniuk, K., Simon, P., Skelton, R., Sloan, J. J., Soucy, M., Strong, K., Tremblay, P., Turnbull, D., Walker, K. A., Walkty, I., Wardle, D. A., Wehrle, V., Zander, R., and Zou, J.: Atmospheric Chemistry Experiment (ACE): Mission overview, Geophys. Res. Lett., 32(15), L15S01, doi:10.1029/2005GL022386, 2005.

Blumenstock, T., Hase, F., Schneider, M., García, O. E., and Sepúlveda, E.: TCCON data from Izana, Tenerife, Spain, release GGG2014R0, TCCON data archive, hosted by the Carbon Dioxide Information Analysis Center, Oak Ridge National Laboratory, Oak Ridge, Tennessee, USA, doi:10.14291/tccon.ggg2014.izana01.R0/1149295, 2014.

Boone, C. D.,Walker, K. A., and Bernath, P. F.: Version 3 Retrievals for the Atmospheric Chemistry Experiment Fourier Transform Spectrometer (ACE-FTS), in: The Atmospheric Chemistry Experiment ACE at 10: A Solar Occultation Anthology, edited by Bernath, P. F., pp. 103–127, A. Deepak Publishing, Hampton, Virginia, USA, 2013.

Brühl, C. and Crutzen, P. J.: The MPIC 2D model, in: NASA Ref. Publ. 1292, 1, 103–104, 1993.

Burrows, J. P., Hölzle, E., Goede, A. P. H., Visser, H., and Fricke, W.: SCIAMACHY – Scanning Imaging Absorption Spectrometer for Atmospheric Chartography, Acta Astronautica, 35(7), 445–451, 1995.

Cressot, C., Chevallier, F., Bousquet, P., Crevoisier, C., Dlugokencky, E. J., Fortems-Cheiney, A., Frankenberg, C., Parker, R., Pison, I., Scheepmaker, R. A., Montzka, S. A., Krummel, P. B., Steele, L. P., and Langenfelds, R. L.: On the consistency between global and regional methane emissions inferred from SCIAMACHY, TANSO-FTS, IASI and surface measurements, Atmos. Chem. Phys., 14, 577-592, doi:10.5194/acp-14-577-2014, 2014.

Buzan, E. M., Beale, C. A., Boone, C. D., and Bernath, P. F.: Global stratospheric measurements of the isotopologues of methane from the Atmospheric Chemistry Experiment Fourier Transform Spectrometer, Atmos. Meas. Tech. Discuss., 8, 11171-11207, doi:10.5194/amtd-8-11171-2015, 2015.

Dee, D. P., Uppala, S. M., Simmons, A. J., Berrisford, P., Poli, P., Kobayashi, S., Andrae, U., Balmaseda, M. A., Balsamo, G., Bauer, P. Bechtold, P., Beljaars, A. C. M., van de Berg, L., Bidlot, J., Bormann, N., Delsol, C., Dragani, R., Fuentes, M., Geer, A. J., Haimberger, L., Healy, S. B., Hersbach, H., H´olm, E. V., Isaksen, L., K°allberg, P., K¨ohler, M., Matricardi, M., McNally, A. P., Monge-Sanz, B. M., Morcrette, J.-J., Park, B.-K., Peubey, C., de Rosnay, P., Tavolato, C., Th´epaut, J.-N., and Vitart, F.: The ERA-Interim reanalysis: configuration and performance of the data assimilation system, Q. J. Roy. Meteor. Soc., 137, 553–597, doi:10.1002/qj.828, 2011.

Deutscher, N., Notholt, J., Messerschmidt, J., Weinzierl, C., Warneke, T., Petri, C., Gruppe, P., and Katrynski, K.: TCCON data from Bialystok, Poland, Release GGG2014R0. TCCON data archive, hosted by the Carbon Dioxide Information Analysis Center, Oak Ridge National Laboratory, Oak Ridge, Tennessee, U.S.A., http://dx.doi.org/10.14291/tccon.ggg2014.bialystok01.R0/1149277, 2014

Diallo, M., Legras, B., and Chédin, A.: Age of stratospheric air in the ERA-Interim, Atmos. Chem. Phys., 12, 12133-12154, doi:10.5194/acp-12-12133-2012, 2012.

Dils, B., Buchwitz, M., Reuter, M., Schneising, O., Boesch, H., Parker, R., Guerlet, S., Aben, I., Blumenstock, T., Burrows, J. P., Butz, A., Deutscher, N. M., Frankenberg, C., Hase, F., Hasekamp, O. P., Heymann, J., De Mazière, M., Notholt, J., Sussmann, R., Warneke, T., Griffith, D., Sherlock, V., and Wunch, D.: The Greenhouse Gas Climate Change Initiative (GHG-CCI): comparative validation of GHG-CCI SCIAMACHY/ENVISAT and TANSO-FTS/GOSAT CO_2 and CH_4 retrieval algorithm products with measurements from the TCCON, Atmos. Meas. Tech., 7, 1723-1744, doi:10.5194/amt-7-1723-2014, 2014.

Ebita, A., Kobayashi, S., Ota, Y., Moriya, M., Kumabe, R., Onogi, K., Harada, Y., Yasui, S., Miyaoka, K., Takahashi, K., Kamahori, H., Kobayashi, C., Endo, H., Soma, M., Oikawa, Y., and Ishimizu, T.: The Japanese 55-year Reanalysis “JRA-55”: An interim report, SOLA, 7, 149–152, doi:10.2151/sola.2011-038, 2011.

Engel, A., Möbius, T., Bönisch, H., Schmidt, U., Heinz, R., Levin, I., Atlas, E., Aoki, S., Nakazawa, T., Sugawara, S., Moore, F., Hurst, D., Elkins, J., Schauffler, S., Andrews, A., and Boering, K.: Age of stratospheric air unchanged within uncertainties over the past 30 years, Nature Geosci., 2, 28–31, doi:10.1038/ngeo388, 2009.

Fischer, H., Birk, M., Blom, C., Carli, B., Carlotti, M., von Clarmann, T., Delbouille, L., Dudhia, A., Ehhalt, D., Endemann, M., Flaud, J. M., Gessner, R., Kleinert, A., Koopman, R., Langen, J., López-Puertas, M., Mosner, P., Nett, H., Oelhaf, H.,

Perron, G., Remedios, J., Ridolfi, M., Stiller, G., and Zander, R.: MIPAS: an instrument for atmospheric and climate research, Atmos. Chem. Phys., 8, 2151-2188, doi:10.5194/acp-8-2151-2008, 2008.

Frankenberg, C., Aben, I., Bergamaschi, P., Dlugokencky, E. J., van Hees, R., Houweling, S., van der Meer, P., Snel, R., and Tol, P.: Global column-averaged methane mixing ratios from 2003 to 2009 as derived from SCIAMACHY: Trends and variability, J. Geophys. Res., 116, D04302, doi:10.1029/2010JD014849, 2011.

Fraser, A., Palmer, P. I., Feng, L., Boesch, H., Cogan, A., Parker, R., Dlugokencky, E. J., Fraser, P. J., Krummel, P. B., Langenfelds, R. L., O'Doherty, S., Prinn, R. G., Steele, L. P., van der Schoot, M., and Weiss, R. F.: Estimating regional methane surface fluxes: the relative importance of surface and GOSAT mole fraction measurements, Atmos. Chem. Phys., 13, 5697–5713, doi:10.5194/acp-13-5697-2013, 2013.

Fraser, A., Palmer, P. I., Feng, L., Bösch, H., Parker, R., Dlugokencky, E. J., Krummel, P. B., and Langenfelds, R. L.: Estimating regional fluxes of CO2 and CH4 using space-borne observations of XCH_4: XCO_2, Atmos. Chem. Phys., 14, 12883-12895, doi:10.5194/acp-14-12883-2014, 2014.

Geibel, M. C., Messerschmidt, J., Gerbig, C., Blumenstock, T., Chen, H., Hase, F., Kolle, O., Lavriĉ, J. V., Notholt, J., Palm, M., Rettinger, M., Schmidt, M., Sussmann, R., Warneke, T., and Feist, D. G.: Calibration of column-averaged CH_4 over European TCCON FTS sites with airborne in-situ measurements, Atmos. Chem. Phys., 12, 8763–8775, doi:10.5194/acp-12-8763-2012, 2012.

Griffith, D. W. T., Deutscher, N., Velazco, V. A., Wennberg, P. O., Yavin, Y., Keppel Aleks, G., Washenfelder, R., Toon, G. C., Blavier, J.-F., Murphy, C., Jones, N., Kettlewell, G., Connor, B., Macatangay, R., Roehl, C., Ryczek, M., Glowacki, J., Culgan, T., and Bryant, G.: TCCON data from Darwin, Australia, Release GGG2014R0. TCCON data archive, hosted by the Carbon Dioxide Information Analysis Center, Oak Ridge National Laboratory, Oak Ridge, Tennessee, U.S.A., http://dx.doi.org/10.14291/tccon.ggg2014.darwin01.R0/1149290, 2014a.

Griffith, D. W. T., Velazco, V. A., Deutscher, N., Murphy, C., Jones, N., Wilson, S., Macatangay, R., Kettlewell, G., Buchholz, R. R., and Riggenbach, M.: TCCON data from Wollongong, Australia, Release GGG2014R0. TCCON data archive, hosted by the Carbon Dioxide Information Analysis Center, Oak Ridge National Laboratory, Oak Ridge, Tennessee, U.S.A. http://dx.doi.org/10.14291/tccon.ggg2014.wollongong01.R0/1149291, 2014b.

Haenel, F. J., Stiller, G. P., von Clarmann, T., Funke, B., Eckert, E., Glatthor, N., Grabowski, U., Kellmann, S., Kiefer, M., Linden, A., and Reddmann, T.: Reassessment of MIPAS age of air trends and variability, Atmos. Chem. Phys., 15, 13161-13176, doi:10.5194/acp-15-13161-2015, 2015.

Hase, F., Blumenstock, T., Dohe, S., Groß, J., and Kiel, M.: TCCON data from Karlsruhe, Germany, Release GGG2014R0. TCCON data archive, hosted by the Carbon Dioxide Information Analysis Center, Oak Ridge National Laboratory, Oak Ridge, Tennessee, U.S.A., http://dx.doi.org/10.14291/tccon.ggg2014.karlsruhe01.R0/1149270, 2014.

Hourdin, F., Musat, I., Bony, S., Braconnot, P., Codron, F., Dufresne, J., Fairhead, L., Filiberti, M., Friedlingstein, P., Grandpeix, J., Krinner, G., Levan, P., Li, Z., and Lott, F.: The LMDz4 general circulation model: climate performance and

sensitivity to parametrized physics with emphasis on tropical convection, Clim. Dynam., 27, 787–813, doi:10.1007/s00382-006-0158-0, 2006.

Houweling, S., Krol, M., Bergamaschi, P., Frankenberg, C., Dlugokencky, E. J., Morino, I., Notholt, J., Sherlock, V.,Wunch, D., Beck, V., Gerbig, C., Chen, H., Kort, E. A., Röckmann, T., and Aben, I.: A multi-year methane inversion using SCIAMACHY, accounting for systematic errors using TCCON measurements, Atmos. Chem. Phys., 14, 3991–4012, doi:10.5194/acp-14-3991-2014, 2014.

Inoue, M., Morino, I., Uchino, O., Nakatsuru, T., Yoshida, Y., Yokota, T., Wunch, D., Wennberg, P. O., Roehl, C. M., Griffith, D. W. T., Velazco, V. A., Deutscher, N. M., Warneke, T., Notholt, J., Robinson, J., Sherlock, V., Hase, F., Blumenstock, T., Rettinger, M., Sussmann, R., Kyrö, E., Kivi, R., Shiomi, K., Kawakami, S., De Mazière, M., Arnold, S. G., Feist, D. G., Barrow, E. A., Barney, J., Dubey, M., Schneider, M., Iraci, L., Podolske, J. R., Hillyard, P., Machida, T., Sawa, Y., Tsuboi, K., Matsueda, H., Sweeney, C., Tans, P. P., Andrews, A. E., Biraud, S. C., Fukuyama, Y., Pittman, J. V., Kort, E. A., and Tanaka, T.: Bias corrections of GOSAT SWIR XCO_2 and XCH_4 with TCCON data and their evaluation using aircraft measurement data, Atmos. Meas. Tech. Discuss., doi:10.5194/amt-2015-366, in review, 2016.

Karion, A., Sweeney, C., Tans, P., and Newberger, T.: Aircore: an innovative atmospheric sampling system, J. Atmos. Oceanic Technol., 27, 1839|-1853, doi:10.1175/2010JTECHA1448.1, 2010.

Kivi, R., Heikkinen, P., and Kyro, E.: TCCON data from Sodankyla, Finland, Release GGG2014R0. TCCON data archive, hosted by the Carbon Dioxide Information Analysis Center, Oak Ridge National Laboratory, Oak Ridge, Tennessee, U.S.A., http://dx.doi.org/10.14291/tccon.ggg2014.sodankyla01.R0/1149280, 2014.

Krol, M., Houweling, S., Bregman, B., van den Broek, M., Segers, A., van Velthoven, P., Peters, W., Dentener, F., and Bergamaschi, P.: The two-way nested global chemistry-transport zoom model TM5: algorithm and applications, Atmos. Chem. Phys., 5, 417–432, doi:10.5194/acp-5-417-2005, 2005.

Kulawik, S. S., Wunch, D., O'Dell, C., Frankenberg, C., Reuter, M., Oda, T., Chevallier, F., Sherlock, V., Buchwitz, M., Osterman, G., Miller, C., Wennberg, P., Griffith, D. W. T., Morino, I., Dubey, M., Deutscher, N. M., Notholt, J., Hase, F., Warneke, T., Sussmann, R., Robinson, J., Strong, K., Schneider, M., and Wolf, J.: Consistent evaluation of GOSAT, SCIAMACHY, CarbonTracker, and MACC through comparisons to TCCON, Atmos. Meas. Tech. Discuss., 8, 6217-6277, doi:10.5194/amtd-8-6217-2015, 2015.

Kurylo, M. J.: Network for the detection of stratospheric change, Proc. SPIE 1491, P. Soc. Photo-Opt. Ins., 168 (September 1, 1991), doi:10.1117/12.46658, 1991.

Kuze, A., Suto, H., Nakajima, M., and Hamazaki, T.: Thermal and near infrared sensor for carbon observation Fourier-transform spectrometer on the Greenhouse Gases Observing SATellite for greenhouse gases monitoring, Appl. Optics, 48, 6716–6733, doi:10.1364/AO.48.006716, 2009.

Laeng, A., Plieninger, J., von Clarmann, T., Grabowski, U., Stiller, G., Eckert, E., Glatthor, N., Haenel, F., Kellmann, S., Kiefer, M., Linden, A., Lossow, S., Deaver, L., Engel, A., Hervig, M., Levin, I., McHugh, M., Noël, S., Toon, G., and

Walker, K.: Validation of MIPAS IMK/IAA methane profiles, Atmos. Meas. Tech., 8, 5251-5261, doi:10.5194/amt-8-5251-2015, 2015.

Locatelli, R., Bousquet, P., Saunois, M., Chevallier, F., and Cressot, C.: Sensitivity of the recent methane budget to LMDz sub-grid-scale physical parameterizations, Atmos. Chem. Phys., 15, 9765-9780, doi:10.5194/acp-15-9765-2015, 2015.

Meirink, J. F., Bergamaschi, P., and Krol, M. C.: Four-dimensional variational data assimilation for inverse modelling of atmospheric methane emissions: method and comparison with synthesis inversion, Atmos. Chem. Phys., 8, 6341-6353, doi:10.5194/acp-8-6341-2008, 2008.

Locatelli, R., Bousquet, P., Chevallier, F., Fortems-Cheney, A., Szopa, S., Saunois, M., Agusti-Panareda, A., Bergmann, D., Bian, H., Cameron-Smith, P., Chipperfield, M. P., Gloor, E., Houweling, S., Kawa, S. R., Krol, M., Patra, P. K., Prinn, R. G., Rigby, M., Saito, R., and Wilson, C.: Impact of transport model errors on the global and regional methane emissions estimated by inverse modelling, Atmos. Chem. Phys., 13, 9917-9937, doi:10.5194/acp-13-9917-2013, 2013.

Locatelli, R., Bousquet, P., Saunois, M., Chevallier, F., and Cressot, C.: Sensitivity of the recent methane budget to LMDz sub-grid-scale physical parameterizations, Atmos. Chem. Phys., 15, 9765-9780, doi:10.5194/acp-15-9765-2015, 2015.

Messerschmidt, J., Geibel, M. C., Blumenstock, T., Chen, H., Deutscher, N. M., Engel, A., Feist, D. G., Gerbig, C., Gisi, M., Hase, F., Katrynski, K., Kolle, O., Lavriˇc, J. V., Notholt, J., Palm, M., Ramonet, M., Rettinger, M., Schmidt, M., Sussmann, R., Toon, G. C., Truong, F., Warneke, T., Wennberg, P. O., Wunch, D., and Xueref-Remy, I.: Calibration of TCCON column-averaged CO_2: the first aircraft campaign over European TCCON sites, Atmos. Chem. Phys., 11, 10765–10777, doi:10.5194/acp-11-10765-2011, 2011.

Monge-Sanz, B. M., Chipperfield, M. P., Simmons, A. J., and Uppala, S. M.: Mean age of air and transport in a CTM: comparison of different ECMWF analyses, Geophys. Res. Lett., 340, L04801, doi:10.1029/2006GL028515, 2007.

Monge-Sanz, B. M., Chipperfield, M. P., Dee, D. P., Simmons, A. J., and Uppala, S. M.: Improvements in the stratospheric transport achieved by a chemistry transport model with ECMWF (re)analyses: identifying effects and remaining challenges, Q. J. R. Meteorol. Soc., doi:10.1002/qj.1996, 2012.

Monteil, G., Houweling, S., Butz, A., Guerlet, S., Schepers, D., Hasekamp, O., Frankenberg, C., Scheepmaker, R., Aben, I., and Röckmann, T.: Comparison of CH_4 inversions based on 15 months of GOSAT and SCIAMACHY observations, J. Geophys. Res. Atmos., 118, 11,807–11,823, doi:10.1002/2013JD019760, 2013.

Onogi, K., Tsutusi, J., Koide, H., Sakamoto, M., Kobayashi, S., Hatsushika, H., Matsumoto, T., Yamazaki, N., Kamahori, H., Takahashi, K., Kadokura, S., Wada, K., Kato, K., Oyama, R., Ose, T., Mannoji, N., and Taira, R.: The JRA-25 reanalysis, J. Meteor, Soc. Japan, 85, 369–432, 2007.

Ostler, A., Sussmann, R., Rettinger, M., Deutscher, N. M., Dohe, S., Hase, F., Jones, N., Palm, M., and Sinnhuber, B.-M.: Multistation intercomparison of column-averaged methane from NDACC and TCCON: impact of dynamical variability, Atmos. Meas. Tech., 7, 4081-4101, doi:10.5194/amt-7-4081-2014, 2014.

Pandey, S., Houweling, S., Krol, M., Aben, I., Chevallier, F., Dlugokencky, E. J., Gatti, L. V., Gloor, M., Miller, J. B., Detmers, R., Machida, T., and Röckmann, T.: Inverse modeling of GOSAT-retrieved ratios of total column CH_4 and CO_2 for 2009 and 2010, Atmos. Chem. Phys. Discuss., doi:10.5194/acp-2016-77, in review, 2016.

Parker, R., Boesch, H., Cogan, A., Fraser, A., Feng, L., Palmer, P. I., Messerschmidt, J., Deutscher, N., Griffith, D. W. T., Notholt, J., Wennberg, P. O., and Wunch, D.: Methane observations from the Greenhouse Gases Observing SATellite: Comparison to ground-based TCCON data and model calculations, Geophys. Res. Lett., 38, L15807, doi:10.1029/2011GL047871, 2011

Parker, R. J., Boesch, H., Byckling, K., Webb, A. J., Palmer, P. I., Feng, L., Bergamaschi, P., Chevallier, F., Notholt, J., Deutscher, N., Warneke, T., Hase, F., Sussmann, R., Kawakami, S., Kivi, R., Griffith, D. W. T., and Velazco, V.: Assessing 5 years of GOSAT Proxy XCH_4 data and associated uncertainties, Atmos. Meas. Tech., 8, 4785-4801, doi:10.5194/amt-8-4785-2015, 2015.

Patra, P. K., Takigawa, M., Ishijima, K., Choi, B.-C., Cunnold, D., Dlugokencky, E. J., Fraser, P., Gomez-Pelaez, A. J., Goo, T.-Y., Kim, J.-S., Krummel, P., Langenfelds, R., Meinhardt, F., Mukai, H., O'Doherty, S., Prinn, R. G., Simmonds, P., Steele, P., Tohjima, Y., Tsuboi, K., Uhse, K., Weiss, R., Worthy, D., and Nakazawa, T.: Growth rate, seasonal, synoptic, diurnal variations and budget of methane in lower atmosphere, J. Meteorol. Soc. Jpn., 87, 635–663, 2009a.

Patra, P. K., Takigawa, M., Dutton, G. S., Uhse, K., Ishijima, K., Lintner, B. R., Miyazaki, K., and Elkins, J. W.: Transport mechanisms for synoptic, seasonal and interannual SF_6 variations and "age" of air in troposphere, Atmos. Chem. Phys., 9, 1209–1225, doi:10.5194/acp-9-1209-2009, 2009b.

Patra, P. K., Houweling, S., Krol, M., Bousquet, P., Belikov, D., Bergmann, D., Bian, H., Cameron-Smith, P., Chipperfield, M. P., Corbin, K., Fortems-Cheiney, A., Fraser, A., Gloor, E., Hess, P., Ito, A., Kawa, S. R., Law, R. M., Loh, Z., Maksyutov, S., Meng, L., Palmer, P. I., Prinn, R. G., Rigby, M., Saito, R., and Wilson, C.: TransCom model simulations of CH_4 and 15 related species: linking transport, surface flux and chemical loss with CH_4 variability in the troposphere and lower stratosphere, Atmos. Chem. Phys., 11, 12813–12837, doi:10.5194/acp-11-12813-2011, 2011.

Patra, P. K., Krol, M. C., Montzka, S. A., Arnold, T., Atlas, E. L., Lintner, B. R., Stephens, B. B., Xiang, B., Elkins, J. W., Fraser, P. J., Ghosh, A., Hintsa, E. J., Hurst, D. F., Ishijima, K., Krummel, P. B., Miller, B. R., Miyazaki, K., Moore, F. L., Mühle, J., O'Doherty, S., Prinn, R. G., Steele, L. P., Takigawa, M., Wang, H. J., Weiss, R. F., Wofsy, S. C., and Young, D.: Observational evidence for interhemispheric hydroxyl parity, Nature, 513, 219–223, 2014.

Patra, P. K., Saeki, T., Dlugokencky, E. J., Ishijima1, K., Umezawa, T., Ito, A., Aoki, S., Morimoto, S., Kort, E. A., Crotwell, A., Ravi Kumar, K., and Nakazawa, T.: Regional methane emission estimation based on observed atmospheric concentrations (2002–2012), J. Meteorol. Soc. Jpn., 94, doi:10.2151/jmsj.2016-006, 2016.

Plieninger, J., von Clarmann, T., Stiller, G. P., Grabowski, U., Glatthor, N., Kellmann, S., Linden, A., Haenel, F., Kiefer, M., Höpfner, M., Laeng, A., and Lossow, S.: Methane and nitrous oxide retrievals from MIPAS-ENVISAT, Atmos. Meas. Tech., 8, 4657-4670, doi:10.5194/amt-8-4657-2015, 2015.

Plieninger, J., Laeng, A., Lossow, S., von Clarmann, T., Stiller, G. P., Kellmann, S., Linden, A., Kiefer, M., Walker, K. A., Noël, S., Hervig, M. E., McHugh, M., Lambert, A., Urban, J., Elkins, J. W., and Murtagh, D.: Validation of revised methane and nitrous oxide profiles from MIPAS–ENVISAT, Atmos. Meas. Tech., 9, 765-779, doi:10.5194/amt-9-765-2016, 2016..

Saad, K. M., Wunch, D., Toon, G. C., Bernath, P., Boone, C., Connor, B., Deutscher, N. M., Griffith, D. W. T., Kivi, R., Notholt, J., Roehl, C., Schneider, M., Sherlock, V., and Wennberg, P. O.: Derivation of tropospheric methane from TCCON CH_4 and HF total column observations, Atmos. Meas. Tech., 7, 2907-2918, doi:10.5194/amt-7-2907-2014, 2014.

Saito, R., Patra, P. K., Deutscher, N., Wunch, D., Ishijima, K., Sherlock, V., Blumenstock, T., Dohe, S., Griffith, D., Hase, F., Heikkinen, P., Kyrö, E., Macatangay, R., Mendonca, J., Messerschmidt, J., Morino, I., Notholt, J., Rettinger, M., Strong, K., Sussmann, R., and Warneke, T.: Technical Note: Latitude-time variations of atmospheric column-average dry air mole fractions of CO_2, CH_4 and N_2O, Atmos. Chem. Phys., 12, 7767-7777, doi:10.5194/acp-12-7767-2012, 2012.

Schepers, D., Guerlet, S., Butz, A., Landgraf, J., Frankenberg, C., Hasekamp, O., Blavier, J.-F., Deutscher, N. M., Griffith, D. W. T., Hase, F., Kyro, E., Morino, I., Sherlock, V., Sussmann, R., and Aben, I.: Methane retrievals from Greenhouse Gases Observing Satellite (GOSAT) shortwave infrared measurements: Performance comparison of proxy and physics retrieval algorithms, J. Geophys. Res., 117, D10307, doi:10.1029/2012JD017549, 2012.

Sepúlveda, E., Schneider, M., Hase, F., García, O. E., Gomez-Pelaez, A., Dohe, S., Blumenstock, T., and Guerra, J. C.: Longterm validation of tropospheric column-averaged CH_4 mole fractions obtained by mid-infrared ground-based FTIR spectrometry, Atmos. Meas. Tech., 5, 1425–1441, doi:10.5194/amt-5-1425-2012, 2012.

Sepúlveda, E., Schneider, M., Hase, F., Barthlott, S., Dubravica, D., García, O. E., Gomez-Pelaez, A., González, Y., Guerra, J. C., Gisi, M., Kohlhepp, R., Dohe, S., Blumenstock, T., Strong, K., Weaver, D., Palm, M., Sadeghi, A., Deutscher, N. M., Warneke, T., Notholt, J., Jones, N., Griffith, D. W. T., Smale, D., Brailsford, G. W., Robinson, J., Meinhardt, F., Steinbacher, M., Aalto, T., and Worthy, D.: Tropospheric CH_4 signals as observed by NDACC FTIR at globally distributed sites and comparison to GAW surface in situ measurements, Atmos. Meas. Tech., 7, 2337–2360, doi:10.5194/amt-7-2337-2014, 2014.

Sherlock, V., Connor, B., Robinson, J., Shiona, H., Smale, D., and Pollard, D.: TCCON data from Lauder, New Zealand, 120HR, Release GGG2014R0. TCCON data archive, hosted by the Carbon Dioxide Information Analysis Center, Oak Ridge National Laboratory, Oak Ridge, Tennessee, U.S.A., http://dx.doi.org/10.14291/tccon.ggg2014.lauder01.R0/1149293, 2014.

Sherlock, V., B., Connor, B., Robinson, J., Shiona, H., Smale, D., and Pollard, D.: TCCON data from Lauder, New Zealand, 125HR, Release GGG2014R0. TCCON data archive, hosted by the Carbon Dioxide Information Analysis Center, Oak Ridge National Laboratory, Oak Ridge, Tennessee, U.S.A., http://dx.doi.org/10.14291/tccon.ggg2014.lauder02.R0/1149298, 2014.

Spivakovsky, C., Logan, J. A., Montzka, S. A., Balkanski, Y. J., Foreman-Fowler, M., Jones, D. B. A., Horowitz, L. W., Fusco, A. C., Brenninkmeijer, C. A. M., Prather, M. J., Wofsy, S. C., McElroy, M. B.: Three-dimensional climatological distribution of tropospheric OH: update and evaluation, J. Geophys. Res., 105, 8931–8980, 2000.

Stiller, G. P., von Clarmann, T., Haenel, F., Funke, B., Glatthor, N., Grabowski, U., Kellmann, S., Kiefer, M., Linden, A., Lossow, S., and López-Puertas, M.: Observed temporal evolution of global mean age of stratospheric air for the 2002 to 2010 period, Atmos. Chem. Phys., 12, 3311-3331, doi:10.5194/acp-12-3311-2012, 2012.

Strahan, S., Douglass, A., Stolarski, E., Akiyoshi, H., Bekki, S., Braesicke, P., Butchart, N., Chipperfield, M. P., Cugnet, D., Dhomse, S., Frith, S.M., Gettelman, A., Hardiman, S. C., Kinnison, D. E., Lamarque, J. F., Mancini, E., Marchand, M., Michou, M., Morgenstern, O., Nakamura, T., Olivie, D., Pawson, S., Pitari, G., Plummer, D. A., Pyle, J. A., Scinocca, J. F., Shepherd, T. G., Shibata, K., Smale, D., Teyssedre, H., Tian. W, and Yamashita, Y.: Using transport diagnostics to understand chemistry climate model ozone simulations, J. Geophys. Res., 116, D17302, doi:10.1029/2010JD015360, 2011.

Szopa, S., Balkanski, Y., Schulz, M., Bekki, S., Cugnet, D., Fortems-Cheney, A., Turquety, S., Cozic, A., Dandreis, C., Hauglustaine, D., Idelkadi, A., Lathière, J., Lefevre, F., Marchand, M., Vuolo, R., Yan, N., and Dufresne, J.-L.: Aerosol and ozone changes as forcing for climate evolution between 1850 and 2100, Clim. Dynam., 40, 2223–2250, doi:10.1007/s00382-012-1408, 2013.

Sussmann, R., and Rettinger, M.: TCCON data from Garmisch, Germany, Release GGG2014R0. TCCON data archive, hosted by the Carbon Dioxide Information Analysis Center, Oak Ridge National Laboratory, Oak Ridge, Tennessee, U.S.A., http://dx.doi.org/10.14291/tccon.ggg2014.garmisch01.R0/1149299, 2014.

Takigawa, M., Takahashi, M., and Akiyoshi, H.: Simulation of ozone and other chemical species using a Center for Climate System Research/National Institute for Environmental Studies atmospheric GCM with coupled stratospheric chemistry, J. Geophys. Res., 104, 14003–14018, doi:10.1029/1998JD100105, 1999.

Turner, A. J., Jacob, D. J., Wecht, K. J., Maasakkers, J. D., Lundgren, E., Andrews, A. E., Biraud, S. C., Boesch, H., Bowman, K. W., Deutscher, N. M., Dubey, M. K., Griffith, D. W. T., Hase, F., Kuze, A., Notholt, J., Ohyama, H., Parker, R., Payne, V. H., Sussmann, R., Sweeney, C., Velazco, V. A., Warneke, T., Wennberg, P. O., and Wunch, D.: Estimating global and North American methane emissions with high spatial resolution using GOSAT satellite data, Atmos. Chem. Phys., 15, 7049-7069, doi:10.5194/acp-15-7049-2015, 2015.

von Clarmann, T., Glatthor, N., Grabowski, U., Höpfner, M., Kellmann, S., Kiefer, M., Linden, A., Mengistu Tsidu, G., Milz, M., Steck, T., Stiller, G. P., Wang, D.-Y., Fischer, H., Funke, B., Gil-López, S., and López-Puertas, M.: Retrieval of temperature and tangent altitude pointing from limb emission spectra recorded from space by the Michelson Interferometer for Passive Atmospheric Sounding (MIPAS), J. Geophys. Res., 108, doi:10.1029/2003JD003602, 2003.

Wang, Z., Deutscher, N. M.,Warneke, T., Notholt, J., Dils, B., Griffith, D. W. T., Schmidt, M., Ramonet, M., and Gerbig, C.: Retrieval of tropospheric column-averaged CH_4 mole fraction by solar absorption FTIR-spectrometry using N2O as a proxy, Atmos. Meas. Tech., 7, 3295–3305, doi:10.5194/amt-7-3295-2014, 2014.

Warneke, T., Messerschmidt, J., Notholt, J., Weinzierl, C., Deutscher, N., Petri, C., Gruppe, P., Vuillemin, C., Truong, F., Schmidt, M., Ramonet, M., and Parmentier, E.: TCCON data from Orleans, France, Release GGG2014R0. TCCON data archive, hosted by the Carbon Dioxide Information Analysis Center, Oak Ridge National Laboratory, Oak Ridge, Tennessee, U.S.A., http://dx.doi.org/10.14291/tccon.ggg2014.orleans01.R0/1149276, 2014.

Washenfelder, R. A., Wennberg, P. O., and Toon, G. C.: Tropospheric methane retrieved from ground-based near-IR solar absorption spectra, Geophys. Res. Lett., 30, 2226, doi:10.1029/2003GL017969, 2003.

Waugh, D. W., and Hall T. M., Age of stratospheric air: Theory, observations, and models, Rev. Geophys., 40(4), 1010, doi:10.1029/2000RG000101, 2002.

Wecht, K. J., Jacob D. J., Frankenberg C., Jiang Z., and Blake D. R.: Mapping of North American methane emissions with high spatial resolution by inversion of SCIAMACHY satellite data, J. Geophys. Res. Atmos., 119, 7741–7756, doi:10.1002/2014JD021551, 2014.

Wennberg, P. O., Wunch, D., Roehl, C., Blavier, J.-F., Toon, G. C., Allen, N., Dowell, P., Teske, K., Martin, C., Martin, J.: TCCON data from Lamont, Oklahoma, USA, Release GGG2014R0. TCCON data archive, hosted by the Carbon Dioxide Information Analysis Center, Oak Ridge National Laboratory, Oak Ridge, Tennessee, U.S.A., http://dx.doi.org/10.14291/tccon.ggg2014.lamont01.R0/1149159, 2014a.

Wennberg, P. O., Roehl, C., Wunch, D., Toon, G. C., Blavier, J.-F., Washenfelder, R., Keppel-Aleks, G., Allen, N., and Ayers, J.: TCCON data from Park Falls, Wisconsin, USA, Release GGG2014R0. TCCON data archive, hosted by the Carbon Dioxide Information Analysis Center, Oak Ridge National Laboratory, Oak Ridge, Tennessee, U.S.A., http://dx.doi.org/10.14291/tccon.ggg2014.parkfalls01.R0/1149161, 2014b.

Wunch, D., Toon, G. C., Wennberg, P. O., Wofsy, S. C., Stephens, B. B., Fischer, M. L., Uchino, O., Abshire, J. B., Bernath, P., Biraud, S. C., Blavier, J.-F. L., Boone, C., Bowman, K. P., Browell, E. V., Campos, T., Connor, B. J., Daube, B. C., Deutscher, N. M., Diao, M., Elkins, J. W., Gerbig, C., Gottlieb, E., Griffith, D. W. T., Hurst, D. F., Jim´enez, R., Keppel-Aleks, G., Kort, E. A., Macatangay, R., Machida, T., Matsueda, H., Moore, F., Morino, I., Park, S., Robinson, J., Roehl, C. M., Sawa, Y., Sherlock, V., Sweeney, C., Tanaka, T., and Zondlo, M. A.: Calibration of the Total Carbon Column Observing Network using aircraft profile data, Atmos. Meas. Tech., 3, 1351–1362, doi:10.5194/amt-3-1351-2010, 2010.

Wunch, D., Toon, G. C., Blavier, J.-F. L., Washenfelder, R. A., Notholt, J., Connor, B. J., Griffith, D. W. T., Sherlock, V., and Wennberg, P. O.: The Total Carbon Column Observing Network, Phil. Trans. R. Soc. A, 369, 2087–2112, doi:10.1098/rsta.2010.0240, 2011.

Yokota, T., Yoshida, Y., Eguchi, N., Ota, Y., Tanaka, T., Watanabe, H., and Maksyutov, S.: Global concentrations of CO_2 and CH_4 retrieved from GOSAT, first preliminary results, SOLA, 5, 160–163, doi:10.2151/sola.2009-041, 2009.

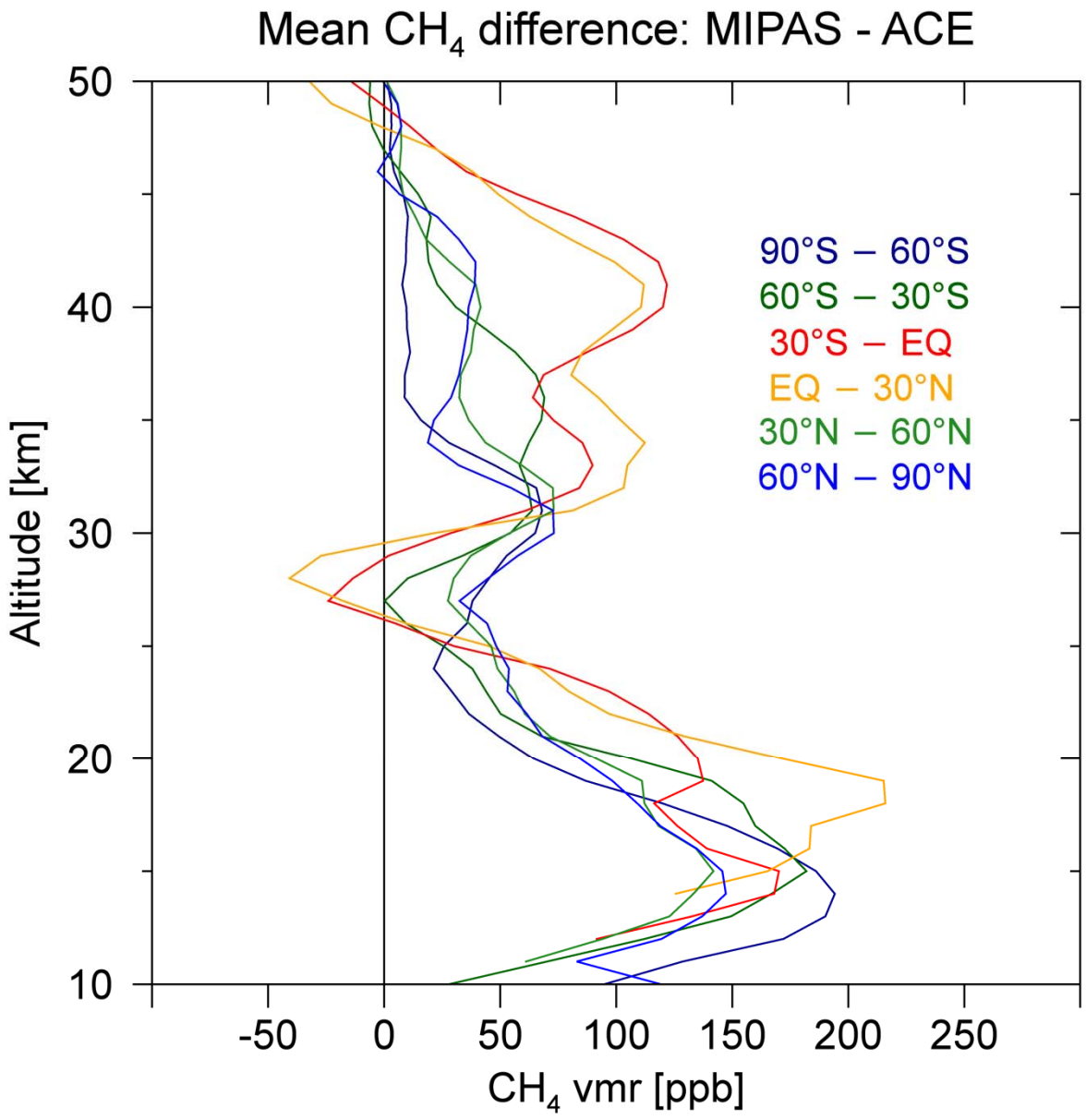

Figure 1. Mean CH_4 differences between collocated MIPAS and ACE-FTS CH_4 profiles measured in the year 2010. Mean CH_4 differences in parts per billion (ppb) are derived for 30° latitudinal bands indicated by different colours.

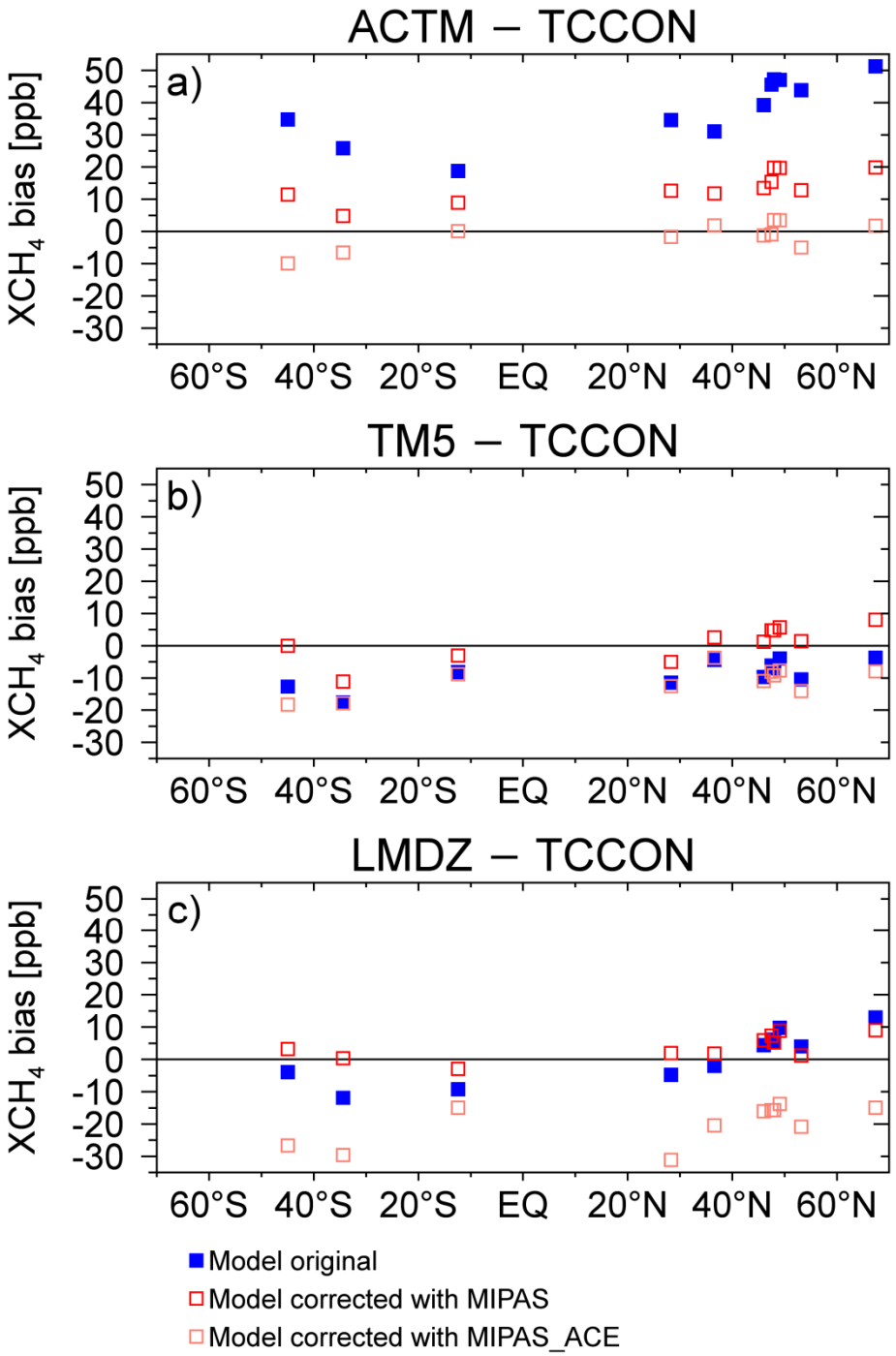

Figure 2. Site-specific model XCH_4 biases with respect to TCCON observations in parts per billion (ppb) for the year 2010. Different colors indicate different stratospheric CH_4 fields used for the calculation of model XCH_4.

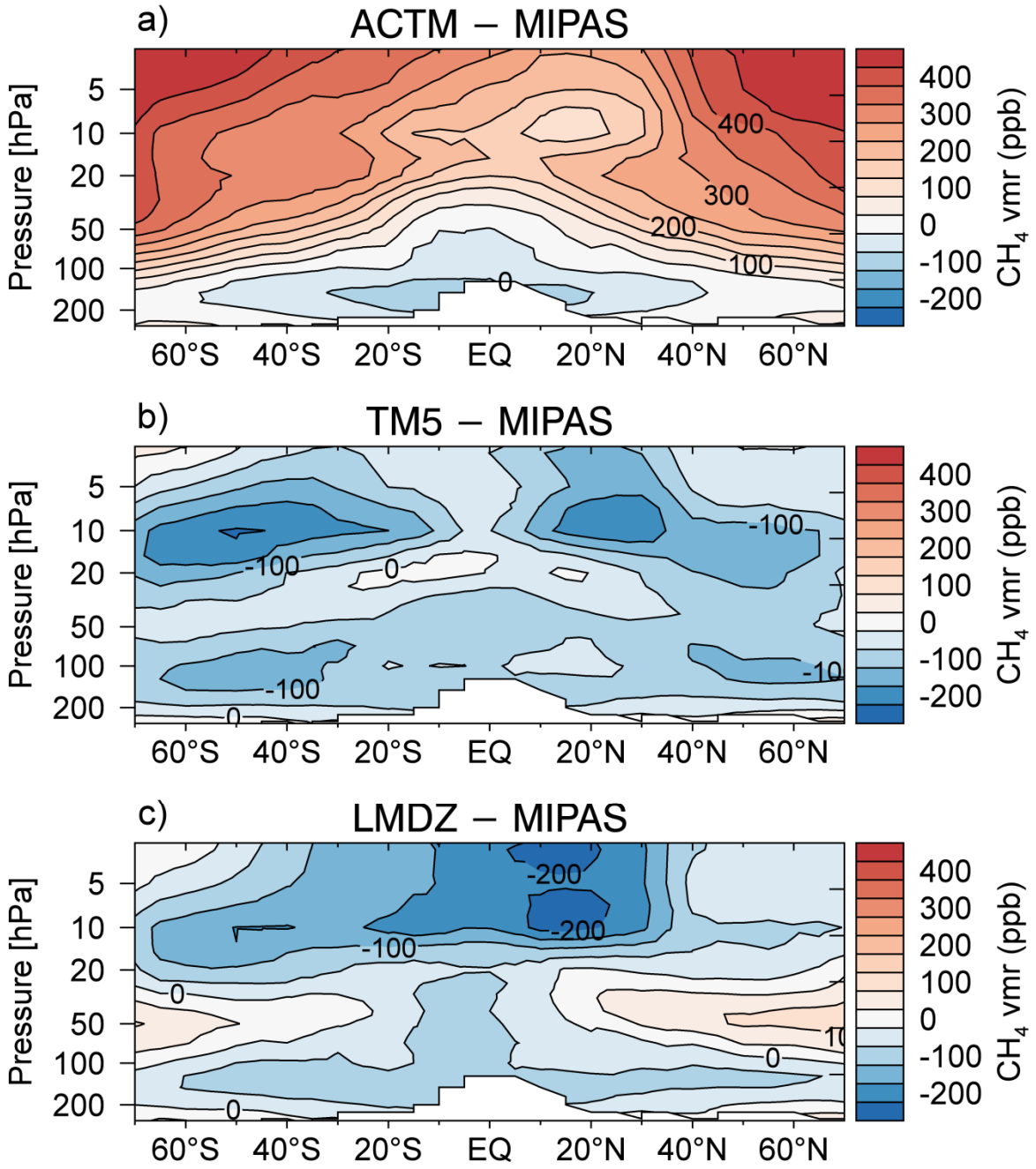

Figure 3. Model-MIPAS differences of stratospheric CH_4 volume mixing ratios (vmr) in parts per billion (ppb). Zonally-averaged CH_4 vmr differences are annual means for the year 2010.

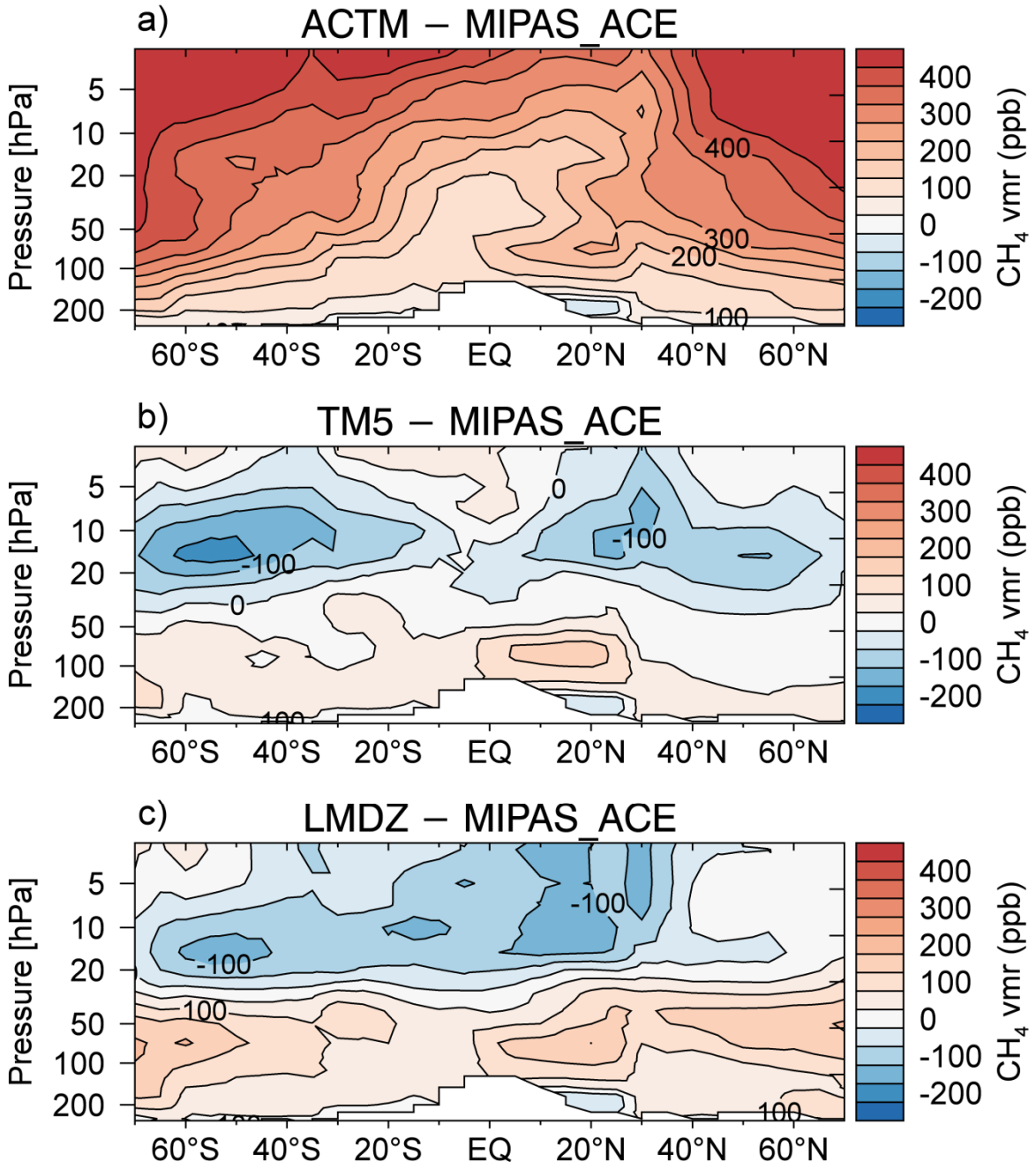

Figure 4. Model-MIPAS_ACE differences of stratospheric CH_4 volume mixing ratios (vmr) in parts per billion (ppb). Zonally-averaged CH_4 vmr differences are annual means for the year 2010.

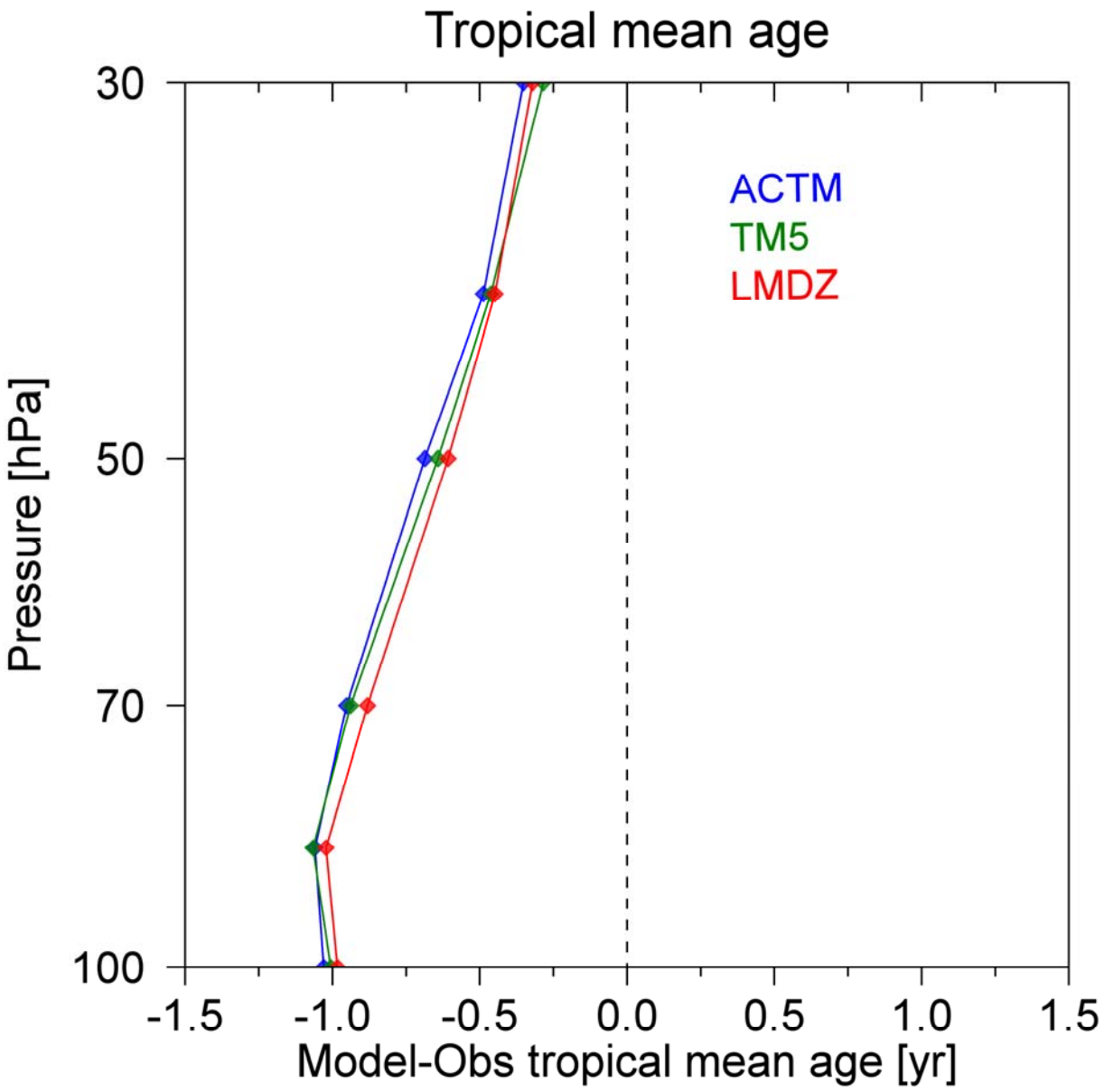

Figure 5. Model-MIPAS differences of mean age for the tropical lower. Mean age data in years (yr) are calculated as annual means on the MIPAS pressure-latitude grid.

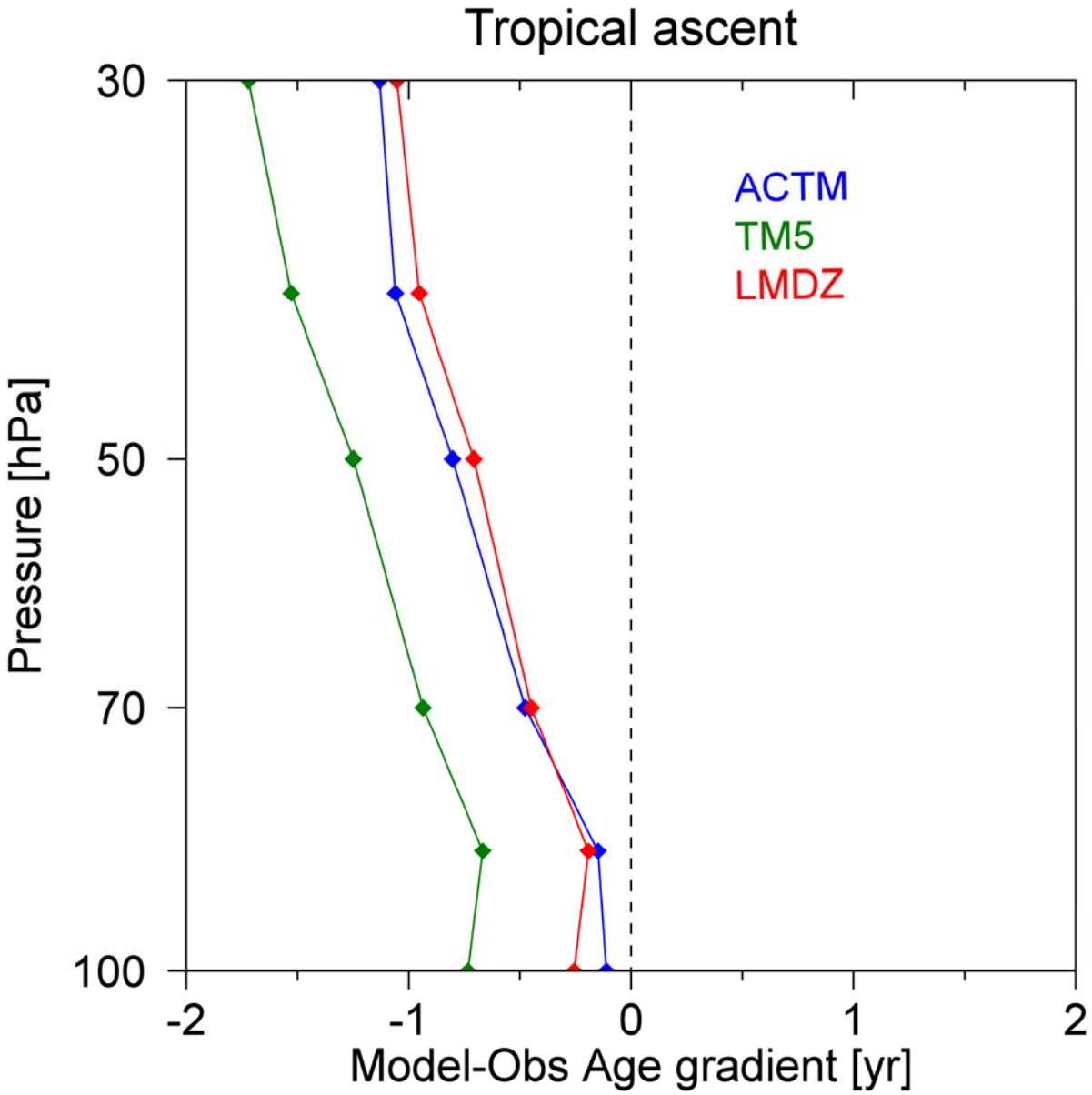

Figure 6. Model-MIPAS differences of the mean age gradient as a transport diagnostics for tropical ascent. The mean age gradient was calculated as difference between the lower stratospheric mean ages averaged over 35°N–50°N and 10°S–10°N. Mean age data in years (yr) are calculated as annual means on the MIPAS pressure-latitude grid.

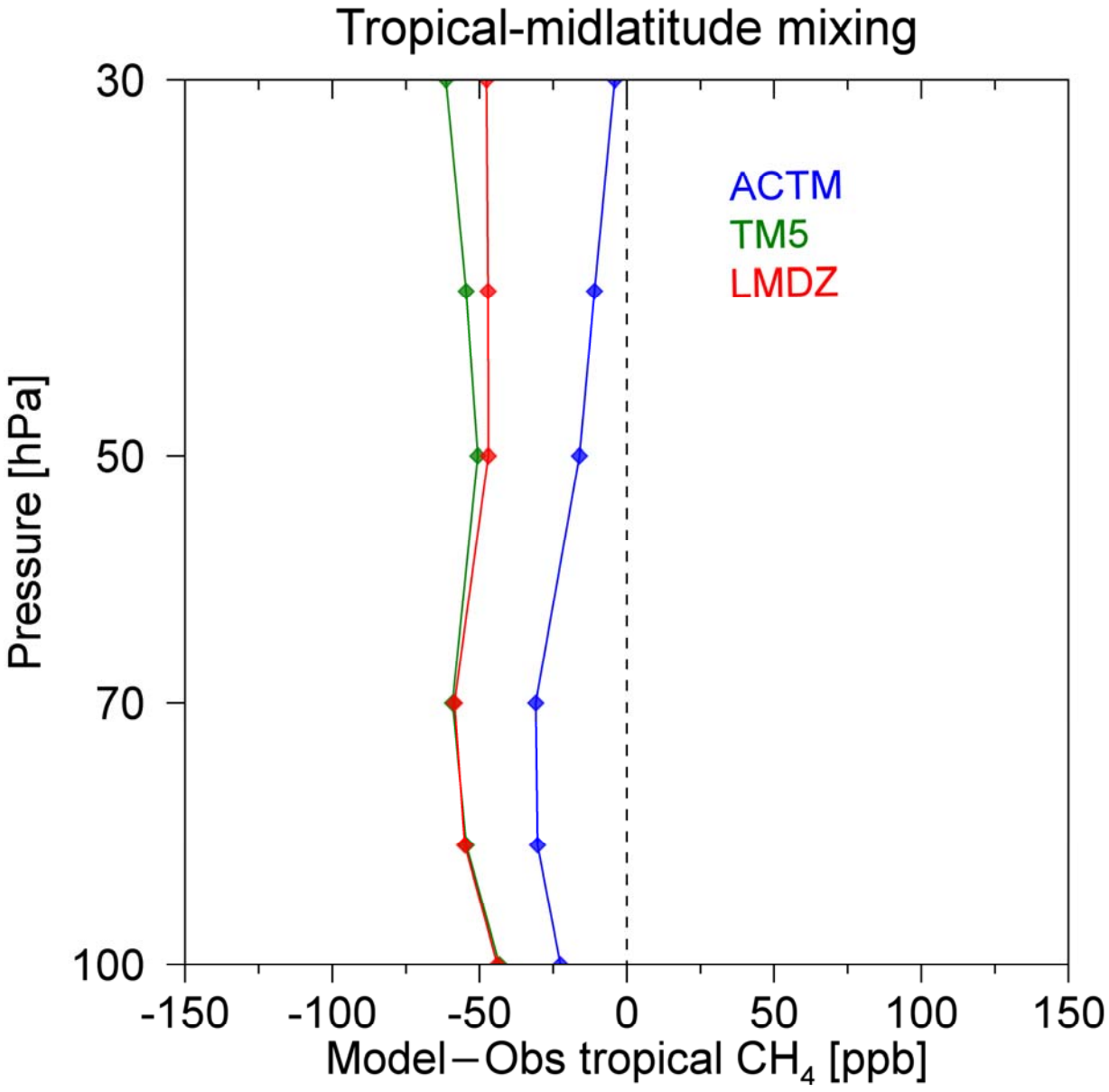

Figure 7. Model-MIPAS differences of tropical CH_4 mixing ratios as a transport diagnostics for horizontal mixing. The CH_4 differences are calculated as annual means on the MIPAS pressure-latitude grid.

Table 1. Overview of CTMs used for model-TCCON comparison

Model name	**Institution**	**Resolution**		**Output**	**Mean age derived from**	**Reference**
		horizontal[a]	**vertical**[b]	**CH_4**		
ACTM	JAMSTEC	~2.8 × 2.8 °	67σ	1-hourly, monthly	idealized transport tracer simulations	Patra et al. (2016)
TM5	SRON	~6 × 4 °	25η	daily	SF_6 simulations	Pandey et al. (2016)
LMDz	LSCE	~3.75 × 1.875 °	39η	monthly	SF_6 simulations	Locatelli et al. (2015)

[a] Longitude × Latitude

[b] vertical coordinates in sigma-pressure σ (pressure divided by surface pressure) and hybrid sigma-pressure η

Table 2. Overview of TCCON measurement sites used for the evaluation of chemical transport models. Abbreviations of the site names, information about geographical location, and number of measurement days in 2010 are provided.

TCCON site	Abbreviation	Latitude	Longitude	Days	Reference
Sodankylä (Finland)	SOD	67.4 °N	26.6 °E	78	Kivi et al. (2014)
Białystok (Poland)	BIA	53.2 °N	23.0 °E	120	Deutscher et al. (2014)
Karlsruhe (Germany)	KAR	49.1 °N	8.4 °E	79	Hase et al. (2014)
Orléans (France)	ORL	48.0 °N	2.1 °E	91	Warneke et al. (2014)
Garmisch (Germany)	GAR	47.5 °N	11.1 °E	120	Sussmann et al. (2014)
Park Falls (USA)	PAR	46.0 °N	90.3 °W	155	Wennberg et al. (2014a)
Lamont (USA)	LAM	36.6 °N	97.5 °W	299	Wennberg et al. (2014b)
Izaña (Tenerife)	IZA	28.3 °N	16.5 °W	50	Blumenstock et al. (2014)
Darwin (Australia)	DAR	12.4 °S	130.9 °E	64	Griffith et al. (2014a)
Wollongong (Australia)	WOL	34.4 °S	150.9 °E	142	Griffith et al. (2014b)
Lauder (New Zealand)	LAU	45.0 °S	169.7 °E	142	Sherlock et al. (2014a, b)

Table 3. Site-specific model XCH_4 biases with respect to TCCON observations in 2010. The model-TCCON agreement in XCH_4 is evaluated with different stratospheric CH_4 model fields: the original model distribution (**orig**), the MIPAS-based stratospheric CH_4 (**MIPAS**), and the MIPAS-based stratospheric CH_4 ajusted to ACE-FTS observations (**MIPAS_ACE**). XCH_4 biases and corresponding 2-σ standard errors (in brackets) are in parts per billion (ppb).

	ACTM			TM5			LMDz		
Site	orig	MIPAS	MIPAS_ACE	orig	MIPAS	MIPAS_ACE	orig	MIPAS	MIPAS_ACE
SOD	51.3 (±2.7)	19.9 (±2.9)	1.8 (±2.8)	-3.7 (±1.7)	8.1 (±2.6)	-8.0 (±2.5)	13.0 (±3.0)	9.1 (±3.2)	-15.0 (±3.6)
BIA	43.9 (±1.7)	12.8 (±1.7)	-5.0 (±1.9)	-10.5 (±1.3)	1.4 (±1.6)	-14.1 (±1.6)	4.0 (±1.7)	1.2 (±1.8)	-20.9 (±2.1)
KAR	47.0 (±2.0)	19.7 (±1.8)	3.5 (±1.9)	-4.0 (±1.4)	5.7 (±1.5)	-7.7 (±1.6)	9.8 (±2.0)	8.8 (±2.1)	-13.8 (±2.2)
ORL	47.2 (±1.7)	19.8 (±2.2)	3.5 (±2.3)	-7.0 (±1.5)	4.8 (±1.6)	-9.2 (±1.7)	5.4 (±2.1)	5.3 (±2.0)	-15.7 (±2.1)
GAR	45.6 (±1.8)	15.4 (±1.8)	-0.9 (±2.0)	-6.1 (±1.3)	4.7 (±1.5)	-8.1 (±1.5)	6.1 (±1.8)	7.3 (±1.8)	-15.7 (±1.8)
PAR	39.2 (±1.5)	13.5 (±1.6)	-1.3 (±1.6)	-9.7 (±1.2)	1.2 (±1.2)	-11.0 (±1.2)	4.4 (±1.4)	5.9 (±1.6)	-16.0 (±1.6)
LAM	31.1 (±1.3)	11.8 (±1.2)	1.8 (±1.1)	-4.4 (±0.8)	2.6 (±0.9)	-3.7 (±0.8)	-2.0 (±1.1)	1.7 (±1.1)	-20.4 (±1.2)
IZA	34.6 (±2.0)	12.6 (±2.2)	-1.6 (±2.2)	-11.4 (±1.5)	-5.0 (±1.5)	-12.6 (±1.5)	-4.8 (±1.9)	1.9 (±2.2)	-31.1 (±2.2)
DAR	18.8 (±1.6)	8.9 (±1.7)	0.1 (±1.8)	-8.1 (±1.0)	-3.1 (±1.1)	-8.8 (±1.1)	-9.2 (±1.6)	-2.9 (±2.6)	-15.0 (±1.4)
WOL	25.8 (±1.5)	4.8 (±1.6)	-6.6 (±1.6)	-17.6 (±1.4)	-11.1 (±1.4)	-17.9 (±1.3)	-11.9 (±1.8)	0.4 (±1.7)	-29.6 (±1.9)
LAU	34.8 (±1.0)	11.4 (±1.2)	-9.9 (±1.3)	-12.7 (±1.2)	0.0 (±1.3)	-18.3 (±1.3)	-4.0 (±1.4)	3.2 (±1.4)	-26.6 (±1.6)
range	32.5	15.1	13.4	13.9	19.2	14.6	24.9	12.0	17.3

Table 4. Average model XCH_4 bias with respect to TCCON observations in 2010 computed as mean of absolute site-specific biases (see Table 3). Average XCH_4 biases in ppb are derived for different model stratospheric CH_4 fields.

	mean XCH_4 bias		
Model stratospheric CH_4 field	ACTM	TM5	LMDz
Original model	38.1	8.7	6.8
MIPAS	13.7	4.3	4.3
MIPAS_ACE	3.3	10.8	20.0

Appendix B:

Personal contribution to the publications comprising this dissertation thesis

[**1**] Sussmann, R., **Ostler, A.**, Forster, F., Rettinger, M., Deutscher, N. M., Griffith, D. W. T., Hannigan, J. W., Jones, N., and Patra, P. K.: First intercalibration of column-averaged methane from the Total Carbon Column Observing Network and the Network for the Detection of Atmospheric Composition Change, Atmos. Meas. Tech., 6, 397–418, doi:10.5194/amt-6-397-2013, 2013.

- Performed batch processing of Garmisch NDACC retrievals and a priori corrections for both NDACC and TCCON retrievals in collaboration with F. Forster.
- Refined the a priori correction and the conversion of CH_4 total column retrievals into XCH_4 data.
- Computed XCH_4 data from NDACC retrievals of Garmisch and Wollongong.
- Evaluated the agreement of NDACC and TCCON XCH_4 data in terms of linear regression, trend analysis, auto-/cross-corelation, tests on statistical significance (t-test), and sensitivity of XCH_4 retrievals to airmass.
- Designed paper plots in cooperation with M. Rettinger.

- Provided general input to improve the paper, in particular during the review-process.

[2] Ostler, A., Sussmann, R., Rettinger, M., Deutscher, N. M., Dohe, S., Hase, F., Jones, N., Palm, M. and Sinnhuber, B.-M.: Multistation intercomparison of column-averaged methane from NDACC and TCCON: impact of dynamical variability, Atmos. Meas. Tech., 7, 4081–4101, doi:10.5194/amt-7-4081-2014, 2014.

- Developed the ideas and concepts for the paper in iteration with Ralf Sussmann.
- Performed batch processing of Garmisch NDACC retrievals and a priori corrections for both NDACC and TCCON retrievals.
- Computed XCH_4 data from NDACC retrievals of Garmisch, Wollongong, Karlsruhe, Izaña and Ny-Ålesund.
- Analyzed STE-trajectories.
- Performed all paper writing with feedback from Ralf Sussmann (feedback on English language by Nicholas M. Deutscher).
- Made all response to peer review and paper revision.

[3] Ostler, A., Sussmann, R., Patra, P. K., Houweling, S., De Bruine, M., Stiller, G. P., Haenel, F. J., Plieninger, J., Bousquet, P., Yin, Y., Saunois, M., Walker, K. A., Deutscher, N. M., Griffith, D. W. T., Blumenstock, T., Hase, F., Warneke, T., Wang, Z., Kivi, R., and Robinson, J.: Model − TCCON comparisons of column-averaged methane with a focus on the stratosphere, submitted to Atmos. Meas. Tech., 2016.

- Developed ideas and designed the concept of the published work based on input and feedback from Ralf Sussmann, Sander Houweling, Prabir K. Patra and Philipe Bousquet.
- Conducted the analysis of all model, TCCON, and satellite data sets.
- Developed figures and wrote the paper with conceptual advice from Ralf Sussmann, Sander Houweling and Prabir K. Patra.

Bibliography

Alexe, M., Bergamaschi, P., Segers, A., Detmers, R., Butz, A., Hasekamp, O., Guerlet, S., Parker, R., Boesch, H., Frankenberg, C., Scheepmaker, R. A., Dlugokencky, E., Sweeney, C., Wofsy, S. C., and Kort, E. A.: Inverse modelling of CH_4 emissions for 2010–2011 using different satellite retrieval products from GOSAT and SCIAMACHY, Atmos. Chem. Phys., 15, 113–133, doi:10.5194/acp-15-113-2015, 2015.

Angelbratt, J., Mellqvist, J., Blumenstock, T., Borsdorff, T., Brohede, S., Duchatelet, P., Forster, F., Hase, F., Mahieu, E., Murtagh, D., Petersen, A. K., Schneider, M., Sussmann, R., and Urban, J.: A new method to detect long term trends of methane (CH_4) and nitrous oxide (N_2O) total columns measured within the NDACC ground-based high resolution solar FTIR network, Atmos. Chem. Phys., 11, 6167–6183, doi:10.5194/acp-11-6167-2011, 2011.

Beck, V., Chen, H., Gerbig, C., Bergamaschi, P., Bruhwiler, L., Houweling, S., Röckmann, T., Kolle, O., Steinbach, J., Koch, T., Sapart, C. J., van der Veen, C., Frankenberg, C., Andreae, M. O., Artaxo, P., Longo, K. M., and Wofsy, S. C.: Methane airborne measurements and comparison to global models during BARCA, J. Geophys. Res., 117, D15310, doi:10.1029/2011JD017345, 2012.

Bergamaschi, P., Frankenberg, C., Meirink, J. F., Krol, M., Villani, M. G., Houweling, S., Dentener, F., Dlugokencky, E. J., Miller, J. B., Gatti, L. V., Engel, A., and Levin, I.: Inverse modeling of global and regional CH_4 emissions using SCIAMACHY satellite retrievals, J. Geophys. Res., 114, D22301, doi:10.1029/2009JD012287, 2009.

Bergamaschi, P., Houweling, S., Segers, A., Krol, M., Frankenberg, C., Scheepmaker, R. A., Dlugokencky, E., Wofsy, S. C., Kort, E. A., Sweeney, C., Schuck, T., Brenninkmeijer, C., Chen, H., Beck, V., and Gerbig, C.: Atmospheric CH_4 in the first decade of the 21st century: Inverse modeling analysis using SCIAMACHY satellite

retrievals and NOAA surface measurements, J. Geophys. Res., 118, 7350–7369, doi: 10.1002/jgrd.50480, 2013.

Bergamaschi, P., Corazza, M., Karstens, U., Athanassiadou, M., Thompson, R. L., Pison, I., Manning, A. J., Bousquet, P., Segers, A., Vermeulen, A. T., Janssens-Maenhout, G., Schmidt, M., Ramonet, M., Meinhardt, F., Aalto, T., Haszpra, L., Moncrieff, J., Popa, M. E., Lowry, D., Steinbacher, M., Jordan, A., O'Doherty, S., Piacentino, S., and Dlugokencky, E.: Top-down estimates of European CH_4 and N_2O emissions based on four different inverse models, Atmos. Chem. Phys., 15, 715–736, doi:10.5194/acp-15-715-2015, 2015.

Bernath, P. F., McElroy, C. T., Abrams, M. C., Boone, C. D., Butler, M., Camy-Peyret, C., Carleer, M., Clerbaux, C., Coheur, P.-F., Colin, R., DeCola, P., DeMazière, M., Drummond, J. R., Dufour, D., Evans, W. F. J., Fast, H., Fussen, D., Gilbert, K., Jennings, D. E., Llewellyn, E. J., Lowe, R. P., Mahieu, E., McConnell, J. C., McHugh, M., McLeod, S. D., Michaud, R., Midwinter, C., Nassar, R., Nichitiu, F., Nowlan, C., Rinsland, C. P., Rochon, Y. J., Rowlands, N., Semeniuk, K., Simon, P., Skelton, R., Sloan, J. J., Soucy, M.-A., Strong, K., Tremblay, P., Turnbull, D., Walker, K. A., Walkty, I., Wardle, D. A., Wehrle, V., Zander, R., and Zou, J.: Atmospheric Chemistry Experiment (ACE): Mission overview, Geophys. Res. Lett., 32, doi:10.1029/2005GL022386, 2005.

Brandt, A. R., Heath, G. A., Kort, E. A., O'Sullivan, F., Pétron, G., Jordaan, S. M., Tans, P., Wilcox, J., Gopstein, A. M., Arent, D., Wofsy, S., Brown, N. J., Bradley, R., Stucky, G. D., Eardley, D., and Harriss, R.: Methane Leaks from North American Natural Gas Systems, Science, 343, 733–735, doi:10.1126/science.1247045, 2014.

Ciais, P., Sabine, C., Bala, G., Bopp, L., Brovkin, V., Canadell, J., Chhabra, A., DeFries, R., Galloway, J., Heimann, M., Jones, C., Le Quéré, C., Myneni, R., Piao, S., and Thornton, P.: Carbon and Other Biogeochemical Cycles, book section 6, p. 465–570, Cambridge University Press, Cambridge, United Kingdom and New York, NY, USA, doi:10.1017/CBO9781107415324.015, 2013.

Cressot, C., Chevallier, F., Bousquet, P., Crevoisier, C., Dlugokencky, E. J., Fortems-Cheiney, A., Frankenberg, C., Parker, R., Pison, I., Scheepmaker, R. A., Montzka, S. A., Krummel, P. B., Steele, L. P., and Langenfelds, R. L.: On the consistency

between global and regional methane emissions inferred from SCIAMACHY, TANSO-FTS, IASI and surface measurements, Atmos. Chem. Phys., 14, 577–592, doi:10.5194/acp-14-577-2014, 2014.

Dils, B., Buchwitz, M., Reuter, M., Schneising, O., Boesch, H., Parker, R., Guerlet, S., Aben, I., Blumenstock, T., Burrows, J. P., Butz, A., Deutscher, N. M., Frankenberg, C., Hase, F., Hasekamp, O. P., Heymann, J., De Mazière, M., Notholt, J., Sussmann, R., Warneke, T., Griffith, D., Sherlock, V., and Wunch, D.: The Greenhouse Gas Climate Change Initiative (GHG-CCI): comparative validation of GHG-CCI SCIAMACHY/ENVISAT and TANSO-FTS/GOSAT CO_2 and CH_4 retrieval algorithm products with measurements from the TCCON, Atmos. Meas. Tech., 7, 1723–1744, doi:10.5194/amt-7-1723-2014, 2014.

Dlugokencky, E. J., Nisbet, E. G., Fisher, R., and Lowry, D.: Global atmospheric methane: budget, changes and dangers, Phil. Trans. R. Soc. A, 369, 2058–2072, doi:10.1098/rsta.2010.0341, 2011.

Fischer, H., Birk, M., Blom, C., Carli, B., Carlotti, M., von Clarmann, T., Delbouille, L., Dudhia, A., Ehhalt, D., Endemann, M., Flaud, J. M., Gessner, R., Kleinert, A., Koopman, R., Langen, J., López-Puertas, M., Mosner, P., Nett, H., Oelhaf, H., Perron, G., Remedios, J., Ridolfi, M., Stiller, G., and Zander, R.: MIPAS: an instrument for atmospheric and climate research, Atmos. Chem. Phys., 8, 2151–2188, doi:10.5194/acp-8-2151-2008, 2008.

Franco, B., Bader, W., Toon, G., Bray, C., Perrin, A., Fischer, E., Sudo, K., Boone, C., Bovy, B., Lejeune, B., Servais, C., and Mahieu, E.: Retrieval of ethane from ground-based FTIR solar spectra using improved spectroscopy: Recent burden increase above Jungfraujoch, J. Quant. Spectrosc. Radiat. Transf., 160, 36 – 49, doi:10.1016/j.jqsrt.2015.03.017, 2015.

Frankenberg, C., Meirink, J. F., van Weele, M., Platt, U., and Wagner, T.: Assessing Methane Emissions from Global Space-Borne Observations, Science, 308, 1010–1014, doi:10.1126/science.1106644, 2005.

Frankenberg, C., Bergamaschi, P., Butz, A., Houweling, S., Meirink, J. F., Notholt, J., Petersen, A. K., Schrijver, H., Warneke, T., and Aben, I.: Tropical methane emissions:

A revised view from SCIAMACHY onboard ENVISAT, Geophys. Res. Lett., 35, doi: 10.1029/2008GL034300, 2008.

Frankenberg, C., Aben, I., Bergamaschi, P., Dlugokencky, E. J., van Hees, R., Houweling, S., van der Meer, P., Snel, R., and Tol, P.: Global column-averaged methane mixing ratios from 2003 to 2009 as derived from SCIAMACHY: Trends and variability, J. Geophys. Res., 116, D04302, doi:10.1029/2010JD014849, 2011.

Fraser, A., Palmer, P. I., Feng, L., Boesch, H., Cogan, A., Parker, R., Dlugokencky, E. J., Fraser, P. J., Krummel, P. B., Langenfelds, R. L., O'Doherty, S., Prinn, R. G., Steele, L. P., van der Schoot, M., and Weiss, R. F.: Estimating regional methane surface fluxes: the relative importance of surface and GOSAT mole fraction measurements, Atmos. Chem. Phys., 13, 5697–5713, doi:10.5194/acp-13-5697-2013, 2013.

Garcia, R. R., Marsh, D. R., Kinnison, D. E., Boville, B. A., and Sassi, F.: Simulation of secular trends in the middle atmosphere, 1950–2003, J. Geophys. Res., 112, D09301, doi:10.1029/2006JD007485, 2007.

Geibel, M. C., Messerschmidt, J., Gerbig, C., Blumenstock, T., Chen, H., Hase, F., Kolle, O., Lavrič, J. V., Notholt, J., Palm, M., Rettinger, M., Schmidt, M., Sussmann, R., Warneke, T., and Feist, D. G.: Calibration of column-averaged CH_4 over European TCCON FTS sites with airborne in-situ measurements, Atmos. Chem. Phys., 12, 8763–8775, doi:10.5194/acp-12-8763-2012, 2012.

Griffiths, Peter, R. and de Haseth, James, A.: Fourier Transform Infrared Spectrometry, John Wiley & Sons, Inc., doi:10.1002/047010631X, 2007.

Hausmann, P., Sussmann, R., and Smale, D.: Contribution of oil and natural gas production to renewed increase in atmospheric methane (2007–2014): top–down estimate from ethane and methane column observations, Atmospheric Chemistry and Physics, 16, 3227–3244, doi:10.5194/acp-16-3227-2016, 2016.

Houweling, S., Krol, M., Bergamaschi, P., Frankenberg, C., Dlugokencky, E. J., Morino, I., Notholt, J., Sherlock, V., Wunch, D., Beck, V., Gerbig, C., Chen, H., Kort, E. A., Röckmann, T., and Aben, I.: A multi-year methane inversion using SCIAMACHY, accounting for systematic errors using TCCON measurements, Atmos. Chem. Phys., 14, 3991–4012, doi:10.5194/acp-14-3991-2014, 2014.

Jørgensen, J. C., Johansen, K. M. L., Westergaard-Nielsen, A., and Elberling, B.: Net regional methane sink in High Arctic soils of northeast Greenland, Nat. Geosci., 8, 20–23, doi:10.1038/ngeo2305, 2015.

Karion, A., Sweeney, C., Tans, P., and Newberger, T.: Aircore: an innovative atmospheric sampling system, J. Atmos. Oceanic Technol., 27, 1839—-1853, doi: http://dx.doi.org/10.1175/2010JTECHA1448.1, 2010.

Keppel-Aleks, G., Wennberg, P. O., and Schneider, T.: Sources of variations in total column carbon dioxide, Atmos. Chem. Phys., 11, 3581–3593, doi:10.5194/acp-11-3581-2011, 2011.

Kirschke, S., Bousquet, P., Ciais, P., Saunois, M., Canadell, J., Dlugokencky, E., Bergamaschi, P., Bergmann, D., Blake, D., Bruhwiler, L., Cameron-Smith, P., Castaldi, S., Chevallier, F., Feng, L., Fraser, A., Heimann, M., Hodson, E., Houweling, S., Josse, B., Fraser, P., Krummel, P., Lamarque, J.-F., Langenfelds, R., Le Quere, C., Naik, V., O'Doherty, S., Palmer, P., Pison, I., Plummer, D., Poulter, B., Prinn, R., Rigby, M., Ringeval, B., Santini, M., Schmidt, M., Shindell, D., Simpson, I., Spahni, R., Steele, L., Strode, S., Sudo, K., Szopa, S., van der Werf, G., Voulgarakis, A., van Weele, M., Weiss, R., Williams, J., and Zeng, G.: Three decades of global methane sources and sinks, Nat. Geosci., 6, 813–823, doi:10.1038/NGEO1955, 2013.

Liou, K. N.: An Introduction to Atmospheric Radiation, Volume 84, Second Edition (International Geophysics), Academic Press, 2 edn., 2002.

Locatelli, R., Bousquet, P., Saunois, M., Chevallier, F., and Cressot, C.: Sensitivity of the recent methane budget to LMDz sub-grid-scale physical parameterizations, Atmos. Chem. Phys., 15, 9765–9780, doi:10.5194/acp-15-9765-2015, 2015.

Mahieu, E., Chipperfield, M. P., Notholt, J., Reddmann, T., Anderson, J., Bernath, P. F., Blumenstock, T., Coffey, M. T., Dhomse, S. S., Feng, W., Franco, B., Froidevaux, L., Griffith, D. W. T., Hannigan, J. W., Hase, F., Hossaini, R., Jones, N. B., Morino, I., Murata, I., Nakajima, H., Palm, M., Paton-Walsh, C., Russell, Schneider, M., Servais, C., Smale, D., and Walker, K. A.: Recent Northern Hemisphere stratospheric HCl increase due to atmospheric circulation changes, Nature, 515, 104–107, doi:10.1038/nature13857, 2014.

McKain, K., Down, A., Raciti, S. M., Budney, J., Hutyra, L. R., Floerchinger, C., Herndon, S. C., Nehrkorn, T., Zahniser, M. S., Jackson, R. B., Phillips, N., and Wofsy, S. C.: Methane emissions from natural gas infrastructure and use in the urban region of Boston, Massachusetts, Proc. Natl. Acad. Sci. U.S.A., 112, 1941–1946, doi: 10.1073/pnas.1416261112, 2015.

Meirink, J. F., Bergamaschi, P., Frankenberg, C., d'Amelio, M. T. S., Dlugokencky, E. J., Gatti, L. V., Houweling, S., Miller, J. B., Röckmann, T., Villani, M. G., and Krol, M. C.: Four-dimensional variational data assimilation for inverse modeling of atmospheric methane emissions: Analysis of SCIAMACHY observations, J. Geophys. Res., 113, D17301, doi:10.1029/2007JD009740, 2008.

Melton, J. R., Wania, R., Hodson, E. L., Poulter, B., Ringeval, B., Spahni, R., Bohn, T., Avis, C. A., Beerling, D. J., Chen, G., Eliseev, A. V., Denisov, S. N., Hopcroft, P. O., Lettenmaier, D. P., Riley, W. J., Singarayer, J. S., Subin, Z. M., Tian, H., Zürcher, S., Brovkin, V., van Bodegom, P. M., Kleinen, T., Yu, Z. C., and Kaplan, J. O.: Present state of global wetland extent and wetland methane modelling: conclusions from a model inter-comparison project (WETCHIMP), Biogeosciences, 10, 753–788, doi:10.5194/bg-10-753-2013, 2013.

Miller, S. M., Wofsy, S. C., Michalak, A. M., Kort, E. A., Andrews, A. E., Biraud, S. C., Dlugokencky, E. J., Eluszkiewicz, J., Fischer, M. L., Janssens-Maenhout, G., Miller, B. R., Miller, J. B., Montzka, S. A., Nehrkorn, T., and Sweeney, C.: Anthropogenic emissions of methane in the United States, Proc. Natl. Acad. Sci. U.S.A., 110, 20 018–20 022, doi:10.1073/pnas.1314392110, 2013.

Monteil, G., Houweling, S., Butz, A., Guerlet, S., Schepers, D., Hasekamp, O., Frankenberg, C., Scheepmaker, R., Aben, I., and Röckmann, T.: Comparison of CH_4 inversions based on 15 months of GOSAT and SCIAMACHY observations, J. Geophys. Res., 118, 11,807–11,823, doi:10.1002/2013JD019760, 2013.

Montzka, S. A., Krol, M., Dlugokencky, E., Hall, B., Jöckel, P., and Lelieveld, J.: Small Interannual Variability of Global Atmospheric Hydroxyl, Science, 331, 67–69, doi: 10.1126/science.1197640, 2011.

Morino, I., Uchino, O., Inoue, M., Yoshida, Y., Yokota, T., Wennberg, P. O., Toon, G. C., Wunch, D., Roehl, C. M., Notholt, J., Warneke, T., Messerschmidt, J., Griffith,

D. W. T., Deutscher, N. M., Sherlock, V., Connor, B., Robinson, J., Sussmann, R., and Rettinger, M.: Preliminary validation of column-averaged volume mixing ratios of carbon dioxide and methane retrieved from GOSAT short-wavelength infrared spectra, Atmos. Meas. Tech., 4, 1061–1076, doi:10.5194/amt-4-1061-2011, 2011.

Myhre, G., Shindell, D., Bréon, F.-M., Collins, W., Fuglestvedt, J., Huang, J., Koch, D., Lamarque, J.-F., Lee, D., Mendoza, B., Nakajima, T., Robock, A., Stephens, G., Takemura, T., and Zhang, H.: Anthropogenic and Natural Radiative Forcing, book section 8, p. 659–740, Cambridge University Press, Cambridge, United Kingdom and New York, NY, USA, doi:10.1017/CBO9781107415324.018, 2013.

Nisbet, E. and Weiss, R.: Top-Down Versus Bottom-Up, Science, 328, 1241–1243, doi:10.1126/science.1189936, 2010.

Nisbet, E. G., Dlugokencky, E. J., and Bousquet, P.: Methane on the Rise—Again, Science, 343, 493–495, doi:10.1126/science.1247828, 2014.

NOAA, NASA, and USAF: U.S. Standard Atmosphere, U.S. Governement Printing Office, Washington D.C., 1st edn., 1976.

Olsen, S. C. and Randerson, J. T.: Differences between surface and column atmospheric CO_2 and implications for carbon cycle research, J. Geophys. Res., 109, D02301, doi:10.1029/2003JD003968, 2004.

Ostler, A., Sussmann, R., Rettinger, M., Deutscher, N. M., Dohe, S., Hase, F., Jones, N., Palm, M., and Sinnhuber, B.-M.: Multistation intercomparison of column-averaged methane from NDACC and TCCON: impact of dynamical variability, Atmos. Meas. Tech., 7, 4081–4101, doi:10.5194/amt-7-4081-2014, 2014.

Ostler, A., Sussmann, R., Patra, P. K., Houweling, S., De Bruine, M., Stiller, G. P., Haenel, F. J., Plieninger, J., Bousquet, P., Yin, Y., Saunois, M., Walker, K. A., Deutscher, N. M., Griffith, D. W. T., Blumenstock, T., Hase, F., Warneke, T., Wang, Z., Kivi, R., and Robinson, J.: Model − TCCON comparisons of column-averaged methane with a focus on the stratosphere, submitted to Atmos. Meas. Tech., 2016.

Pandey, S., Houweling, S., Krol, M., Aben, I., Chevallier, F., Dlugokencky, E. J., Gatti, L. V., Gloor, M., Miller, J. B., Detmers, R., Machida, T., and Röckmann, T.: Inverse modeling of GOSAT-retrieved ratios of total column CH_4 and CO_2 for 2009 and 2010, Atmos. Chem. Phys. Discuss., 2016, 1–32, doi:10.5194/acp-2016-77, 2016.

Patra, P. K., Houweling, S., Krol, M., Bousquet, P., Belikov, D., Bergmann, D., Bian, H., Cameron-Smith, P., Chipperfield, M. P., Corbin, K., Fortems-Cheiney, A., Fraser, A., Gloor, E., Hess, P., Ito, A., Kawa, S. R., Law, R. M., Loh, Z., Maksyutov, S., Meng, L., Palmer, P. I., Prinn, R. G., Rigby, M., Saito, R., and Wilson, C.: TransCom model simulations of CH_4 and related species: linking transport, surface flux and chemical loss with CH_4 variability in the troposphere and lower stratosphere, Atmos. Chem. Phys., 11, 12 813–12 837, doi:10.5194/acp-11-12813-2011, 2011.

Patra, P. K., Krol, M. C., Montzka, S. A., Arnold, T., Atlas, E. L., Lintner, B. R., Stephens, B. B., Xiang, B., Elkins, J. W., Fraser, P. J., Ghosh, A., Hintsa, E. J., Hurst, D. F., Ishijima, K., Krummel, P. B., Miller, B. R., Miyazaki, K., Moore, F. L., Muhle, J., O/'Doherty, S., Prinn, R. G., Steele, L. P., Takigawa, M., Wang, H. J., Weiss, R. F., Wofsy, S. C., and Young, D.: Observational evidence for interhemispheric hydroxyl-radical parity, Nature, 513, 219–223, doi:10.1038/nature13721, 2014.

Patra, P. K., Saeki, T., Dlugokencky, E. J., Ishijima, K., Umezawa, T., Ito, A., Aoki, S., Morimoto, S., Kort, E. A., Crotwell, A., Ravi Kumar, K., and Nakazawa, T.: Regional methane emission estimation based on observed atmospheric concentrations (2002–2012), J. Meteorol. Soc. Jpn., 94, doi:doi:10.2151/jmsj.2016-006, 2016.

Petrescu, A. M. R., Lohila, A., Tuovinen, J.-P., Baldocchi, D. D., Desai, A. R., Roulet, N. T., Vesala, T., Dolman, A. J., Oechel, W. C., Marcolla, B., Friborg, T., Rinne, J., Matthes, J. H., Merbold, L., Meijide, A., Kiely, G., Sottocornola, M., Sachs, T., Zona, D., Varlagin, A., Lai, D. Y. F., Veenendaal, E., Parmentier, F.-J. W., Skiba, U., Lund, M., Hensen, A., van Huissteden, J., Flanagan, L. B., Shurpali, N. J., Grünwald, T., Humphreys, E. R., Jackowicz-Korczyński, M., Aurela, M. A., Laurila, T., Grüning, C., Corradi, C. A. R., Schrier-Uijl, A. P., Christensen, T. R., Tamstorf, M. P., Mastepanov, M., Martikainen, P. J., Verma, S. B., Bernhofer, C., and Cescatti, A.: The uncertain climate footprint of wetlands under human pressure, Proc. Natl. Acad. Sci. U.S.A., 112, 4594–4599, doi:10.1073/pnas.1416267112, 2015.

Plieninger, J., Laeng, A., Lossow, S., von Clarmann, T., Stiller, G. P., Kellmann, S., Linden, A., Kiefer, M., Walker, K. A., Noël, S., Hervig, M. E., McHugh, M., Lambert, A., Urban, J., Elkins, J. W., and Murtagh, D.: Validation of revised methane and nitrous oxide profiles from MIPAS–ENVISAT, Atmospheric Measurement Techniques, 9, 765–779, doi:10.5194/amt-9-765-2016, 2016.

Rogelj, J., Schaeffer, M., Meinshausen, M., Shindell, D. T., Hare, W., Klimont, Z., Velders, G. J. M., Amann, M., and Schellnhuber, H. J.: Disentangling the effects of CO_2 and short-lived climate forcer mitigation, Proc. Natl. Acad. Sci. U.S.A., 111, 16 325–16 330, doi:10.1073/pnas.1415631111, 2014.

Saad, K. M., Wunch, D., Toon, G. C., Bernath, P., Boone, C., Connor, B., Deutscher, N. M., Griffith, D. W. T., Kivi, R., Notholt, J., Roehl, C., Schneider, M., Sherlock, V., and Wennberg, P. O.: Derivation of tropospheric methane from TCCON CH_4 and HF total column observations, Atmos. Meas. Tech., 7, 2907–2918, doi:10.5194/amt-7-2907-2014, 2014.

Schepers, D., Guerlet, S., Butz, A., Landgraf, J., Frankenberg, C., Hasekamp, O., Blavier, J.-F., Deutscher, N. M., Griffith, D. W. T., Hase, F., Kyro, E., Morino, I., Sherlock, V., Sussmann, R., and Aben, I.: Methane retrievals from Greenhouse Gases Observing Satellite (GOSAT) shortwave infrared measurements: Performance comparison of proxy and physics retrieval algorithms, J. Geophys. Res., 117, D10307, doi:10.1029/2012JD017549, 2012.

Schneising, O., Bergamaschi, P., Bovensmann, H., Buchwitz, M., Burrows, J. P., Deutscher, N. M., Griffith, D. W. T., Heymann, J., Macatangay, R., Messerschmidt, J., Notholt, J., Rettinger, M., Reuter, M., Sussmann, R., Velazco, V. A., Warneke, T., Wennberg, P. O., and Wunch, D.: Atmospheric greenhouse gases retrieved from SCIAMACHY: comparison to ground-based FTS measurements and model results, Atmos. Chem. Phys., 12, 1527–1540, doi:10.5194/acp-12-1527-2012, 2012.

Schuur, E. A. G., McGuire, A. D., Schädel, C., Grosse, G., Harden, J. W., Hayes, D. J., Hugelius, G., Koven, C. D., Kuhry, P., Lawrence, D. M., Natali, S. M., Olefeldt, D., Romanovsky, V. E., Schaefer, K., Turetsky, M. R., Treat, C. C., and Vonk, J. E.: Climate change and the permafrost carbon feedback, Nature, 520, 171–179, doi:10.1038/nature14338, 2015.

Sepúlveda, E., Schneider, M., Hase, F., García, O. E., Gomez-Pelaez, A., Dohe, S., Blumenstock, T., and Guerra, J. C.: Long-term validation of tropospheric column-averaged CH_4 mole fractions obtained by mid-infrared ground-based FTIR spectrometry, Atmos. Meas. Tech., 5, 1425–1441, doi:10.5194/amt-5-1425-2012, 2012.

Sepúlveda, E., Schneider, M., Hase, F., Barthlott, S., Dubravica, D., García, O. E., Gomez-Pelaez, A., González, Y., Guerra, J. C., Gisi, M., Kohlhepp, R., Dohe, S., Blumenstock, T., Strong, K., Weaver, D., Palm, M., Sadeghi, A., Deutscher, N. M., Warneke, T., Notholt, J., Jones, N., Griffith, D. W. T., Smale, D., Brailsford, G. W., Robinson, J., Meinhardt, F., Steinbacher, M., Aalto, T., and Worthy, D.: Tropospheric CH_4 signals as observed by NDACC FTIR at globally distributed sites and comparison to GAW surface in situ measurements, Atmos. Meas. Tech., 7, 2337–2360, doi:10.5194/amt-7-2337-2014, 2014.

Shindell, D., Kuylenstierna, J. C. I., Vignati, E., van Dingenen, R., Amann, M., Klimont, Z., Anenberg, S. C., Muller, N., Janssens-Maenhout, G., Raes, F., Schwartz, J., Faluvegi, G., Pozzoli, L., Kupiainen, K., Höglund-Isaksson, L., Emberson, L., Streets, D., Ramanathan, V., Hicks, K., Oanh, N. T. K., Milly, G., Williams, M., Demkine, V., and Fowler, D.: Simultaneously Mitigating Near-Term Climate Change and Improving Human Health and Food Security, Science, 335, 183–189, doi:10.1126/science.1210026, 2012.

Simpson, I., Andersen, M., Meinardi, S., Bruhwiler, L., Blake, N., Helmig, D., Rowland, F., and Blake, D.: Long-term decline of global atmospheric ethane concentrations and implications for methane, Nature, 488, 490–4, doi:10.1038/nature11342, 2012.

Sjögersten, S., Black, C. R., Evers, S., Hoyos-Santillan, J., Wright, E. L., and Turner, B. L.: Tropical wetlands: A missing link in the global carbon cycle?, Global Biogeochem. Cycles, 28, 1371–1386, doi:10.1002/2014GB004844, 2014.

Stohl, A., Bonasoni, P., Cristofanelli, P., Collins, W., Feichter, J., Frank, A., Forster, C., Gerasopoulos, E., Gäggeler, H., James, P., Kentarchos, T., Kromp-Kolb, H., Krüger, B., Land, C., Meloen, J., Papayannis, A., Priller, A., Seibert, P., Sprenger, M., Roelofs, G. J., Scheel, H. E., Schnabel, C., Siegmund, P., Tobler, L., Trickl, T., Wernli, H., Wirth, V., Zanis, P., and Zerefos, C.: Stratosphere-troposphere exchange: A review, and what we have learned from STACCATO, J. Geophys. Res., 108(D12), 8516, doi:10.1029/2002JD002490, 2003.

Strahan, S. E., Douglass, A. R., Stolarski, R. S., Akiyoshi, H., Bekki, S., Braesicke, P., Butchart, N., Chipperfield, M. P., Cugnet, D., Dhomse, S., Frith, S. M., Gettelman, A., Hardiman, S. C., Kinnison, D. E., Lamarque, J.-F., Mancini, E., Marchand, M., Michou, M., Morgenstern, O., Nakamura, T., Olivié, D., Pawson, S., Pitari,

G., Plummer, D. A., Pyle, J. A., Scinocca, J. F., Shepherd, T. G., Shibata, K., Smale, D., Teyssèdre, H., Tian, W., and Yamashita, Y.: Using transport diagnostics to understand chemistry climate model ozone simulations, J. Geophys. Res., 116, D17302, doi:10.1029/2010JD015360, 2011.

Sussmann, R., Stremme, W., Buchwitz, M., and de Beek, R.: Validation of ENVISAT/SCIAMACHY columnar methane by solar FTIR spectrometry at the Ground-Truthing Station Zugspitze, Atmos. Chem. Phys., 5, 2419–2429, doi:10.5194/acp-5-2419-2005, 2005.

Sussmann, R., Forster, F., Rettinger, M., and Jones, N.: Strategy for high-accuracy-and-precision retrieval of atmospheric methane from the mid-infrared FTIR network, Atmos. Meas. Tech., 4, 1943–1964, doi:10.5194/amt-4-1943-2011, 2011.

Sussmann, R., Ostler, A., Forster, F., Rettinger, M., Deutscher, N. M., Griffith, D. W. T., Hannigan, J. W., Jones, N., and Patra, P. K.: First intercalibration of column-averaged methane from the Total Carbon Column Observing Network and the Network for the Detection of Atmospheric Composition Change, Atmos. Meas. Tech., 6, 397–418, doi:10.5194/amt-6-397-2013, 2013.

Turner, A. J., Jacob, D. J., Wecht, K. J., Maasakkers, J. D., Biraud, S. C., Boesch, H., Bowman, K. W., Deutscher, N. M., Dubey, M. K., Griffith, D. W. T., Hase, F., Kuze, A., Notholt, J., Ohyama, H., Parker, R., Payne, V. H., Sussmann, R., Velazco, V. A., Warneke, T., Wennberg, P. O., and Wunch, D.: Estimating global and North American methane emissions with high spatial resolution using GOSAT satellite data, Atmos. Chem. Phys. Discuss., 15, 4495–4536, doi:10.5194/acpd-15-4495-2015, 2015.

Wang, Z., Deutscher, N. M., Warneke, T., Notholt, J., Dils, B., Griffith, D. W. T., Schmidt, M., Ramonet, M., and Gerbig, C.: Retrieval of tropospheric column-averaged CH_4 mole fraction by solar absorption FTIR-spectrometry using N_2O as a proxy, Atmos. Meas. Tech., 7, 3295–3305, doi:10.5194/amt-7-3295-2014, 2014.

Washenfelder, R. A., Wennberg, P. O., and Toon, G. C.: Tropospheric methane retrieved from ground-based near-IR solar absorption spectra, Geophys. Res. Lett., 30(23), 2226, doi:10.1029/2003GL017969, 2003.

Waugh, D. and Hall, T.: AGE OF STRATOSPHERIC AIR: THEORY, OBSERVATIONS, AND MODELS, Rev. Geophys., 40(4), 1–26, doi:10.1029/2000RG000101, 2002.

Wecht, K. J., Jacob, D. J., Frankenberg, C., Jiang, Z., and Blake, D. R.: Mapping of North American methane emissions with high spatial resolution by inversion of SCIAMACHY satellite data, J. Geophys. Res., 119, 7741–7756, doi:10.1002/2014JD021551, 2014.

Wennberg, P. O.: Atmospheric chemistry: Radicals follow the Sun, Nature, 442, 145–146, doi:10.1038/442145a, 2006.

Wennberg, P. O., Mui, W., Wunch, D., Kort, E. A., Blake, D. R., Atlas, E. L., Santoni, G. W., Wofsy, S. C., Diskin, G. S., Jeong, S., and Fischer, M. L.: On the Sources of Methane to the Los Angeles Atmosphere, Environ. Sci. Technol., 46, 9282–9289, doi:10.1021/es301138y, 2012.

Wunch, D., Toon, G. C., Wennberg, P. O., Wofsy, S. C., Stephens, B. B., Fischer, M. L., Uchino, O., Abshire, J. B., Bernath, P., Biraud, S. C., Blavier, J.-F. L., Boone, C., Bowman, K. P., Browell, E. V., Campos, T., Connor, B. J., Daube, B. C., Deutscher, N. M., Diao, M., Elkins, J. W., Gerbig, C., Gottlieb, E., Griffith, D. W. T., Hurst, D. F., Jiménez, R., Keppel-Aleks, G., Kort, E. A., Macatangay, R., Machida, T., Matsueda, H., Moore, F., Morino, I., Park, S., Robinson, J., Roehl, C. M., Sawa, Y., Sherlock, V., Sweeney, C., Tanaka, T., and Zondlo, M. A.: Calibration of the Total Carbon Column Observing Network using aircraft profile data, Atmos. Meas. Tech., 3, 1351–1362, doi:10.5194/amt-3-1351-2010, 2010.

Wunch, D., Toon, G. C., Blavier, J.-F. L., Washenfelder, R. A., Notholt, J., Connor, B. J., Griffith, D. W. T., Sherlock, V., and Wennberg, P. O.: The Total Carbon Column Observing Network, Phil. Trans. R. Soc. A, 369, 2087–2112, doi:10.1098/rsta.2010.0240, 2011.

Yoshida, Y., Kikuchi, N., Morino, I., Uchino, O., Oshchepkov, S., Bril, A., Saeki, T., Schutgens, N., Toon, G. C., Wunch, D., Roehl, C. M., Wennberg, P. O., Griffith, D. W. T., Deutscher, N. M., Warneke, T., Notholt, J., Robinson, J., Sherlock, V., Connor, B., Rettinger, M., Sussmann, R., Ahonen, P., Heikkinen, P., Kyrö, E., Mendonca,

J., Strong, K., Hase, F., Dohe, S., and Yokota, T.: Improvement of the retrieval algorithm for GOSAT SWIR XCO_2 and XCH_4 and their validation using TCCON data, Atmos. Meas. Tech., 6, 1533–1547, doi:10.5194/amt-6-1533-2013, 2013.

Zdunkowski, W., Trautmann, T., and Bott, A.: Radiation in the atmosphere : a course in theoretical meteorology, Cambridge University Press, Cambridge, UK; New York, 2007.